การผลิตเซรามิกซ์ไฮดรอกซี่แอพาไทต์ชนิดพรุน

นาย สุจินต์ วุฒิชัยวัฒน์

วิทยานิพนธ์นี้เป็นส่วนหนึ่งของการศึกษาตามหลักสูตรปริญญาวิศวกรรมศาสตรดุษฎีบัณฑิต
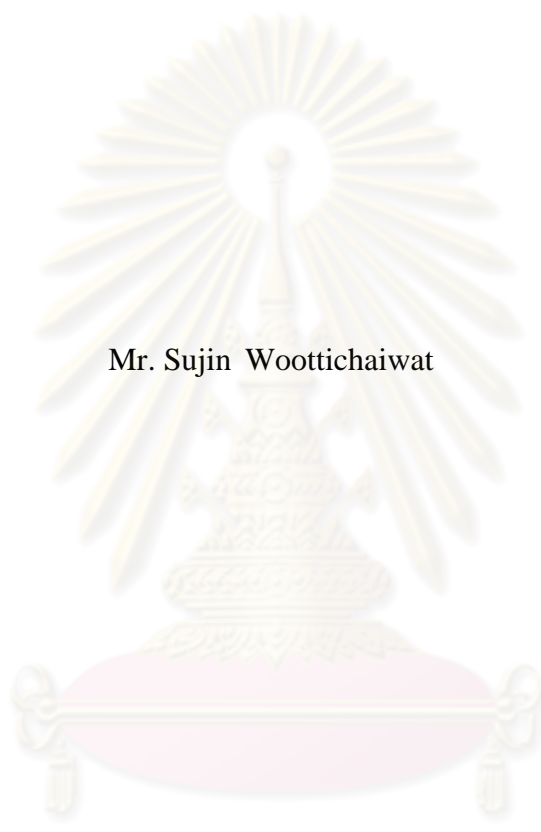สาขาวิชาวิศวกรรมอุตสาหการ   ภาควิชาวิศวกรรมอุตสาหการ
คณะวิศวกรรมศาสตร์ จุฬาลงกรณ์มหาวิทยาลัย
ปีการศึกษา 2553

THE PRODUCTION OF POROUS HYDROXYAPATITE CERAMICS

Mr. Sujin Woottichaiwat

A Dissertation Submitted in Partial Fulfillment of the Requirements

for the Degree of Doctor of Philosophy Program in Industrial Engineering

Department of Industrial Engineering

Faculty of Engineering

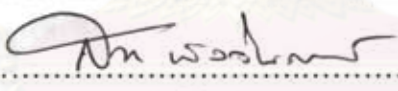Chulalongkorn University

Academic Year 2010

Thesis Title	THE PRODUCTION OF POROUS HYDROXYAPATITE CERAMICS
By	Mr. Sujin Woottichaiwat
Field of Study	Industrial Engineering
Thesis Advisor	Assistant Professor Somchai Puajindanetr, Ph.D.

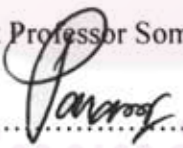
Accepted by the Faculty of Engineering, Chulalongkorn University in Partial Fulfillment of the Requirements for the Doctoral Degree
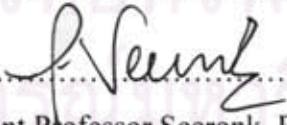
.... Dean of the Faculty of Engineering

(Associate Professor Boonsom Lerdhirunwong, Dr.Ing.)
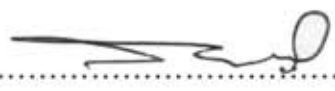
THESIS COMMITTEE

.... Chairman

(Associate Professor Damrong Thawesaengskulthai.)

.... Thesis Advisor

(Assistant Professor Somchai Puajindanetr, Ph.D.)

.... Examiner

(Associate Professor Parames Chutima, Ph.D.)

.... Examiner

(Assistant Professor Seeronk Prichanont, Ph.D.)

.... External Examiner

(Associate Professor Somchai Puangphuaksook)

สุจินต์ วุฒิชัยวัฒน์ : การผลิตเซรามิกซ์ไฮดรอกซี่แอพาไทต์ชนิดพรุน (THE PRODUCTION OF POROUS HYDROXYAPATITE CERAMICS) อ.ที่ปรึกษาวิทยานิพนธ์หลัก : ผศ.ดร. สมชาย พัวจินดาเนตร, 240 หน้า.

วัตถุประสงค์ของงานวิจัยนี้ เพื่อ (1) พัฒนากระบวนการผลิตเซรามิกซ์ไฮดรอกซี่อะพาไทต์ (HA) ชนิด พรุนที่สามารถควบคุมความพรุนได้ และ (2) ศึกษาปัจจัยสำคัญในการขึ้นรูปที่มีผลต่อความพรุนและความ ทนทานแรงทางกล   ผง HA ที่ใช้ในการขึ้นรูปชิ้นงานตัวอย่างถูกสังเคราะห์ด้วยวิธีการตกตะกอนจากปฏิกิริยาเคมี ระหว่างแคลเซียมไฮดรอกไซด์และกรดออร์โธฟอสฟอริค ผง HA ถูกเตรียมเป็นชิ้นงานพรุนด้วย 3 วิธีการ ทั้งไม่เติม และเติมสารลดความตึงผิวร้อยละ 1 โดยน้ำหนัก (ในที่นี้ใช้ผงอะการ์) ได้แก่ (1) การใช้โพลีเมธิวเมธาไครเลท (PMMA) เป็นแม่แบบที่สลายได้ ในช่วงร้อยละ 5-50 โดยน้ำหนัก (2) การใช้ไฮโครเจนเปอร์ออกไซด์ (H_2O_2) สร้าง ฟองอากาศ ในช่วงร้อยละ 1-30 โดยน้ำหนัก และ (3) การรวมวิธีการทั้งสองโดยใช้ทั้ง PMMA และ H_2O_2 ด้วย อัตราส่วนของเหลวต่อผง HA ที่ระดับ 1.3 และ 1.5 มิลลิลิตรต่อกรัม หลังจากนั้นนำชิ้นงานเผาที่อุณหภูมิ 1,100 องศาเซลเซียส เป็นเวลา 2 ชั่วโมง และปล่อยให้เย็นตัวในเตา ก่อนการเตรียมชิ้นงานพรุน นำผง HA ตรวจสอบ คุณสมบัติทางกายภาพด้วยเทคนิค X-ray Diffraction (XRD) Fourier Transform Infrared (FTIR) Particle Size Analysis (PSA) และ Scanning Electron Microscope (SEM) นำชิ้นงานหลังการเผามาตรวจสอบความพรุน โครงสร้างจุลภาค ความทนทานแรงกดและแรงดัด และโมดูลัสแรงกดและแรงดัด

จากการศึกษา พบว่า (1) วิธีที่ 1 สร้างรูพรุนที่มีขนาด 100-300 ไมโครเมตร ความพรุน 52-74% ความ ทนทานแรงกดและแรงดัด 0.5-36 และ 0.06-7 เมกะปาสคาล ตามลำดับ และโมดูลัสแรงกดและแรงดัด 33-5,530 กิโลนิวตันต่อตารางเมตร และ 8-730 เมกะนิวตันต่อตารางเมตร ตามลำดับ (2) วิธีที่ 2 สร้างรูพรุนที่มีขนาด 100-1,000 ไมโครเมตร ความพรุน 80-85% ความทนทานแรงกดและแรงดัด 0.07-0.7 และ 0.1-1.1 เมกะปาสคาล ตามลำดับ และโมดูลัสแรงกดและแรงดัด 60-550 กิโลนิวตันต่อตารางเมตร และ 2-75 เมกะนิวตันต่อตารางเมตร ตามลำดับ (3) วิธีที่ 3 สร้างรูพรุนที่มีขนาด 100-1,000 ไมโครเมตร ความพรุน 82-90% ความทนทานแรงกดและ แรงดัด 0.03-0.5 และ 0.1-0.7 เมกะปาสคาล และโมดูลัสแรงกดและแรงดัด 13-440 กิโลนิวตันต่อตารางเมตร และ 0.5-45 เมกะนิวตันต่อตารางเมตร ตามลำดับ (4) วิธีที่ 3 สามารถสร้างรูพรุนที่มีช่องเชื่อมต่อกัน ในขณะที่สองวิธี แรกจะสร้างรูพรุนที่มีลักษณะปิด (5) วิธีที่ 1 เป็นวิธีที่สามารถควบคุมความพรุนของชิ้นงานได้มากที่สุด (6) การ เพิ่มปริมาณการใช้ PMMA ความเข้มข้นของ H_2O_2 และอัตราส่วนของเหลวต่อผง HA ต่างส่งผลให้ความพรุน เพิ่มขึ้นและความทนทานแรงทางกลลดลง และ (7) การเติมสารลดความตึงผิวมีผลต่อการเพิ่มขึ้นของความ ทนทานแรงกดของชิ้นงานพรุนที่ขึ้นรูปด้วยวิธีที่ 2 อย่างมีนัยสำคัญ ที่ระดับความเชื่อมั่น 95% ในช่วงความเข้มข้น ของ H_2O_2 ระหว่างร้อยละ 5-20 โดยน้ำหนัก ความทนทานแรงกดมีค่าเพิ่มขึ้นจาก 0.29 ถึง 0.46 เมกะปาสคาล หรือ เพิ่มขึ้นคิดเป็นร้อยละ 60

ภาควิชา ...วิศวกรรมอุตสาหการ... ลายมือชื่อนิสิต...............................

สาขาวิชา.. วิศวกรรมอุตสาหการ... ลายมือชื่อ อ. ที่ปรึกษาวิทยานิพนธ์หลัก..............

ปีการศึกษา ...2553...

4771868921 : MAJOR INDUSTRIAL ENGINEERING
KEYWORDS: POROUS HYDROXYAPATITE / FABRICATION / SACRIFICIAL TEMPLATE / DIRECT FOAMING

SUJIN WOOTTICHAIWAT: THE PRODUCTION OF POROUS HYDROXYAPATITE CERAMICS, ADVISOR: ASST. PROF. SOMCHAI PUAJINDANETR, Ph.D., 240 pp.

The objectives of this research were to (1) develop the production process of porous hydroxyapatite (HA) ceramics with controllable porosity and (2) study key forming factors affecting on porosity and mechanical strength of porous HA scaffolds. The HA powder was synthesized through a precipitation reaction between calcium hydroxide and orthophosphoric acid. The porous samples were prepared from HA powder without and with 1wt% surfactant (agar powder) through three methods; including (1) sacrificial template technique using polymethyl methacrylate (PMMA) granule ranging from 5 to 50wt% in content, (2) direct foaming technique using hydrogen peroxide (H_2O_2) solution ranging from 1 to 30wt% in concentration, and (3) combination technique between sacrificial template and direct foaming techniques using PMMA and H_2O_2, at liquid to powder ratio of 1.3 ml/g and 1.5 ml/g. Afterwards, the porous samples were sintered at 1,100°C for 2 hours and then cooled in the furnace. Moreover, the HA powder was characterized by X-ray Diffraction (XRD), Fourier Transform Infrared (FTIR), Particle Size Analysis (PSA) and Scanning Electron Microscope (SEM). The porous samples were investigated for porosity, microstructure, compressive and flexural strength, and stiffness.

The study found that (1) sacrificial template technique using PMMA provided pore sizes ranging between 100-300 μm, porosity ranging between 52-74%, compressive and flexural strengths ranging between 0.5-36 MPa and 0.6-7 MPa, respectively, compressive and flexural stiffness ranging between 33-5,530 kN/m^2 and 8-730 MN/m^2, respectively; (2) direct foaming technique using H_2O_2 provided pore sizes ranging between 100-1,000 μm, porosity ranging between 80-85%, compressive and flexural strengths ranging between 0.07-0.7 MPa and 0.1-1.1 MPa, respectively, and compressive and flexural stiffness ranging between 60-550 kN/m^2 and 2-75 MN/m^2, respectively; (3) combination technique using PMMA and H_2O_2 provided pore sizes ranging between 100-1,000 μm, porosity ranging between 82-90%, compressive and flexural strengths ranging between 0.03-0.5 MPa and 0.1-0.7 MPa, respectively, and compressive and flexural stiffness ranging between 13-440 KN/m^2 and 0.5-45 MN/m^2, respectively; (4) the combination technique provided the interconnected pores, while the sacrificial template and the direct foaming techniques performed the closed pores; (5) the sacrificial template technique was the best method to control the porosity; (6) Increasing PMMA content, H_2O_2 concentration and L/P ratio affected an increase of porosity and a decrease of mechanical strength; and (7) addition of surfactant was a significant effect on an increasing compressive strength of the porous samples prepared via direct foaming technique using H_2O_2, at 95% confident interval. At the H_2O_2 concentration between 5wt% and 20wt%, the compressive strength increased from approximately 0.29 to 0.46 MPa (increased about 60%).

Department....Industrial Engineering... Student's signature...................

Field of study...Industrial Engineering... Advisor's signature...................

Academic year...2010...

ACKNOWLEDGEMENTS

Firstly, I would like to sincerely thank my venerable advisor, Assistant Professor Dr. Somchai Puajindanetr, for his merciful support, encouragement and invaluable suggestions that enhance my knowledge, wisdom and experience.

I truly appreciate with my examination committees, Associate Professor Damrong Thawesaengskulthai, Associate Professor Dr. Parames Chutima, Chairman, Assistant Professor Dr. Seeronk Prichanont and Associate Professor Somchai Puangphuaksook, for their helpful comments and suggestions.

I would like to acknowledge the Commission of Higher Education, Ministry of Education, for scholarship and also thank Department of Industrial Engineering, Faculty of Engineering, Chulalongkorn University for all facilities throughout my Ph.D. program. Special thanks were also passed to faculties and staffs at the Department of Industrial Engineering. Without their supports, this dissertation would never be completed.

I would like to extend my appreciation to Professor Dr. Serena M. Best, Department of Material Science and Metallurgy, University of Cambridge, England, for inspiring the idea and giving the great opportunity and also thank all staffs and members of the CCMM group at the Department of Material Science and Metallurgy for their supports throughout the time I spent in Cambridge.

Finally, I dedicate this dissertation to my family. Without their endless love, encouragement and support, I would never come this far.

CONTENTS

LIST OF TABLES

LIST OF FIGURES

Figure   **Page**

Figure		**Page**

Figure   **Page**

ศูนย์วิทยทรัพยากร

จุฬาลงกรณ์มหาวิทยาลัย

CHAPTER I

INTRODUCTION

1.1 Background

From the advent of fire, ceramics have been developed to facilitate human life for many decades ago. The remarkable evolution of using ceramics is for the medical purposes, including repair, reconstruction and replacement of diseased or damaged parts of human organs. Ceramics used for this purpose are termed "*Bioceramics*" (Hench, 1998). According to an increasing demand of patients suffering from losing their organs, such ceramics have become an integral part of the modern health care system.

Recently, bioceramics have been developed for various uses in medical industry, for example implant devices for bone and joint surgery, prostheses for orbital implant, or carriers for drug delivery system. Furthermore, bioceramics are also used in dentistry, e.g. dental cements, tooth filler or tooth root. The prime example of bioceramics is hydroxyapatite, the most popular bioactive material utilized in medical application. Many studies focused on hydroxyapatite (HA) because of its identical chemical composition to human bone and its excellent biocompatibility with human tissue (Liu, 1997). There are some examples of clinical applications of HA, including orthopedic surgery, orbital implant, surgical application, dental application and drug delivery system.

Clinically, hydroxyapatite can be used in various forms, depending on the purpose of medical application, i.e. granules for bone filler, dense and porous block for artificial bone, composite for making artificial device or microcrystal for drug delivery carrier (Aoki, 1994), as well as thin layer for coating on metallic implant (Gibson, 2001).

Interestingly, porous HA favors more growth of cells and tissue than dense one due to the surface area of porous form greater than dense form. In addition, a rough surface of porous HA can improve the mechanical strength of the attachment between the implanted material and the surrounding tissue, providing a greater

mechanical stability at the critical interface. Moreover, interconnections are also necessary for a formation of new bone and tissue because they allow migration and proliferation of osteoblast, a type of bone cells, and vascularization (Lu *et al*, 1999). Additionally, pore size larger than 300 μm (Karageorgiou and Kaplan, 2005) and interconnected pore size larger than 50 μm (Flautre *et al*, 2001) are required to achieve this purpose. Therefore, porous HA with suitable size is an appropriate material for making devices or prostheses attached to the biological surrounding environment.

Generally, porous ceramics can be grouped into two general groups, including reticulate ceramics and foam ceramics. The former is composed of interconnected voids surrounding by a web of ceramic whereas the latter is comprised of closed voids within a continuous ceramic matrix (Li et al, 2003). Besides the structure, the sizes of pore are also classified, including micropores (<20 nm), mesopores (between 20 and 50 nm) and macropores (>50 nm). Consequently, the reticulate ceramic with macropores seems to be suitable to fulfill the requirement of tissue engineering.

Nevertheless, all porous materials have a common limitation that is the inherent lack of strength associated with porosity. So, their application tends to be limited to low-stress location. The porous HA is frequently used in low-load bearing applications. The outstanding example of low-load bearing application is the use of a porous hydroxyapatite eyeball in orbital implant. That is why a lot of commercial products are manufactured from natural materials which have an appropriate porous structure, e.g. Biocoral® is derived from natural coral and Endobon® is produced from bovine bone.

In fact, porous HA can be produced from both natural sources and completely synthetic routes. But, the use of porous HA derived from natural source, e.g. coralline HA, is restricted by the scarce resources, as well as a risk of contamination from remaining organic matters and undesirable minerals. Thus, HA derived from synthetic route has become an alternative for making porous material. For all above reasons, many attentions focus on how to fabricate a suitable porous structure.

Until now, numerous methods of making macroporous HA have been presented. In addition, the route to fabricate porous ceramics has been classified into three techniques, including replica technique, sacrificial template technique and direct

foaming technique (Studart *et al*, 2006). Replica technique is based on the replication of the morphological structure of the original template. Sacrificial template technique is found on the use of the template as a pore former. And direct foaming technique is ground on incorporating gaseous bubbles into ceramic suspension. The schemata of these techniques are shown in Figure 2.6 in chapter 2.

Although there are previous studies on fabrication of macroporous HA, they have mainly focused on using a single technique. For instance, replica techniques such as replamineform (White *et al*, 1975), hydrothermal (Roy, 1975; Hing *et al*, 1999; Xu *et al*, 2001) and impregnation (Tian *et al*, 2001); sacrificial template technique such as dual-phase mixing (Li *et al*, 2003) and starch consolidation (Rodriguez *et al*, 1998); and direct foaming technique such as foaming method (Almirall *et al*, 2004) and gelcasting (Sepulveda *et al*, 2000). Surprisingly, a few works focused on the fabrication of porous HA using a combination between replica and direct foaming techniques, e.g. a combination of PU impregnation and gelcasting (Padilla *et al*, 2002). Therefore, it seems there is no study focused on using a combination between sacrificial template and direct foaming techniques, which may be a new approach to producing porous HA scaffolds.

In this dissertation, the production process of porous HA was developed. HA powder used in this study was synthesized from an aqueous precipitation reaction between calcium hydroxide and orthophosphoric acid. Porous HA scaffold was prepared via direct foaming, sacrificial template and combination techniques. The key process parameters affecting on porosity and mechanical strength were also studied. The prepared HA powder and the resultant porous HA samples were characterized as well.

1.2 Objectives of Study

The objectives of this study are as follows,

1. To develop the production process of porous HA ceramics with controllable porosity.

2. To study key forming factors affecting on porosity and mechanical strength of porous HA scaffolds

1.3 Scopes of Study

The scopes of this study are as follows,

1. Synthesized hydroxyapatite derived from an aqueous precipitation reaction between calcium hydroxide and orthophosphoric acid will be used as a material for making the specimens in this dissertation.

2. Sacrificial template method, direct foaming method and combination technique between the both methods will be used for the fabrication of porous hydroxyapatite ceramics.

1.4 Expected Outcomes

Expected outcomes of this study were as follows,

1. Pure hydroxyapatite powder could be produced.

2. Porous hydroxyapatite scaffolds could be prepared using sacrificial template, direct foaming and combination methods.

3. Comparison between sacrificial template method and direct foaming method were studied.

4. Relationship between key process parameters affecting on porosity and mechanical properties of the porous samples were investigated.

CHAPTER II

LITERATURE REVIEWS

In this chapter, the previous studies of bioceramics, hydroxyapatite, porous bioceramics, fabrication methodologies of porous bioceramics, and heat treatment of bioceramics were reviewed.

2.1 Bioceramics

Many years ago, ceramics have been developed to improve the quality of human life. The considerable breakthrough is the innovative use of specially designed ceramics for the repair, reconstruction, and replacement of diseased or damaged parts of the body. Ceramics used for this purpose are termed "*Bioceramics*." Bioceramics can be polycrystalline, bioactive, or porous for tissue ingrowths (Hench, 1998). This particular ceramics has become an integral and vital segment of the modern health care delivery system.

2.1.1 Needs of Bioceramics

Bioceramics are needed to relieve pain and restore function to diseased or damaged parts of the body. A major contributor to the need for spare parts for the body is the progressive deterioration of tissue with age. Bone is especially vulnerable to fracture in older people because of a loss of bone density and strength with age.

Figure 2.1 showed the effect of age on bone strength and fracture probability from the age of 30 years onward. The bone strength decreases, but the fracture probability increases, with an increasing age. Particularly, the effect is severe in women because of hormonal changes associated with menopause. As a result, bone density decreases because bone-growing cells (osteoblast) become progressively less productive in making new bone and repairing micro-fractures. The lower density greatly deteriorates the strength of the porous bone, called *trabecular* or *cancellous bone*, in the ends of long bones and invertebrae. An unfortunate consequence is that

many old people possibly fracture their hips or have collapsed vertebrae and spinal problems.

The great challenge of using ceramics in the body is to replace original deteriorating bone with a material that can function the remaining years of the patient's life. According to the fact that the average longevity of human is now over 80 years and the need for body spare parts begins at around 60 years of age, bioceramics need to last for over 20 years. This demanding requirement of survivability is under conditions of use that are especially harsh to ceramic materials (e.g. corrosive saline solutions at 37°C under variable, multi-axial, and cyclical mechanical loads). So, the specially designed bioceramics can satisfy this requirement with the excellent performance.
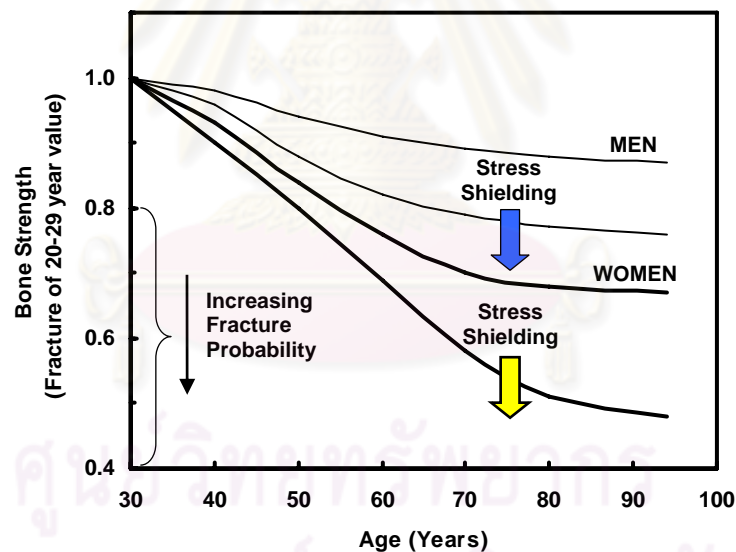
Figure 2.1   Effect of age on the strength of bone and probability of fracture
(Hench, 1998)

2.1.2 Classification of Bioceramics

To consider the classification of bioceramics, it is essential to recognize the level of survivability of bioceramics and bioreactivity of tissue attachment. Generally, bioceramics can be classified into 3 types, according to biological response of cells and tissues. There are (A) bioinert, (B) bioactive and (C) bioresorbable.

(A) Bioinert Ceramics

The term bioinert refers to any bioceramics once placed into the human body has biologically minimal interaction or inactive with its surrounding tissue, but promotes the formation of fibrous tissue. Their general function is to sustain high mechanical loads. For this role, they are used to realize parts in which the applied compressive load is very high. Consequently, they are particularly employed to produce joint parts of prostheses, such as the head of a hip joint or the plates of knee joint. The most utilized examples of such bioceramics are alumina (Al_2O_3) and zirconia (ZrO_2)

(B) Bioactive Ceramics

Unlike inert bioceramics, this type of bioceramics is the most favorable to medical application because it encourages the surrounding tissue. Generally, they are calcium phosphates. The prime example of these materials is hydroxyapatite (HA). Their function is generally to sustain repair or growth of bone; therefore, their main application is in the bone, where a mineral component is similar to that of hydroxyapatite.

Bioactivity is an interfacial response of the tissue toward material, which results at the end in a tissue bonding. The bioactivity of a material can be subdivided into (1) *osteoinduction* (the repair or growth of tissue due to the ions freed in the biological environment) and (2) *osteoconduction* (the process by which bone is directed to conform to the surface of the material).

(C) Bioresorbable Ceramics

Upon placement within the human body, bioresorbable (or biodegradable) ceramics starts to dissolve and be slowly replaced by the surrounding tissues. The examples of such ceramics are calcium phosphate salts, tri-calcium phosphate (TCP), calcium oxide (CaO), and calcium carbonate. Usually, bioresorbable ceramics have the high level of bioresorption (the process of removal of material for degradation exercised by the biological environment), whereas bioactive hydroxyapatite exhibits high biostability (the capacity of a material to resist changes in a biological environment) (Barbucci, 2002).

2.1.3 Calcium Phosphates Family

There are several forms of Calcium phosphate, forming a family of compounds called "*apatites.*" Apparently, the main inorganic components of bone and teeth are hydroxyapatite which has calcium and phosphate as the major constituents (Guelcher and Hollenger, 2006). However, the exact structure of biological apatites is not clear due to the numerous forms of their morphology and variation in non-stoichiometry. Therefore, the most convenient way to classify calcium phosphate compound is by groups of definite Ca/P atomic ratios. Table 2.1 presents several types of calcium phosphates categorized by sorting according to respective Ca/P atomic ratios.

Generally, various types of calcium phosphates, having different Ca/P ratios from 2.0 to 0.5, can be synthesized by mixing a calcium and phosphate ion solution under acid or alkaline conditions. The calcium phosphate compounds with high Ca/P ratios can be synthesized in alkaline environment, whilst those with low Ca/P ratios can be precipitated in acid solution. Hydroxyapatite can be produced in both neutral and alkaline condition. Usually, the stability of calcium phosphate in solution increases with increasing Ca/P ratios. Interestingly, hydroxyapatite is the most popular material among its family since it is found in natural hard tissues as mineral phase.

Table 2.1   Various calcium phosphate with their respective Ca/P atomic ratios
(Adapted from Aoki: 6, 1994)

Name	Abbreviation	Chemical Formula	Ca/P
Tetracalcium phosphate monoxide (Hilgenstockite)	TCPM (TTCP/TetCP)	$Ca_4O(PO_4)_2$	2.00
Hydroxyapatite	HA	$Ca_{10}(PO_4)_6(OH)_2$	1.67
Amorphous calcium phosphate	ACP	$Ca_x(PO4)_y$	
Tricalcium phosphate	TCP		
Alpha tricalcium phosphate	α-TCP	$Ca_3(PO_4)_2$	1.50
Beta tricalcium phosphate (whitlockite)	β-TCP	$Ca_3P_2O_8$	1.50
Octacalcium phosphate	OCP	$Ca_8H_2(PO_4)_6.5H_2O$	1.33
Dicalcium phosphate dehydrate (Brushite)	DCPD	$CaHPO_4.2H_2O$	1.00
Dicalcium phosphate anhydrous (Monetite)	DCPA	$CaHPO_4$	1.00
Calcium pyrophosphate	CPP	$Ca_2P_2O_7$	1.00
Calcium pyrophosphate dihydrate	CPPD	$Ca_2P_2O_7.H_2O$	1.00
Heptacalcium phosphate (Tromelite)	HCP	$Ca_7(P_5O_{16})_2$	0.70
Tetracalcium dihydrogen phosphate	TDHP	$Ca_4H_2P_6O_{20}$	0.67
Monocalcium phosphate monohydrate	MCPM	$Ca(H_2PO_4)_2.H_2O$	0.50
Monocalcium phosphate anhydrous	MCPA	$Ca(H_2PO_4)_2$	0.50

2.1.4 Coralline

Coral is a natural substance made by marine invertebrate which has a unique interconnected porous structure. Clinically, corals for use as bone implants were selected mainly on the basis of their structural similarity to bone. It provides an excellent structure for the ingrowth of cells and hard tissue (bone), and the main component is gradually degraded by the body.

Chemically, the main constituent of coral is calcium carbonate, $CaCO_3$, (or Aragonite). In 1975, Roy patented the first hydrothermal method to convert carbonate life forms to HA. Recently, Guelcher and Hollenger (2006) also converted corals to HA by a hydrothermal ion exchange process. Additionally, Hu *et al.* (2001) and Xu *et al.* (2001) also reported that corals genus '*Goniopora*' and '*Porites*' can be used as

original materials because of its inimitable microstructure and favourable strength. For example, Interpore-200 and Biocoral are commercial names of the coralline HA which resembles cancellous bone. Currently, both pure coral and coralline HA derived from coral are utilized to repair damaged bone, to replace diseased bone and to reconstruct a number of bone defects.

Figure 2.2 exhibited the microstructure of the pure coral (Biocoral) which is composed of crystalline calcium carbonate or aragonite and that of human cancellous bone. The compressive strength of the pure coral varies from 26 MPa (50% porosity) to 395 MPa (dense) depending on the porosity. Similarly, the elastic modulus ranges from 8 (50% porous) to 100 GPa (dense).

(a) Pure coral   (b) Human cancellous bone
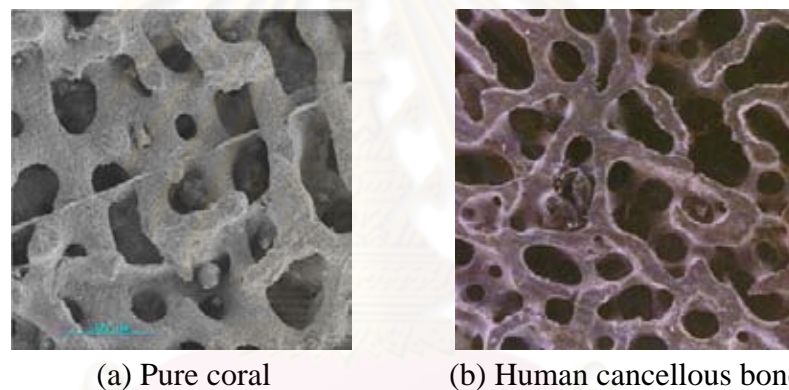
Figure 2.2 The microstructure of the section of (a) Biocoral at 50% porosity and (b) the section of human cancellous bone (from http://www.biocoral.com)

2.1.5 Human Bone

Bone is a composite material, consisting of approximately 10% water, 20% organic material, and 70% mineral matter, by weight. The organic component is mainly composed of collagen fibrils. The remainder of the organic material is made up of other proteins, a cement-like substance, and a cellular component, comprised of (1) *Osteoblasts*, (2) *Osteocytes*, and (3) *Osteoclasts*, which aid in dissolution, deposition, and nourishment of the bone. The inorganic, mineral component is a calcium-deficient carbonate-substituted apatite containing calcium and phosphate ions, similar in structure and composition to Hydroxyapatite ($Ca_{10}(PO_4)_6(OH)_2$) (White *et al*, 2007).

There are several types of cells constituting the bone, including

(1) Osteoblasts:

Osteoblasts are mononucleate bone-forming cells which descend from osteoprogenitor cells. They are located on the surface of osteoid seams and make a protein mixture known as '*Osteoid*', which mineralizes to become bone. Osteoid is primarily composed of type I collagen. Osteoblasts also manufacture hormones, such as *prostaglandins*, to act on the bone itself. They robustly produce alkaline *phosphatase*, an enzyme that has a role in the mineralization of bone, as well as many matrix proteins. Osteoblasts are the immature bone cells.

(2) Osteocytes:

Osteocytes originate from osteoblasts which have migrated into and become trapped and surrounded by bone matrix which they themselves produce. The spaces which they occupy are known as lacunae. Osteocytes have many processes which reach out to meet osteoblasts and other osteocytes probably for the purposes of communication. Their functions include to varying degrees: formation of bone, matrix maintenance and calcium homeostasis. They have also been shown to act as mechano-sensory receptors, regulating the bone's response to stress and mechanical load. They are mature bone cells.

(3) Osteoclasts:

Osteoclasts are the cells responsible for bone resorption (remodeling of bone to reduce its volume). Osteoclasts are large, multinucleated cells located on bone surfaces in what are called *Howship's lacunae* or resorption pits. These lacunae, or resorption pits, are left behind after the breakdown of bone and often present as scalloped surfaces. Because the osteoclasts are derived from a monocyte stem-cell lineage, they are equipped with engulfment strategies similar to circulating macrophages. Osteoclasts mature and/or migrate to discrete bone surfaces. Upon arrival, active enzymes, such as tartrate resistant acid phosphatase, are secreted against the mineral substrate.

Figure 2.3 showed the hierarchical structure of bone. Hydroxyapatite micro crystals are arranged between the ends of collagen fibrils, which are then arranged into sheets called '*lamellae*.' The morphology of the hydroxyapatite microcrystals is generally agreed to be plate like with dimensions on the scale of 10-100s of angstroms. The collagen lamellae are either arranged in concentric circles, called '*Tubular Haversian Systems*,' or in sheets. These sheets form the spongy, cancellous bone (or trabecular bone) found inside the structure and at bone ends. The Haversian system configuration, on the other hand, leads to the dense, *cortical bone*, which comprises 80% of bone mass and surrounds the cancellous bone.
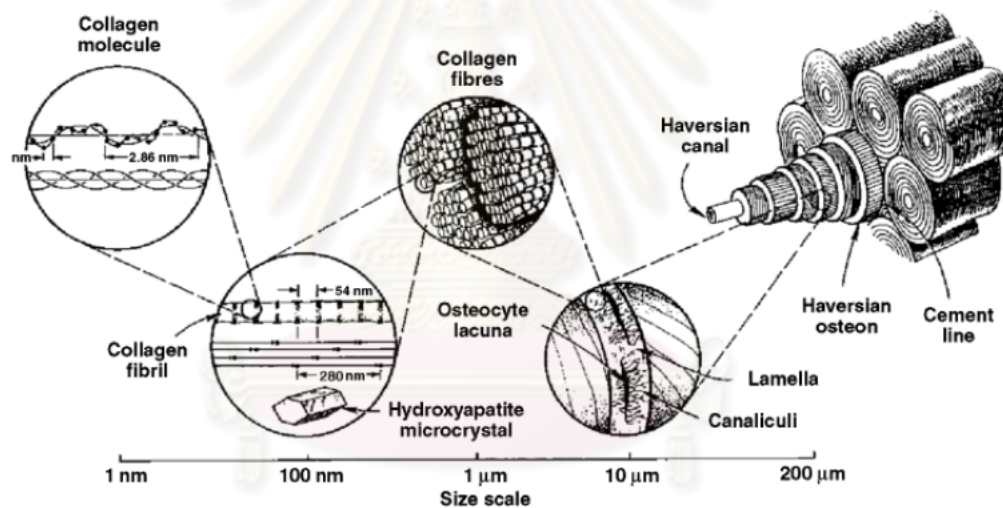
Figure 2.3   The hierarchical structure of bone (White *et al.*, 2007)

2.2 Hydroxyapatite

Hydroxyapatite (HA) has been extensively utilized as raw materials for the application in the biomedical fields. HA has become the most attractive bioceramics due to its chemically identical to human bone and its biocompatibility.

2.2.1 Crystal Structure of Hydroxyapatite

Hydroxyapatite is the one of calcium phosphate's family with hydroxide ion and has the main chemical component of tooth and bone minerals. Table 2.2 summarized the crystal data of HA. Its chemical formula is $Ca_{10}(PO_4)_6(OH)_2$. Chemically, hydroxyapatite has the molecular weight of 1004.8 g/mol, the Ca/P atomic ratio of 1.67 and the lattice parameters of a = 9.42148 Å, b = 2a and c = 6.81447 Å (Guelcher and Hollenger, 2006).

Table 2.2   The crystal data of hydroxyapatite (Aoki: 3, 1994)

Crystal data	Details
Chemical formula	$Ca_{10}(PO_4)_6(OH)_2$
Molecular weight (g/mol)	1004.8
Crystal system	Hexagonal
Ca/P atomic ratio	1.67
Lattice constants (Å)	a = 9.423, c = 6.875
Chemical unit number	Z = 1

Figure 2.4 illustrated the crystal structure of hydroxyapatite. The crystal structure of HA is hexagonal. There are two crystallographically Ca atoms in the unit cell. The former is surrounded by six O atoms belonging to PO_4 groups and OH groups, whereas the latter is nearly surrounded by six O atoms. Apparently, the chemical component and crystal structure of HA are also similar to those of the mineral component of human bone, are the most important factors to its in bioactivity.
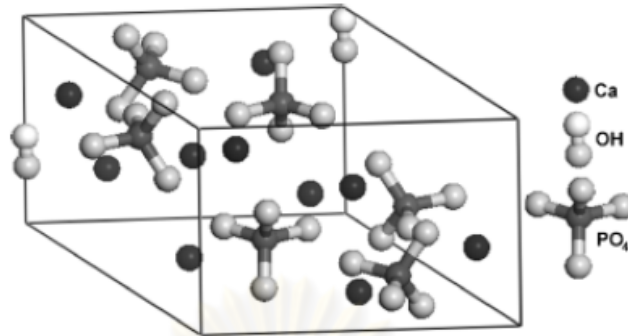
Figure 2.4   Crystal structure of hydroxyapatite (White *el al.*, 2007)

2.2.2 Properties of Hydroxyapatite

Admittedly, the synthesis parameters, forming method and exactly stoichiometry will have a direct effect on the properties of synthesized hydroxyapatite. In this section, solubility, biological and mechanical properties of HA were discussed.

(A) Solubility

Hydroxyapatite is soluble in an acidic solution, while insoluble in an alkaline solution, and slightly soluble in water. In 1999, Paul and Sharma reported that the solubility of calcium phosphate increased in the following phase sequence: HA, β-TCP and α-TCP. Hamdi and Ide-Ektessabi (2007) also summarized that the solubility of HA was mainly dependent on many factors, such as the amount of electrolyte in solution, the condition of pressure, temperature and pH level, as well as chemical composition, morphology, particle size, porosity, density, crystal size and crystallinity of HA particles.

In deionized water, Zhang *et al*. (2001) found that HA had a higher dissolubility under the hydrothermal condition than under normal pressure and temperature as well as the solubility of HA decreased with the increasing pH value. Moreover, Sun *et al*. (2006) confirmed that the difference in surface density and crystallinity of HA had an effect on its solubility rate. Aoki (205-225; 1994) indicated that the solubility of HA was strongly related to biocompatibility with tissues and chemical reaction.

In the Ringer's solution, Kwon *et al.* (2003) reported that TCP showed a higher dissolution rate than HA-TCP composite, exhibiting an intermediate dissolution behavior between that of HA and TCP.

(B) Biological Properties

Among the various properties of HA, the most interesting properties is its excellent biocompatibility. Indeed, it appears to form a direct chemical bond with hard tissues when HA is implanted into the environment of such tissues, since the composition and crystal structure of HA are similar to that of the mineral component of bone. There are four factors, reviewed by White *et al.* (2007), having an influence on cellular response: including (1) Ca/P ratio (phase purity), (2) trace element impurities, (3) ceramic handling properties, and (4) sintering characteristics.

Particularly, the bioactivity of the ceramic is very sensitive to the Ca/P ratio. Synthesis conditions, such as pH and reaction rate, and sintering parameters can affect the Ca/P ratio. Stoichiometric HA has a Ca/P ratio of 1.67 and is classified as bioactive ceramic, forming a stable bond of carbonated apatite at the HA/bone interface through a process of dissolution, precipitation, and ion exchange. In vivo studies have confirmed this bond, showing that failure typically occurs in the bone or HA, but not at the HA/bone interface.

Synthetic materials pose their own set of challenges. Hench (1998) identified two key components to the clinical success of a biomaterial: (1) it must be able to form a stable interface with the surrounding tissue and (2) it must functionally match the mechanical behavior of the tissue to be replaced.

(C) Mechanical Properties

While HA has excellent bioactivity, its poor mechanical properties compared with bone have hindered its use in clinical applications. Table 2.3 summarized the mechanical properties of hydroxyapatite in various forms. White *et al.* (2007) reported that dense HA had a compressive strength four times that of cortical bone, and yet a significantly lower tensile strength and fracture toughness. However, it must be noted that even among studies of dense, single-phase HA, the values reported for mechanical properties vary widely due to differences in the preparation process and

the measurement techniques. As well as the final firing conditions can be resulted in the phase transition between HA and TCP. Even with this consideration, HA does not match the mechanical behavior of natural bone and thus can not be used in major load-bearing applications in its present form.

Table 2.3   Reviews of mechanical properties of hydroxyapatite in various forms

Materials	Authors (Year)	Compressive strength (MPa)	Flexural/tensile strength (MPa)	Elastic Modulus (GPa)	Fracture toughness (MPa.m$^{1/2}$)
Cortical bone	White *et al* (2007)	100-230	50-150	n/a	2-12
Cancellous bone	White *et al* (2007)	2-12	10-20	n/a	n/a
Dense HA	Kothapalli *et al* (2004)	n/a	57.4	n/a	n/a
Dense HA	White *et al* (2007)	430-920	17-110	n/a	1
Dense HA	Park and Lakes (2007)	294	147	40-117	n/a
Dense HA	He *et al* (2008)	n/a	n/a	13.86	n/a

Note: n/a = No data available

Table 2.4 listed the physical properties of synthetic hydroxyapatite. Park and Lakes (2007) reported that the synthetic HA had the elastic modulus ranging between 40 and 117 GPa, the compressive strength of around 294 MPa and bending strength of approximately 147 MPa. The hardness in Vickers' scale of the synthetic HA was 3.43. Poisson's ratio for the mineral or synthetic HA was about 0.27, which is close to that of bone (around 0.3). Furthermore, the theoretical density of synthetic HA was 3.156 g/cm^3.

Table 2.4   Physical properties of synthetic hydroxyapatite
             (Park and Lakes: 153, 2007)

Properties	values
Elastic Modulus (GPa)	40-117
Compressive Strength (MPa)	294
Bending Strength (MPa)	147
Hardness (Vickers, GPa)	3.43
Poisson's ratio	0.27
Theoretical Density (g/cm^3)	3.156

2.2.3 Medical Application of Hydroxyapatite

Hydroxyapatite has been widely used in medical applications due to its identical chemical composition and high biocompatibility with human bones. Table 2.5 summarized the medical applications of hydroxyapatite in many forms. HA has been synthesized and used for manufacturing various forms of implants as well as for solid or porous coating on other implants. In this section, various medical applications of hydroxyapatite were reviewed.

Table 2.5   Medical applications of hydroxyapatite in many forms
(Adapted from Table 5-1, Aoki: 90, 1994)

Applications	Forms of Hydroxyapatite					
	Dense	Porous	Granule	Micro-crystal	Coating	Composite
Orthopedic Applications						
- Artificial bone	✓	✓				
- Artificial joint	✓	✓			✓	
- Bone fillers		✓	✓			
- Bone formation promoter				✓		
Orbital implant		✓				
Surgical Applications						
- Artificial Blood Vessel	✓					✓
- Artificial Heart Valve	✓					✓
- Artificial Trachea	✓					✓
Dental application						
- Toothpaste			✓			
- Dental cement						✓
- Bone fillers	✓	✓				
- Tooth root	✓				✓	
Drug Delivery Carrier		✓		✓		

(A) Orthopedic Applications

Orthopedic applications of hydroxyapatite reported by White *et al*. (2007); including bone grafts, autografts and allografts, bone filler, as well as artificial bones and joints, are already being utilized clinically worldwide. When bone defect occur due to diseases or accidents, bone grafts are introduced to perform both a mechanical and biological role, serving to restore skeletal integrity, fill voids, and enhance bone repair.

Murugan and Ramakrishna (2005) indicated that HA is an appropriate material for bone grafting due to its bioactivity, osteoconductivity and crystallographic structure similar to bone mineral. Dense and porous HA are also used to produce

artificial bone. Autografts involve a second incision to harvest the replacement tissue from another area of the patient's own body. This requires additional healing at the donation site and can involve long-term postoperative pain. Allografts, as they come from a foreign body, carry with them the risk of viral infection, immune system rejection, and resorption due to immunological responses.

The potential advantage offered by a porous bioceramic implant is the mechanical stability of the highly convoluted interface developed when bone grows into the pores of the ceramics. There are two primary clinical applications of porous ceramics, including bone filler and joint replacement. For Bone fillers, HA granules or porous bodies can be used as prostheses for bone repair in non-load bearing location. Bone formation promoter is made of microcrystal HA.

For joint replacement, hydroxyapatite has been used as a coating material on metal and alloy (e.g. stainless steel or titanium alloy) in order to prevent loosening and corrosion of using uncoated metals and alloys. There are many artificial joint, including hip, knee, shoulder, finger and other joints.

(B) Orbital Implants

Lloyd *et al.* (2001) indicated that orbital implant is needed due to the fact that removal of the globe or its internal contents requires the insertion of a solid implant to maintain the orbital volume. To repair these, artificial eye ball are implanted into eye socket. Recently, porous ocular implants made of Hydroxyapatite are widely accepted for reconstruction of the artificial eyes after surgery. Porous HA capable of sustaining fibrovascular growth are termed as integrated implants. Porous implants have an advantage of becoming infiltrated by fibrovascular tissue, thereby providing resistance to infection, migration and extrusion (Kundu *et al*, 2004).

Porous HA for orbital implant can be produced from natural sources or synthetic materials. From natural source, it seems coral is a perfect precursor for making eye ball due to its unique cellular structure and mechanical strength. Many methods of using coral as original templates are proposed by White et al (1975), Roy (1975) and Xu *et al* (2001). In addition to natural sources, porous HA eye ball can be synthetically produced through various methods, such as replica methods, sacrificial template or direct foaming method. The details will be given in the other section.

(C) Surgical Applications

In surgical field, artificial blood vessels, heart valve, trachea and urea tubes made of sintered hydroxyapatite have been developed. Recently, all available artificial bold vessels are made of polymer materials because of their softness and flexibility. A vascular access tube, developed by Aoki and his colleagues, are made of sintered HA.

The trachea is an important part of respiratory system. Since HA is known as the best materials among others, a sintered HA tube was applied for making the artificial trachea in combination with yttrium aluminum YAG laser irradiation.

(D) Dental Applications

In dental applications, many types of dental materials based on hydroxyapatite have been developed, including toothpaste, dental cement, root canal, tooth and bone fillers, and tooth root. Some toothpaste had included hydroxyapatite fine powder in order to improve properties in preventing caries (decay in teeth) and pyorrhea (disease from infected gum).

Generally, dental cements must be nontoxic and demonstrate great bonding to teeth and artificial teeth as well as possess outstanding mechanical and chemical properties. Furthermore these cements must have suitable properties to resist against saliva. To fulfill this requirement, HA and polyacrylic acid copolymer are used as dental cement. For bone reconstruction, granules and porous bodies of HA have been recently used. Additionally, tooth root can be made of sintered HA or HA coated titanium, depending on implant location. Hydroxyapatite has been also used for coatings on metallic pins and to fill large bone voids resulting from disease or trauma.

(E) Drug Delivery Systems

Friefs and Warner (2002) noted that porous HA has been extensively used as scaffolds for controlled drug delivery system. In cases of chronic disease or localized surgical intervention, in which a sustained local drug delivery becomes important, such porous HA blocks have been utilized as local drug delivery systems, allowing slow release of antibiotic substances. Additionally, drug delivery carriers made of hydroxyapatite microcrystals have been developed (Aoki: 104-106, 1994).

2.2.4 Synthesis of Hydroxyapatite

Recently, various methods of synthesizing hydroxyapatite have been reported. Generally, there are three main techniques to synthesize HA, including (1) wet chemical process such as precipitation, hydrothermal and hydrolysis method; (2) solid-state reaction process such as mechanochemical synthesis; and (3) solvent evaporation process such as sol-gel method. In this section, the synthesis methodologies based on these techniques are reviewed. Additionally, the other techniques such as biomimetic and electrochemical deposition are also referred.

(A) Wet Chemical Precipitation

The precipitation method is the most commonly used techniques for synthesis of hydroxyapatite due to its convenient and effective process. This method is suitable for mass production of small crystalline or non-crystalline hydroxyapatite powders. There are typically two kinds of process in the precipitation method (Aoki: 176, 1994). The former is a process involving a neutral reaction of acid and alkaline solution, as shown in Equation 2.1. The latter involves the reaction of calcium salts and phosphate salts, such as the chemical reactions shown in Equation 2.2 and 2.3.

$$10Ca(OH)_2 + 6H_3PO_4 \rightarrow Ca_{10}(PO_4)_6(OH)_2 + 18H_2O \tag{2.1}$$

$$10Ca(NO_3)_2 + 6(NH_4)_2HPO_4 + 8NH_4OH \rightarrow Ca_{10}(PO_4)_6(OH)_2 + 20NH_4NO_3 + 6H_2O \tag{2.2}$$

$$10CaCl_2 + 6(NH_4)_2HPO_4 + 2H_2O \rightarrow Ca_{10}(PO_4)_6(OH)_2 + 12NH_4Cl + 8HCl \tag{2.3}$$
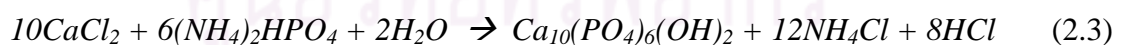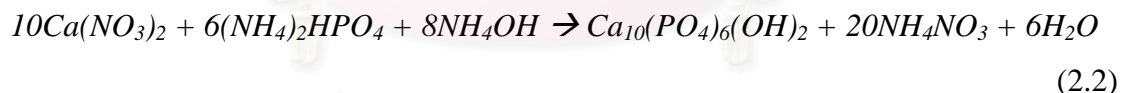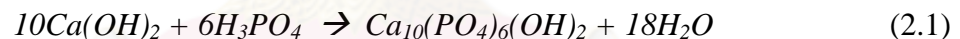
As mentioned, the first process of this method is the reaction between calcium hydroxide suspension and orthophosphoric acid with initial Ca/P molar ratio of 1.67. The resulting product is hydroxyapatite and the only by-product is water, whereas the latter (equation 2.2 and 2.3) results the undesirable by-products.

In addition, Kweh *et al* (1999) studied on the production of HA through two precipitation reactions (Equation 2.1 and 2.2). They reported that the disadvantage of equation 2.3 is that the purity of the precipitated HA powder is affected by the purity of the calcium nitrate and the excess ammonia and ammonium by-products must be

removed by extensive washing. In contrast to equation 2.2, the reaction in equation 2.1 is a more convenient process and suitable for the industrial production of HA.

Although Kweh and colleagues (1999) referred that using ammonium solution is no need for the synthesis through equation 2.1, many researchers, in practice, used ammonium solution to maintain pH level of the reaction (Liu, 1997; Yeong *et al*, 1999; Gibson *et al*, 2001; Patel *et al*, 2001). The addition of ammonium solution into the reaction between $Ca(OH)_2$ and H_3PO_4 is necessary because orthophosphoric acid dissociates well in environment of high pH level (generally pH over 10.5), resulting in completed reaction. So, it seems washing excess ammonia by-product is still an indispensable process.

Besides adding ammonium solution, some previous works applied heat in the synthesis of HA through equation 2.1, resulting in nano-crystalline HA (Lazic *et al*, 2001; Afshar *et al*, 2003; Saeri *et al*, 2003). Some researches synthesized HA at $90^{o}C$ to gain polycrystalline HA (Bouyer *et al*, 2000; Padilla *et al*, 2002).

Moreover, heating during the reaction in Equation 2.2 was carried out by Tas *et al*. (1997); Kivrak and Tas (1998); and Kothapalli *et al*. (2004). Also, use of heat during the reaction in Equation 2.3 was conducted by Pang and Bao (2003). The heat was used for improving the crystallinity and crystal size of HA crystals. The effect of temperature on synthesis of HA will be discussed in section 2.2.5.

(B) Hydrothermal Reaction

The hydrothermal method is one of the most mentioned techniques for preparing hydroxyapatite powders and other forms; however, this techniques seem to have complicated and time-consuming process. This method involves converting the calcium carbonate into the calcium phosphate under conditions of high temperature and pressure. Moreover, this method can be employed either organic or inorganic as the source of calcium phosphate.

The hydrothermal method was firstly introduced by Roy in 1975. Roy patented the process for hydroxyapatite converting directly from natural carbonate skeleton of marine life; such as echinoderm and coral. It was informed that the complete replacement of aragonite ($CaCO_3$) by phosphatic material was achieved by using the hydrothermal process. In 1996, hydroxyapatite derived from Indian coral,

genus "*Goniopora*", using hydrothermal process was reported by Siva-Kumar and co-workers. This method involves reacting a mixture of calcium carbonate ($CaCO_3$) and di-ammonium hydrogen phosphate (($NH_4)_2HPO_4$), as Equation 2.4. The resultant material of this method is known as coralline hydroxyapatite, whether in the porous structure or in the powdered form. Instead of coral, other invertebrate marine life is eligible to be used as calcium templates. For example, cuttlefish and seashells were utilized as calcium source by Rocha *et al* (2005) and Zhang and Vecchio (2006) respectively.

$$10CaCO_3 + 6(NH_4)_2HPO_4 + 2H_2O \rightarrow Ca_{10}(PO_4)_6(OH)_2 + 6(NH_4)_2CO_3 + 4H_2CO_3$$

$$(2.4)$$
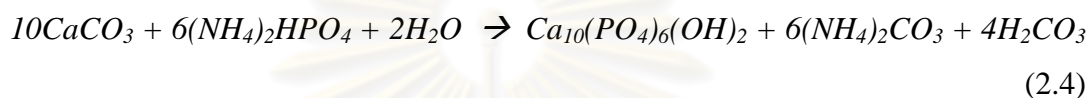
In addition to the marine life, bovine bone was also used as the calcium source materials. In 2002, Jinawath and colleagues presented the process of the hydrothermal synthesis of hydroxyapatite from di-calcium phosphate di-hydrate ($CaHPO_4.2H_2O$, DCPD or brushite) and anhydrous di-calcium phosphate ($CaHPO_4$, DCPA) powders, extracted from the by-product in the manufacture of gelatin from bovine bone.

(C) Hydrolysis Reaction

Hydrolysis reaction is the process in which a molecule is split into two parts by reacting with a molecule of water. In 1996, Graham and Brown studied on the hydrolysis reaction of octacalcium phosphate (OCP) with tetra-calcium phosphate (TetCP) or calcium hydroxide to form Stoichiometric HA. They indicated that the rate of OCP hydrolysis to HA was reduced when calcium hydroxide was present. In 2004, Shih, Chen and others investigated on the nanosized hydroxyapatite powders synthesized from DCPD and Calcium carbonate by hydrolysis method in which crystallinity of HA is improved with increasing annealing temperature. Afterwards, Shih, Wang and coworkers (2006) studied on the phase transformation of HA synthesized by the previous method and reported that HA was crystallized at 600°C and maintained as the major phase until 1400°C. At 1500°C, the HA steadily transformed to the α-TCP.

In addition to the synthesis of HA particles, the hydrolysis synthesis of HA whiskers was also studied. Yoon and colleagues (2005) synthesized HA whiskers by a

hydrolysis reaction of α-TCP at 70°C for 15 hours, using microwave heating. At this condition, HA whiskers with a nearly complete conversion of α-TCP to HA were obtained.

(D) Mechanochemical Synthesis

Mechanochemical method involves reacting powder mixtures of suitable composition by the use of grinding media. Usually, DCPA or DCPD and calcium compound are used as starting materials for preparation of hydroxyapatite, with ball milling under low temperature. In 1991, Brown and Fulmer used DCPA and tetra-calcium phosphate ($Ca_4(PO_4)_2O$) as reactants and ball milled in anhydrous ethanol followed by drying at 80°C, as in Equation 2.5. Additionally, Yeong *et al* (2001) used DCPD and calcium oxide (CaO) as the starting materials, as in Equation 2.6. This reaction provides the product of HA with the by-product of water in form of moisture.

$$2CaHPO_4 + 2Ca_4(PO_4)_2O \rightarrow Ca_{10}(PO_4)_6(OH)_2 \tag{2.5}$$

$$6CaHPO_4.2H_2O + 4CaO \rightarrow Ca_{10}(PO_4)_6(OH)_2 + 14H_2O \tag{2.6}$$
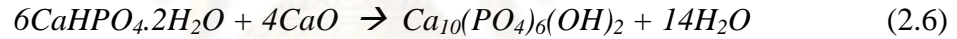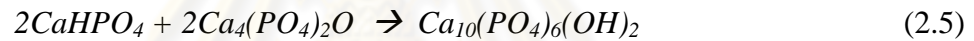
(E) Sol-gel Method

The sol-gel process involves the transition of a system from colloid in a suspension (the sol) into a solid (the gel) phase. This method is favorable for preparing hydroxyapatite thin film. Many researchers focus on the synthesis process of HA with different starting materials. In 1998, Layrolle and others used calcium di-ethoxide ($Ca(OEt)_2$) and phosphoric acid (H_3PO_4) as starting materials in order to synthesize amorphous calcium phosphate, afterwards sintered into pure hydroxyapatite.

In 2001, Hsieh and co-workers studied the conversion of hydroxyapatite synthesis from gel to ceramic using solid-state nuclear magnetic resonance (NMR) spectroscopy and X-ray diffraction. Calcium nitrate tetra-hydrate ($Ca(NO_3)_2.4H_2O$) and tri-ethyl phosphate (($C_2H_6O)_3PO$) was mixed in 2-methoxy ethanol. They indicated that indicated that the existence of a CaO impurity might affect OH─O=PO$_3$ linkages in a HA unit cell and result in longer P spin-lattice time.

Subsequently, Hsieh *et al* (2002) investigated the formation mechanisms of sol-gel-derived HA using different thermal processings, a Rapid-Thermal-Calcination (RTC) heating at 100–600°C/min and a Conventional-Furnace-Calcination (CFC) heating at 1.67°C/min. It indicated that RTC can quickly remove organic portion of the gel networks, leading to a porous surface morphology and a collapse of gel networks at local areas, On the other hand, slow evolution of organics during CFC leads to carbonaceous residues that isolate the inorganic species and inhibit nucleation of HA crystallites until at a higher temperature.

In 2003, Bose and Saha studied on synthesis of hydroxyapatite nanopowders via sucrose-template sol-gel method. Using sucrose as a gelling agent, nanocrystalline HA was synthesized using a sol-gel method from an aqueous solution of calcium nitrate tetra-hydrate and ammonium hydrogen phosphate ($(NH_4)_2HPO_4$). Furthermore Bezzi and others (2003) proposed the simply sol-gel method using etilen-diammine-tetraacetic acid (EDTA) and urea as gelling and ammonium donor agent.

Many reports indicated that sol-gel processes require a strict pH control, vigorous agitation and a long time for processing. However, Wang *et al* (2005) proposed a simple sol-gel method, which did not require controlling pH value and vigorously stirring, for preparing HA nanopowders from calcium nitrate tetra-hydrate and phosphoric pentoxide (P_2O_5) dissolved in ethanol without controlling pH value, vigorously stirring, and long time process. The result shows that crystalline degree and morphology of HA powder are dependent on sintering temperature and aging time.

(F) Other Techniques

In addition to the previous mentioned common methods, hydroxyapatite can be synthesized by other techniques. However, these techniques are applied for a specific purpose and can produce only a small quantity and different characteristic of HA. Two most referred techniques are electrochemical deposition and biomimetic.

The electrochemical deposition is a technique used for coating apatite on metal substrates, e.g. titanium. From previous studies, there were many key factors on this technique, such as composition of electrolyte, temperature of electrolyte, current loading time, current density and composition of substrate. Ban and Hasegawa (2002)

developed a novel method for coating hydroxyapatite on pure titanium plates with different condition, namely hydrothermal-electrochemical coating method, and found that the size of needle-like apatites remarkably increased with the electrolyte temperature and current loading time, and slightly changed with current density. Nevertheless, previous studies on electrochemical processes were conducted at elevated temperature. Kuo and Yen (2002) studied the electrochemical process of HA coating on titanium at room temperature. They indicated that coatings deposited at room temperature exhibited stronger adhesion than those at elevated temperature.

The biomimetic strategy is based on the principle that nucleation and growth of inorganic crystals in biological environments occur in the presence of biological macromolecules. The synthesis of HA is taken place in simulated body fluid (SBF), containing ion concentration nearly equal to those of human blood plasma. By adapting this technique, Tas (2000) presented the synthesis process of hydroxyapatite from calcium nitrate tetra-hydrate and di-ammonium hydrogen phosphate in SBF rather than in pure water. Boanini and Bigi (2006) studied on synthesis of carbonated hydroxyapatite thin films, deposited on a stearic acid monolayer template at room temperature. They indicated that the stoichiometry of the solution can modulate carbonate content, Ca/P molar ratio, crystallinity, morphology and thermal stability of the deposited film. In addition, Hutchens *et al* (2006) investigated the biomimetic synthesis of calcium-deficient hydroxyapatite (CdHA) deposited in a bacterial cellulose (BC) hydrogel. The SEM results showed that ~1 μm CdHA spherical clusters composed of nano-sized crystallites had formed within the BC network.

2.2.5 Synthesis Parameters Affecting on the Properties of HA

Even numerous synthesis methodologies for preparing synthetic HA are available; the most common method is precipitation reaction still be popular due to its convenient and economical process. Many research indicated that the synthesis parameters have an influence on the characteristic and properties of the resultant HA. Kweh *et al*. (1999) indicated the significant parameters affecting on the overall characteristic of the HA; including reaction temperature, mixing rate (i.e. addition rate of acid), concentration of reactant, pH level and residence time.

This section focused mainly on the synthesis parameters of HA through an aqueous precipitation reaction between calcium hydroxide and orthophosphoric acid, which was the most popular method and probably used in this study.

(A) Reaction Temperature

Reaction temperature is a basic parameter affecting on HA crystal. Recently, many studies have been reported that the reaction temperature has an effect on the stoichiometry (phase purity), morphology, specific surface area, size and crystallinity of HA crystal, as well as rheology and thermal stability of precipitated powder.

From crystallography study of Tampieri *et al*. (2000), the size and crystallinity of the crystals increased with an increase of the preparation temperature. By controlling the reaction temperature between $35^{o}C$ and $95^{o}C$, it is possible to vary the degree of crystallinity of the HA product approximately from 20 to 60%. Lazic *et al.* (2001) reported that HA precipitated at low temperature following an appropriated maturation showed the properties of stoichiometric low crystalline HA and appeared to be very promising as a bioceramic precursor. Contrary to previous study of Bouyer *et al*. (2000), the specific surface area (SSA) of HA particles decreased with an increase of the reaction temperature.

In morphological study, Bouyer and co-workers (2000) discovered that reaction temperature also had a sensitive effect on morphology (shape and size) of HA nanoparticles. Moreover the particles of HA synthesized at low temperature ($<60^{o}C$) was monocrystalline. At low synthesis temperature, the crystals carried a needle shape corresponding to the c-axis of the HA structure. At higher synthesis temperature, nanocrystals seemed to loose the tendency to grow as a monocrystal following the c-axis of the apatite structure. So, increasing the reaction temperature changed the crystal from as-needle shape to a more regular shape close to circular.

For ceramic suspension, the ideal property is good flowability, namely a low viscosity allowing the suspension to be readily pumped by a peristaltic pump. In rheological study, viscosity seems to increase with the synthesis temperature, but the viscosity decreases with an increase of shear rate.

As well as above, the effect on thermal stability has been studied by Lazic *et al*. (2001). HA precipitated at 95°C showed thermal stability even without ripening. Nearly theoretical values for lattice parameters were obtained for the sample precipitated and matured at 95°C, whilst HA precipitated at low temperature after appropriated maturation offered thermally stable composition. Importantly, the thermal stable of HA increased with a decreasing precipitation temperature during maturation stage.

(B) Mixing Rate

In 2000, the same study of Bouyer and co-workers also indicated that the Mixing rate (or addition rate) of orthophosphoric acid into the suspension of calcium hydroxide had an effect on morphology, phase, SSA and rheology. The shape, size and specific surface area of HA nanoparticles were very sensitive to the reactant addition rate. For low addition rate of acid the particles have an as-needle shape and for very high addition rates the particles had an elongated shape with a very small diameter like fiber. The HA particles synthesized at high acid addition rate contained some residual and unreacted calcium hydroxide. Consequently, the acid addition rate seemed to give opposite effects on the SSA of HA particle, increasing the acid addition rate leads to SSA increase.

For phase purity of synthesized HA, a high addition rate of phosphoric acid or in excess could lead to the formation of calcium deficient HA precipitate, resulting in an increase of the unreacted $Ca(OH)_2$ content. Kweh *et al.* (1999) reported that a slow and controlled addition of phosphoric acid in an alkaline environment was necessary to the production of pure stoichiometric HA.

(C) Maturation, Ripening or Aging Conditions

Maturation, ripening or aging condition of suspension after reaction has an effect on characteristic of precipitated HA. Lazic and colleagues (2001) indicated that stoichiometry, size, morphology and ordering of HA crystals precipitated from calcium hydroxide and phosphoric acid are significantly affected by the maturation conditions (i.e. time and temperature). The important of maturation stage in obtaining stoichiometric HA increase with decreasing precipitation temperature. They also

found that the crystals precipitated in temperature range from 20 to 95°C with maturation for 20 hours at the precipitation condition show thermally stable HA. Nearly theoretical values for lattice parameters were obtained for the sample precipitated and matured at 95°C.

Additionally, Saeri and colleagues (2003) noted that aging the HA suspension leads to the growth of the particles and changes the morphology to a more equi-axed status (nearly circular), attributed to the nanoparticles tend to form small agglomerates.

(D) Level of pH

In addition to the reaction temperature and addition rate, the favorable synthesis conditions of pure and monocrystalline HA involves a reasonably high pH at the end of the reaction. Kweh and others (1999) noted that a pH level of about 9 produces the correct stoichiometric condition whereby only pure, single-phase HA is formed. Below a pH of 9, traces of TCP were detected. However, if the slurry suspension's pH swings to the other extreme of pH 11, traces of calcium oxide (CaO) were identified.

Also, Bouyer and co-workers (2000) indicated that the pH at the end of synthesis, which depends on the acid addition rate, is a key parameter, which can be used to determine the purity of the synthesized HA nanocrystals and for the stabilization of the suspension. Additionally, Afshar *et al*. (2003) noted that a decreasing of the pH level can reduce the amount of calcium in the precipitated HA powder.

(E) Ca/P Ratio of Reactant

Basically, the Ca/P ratio is considered as a particularly relevant parameter, because both mechanical properties and biodegradation rate depend on it. The Ca/P atomic ratio of stoichiometric HA is 1.67, but it can preserve its crystalline structure with Ca/P ratios as low as 1.5. Fanovich and Porto-Lopez (1998) found that, upon sintering, the samples with Ca/P ratio of 1.51 transformed to β-TCP and HA, resulting in materials with low densities. Furthermore, the samples with a Ca/P ratio of 1.77, without β-TCP, showed better sinterability and homogeneous microstructures.

Compared to the precipitation reaction between $Ca(NO_3)_2.4H_2O$ and $(NH_4)_2HPO_4$, the Ca/P ratio of the resulting powders was strongly dependent on the pH of the solution and weakly dependent on the initial Ca/P ratio, investigated by Kwon and others (2003). Single phase TCP powder was obtained at pH=7.4 and the initial Ca/P ratio had a little effect on the resulting Ca/P ratio. Biphasic composite powders were prepared at pH=8.0. Moreover, the Ca/P ratio of resulting powder can be easily controlled by adjusting the initial Ca/P ratio.

(F) Ultrasonic Irradiation

So far, the ultrasonic irradiation has been well known as a promising tool to assist the synthetic reactions to prepare fine ceramic powder. This can stimulate the reactivity of chemical species involved, resulting in the acceleration of heterogeneous reactions between liquid and solid reactant effectively. These processes involve dissolution and precipitation of solids through particle size reduction and surface activation by intensive stirring. From previous study of Vargas *et al*. (1998), the ultrasonic vibration, either applied during the aging stage or throughout the chemical synthesis process, can cause a significant reduction in the HA particle size by avoiding the formation of larger agglomerates by flocculation.

The synthesis reaction between $Ca(OH)_2$ and H_3PO_4 via the ultrasonic irradiation, investigated by Kim and Saito (2001), is more effective than that via direct heating method, resulting in the nearly completion of the synthesis reaction by 60 minutes. The ultrasonic irradiation leads to the formation of very fine HA powder with a relatively narrow size distribution. The SSA of the powder sonicated is much higher than that heated. Moreover, prolonged sonicating increases the reactivity of DCPD and stimulates the reaction of DCPD and $Ca(OH)_2$ to produce HA monophase effectively. Comparing this result with those by heating method, although the reaction between DCPD and $Ca(OH)_2$ occurs to produce HA partly, the heating operation alone is not favorable for the preparation of HA monophase. Thus, the high power ultrasonic irradiation is very effective to homogenize the reactants in the suspension, leading to the improvement of reactivity of both solid and liquid by the stimulation of their active surface.

In addition to previous reaction, the effect of ultrasonic irradiation on synthesis reaction between $Ca(NO_3)_2$ and $NH_4H_2PO_4$ was investigated by Cao and colleagues (2005). The result showed that the particle size of the HA crystallites decreased linearly with the increase of ultrasonic power, which can be deduced that the irradiation of ultrasound on the reaction solution during the precipitation process is helpful to make finer particles. It also revealed that the formation of acicular (plated-like) and spherical particles was obtained in different ultrasonic powers of 200 and 300 W, respectively.

(G) Reactant Concentration

Recently, there is no direct investigation on the effect of the reactant concentration of HA synthesis through precipitation reaction between $Ca(OH)_2$ and H_3PO_4. The previous research mostly studied on the reaction between $Ca(NO_3)_2$ and $(NH_4)_2HPO_4$. Many studies confirmed that the crystallinity and morphology of HA crystal are strongly dependent on the concentration of reactant. Kothapalli *et al.* (2004) reported that the aspect ratio (ratio between length and breath of particles) of the HA particles increased with the concentration. Moreover, Cao *et al.* (2005) indicated that the crystallinity improved with an increase of concentration of Ca^{2+} ion.

(H) Other Parameters

In addition to previous major parameters, other conditions were also investigated. The effects of atmosphere controlling, pH, adding extra acid solution, the amount of stirring speed and post-chemical treatment on the properties of HA powder were investigated by Afshar and others (2003). The results clearly reveal that these factors have significant influences on the characteristics of HA precipitated powder, resulting in good purity, stoichiometry and thermal stability.

Controlling atmosphere is very important for synthesizing pure HA particle. Due to the fact that the HA powder is very hospitable for substitution of carbon dioxide in its crystal structure, carbonate ions can substitute hydroxyls or phosphates sites. So, to achieve a pure HA without any carbon dioxide contamination, it is effective to control atmosphere during precipitation process. For example, by using the filtered inert gas, carbonate ion in final HA powder significantly reduced.

An addition of extra acid during aging stage has an effect on the properties of HA powder. The main purpose of adding the extra acid solution is to remove any excess calcium in the HA precipitate. Also, the amount of extra acid has some effects on stoichiometric of precipitated HA, but not in a proportional manner.

Furthermore, the stirring speed and power are also needed. While the stirring speed increased, the amount of $I_{(200)CaO}/I_{(002)HA}$ ratios fell. Using a sufficient speed and power of the stirring (preferably mechanical stirring), the intensity of (2 0 0) plan of CaO in the XRD pattern decreased, resulting in decreasing its stoichiometry.

Moreover, the post-chemical treatment has an influence as well. For instance, washing the suspension of HA with phosphoric acid solution before centrifuging is a significant process to remove any extra calcium in some samples.

In comparison between methods, Mostafa (2005), compared the powder properties of HA synthesized from wet mechanochemical and precipitation method prepared at $100^{o}C$, revealed that the crystallite size and particle size of HA prepared through wet precipitation method are larger than those of HA derived from mechanochemical. Inversely, the surface area of precipitated HA particle is smaller than that of another. While wet mechanochemical leads the powder attaining high sintering density at lower temperature in comparison with those prepared by wet precipitation method at $100^{o}C$.

2.3 Porous Bioceramics

Contrary to metals and polymers, pores have been traditionally avoided in ceramic components due to their inherently brittle nature. However, an increasing number of applications that require porous ceramics have appeared in the last decades, especially for critical environments where high temperatures, extensive wear and corrosive media are involved. Such applications include for example the filtration of molten metals, high-temperature thermal insulation, support for catalytic reactions, filtration of particulates from diesel engine exhaust gases, and filtration of hot corrosive gases in various industrial processes.

Besides the above, the application for medical, such as bone repair, reconstruction or replacement and dental application, needs porous ceramic which is compatible with cell and biological environments. The great example of such ceramic is hydroxyapatite.

2.3.1 Pores and Porosity of Bioceramics

Porosity is defined as the percentages of void space in a material and it is a morphological property independent of the material. Karageorgiou and Kaplan (2005) indicated that pores are necessary for bone tissue formation because they allow migration and proliferation of osteoblasts and mesenchymal cell, as well as vascularisation. In addition, a porous surface improves mechanical interlocking between the implant biomaterials and the surrounding natural bone, providing greater mechanical stability at this critical interface.

Figure 2.5 exhibited the schemas of various types of pores in porous ceramics. Generally, pore can be classified into three types; including (1) opened pore, which has the channels or windows connecting to the surface of materials; (2) closed pore, which is completely isolated from the external surface; and (3) interconnected pore, which link to other pores.

Moreover, Li *et al*. (2003) grouped porous ceramics into two general groups; including (1) reticulate ceramics and (2) foam ceramics. The former is composed of interconnected pores surrounding by a web of ceramic whereas the latter is comprised of only closed pores within a continuous ceramic matrix.
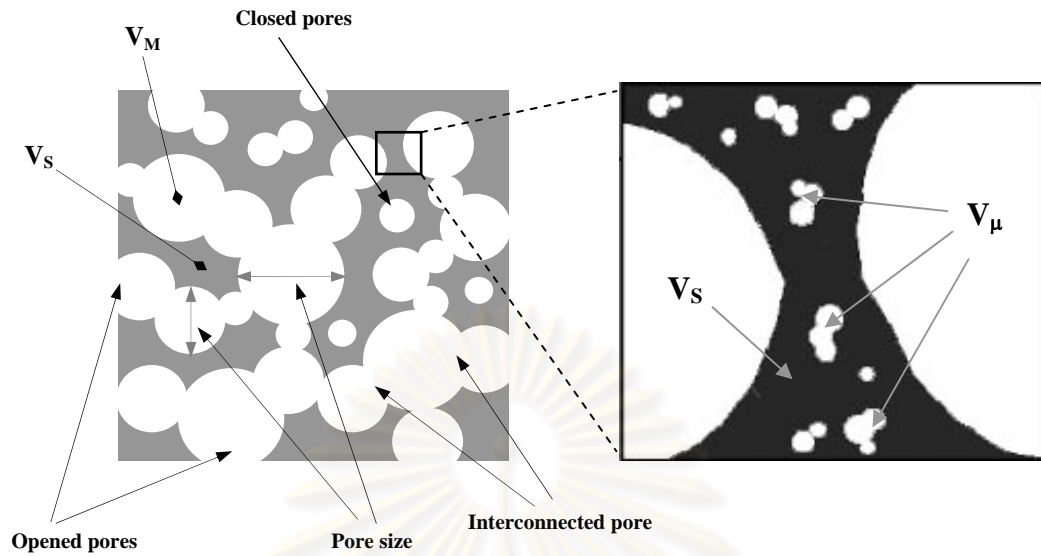
Figure 2.5   Schemas of various types of pores in porous ceramics
(Adapted from Hing, 2005)

Total porosity consists of macroporosity and microporosity. The total porosity can be calculated as in Equation 2.7. When V_M is the total macropore volume, V_μ is the total micropore volume and V_S is the total strut volume or ceramic body volume.

$$\text{Total porosity} = \frac{V_M + V_\mu}{V_S} \tag{2.7}$$

Moreover, Woodard *et al*. (2007) reported that macroporosity (pore size > 50 nm) is thought to contribute to osteogenesis by facilitating cell and ion transport. Microporosity (pore size < 20 nm) improves bone growth into scaffolds by increasing surface area for protein adsorption, increasing ionic solubility in the microenvironment, and providing attachment points for osteoblasts. Pore interconnectivity has been shown to positively influence bone deposition rate and depth of infiltration in vitro and in vivo. Regular interconnected pores provide spacing for the vasculature required to nourish new bone and remove waste products.

2.3.2 Pore Characteristics

The characteristics of porous bioceramics in terms of porosity can be reported by the terms including:

(1) *Pore size*: the pore size can be classified into micropores (<20 nm), mesopores (20-50 nm) and macropores (>50 nm).

(2) *Porosity*: porosity is the ratio between the total pore volume and the materials volume.

(3) *Pore size distribution*: The distribution of pore volume with respect to pore size; alternatively, it may be defined by the related distribution of pore area with respect to pore size.

(4) *Specific Surface Area (SSA):* This is the total surface area of the sample, which is in contact with the external environment. This parameter is mainly dependent on the pore size and the pore volume of material.

2.3.3 Roles of Porosity, Pores and Interconnections in Bioceramics

Clinically, pores and interconnections play an important role in determining the rate and degree of cell and bone ingrowth (Woodard *et al*, 2007). Bone regeneration in a porous scaffold in vivo involves recruitment and penetration of cells from the surrounding bone tissue, as well as vascularisation. Higher porosity is expected to enhance osteogenesis and numerous studies have verified this hypothesis. Mastrogiacomo and colleagues (2006) showed that porosity and pore interconnection of osteoconductive scaffolds can influence the overall amount of bone deposition, the pattern of blood vessels invasion and finally the kinetics of the new bone formation process.

Based on early study of Karageorgiou and Kaplan (2005), the minimum pore size required to regenerate a new bone is considered to be approximately 100 μm due to cell size, migration requirements and transport. However, pore sizes larger than 300 μm are recommended, because of enhanced new bone formation. This was confirmed by Flautre *et al.* (2001). They found that the optimal pore size for osteoconduction was 175-260 μm (larger than 100 μm and approach 300 μm). Moreover, the interconnection size must be over 50 μm to favor new bone ingrowth inside the pores. They also indicated that the interconnection size of 130 μm (larger than 50 μm)

provides the best osteoconduction. In bioresorbable ceramics, Lu *et al*. (1999) reported that pore density and interconnection density are more important than their size, contrary to other bioceramics in which the sizes and the densities are equally important.

Mechanically, Kwon *et al*. (2002) reported that the strength of porous HA samples increased exponentially as the porosity decreased. Although an increasing porosity and pore size facilitate bone ingrowth, the result is a reduction in mechanical properties, because this compromises the structural integrity of the scaffold. The mechanical strength can be adjusted to match the specific requirements by controlling overall porosity of the scaffold. In addition to previous reports, Woodard *et al*. (2007) also indicated that the changes in macroporosity have been shown to affect mechanical properties more than those in microporosity

Table 2.6, Table 2.7 and Table 2.8 presented the reviews of pore size, porosity and mechanical properties of porous calcium phosphate ceramics fabricated by replica technique, sacrificial template technique and direct foaming, respectively. From the reviews, it seems that the compressive strength, elastic modulus and flexural or bending strength are strongly dependent upon the porosity, whilst these mechanical properties are unclearly influenced by the pore size. This may be due to the different fabrication technique of each works. At the pore size less than 100 μm, Deville *et al*. (2006) found that the maximum compressive strength was up to 145 MPa with 40% porosity. At the pore size between 100 and 1,000 μm, the compressive strengths ranged from 0.5 to 45 MPa and the maximum bending strength was approximately 20 MPa. Therefore, the compromise between the mechanical properties of the scaffold and its porosity sets an upper limit in terms of how much the porosity and pore size that can be tolerated in the applied site.

Table 2.6   Reviews of pore size, porosity and mechanical properties of porous

calcium phosphate bioceramics fabricated by replica technique

Authors (year)	Materials	Pore size (μm)	Porosity (%)	Mechanical Properties	Values
White et al (1975)	HA	5-500 μm	n/a	n/a	n/a
Roy (1975)	HA	150-300 μm	n/a	n/a	n/a
Tancred *et al* (1998)	HA/TCP	n/a	< 90 %	n/a	n/a
Hing *et al* (1999)	HA	~500 μm	n/a	Modulus.	1.2 to 3.1MPa
				C.S.	1 to 11 MPa
Hu *et al* (2001)	HA	200-250 μm	n/a	n/a	n/a
Xu *et al* (2001)	HA	~100 μm	n/a	n/a	n/a
Tampieri *et al* (2001)	HA	200-500 μm	n/a	C.S.	21-45 MPa
Tian and Tian (2001)	HA	150-400 μm	58-80 %	C.S.	~15 to 2 MPa
Kwon *et al* (2002)	HA/TCP	~500 μm	65-90 %	C.S.	~3.0 to 0.3 MPa
Padilla *et al* (2002)	HA	30-60 μm	n/a	n/a	n/a
Ramay and Zhang (2003)	HA	200-400 μm	~70-77%	Modulus.	~4 to 7 GPa
				C.S.	~0.5 to 5 MPa
Maio *et al* (2004)	CP	~1,000 μm	~70%	n/a	n/a
Hsu *et al* (2007)	HA	20 and 45 ppi	n/a	F.S.	~18-20 MPa
Saiz *et al* (2007)	HA	100-200 μm	n/a	n/a	n/a
Fidancevska (2007)	HA/TiO$_2$	100-1,000 μm	65±4 %	Modulus	1.7±0.2 GPa
				F.S.	2.1±0.3 MPa
				C.S.	7±1 MPa

Note: *'n/a' = No data available,*
'C.S' = Compressive Strength,
'F.S' = Flexural Strength, and
'T.S' = Tensile Strength

Table 2.7   Reviews of pore size, porosity and mechanical properties of porous
calcium phosphate bioceramics fabricated by sacrificial template
technique

Authors (year)	Materials	Pore size (µm)	Porosity (%)	Mechanical Properties	Values
Liu (1997)	HA	100, 200 and 400 µm	55-70 %	n/a	n/a
Rodiriguez *et al* (1998)	HA	80 µm	45-69 %	F.S.	~14 to 2 MPa
Vaz *et al* (1999)	HA/Li$_3$PO$_4$	100 µm	n/a	n/a	n/a
Rivera *et al* (2001)	HA	10-40 µm	n/a	n/a	n/a
Komlev and Barinov (2002)	HA	100 µm and 500 µm	n/a	T.S.	~4.5 to 1 MPa
Li *et al* (2003)	HA	200-800 µm	< 60 %	n/a	n/a
DeOliveira *et al* (2003)	HA/TCP	300-400 µm	51-78 %	n/a	n/a
Kawata *et al* (2004)	HA	> 100 µm	40-85 %	n/a	n/a
Kundu *et al* (2004)	HA	100-250 µm	75 %	C.S.	10±0.3 MPa
Tadic *et al* (2004)	HA	250-400 µm	15% (macro) 34% (micro)	n/a	n/a
Yao et al (2005)	HA	50-75 µm	~30 %	F.S.	25-27 MPa
		120-150 µm	25-40 %	F.S.	14-23 MPa
		260 350 µm	33.5±0.2 %	F.S.	11.5-13.5 MPa
Madhavi *et al* (2005)	HA	0.8-0.9 µm	n/a	n/a	n/a
Deville *et al* (2006)	HA	> 10 µm	40-65 %	C.S.	65-145 MPa
Zhang and Zhu (2007)	HA	~120 µm	50-75 %	Modulus. C.S.	4.0-10.4 GPa 1.3-7.6 MPa
Lee *et al* (2007)	HA	> 10 µm	56-75 %	C.S.	17 to 0.94 MPa

Note: '*n/a*' = *No data available,*
    '*C.S*' = *Compressive Strength,*
    '*F.S*' = *Flexural Strength, and*
    '*T.S*' = *Tensile Strength*

Table 2.8   Reviews of pore size, porosity and mechanical properties of porous

calcium phosphate bioceramics fabricated by direct foaming technique

Authors (year)	Materials	Pore size (μm)	Porosity (%)	Mechanical Properties	Values
Engin and Tas (2000)	HA	200-400 μm	80-92 %	n/a	n/a
	TCP	100-300 μm	71-78 %	n/a	n/a
Sepulveda *et al* (2000)	HA	17-122 μm	n/a	Modulus C.S	3.6 to 21 GPa 1.6 to 5.8 MPa
Almirall *et al* (2004)	TCP/CdHA	~ 100 μm	45-66 %	n/a	n/a
Potoczek (2008)	HA	130-380 μm	73-92%	C.S.	5.9 to 0.8 MPa
Li *et al* (2009)	CdHA	250-500 μm	70-80%	C.S.	2.2-2.8 MPa

Note: *'n/a' = No data available,*
 'C.S' = Compressive Strength,
 'F.S' = Flexural Strength, and
 'T.S' = Tensile Strength

2.4 Fabrication of Porous Bioceramics

Generally, different fabrication methods and parameters led to a variety of microstructural ranges varying in their application and results with different materials. Similarly, the resultant properties were a fundamental consequence of the microstructures resulting from fabrication (Rice: p.3-9, 1998).

Recently, many novel methods for the fabrication of porous ceramics with different structures were developed. Each technique provided different microstructure and properties. Versatile techniques that allow one to tune the porosity, pore morphology and size distribution, and that can additionally be applied to ceramic materials of many different chemical compositions are demanded. In this section, various techniques for preparing porous ceramics were thoroughly reviewed.

2.4.1 Classification of Pore Forming Techniques for Bioceramics

There are a large number of production methodologies of porous ceramics proposed by many researchers. Interestingly, Studart and others (2006) proposed the classification of processing route based on pore forming technique. According to this classification, the routes to porous bioceramics were categorized into three main techniques; including (1) replica, (2) sacrificial template, and (3) direct foaming techniques. Therefore, the literature reviews of the current available production methods of porous bioceramics were stated.

However, this classification excludes the computerized techniques to produce porous ceramics with complex shape: such as solid freeform fabrication (SFF), creating a precisely controlled pore structure by means of a layer-by-layer and sequential building process, as described by Chu *et al* (2001); robocasting, which allows to build ceramic scaffolds using ceramic inks with minimal organic content (<1wt.%) and without the need for a sacrificial support material or mold, as referred by Miranda *et al* (2006) and Saiz *et al* (2007); and extrusion processes, in which the thermoplastic ceramic and fugitive filaments are aligned alternatively and then the fugitive material is removed with thermal treatment, as explained by Bae *et al* (2006).

2.4.2 Replica Techniques

Figure 2.6 illustrated the schema of replica technique for fabrication of porous bioceramics. This technique is based on the impregnation of a cellular structure with a ceramic suspension or precursor solution in order to produce a porous ceramic exhibiting the same morphology as the original porous material. Thus, the pore size and the structure of the products can be controlled by selecting the different reticulated substrate.

Table 2.9 showed the reviews of replica techniques for porous bioceramics. Many synthetic and natural cellular structures can be used as templates to fabricate porous ceramics through this technique.
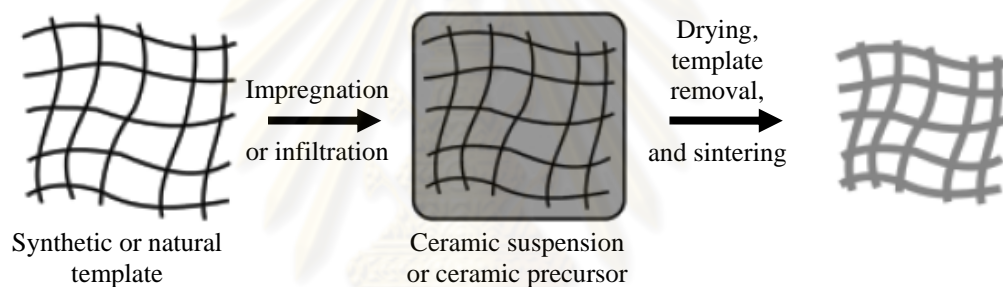
Figure 2.6   Schema of replica techniques for fabrication of porous bioceramics

Table 2.9   Reviews of replica techniques for porous bioceramics

Replica template	Methods	Materials	Author (year)
Synthetic templates			
- Poly urethane foams	Impregnation with	HA	Tian and Tian (2001)
(PU foam)	ceramic suspension	HA/TCP	Kwon *et al* (2002)
		HA	Padilla *et al* (2002)*
		HA	Ramay and Zhang (2003)*
		CP	Miao *et al* (2004)
		HA/TCP	Hsu *et al* (2007)
		HA	Saiz *et al* (2007)
		HA/TiO$_2$	Fidancevska *et al* (2007)**
- Cellulose sponges		HA	Tampieri *et al* (2001)
(Spontex)			
Natural templates			
- Coral	Replamineform	HA	White *et al* (1975)
	Hydrothermal treatment	HA	Roy (1975)
		HA	Hu *et al* (2001)
		HA	Xu *et al* (2001)
- Bovine bone	Replamineform	HA/TCP	Tancred *et al* (1998)
- Natural cancellous bone	Hydrothermal treatment	HA	Hing *et al* (1999)

* = using combination technique / ** = comparing between various techniques

(A) Synthetic Templates

For synthetic templates, polymeric sponges have become the most popular template for preparing macroporous bioceramics with controlled structure because of it simplicity and flexibility. Due to the highly reticulated structure, it seems polyurethane sponge (or PU foam) has been extensively used as a template. This polymer sponge was utilized by Tian and Tian (2001), Kwon *et al* (2002), Padilla *et al* (2002), Ramay and Zhang (2003), Hsu *et al* (2007), Miao *et al* (2004), Saiz *et al* (2007) and Fidancevska *et al* (2007). In addition, cellulose sponge was used as templates by Tampieri *et al* (2001).

Through impregnation method, the selected substrate is soaked with ceramic slurry until the internal pores are saturated with ceramic material. The impregnated sponge is then passed through rollers to remove the excess suspension and distribute the slurry homogeneously (Saiz, 2007). The formation of a thin ceramic coating over the struts of the original substrate is allowed at this stage as well. At this stage, the slurry should be viscous enough to avoid dripping. The ceramic-coated polymeric template should be dried at room temperature no less than 24 hours (Tian and Tian, 2001) and subsequently burned out at temperature over 800°C. Heating rates usually lower than 1°C/min are required to allow the gradual decomposition and diffusion of the polymeric material, avoiding the build-up of pressure within the coated struts. Binder and plasticizers are added to the initial suspension in order to provide ceramic coatings sufficiently strong to prevent cracking the struts during pyrolysis.

A drawback of the sponge replica technique is the fact that the struts of the reticulated structure are often cracked during pyrolysis of the polymeric template, markedly degrading the final mechanical strength of the porous ceramic. The strut flaws reduce the compressive strength of replica-derived porous ceramics to levels usually lower than the strength theoretically predicted for open cell structure.

(B) Natural Templates

In addition to synthetic polymer foams, natural cellular structures have been used as templates for the fabrication of macroporous ceramics through the replica approach. Natural templates are focused on, due mainly to their pore morphology and unique microstructure, which might be difficult to replicate.

Coral have been applied as a natural template for the preparation of macroporous ceramic materials, particularly for the production of scaffold for tissue engineering and bone replacement. In the 1970s, White *et al* employed a lost wax method named "*replamineform*" to replicate the structure of corals and other marine invertebrate skeletons. In this technique, the coral is first impregnated with hot wax under vacuum to obtain negative replica. Afterwards, the calcium carbonate of the coralline skeleton is removed with a strong acid. The porous ceramic is obtained by impregnating the negative wax replica with ceramic slurry and subsequently removing the organic materials by pyrolysis.

In 1975, Roy proposed the method to directly convert the cellular structure of corals into porous hydroxyapatite scaffolds by hydrothermal treatment at high temperature and pressures (as described above in section 2.2.4(B)). This treatment is performed in a phosphate solution, so that carbonate ions present in the coral are partially or totally exchanged by phosphate ions. In 2001, Australian coral and coral genus *Porites* were employed as original templates by Hu *et al* and Xu *et al*, respectively. In addition to corals, natural cancellous bone (e.g. bovine bone) has been utilized as porous templates. The porous hydroxyapatite scaffolds prepared through replamineform and hydrothermal treatment were referred by Tancred *et al.* (1998) and Hing *et al* (1999), respectively.

2.4.3 Sacrificial Template Techniques

Figure 2.7 illustrated the schema of sacrificial template techniques for fabrication of porous bioceramics. This technique is usually based on the preparation of a biphasic composite comprising a matrix of ceramic particles or ceramic precursors and a dispersed sacrificial phase that is initially homogeneously distributed throughout the matrix and is ultimately removed to generate pores within the microstructure. This method leads to porous materials displaying a negative replica of the original sacrificial template, as opposed to the positive morphology obtained from the replica technique.
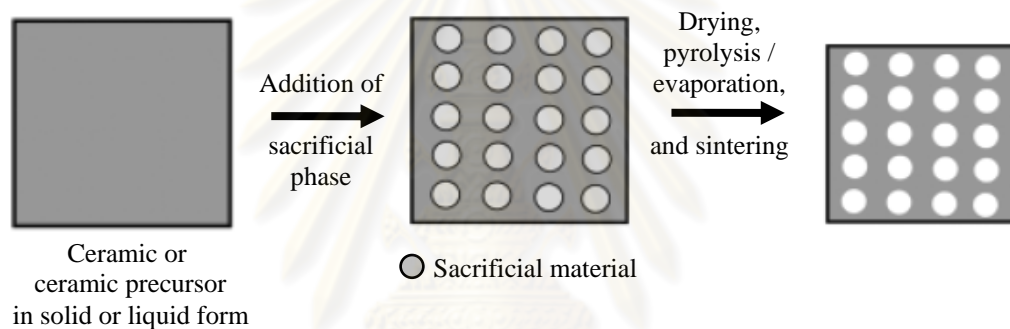
Figure 2.7   Schema of sacrificial template techniques for fabrication of porous bioceramics

The biphasic composite is commonly prepared by (a) pressing a powder mixture of the at least two constituents, (b) forming a two-phase suspension that is subsequently processed by wet colloidal routes such as slip, tape or direct casting or (c) impregnating previously consolidated pre-forming of the sacrificial material with a suspension of ceramic-polymer or ceramic.

The powder pressing (or powder compaction) technique is frequently claimed as the classic route to porous ceramic. These techniques consist of three basic types: including (1) *cold uniaxial pressing*, compressing the powder by piston in a same axis; and (2) *cold isostatic pressing*, applying very high pressure through a device comprising a compression chamber, which is filled with oil to a preformed body, shaped while still in the form of powders, and isolated from the environment by a thin impermeable rubber envelope to preserve the body from contamination by oil; as well

as (3) *hot isostatic pressing*, the powder pressing and heat treatment are performed simultaneously. Among these techniques, cold uniaxial pressing seems to be the most popular way to fabricate porous materials from the mixture of ceramic and porosifier due to its basic and economical method. To fabricate porous HA, this method was used by Liu (1997), Komlev and Barinov (2002), DeOliveira *el al* (2003), Kawata *et al* (2004) and Zhang and Zhu (2007), while the cold isostatic pressing was utilized by Kundu *et al* (2004) and Tadic *et al* (2004).

Additionally, hot pressing techniques were applied to produce porous ceramic. In 2005, Nakahira and colleagues utilized hydrothermal hot pressing technique to fabricate porous HA. The desired amount of powder was added into autoclave with piston and then pressed at the pressure of 10-20 MPa under the temperature of 150-300°C, following by sintering at 1100°C.

Table 2.10 summarized the applied conditions (pressure and temperature) of each compaction from various researches. It seems the isostatic pressing required more pressure than uniaxial pressing.

Table 2.10   Reviews of the various powder compactions to produce porous HA

Compaction Technique	Pressure (MPa)	Temperature (°C)	Materials	Authors
Cold uniaxial pressing	27, 55	Room	HA	Liu (1997)
	10-100	Room	HA	Komlev and Barinov (2002)
	37	Room	HA/TCP	DeOliveira *et al* (2003)
	20-40	Room	HA	Kawata et al (2004)
	50	Room	HA	Zhang and Zhu (2007)
Cold isostatic pressing	160	Room	HA	Kundu *et al* (2004)
	400	Room	HA	Tadic *et al* (2004)
Hot isostatic pressing	10-40	150-300	HA	Nakahira *et al* (2005)

Table 2.11 exhibited the examples of the sacrificial template methods reviewed in this literature. The way that the sacrificial material is extracted from the consolidated composite depends primarily on the type of pore former employed. A wide variety of sacrificial materials have been used as pore formers, including natural and synthetic organics, salts, liquids and ceramic compounds.

Table 2.11　Examples of the sacrificial template methods reviewed in the literature

Sacrificial template	Fabrication method	Materials	Author (year)
Synthetic organics			
- PVB	Uniaxial pressing	HA	Liu (1997)
	Slip casting	HA	Rivera-Munoz *et al* (2001)
- PVC	Slip casting	HA/Li_3PO_4	Vaz *et al* (1999)
- PMMA	Slip casting	A_2O_3	Tang *et al* (2003)
	Slip casting	HA	Yao *et al* (2005)
- Naphthalene	Uniaxial pressing	HA/TCP	DeOliveira *et al* (2003)
	Isostatic pressing	HA	Kundu *et al* (2004)
- Naphthalene and PMMA	Dual phase mixing	HA	Li *et al* (2003)
- Carbon bead & Agar	Uniaxial pressing	HA	Kawata *et al* (2004)
- Carbon fibers	Impregnation	HA/TiO_2	Fidancevska *et al* (2007)**
- Rod-like urea	Uniaxial pressing	HA	Zhang and Zhu (2007)
- Polystyrene (PS) sphere	Impregnation	HA	Madhavi *et al* (2005)
Natural organics			
- Starch	Starch consolidation	HA	Rodriguez-Lorenzo *et al* (1998)
		$CaCO_3$	Lemos and Ferreira (2000)
		A_2O_3	Gregorova *et al* (2006)
		Silica	Mao *et al* (2008)*
Liquids			
- Gelatin and vegetable oils	Uniaxial pressing	HA	Komlev and Barinov (2002)
- Water	Freeze casting	HA	Deville *et al* (2006)
- Camphene	Room-temperature freeze casting	Al_2O_3	Araki and Halloran (2005)
		Al_2O_3	Koh *et al* (2006)
		HA	Lee *et al* (2007)
Salts			
- NaCl & PVA fiber	Isostatic pressing	HA	Tadic *et al* (2004)

*Note: * = using combination technique / ** = comparing between various techniques*

Synthesis and natural organics are often removed through pyrolysis by applying thermal treatment at the temperature below sintering temperature (typically between 200-600°C). The long periods required for completing pyrolysis of the organic matters and the amount of gaseous by-products generated during this process are the main disadvantage of using organic materials as sacrificial phase.

Most of these drawbacks can be partially overcome by using liquid pore formers (such as water and oils) or a solid phase that can be easily sublimated (e.g. naphthalene), as listed in Table 2.11. Even though the burnout process is also time consuming, liquids and volatile oils can be evaporated or sublimated at milder conditions without generating undesired toxic gases during pyrolysis period and excessive stresses during removal of the pore former. For example, Kundu *et al*. (2004) used naphthalene ($C_{10}H_8$) as a sacrificial template which starts to vaporize at around 80^oC. However, during the burnout process, watchfulness on the samples is needed in order to prevent the cracking.

Additionally, freeze casting is an alternative to fabricate porous complex-shaped ceramic. In freeze casting, ceramic slurry is poured into a mold and then frozen at the extremely cold temperature, usually below -40^oC. The frozen solvent, generally water, acts temporarily as a binder to hold the part together for demolding. Subsequently, the part is subject to freeze drying to sublimate the solvent under vacuum, avoiding the drying stresses and shrinkage that may lead to cracks and wrapping during normal drying. After drying, the compacts are sintered in order to fabricate a porous material with improved strength, stiffness and desired porosity. The result is a scaffold with a complex and often anisotropic porous microstructure generated during freezing. By controlling the growth direction of the ice crystals, it is possible to impose a preferential orientation for the porosity in the final material (Deville *et al*, 2006).

To avoid cracking during heat treatment period, some researcher proposed a new strategy to produce porous ceramics without sintering process. In 2004, Tadic and coworkers presented the method to produce porous HA without sintering, using NaCl and polyvinyl alcohol (PVA) fibers as sacrificial templates. The mixture was isostatically pressed at 4000 bar (equivalent to 400 MPa) at room temperature (20^oC). Subsequently, the compacts was submerged in cold water (approximately 20^oC) and then warm water (approximately 50^oC) for 12 hours in order to remove NaCl and PVA fibers, respectively.

2.4.4 Direct Foaming Techniques

Figure 2.8 illustrated the schema of direct foaming techniques for fabrication of porous bioceramics. This technique is based on incorporating air into a suspension or liquid media, which is subsequently set in order to keep the structure of air bubbles created. Generally, the consolidated foams are afterwards sintered at high temperatures to enhance mechanical strength.
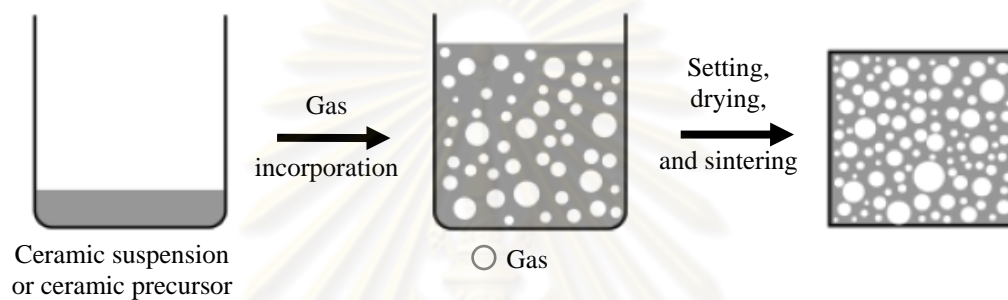
Figure 2.8   Schema of direct foaming techniques for fabrication of porous bioceramics

Table 2.12 presented the examples of direct foaming methods reviewed in this literature. By foaming method, foaming agent is added into the mixture in order to create the gas voids in the ceramic suspension. Recently, there are many kinds of foaming agent used, as shown in Table 2.12. However, it seems adding hydrogen peroxide (H_2O_2) is the most favorable way to create pore in ceramic bodies. The amount of porosity and especially pore size are increased when using a higher concentration of H_2O_2 (Almirall *et al*, 2004).

Besides using a foaming agent, Sepulveda and others (2000) proposed the gelcasting method, which combines foaming and the incorporation of organic monomers into aqueous ceramic suspensions for porosity generation and setting, respectively. The process yields cellular structures with porosity fractions varying from 0.40 to .0.90, with pores closed or open, depending on pore fraction.

By this technique, the total porosity of directly foamed ceramics is proportional to the amount of gas incorporated into the suspension or liquid medium during the foaming process. Furthermore, the pore size is determined by the stability of wet foam before setting occurs. Wet foams are thermodynamically unstable systems due to destabilization processes, including drainage, coalescence and disproportionation (Studart *et al*, 2006). These processes significantly increase the size of incorporated bubbles, resulting in large pores in the final cellular microstructure. Therefore, the critical subject on direct foaming methods is how to stabilize the air bubbles incorporated within the initial suspension or liquid media.

A surfactant is necessary for stabilizing bubbles produced in the slurry by reducing the surface tension at the gas-liquid interfaces (Fuji *et al*, 2006). Intrinsically, surfactants have several long-chain amphiphilic molecules and biomolecules. These molecules retard the coalescence and disproportionation of bubbles by adsorbing at the air bubble surface and reducing the air-water interfacial energy. However, due to the low adsorption energy, surfactant can not prevent the long-term stabilization of foams. Thus, direct foaming methods based on surfactants require a setting agent to consolidate the foam microstructure before extensive coalescence and disproportionation take place.

Numerous processing routes have been developed in the last decades to prepare porous ceramics using direct foaming method based on surfactants. Several chemicals (as shown in Table 2.12) have been used as surfactant in previous works. For example, Sepulveda *et al* (2000) used acrylate-monomer; Ramay and Zhang (2003) used Surfonals DF-58; Fuji *et al* (2006) used poly(oxyethylene)sorbitan monolaurate; Zhang *et al* (2006) used ammonium lauryl sulphate; and Mao *et al* (2008) used sodium carboxy-methyl-cellulose as a surfactant.

Due to toxicity of polymerizable monomer, several setting agents from food industry have been used as a surfactant. Studart *et al.* (2006) indicated that gelling agent such as agar, sucrose and carrageenan gum have been applied as non-toxic processing route for fabrication of porous ceramics.

Table 2.12   Examples of Direct foaming methods reviewed in the literature

Foaming agent / Gas bubbles	Chemicals (function as)	Materials	Author (year)
Foaming method			
- Triton X114	- Ammonium polyacrylate (as deflocculant)	Alumina	Sepulveda and Binner (1999)
- Tween 80	- Acrylate monomer (as sufactant)		
- H_2O_2	No	TCP/CdHA	Almirall _et al_ (2004)
- H_2O_2	- Dolapix CE 64 (as deflocculant)	HA/TiO_2	Fidancevska _et al_ (2007)**
- H_2O_2	- Methyl cellulose (as deflocculant)	CdHA	Li _et al_ (2009)
	- Polyethylene glycol (as viscous agent)		
- Liquid detergent (White Cat ®)	- Sodium carboxymethylcellulose (CMC) (as surfactant)	Silica	Mao _et al_ (2008)*
Gelcasting			
- Air bubble	- Polyacrylate and Acrylic monomers (as gelling agent)	HA	Sepulveda _et al_ (2000)
	- Dispex A40, Allied Colloids (as deflocculant)		
	- Tergitol TMN10, Aldrich (as surfactant)		
- Methyl cellulose	No	HA & TCP	Engin and Tas (2000)
- Air bubble	- Methacrylamide and N,N' Methylenebis-acrylamide (as gelling agent)	HA	Padilla _et al_ (2002)*
	- Ammonium persulfate (as initiator)		
	- N,N,N',N' tetramethylethylene diamine, TEMED (as catalyst)		
	- Darvan 811, R.T.Vanderbilt (as deflocculant)		
- Air bubble	- Acrylamide & N,N' Methylenebis-acrylamide (as gelling agent)	HA	Ramay and Zhang (2003)*
	- Ammonium persulfate (as initiator)		
	- TEMED (as catalyst)		
	- Darvan C, R.T.Vanderbilt (as deflocculant)		
	- Surfonals DF-58 (as surfactant)		
- N_2 gas	- MMA & MBAM (as gelling agent)	Silica glass and Al_2O_3	Fuji _et al_ (2006)
	- Ammonium persulfate (as initiator)		
	- TEMED (as catalyst)		
	- (A) Ammonium lauryl sulphate, (B) Fatty alcohol ethoxy sodium, and (C) Poly(oxyethylene)sorbitan monolaurate (as surfactant)		
	- Ammonium citrate (as deflocculant)		
- N_2 gas	- Ammonium lauryl sulphate (as surfactant)	Silica glass and Al_2O_3	Zhang _et al_ (2006)
	- same chemicals as Fuji _et al_ (2006)		
- Air bubble	- Agarose (as gelling agent)	HA	Potoczek (2008)
	- Darvan 811, R.T.Vanderbilt (as deflocculant)		

* = using combination technique / ** = comparing between various techniques

Moreover, Fuji and colleagues (2006) compared the performance of using three different surfactants (including (1) Ammonium lauryl sulphate, (2) Fatty alcohol ethoxy sodium, and (3) Poly(oxyethylene)sorbitan monolaurate) on their microstructure and some intrinsic properties. They also indicated that the first surfactant with large foaming ability provides low density, highly porous structure, broad pore size distribution and low thermal conductivity, which is suitable for making porous ceramics.

Apparently, each pore forming techniques are based on the basic fabrication methods, e.g. hydrothermal conversion, casting, freeze casting or powder compaction. Table 2.13 listed the reviews of current available methods for producing porous bioceramics, categorized by the fabrication methods and pore forming techniques. However, it seems that casting is the most frequently used method to fabricate porous ceramics. This may be due to the simple and convenience process of this method.

Table 2.13   Reviews of current available methods for producing porous bioceramics, categorized by the fabrication methods and pore forming techniques

Pore forming techniques	Fabrication method			
	Hydrothermal conversion	Casting	Freeze casting	Powder compaction
1. Replica methods	- Replamineform - Hydrothermal treatment	- Polyurethane foam impregnation - Cellulose sponge impregnation	-	-
2. Sacrificial template methods	-	- slip casting with various templates - Dual-phase mixing - Starch consolidation	- Freeze casting (water as a vehicle) - Room temperature freeze casting (camphene as a vehicle)	- Cold Uniaxial pressing - Cold Isostatic pressing - Hot pressing
3. Direct foaming method	-	- foaming method - gelcasting	-	-

2.4.5 Combination Techniques

From above literature reviews, each technique provided a different and unique porous structure. As a result, some studies employed a combination among these techniques. Previous works, using a combination among pore forming techniques for making porous bioceramics, were summarized in Table 2.14.

For a combination between replica and direct foaming techniques, Padilla *et al* (2002) fabricated porous HA samples through Polyurethane foam (PU foam) impregnation and gelcasting, respectively. They found that the porous structure of the sample was a replicate of the cellular foam. Then, Ramay and Zhang (2003) prepared porous HA scaffolds via the same method. They agreed with the previous finding and also indicated that the pore size and shape, depending on the original foam structure, are controllable.

Table 2.14 Previous works using combination among pore forming techniques for making porous bioceramics

Author (year)	Materials	Pore forming techniques		
		Replica	Sacrificial template	Direct foaming
Padilla *et al* (2002)	HA	PU foam impregnation		Gelcasting
Ramay and Zhang (2003)	HA	PU foam impregnation		Gelcasting
Mao *et al* (2008)	Silica		Starch consolidation	Foaming method
Bartuli *et al* (2009)	Zirconia		PE decomposition	Gelcasting
Tulliani *et al*. (2009)	Zirconia		PE decomposition	Gelcasting

For a combination between sacrificial template and direct foaming techniques, Mao *et al* (2008) proposed a combination between starch consolidation and foaming method, respectively, to fabricate porous silica samples. They found the tri-modal hierarchical structure was composed of the large-sized cells, moderate-sized pores and small-sized voids, which were attributed to the bubbles in foams, the elimination of starch particles and the interstices among the silica grains, respectively. Additionally, Bartuli *et al* (2009) and Tulliani *et al* (2009) developed the combined forming technique between sacrificial template and direct foaming techniques for making

porous Zirconia, using PE spheres decomposition and gelcasting, respectively. They found that the amount, size and distribution of macroporosity of the cellular ceramics can be strictly controlled by correctly selecting the size of polyethylene spheres and by optimizing their dispersion in the gelling agent.

Consequently, there were a few works focused on a combination among various pore forming techniques. Particularly, there was no research introducing a combination between sacrificial template and direct foaming techniques for porous hydroxyapatite fabrication.

2.5 Heat Treatments of Hydroxyapatite

In this section, the thermal transformation of calcium phosphate, the calcination behavior and sintering behavior of hydroxyapatite were described, respectively.

2.5.1 Thermal Transformation of Calcium Phosphate

The thermal behavior of phosphates is the subject of an intricate debate due to the fact that each phosphate can remarkably influence the overall process of the transformations which can occur at the different temperatures. Thermal transformations are very important, because a ceramic is obtained through a thermal treatment and consequently all eventual transformations that can occur at high temperatures must be expected as they form the base of the chemical quality of the original powders utilized for the production.

Each calcium phosphate refers to a chemical compound with a defined stoichiometric formula. Most of the compounds crystallize and have many crystallization phases. Generally, the crystallized phases have different names. Sometimes the name used is the chemical one, and a Greek letter is adopted to distinguish the different phases (e.g. α-TCP or β-TCP).

Hydroxyapatite (HA) is a well-defined chemical compound with formula $Ca_{10}(PO_4)_6(OH)_2$. It belongs to a family of homologous compositions, crystallizing in the same spatial group, defined as apatites. The hydroxyl group can be replaced, for example, by fluoride and chloride ion so that fluorapatite $(Ca_{10}(PO_4)_6F)$ and chlorapatite $(Ca_{10}(PO_4)_6Cl_2)$ are obtained, respectively. Also, the cation can be

replaced by other bivalent ions (e.g. Sr^{2+}, Ba^{2+}, Pb^{2+}) to give rise to strontium, barium, and lead hydroxyapatites. All these apatitic compounds crystallize with only one phase; with the specific lattice group $P6_3/m$.

Stoichiometric hydroxyapatite is a very stable compound up to 1400^oC. At temperatures over 1200^oC, HA can transforms into TCP and calcium oxide (CaO) as the chemical Equation 2.8 below. Particularly if CaO is present with HA, TTCP can be occurred as shown in Equation 2.9. By combining both equations, HA can be converted to TCP and TTCP. On the other hand, Equation 2.10 is completely shifted to the right side at 1550^oC.

$$Ca_{10}(PO_4)_6(OH)_2 \rightarrow 3Ca_3(PO_4)_2 + CaO + H_2O \qquad (2.8)$$

$$Ca_{10}(PO_4)_6(OH)_2 + 2\ CaO \rightarrow 3Ca_4O(PO_4)_2 + H_2O \qquad (2.9)$$

$$Ca_{10}(PO_4)_6(OH)_2 \rightarrow 2Ca_3(PO_4)_2 + Ca_4O(PO_4)_2 + H_2O \qquad (2.10)$$
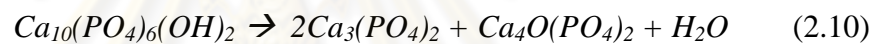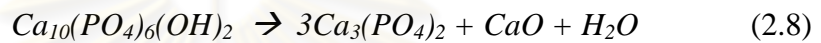
Moreover, the formation of oxyapatite ($Ca_{10}(PO_4)_6O$) through condensation of HA, particularly above 1400^oC, can take place. There are also other cations and anions which, though unable to reach a complete substitution, may be available for playing a role in the formation of solid solutions confined within the apatitic crystal lattice. As regards the Mg^{2+}, it was ascertained to be a characteristic ion not favoring the apatitic structure. This ion can be incorporated into synthetic apatites in quantities lower than 0.4%. Similar ions are $P_2O_7^{4+}$, Sn^{2+} and Al^{3+}, all of which tend to divert the formation of amorphous calcium phosphate compounds (ACP). Other ions, such as CO_3^{2-} may be contained in the apatitic lattice in sufficiently large percentages on condition that Mg^+ is not present. A further ion that may occur in sufficiently large percentage proportions is HPO_4^{2-}.

2.5.2 Calcination Behavior of Hydroxyapatite

Calcination (or calcining) is a thermal treatment process applied to solid materials in order to bring about a thermal decomposition, phase transition, or removal of a volatile fraction. The calcination process normally occurs at temperatures below the melting point of the materials. Calcination is to be distinguished from roasting, in which more complex gas-solid reactions take place between the furnace atmosphere and the solids, however calcination takes place in the absence of air.

It seems that calcination is very important process for preparing HA powder in that calcining allows the powder properties to be controlled in order to optimize the properties of the final product.

(A) Particle Size and Morphology

Juang and Hon (1996) indicated that calcination increased the average particle size of HA powder and also changed the particle size distribution of the powder from multimodal to unimodal because of coalescence of finer particles during calcination.

Moreover, Patel *et al*. (2001) reported that coarsening of the microstructure of the powder surface increased as the calcination temperature increased, corresponding to the decrease in the specific surface area of the powder.

(B) Crystallinity

Calcination is an essential step in order to produce powder with high crystallinity. Kweh *et al*. (1999) found that the XRD spectrum of HA powder calcining at 800°C and above exhibited the sharp, narrow diffraction peaks. Moreover, Patel *et al*. (2001) stated that an increase in calcination temperature to the temperature between 800 to 1000°C resulted in the powders with highly crystalline, fused, sub-micron particles. Additionally, Saeri *et al*. (2003) also confirmed that calcining the as-precipitated HA at 850 and 1200°C caused the reduction of OH group and the increase of crystallinity.

(C) Phase Transformation

Calcination can directly cause the phase transformation of calcium phosphate. From previous study of Kweh *et al*. (1999), it seems the temperature below 1000°C maintained the phase of HA. Furthermore, Juang and Hon (1996) indicated that the HA powder calcining at 900°C showed no phase transformation, while the HA powder calcining at 1000°C and above provided the undesirable phases (such as TCP and CaO).

(D) Flowability

Kweh *et al*. (1999) reported that the flowability of the HA powder was greatly reduced after calcination, which may not be desirable during plasma spraying. Besides, a spherical geometry of the powder was highly desired for enhanced flowability and deposition consistency.

(E) Mechanical Properties

Juang and Hon (1996) indicated that the temperature of 900°C was the beneficial temperature for calcination of the HA samples, resulting in a higher bending strength (about 55 MPa) with finer grain size.

Moreover, Patel *et al*. (2001) reported that no difference in micro-hardness between the calcined powder and non-calcined powder were observed. Therefore, there was no benefit in precalcining the powders prior to sintering.

2.5.3 Sintering Behavior of Hydroxyapatite

Sintering is a firing technique for making objects from powder, through heating the material below its melting point until its particles mutually attach. This technique is commonly the last step in actually making a ceramic body. The sintering methods for hydroxyapatite can be grouped into three common techniques, including (1) normal sintering, (2) hot-pressing, and (3) hot-isostatic pressing.

Although a normal sintering does occur in loose powders, it is greatly enhanced by the powder compaction, and most commercial sintering is done on compacts. Compacting is generally done at room temperature, and the resulting compact is subsequently sintered at elevated temperature without application of

pressure. Secondly, a hot-pressing, ceramic can be sintered simultaneously at high temperature and under high pressure. A hot-pressing apparatus consists of a press machine and furnace. Generally, the hot-press technique has been used for fabrication of dense ceramic at lower temperature compared to the normal sintering technique. Finally, a hot-isostatic pressing (HIP) is a technique for isostatically compressing materials by gaseous pressures at high temperatures. By using this technique, ceramics with small grain sizes and little pores can be obtained at lower sintering temperature. By HIP technique, sintering at 1100°C under the argon gaseous pressure of 160 MPa for 1 hour causes hydroxyapatite to change into transparent form (Aoki, 1994: 271).

Not only the synthesis parameters, but heat treatment also has an influence on the characteristics and properties of HA. Recently, there are many researches investigated on the effect of heat treatment on the properties of HA, and vice versa.

(A) Density and Porosity

White *et al* (2007) stated that many factors; including powder properties, sample preparation, phase purity of the raw materials, sintering temperature, atmosphere, and heating rate, affected the density of the final samples.

Furthermore, Gibson *et al*. (2001) also confirmed that heating rate affected the final density of HA. Higher ramp rates gave a higher final density, but the rate greater than 10°C/min resulted in decomposition of HA. The low crystallinity HA achieves a final sintered density of between 97-98% of the theoretical density at approximately 1200°C, whereas commercial crystalline HA requires a sintering temperature of approximately 1300°C to reach a similar density. Only the sintering temperature significantly affected the sintered density of Lab-HA, whereas the sintering temperature, time, heating rate and compaction pressure all affected the sintered density of commercial HA.

Additionally, Mostasfa (2005) indicated that the sintered density was depended on the particle size, the homogeneity and the agglomeration character of the HA powders. Moreover, He *et al*. (2008) found that the bulk density increased with an increasing sintering temperature, whilst the open porosity and total porosity decreased.

(B) Sinterability

Gibson *et al*. (2001) found that the sinterability of the low crystallinity HA powder, with a median particle size of 22 μm and a high specific surface area (SSA) of 63 cm^2/g, was significantly greater than for a commercial HA powder, which was crystalline and had a median particle size of 5 μm and a low SSA of 16 cm^2/g.

Moreover, Mostasfa (2005) stated that HA prepared from different methods affected different sinterability. The HA powder prepared by mechanochemical route exhibited better sinterability, uniform microstructure and improved mechanical properties, comparing to the HA powder prepared from precipitation method.

(C) Shrinkage

Gibson *et al*. (2001) reported that the linear shrinkage of low crystallinity HA and commercial crystalline HA were approximately 24% and 18%, respectively. Besides, Yang *et al*. (2008) found that the drying shrinkage decreased with an increasing β-TCP content, while the sintering shrinkage increased with an increasing temperature and β-TCP content,

(D) Thermal Stability

One of the main factors affecting the integrity of the final sintered product is the Ca/P ratio. White *et al*. (2007) indicated that even the slightest deviation from the stoichiometric 1.67 Ca/P ratio caused the decomposition during sintering. Typically, a precursor with Ca/P ratio lower than 1.67 caused decomposition to β-TCP (followed by a second conversion to α-TCP at higher temperature) and Tetracalcium phosphate, and a precursor with Ca/P ratio more than 1.67 caused the decomposition to CaO.

Saeri *et al*. (2003) stated that the synthesized HA powder had favorite thermal stability at 1200°C. Moreover, Mostasfa (2005) reported that the start of sintering depended mainly on the Ca/P ratio of HA powers, since the start of sintering of both precipitated Ca-deficient HA and mechanochemical HA start at lower temperatures than precipitated stoichiometric HA.

Additionally, Yang *et al*. (2008) found that the β-TCP-rich samples began sintering at a lower temperature than the HA-rich samples, corresponding to the

previous results of Mostasfa (2005). Although the start of sintering depended on the Ca/P ratio, the relative density at 1100°C was almost the same as the less sintered HA-rich samples because of the lower initial packing efficiency of the β-TCP-rich samples. After sintering the phase composition changed depending on the sintering temperature and phase purity.

(E) Grain size

Basically, grain size increases with sintering temperature and time (Rice: 5-6, 1998). Yeong *et al*. (1999) found that the average grain size increased with increasing sintering time at 1200°C and the increase in average grain size led to a noticeable improvement in fracture toughness of the sintered HA.

(F) Mechanical Properties

The mechanical properties of porous HA are directly related to the density, pore size, porosity and porous structure, influenced by sintering parameters. The higher the degree of sintering, the better the mechanical properties will be, as any porosity will induce cracking and eventually catastrophic failure (White *el al*, 2007).

Gibson and others (2001) found that the hardness of HA ceramic increased with an increase of sintering temperature. Thus, hardness of low crystalline HA and commercial crystalline HA increased with an increasing the sintering temperature. Moreover, they also found that the hardness of low crystalline HA powder was greater than the commercial HA when firing at the lower sintering temperature (below 1200°C).

However, Yeong *et al*. (1999) indicated that the steady decrease in hardness for materials sintered at 1200°C for more than 7 hours was apparently due to the fall in sintered density with prolonged sintering time.

2.6 Summary

In this chapter, the literature review summarized the concept of bioceramics, its classification and some examples of bioceramics, such as calcium phosphate family, coralline and human bone. The crystal structure, properties, medical application and synthesis methodologies of hydroxyapatite were reviewed. In addition to the synthesis methods, the synthesis parameters affecting on the properties of precipitated HA were also examined. The definition of pore and porosity, the characteristics of pore, and roles of porosity, pores and interconnections in bioceramics were mentioned. Moreover, the classification of pore forming techniques and previous works on fabrication of porous bioceramics divided by single technique and combination techniques were explored. Additionally, thermal transition of calcium phosphate and calcination and sintering behavior of hydroxyapatite were determined.

From above reviews, Synthesis through an aqueous precipitation reaction between calcium phosphate and orthophosphoric acid can produce hydroxyapatite with standard quality, high production rate and economical cost. Furthermore, there is no research on fabrication of porous hydroxyapatite through combination between sacrificial template and direct foaming technique.

In this dissertation, the production process of porous HA was developed. HA powder used in this study was synthesized from an aqueous precipitation reaction between calcium hydroxide and orthophosphoric acid. Porous HA samples were prepared through direct foaming, sacrificial template and combination techniques. The key process parameters affecting on porosity and mechanical strength were also studied. The prepared HA powder and the resultant porous HA samples were characterized as well.

CHAPTER III

MATERIALS AND METHODS

In this chapter, the preparation of hydroxyapatite powder, the fabrication procedures of porous samples without and with surfactant, the heat treatment plan, and the characterization of the material and the samples were described.

3.1 Preparation of Hydroxyapatite Powders

In this work, hydroxyapatite (HA) was synthesized using an aqueous precipitation reaction between 0.5M calcium hydroxide ($Ca(OH)_2$, No.31219, Riedel-deHaen, Germany) and 0.3M orthophosphoric acid (H_3PO_4, 85%, Merck, Germany), due to its simple and economical process.

Figure 3.1 showed the production system of synthesized HA via an aqueous precipitation reaction between $Ca(OH)_2$ and H_3PO_4. The reaction was carried out at room temperature and the pH of the reaction was also maintained at 10.5 by the addition of ammonia solution (NH_4OH, 28%, No.2672, APS Finechem, Australia). During the synthesis process, both reactants must be stirred using magnetic stirrer.

To receive the stoichiometric HA, Ca/P molar ratio of the reaction must be preserved at 1.67. The solution of H_3PO_4 acid was slowly dropped into the vigorously stirring suspension of $Ca(OH)_2$ at the addition rate of around 3 ml/minute. Slow dropping was controlled using a peristaltic pump (313U, Watson Marlow, USA). After the ending of the reaction, the reacted suspension was continuously stirred for further 60 minutes and then aged overnight at room temperature.

Figure 3.1 illustrated the preparation process of HA powder. After aging, the resultant precipitate was filtered and repetitively washed using deionized water in order to remove some remaining ammonia and its odor. The filtered cake was dried in the vacuum oven (WTC, Binder, Germany) at $80^{o}C$ overnight and then ground into powder using a pestle and mortar. Subsequently, the powder was passed through a series of sieves. As a result of the sieving process, the desire particle size of the powder has been acquired.

Addition rate of ~3 ml/min.

Stirrer

Drop ammonium solution when pH level drop lower than 10.5

Peristaltic pump

pH/Temperature Probe

H₃PO₄ solution

Ca(OH)₂ suspension

Magnetic stirrer 1

Magnetic stirrer 2
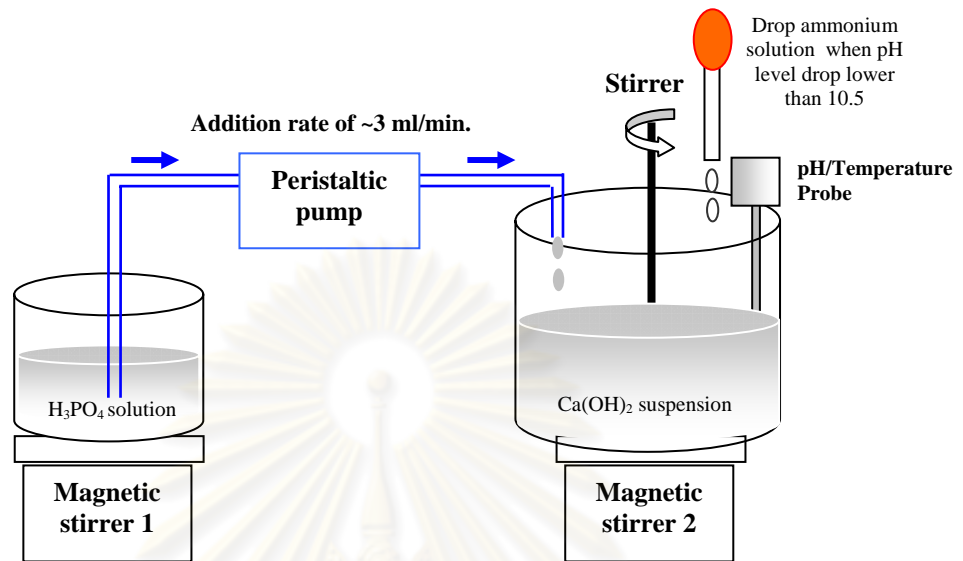
Figure 3.1   Schema of the production system of synthesized HA via an aqueous precipitation reaction between $Ca(OH)_2$ and H_3PO_4

Synthesis   **Aging**   **Filtration**   **Drying**

HA powder   **Sieving**   **Milling**
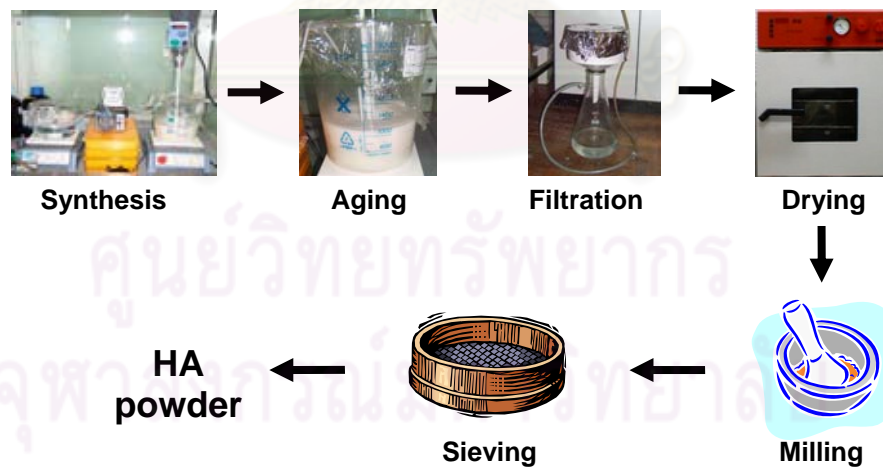
Figure 3.2   Schema of the preparation process of hydroxyapatite powder

3.2 Fabrication of Porous Hydroxyapatite Samples

In this section, the fabrication procedures of porous HA samples without surfactant through three pore forming techniques; including (1) sacrificial template using PMMA, (2) direct foaming using H_2O_2 and (3) combination technique using PMMA and H_2O_2 (combination between sacrificial template and direct foaming), were elaborated.

3.2.1 Sacrificial Template Technique using PMMA

In this work, the commercial poly(methyl methacrylate) granules (PMMA, No.445746, Sigma Aldrich, Germany), which has a molecular weight of around 350,000 and a density of 1.17 g/ml (the details from manufacturer), were selected as a sacrificial template.

Figure 3.3 presented the flow chart of the preparation process of porous HA via sacrificial template technique using PMMA granules. To fabricate the porous samples through this technique, the HA powder was homogeneously mixed with PMMA granule and deionized water. After mixing, the paste was placed into the removable cylindrical molds with a diameter of 25 mm and the bar-shaped molds with dimensions of 10×40×20 mm (width×length×height), and then kept at 60$^{\text{o}}$C in a vacuum oven overnight. Afterwards, the green samples were removed from the mold and heat-treated in a furnace.

Table 3.1 showed the experimental plan and sample names for the HA samples prepared via sacrificial template technique using PMMA granules. To study the effect of PMMA content and L/P ratio, the PMMA granule and deionized water were added with the content of 0, 5, 10, 20, 30, 40 and 50 wt% and with the liquid to powder ratio (L/P ratio) of 1.3 and 1.5 ml/g, respectively.
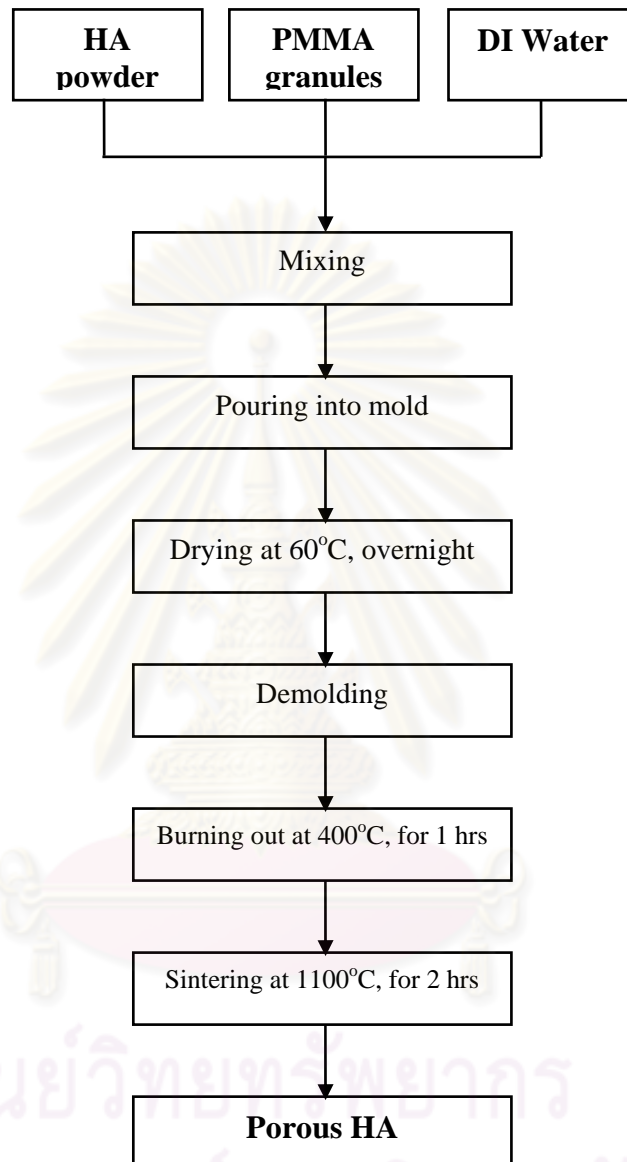
Figure 3.3   Flow chart of the preparation process of porous HA via sacrificial
             template technique using PMMA granules

Table 3.1   Experimental plan and sample names for the HA samples prepared via
sacrificial template technique using PMMA granules

Sample Name	% PMMA content (wt%)	L/P ratio (ml./g.)
H00-P00-L13	0	
H00-P05-L13	5	
H00-P10-L13	10	
H00-P20-L13	20	1.3
H00-P30-L13	30	
H00-P40-L13	40	
H00-P50-L13	50	
H00-P00-L15	0	
H00-P05-L15	5	
H00-P10-L15	10	
H00-P20-L15	20	1.5
H00-P30-L15	30	
H00-P40-L15	40	
H00-P50-L15	50	

Note:
Hxx   *was referred to the sample produced with the H_2O_2 concentration of xx wt%*
Pyy   *was referred to the sample produced with the PMMA content of xx wt%*
Lzz   *was referred to the sample produced with the L/P ratio of 1.3 or 1.5 ml/g*

3.2.2 Direct Foaming Technique using H_2O_2

In this study, the commercial solution of hydrogen peroxide, 30wt% (H_2O_2, Merck, Germany) was used as a foaming agent. To investigate the effect of concentration of H_2O_2, a set of solutions with various concentrations were prepared by diluting the commercial solution with deionized water.

Figure 3.4 illustrated the flow chart of the preparation process of porous HA via direct foaming technique using H_2O_2 solution. The procedure began with the mixture of the HA powder and H_2O_2 solution, and then followed by homogeneous stirring. After mixing, the paste was poured into the removable cylindrical molds with a diameter of 25 mm and the bar-shaped molds with dimensions of 10×40×20 mm (width×length×height) and then left in atmosphere for 15 minutes for expansion. To dry the sample and remove the remaining H_2O_2, the foamed paste was kept at 60°C in a vacuum oven overnight. Afterwards, the green samples were removed from the mold and heat-treated in a furnace.

Table 3.2 exhibited the experimental plan and sample names for the HA samples prepared via direct foaming technique using H_2O_2 solution. To examine the effect of concentration of hydrogen peroxide solution and L/P ratio, the concentration was varied using 0, 1, 3, 5, 10, 20 and 30 wt% with the L/P ratio of 1.3 and 1.5 ml/g.
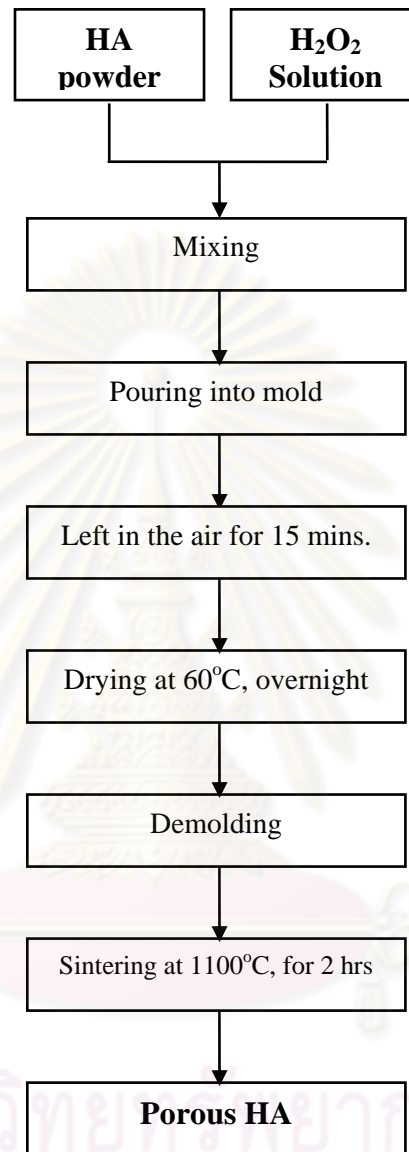
Figure 3.4   Flow chart of the preparation process of porous HA via direct
             foaming technique using H_2O_2 solution

Table 3.2   Experimental plan and sample names for the HA samples prepared via
direct foaming technique using H_2O_2 solution

Sample Name	% H_2O_2 concentration (wt%)	L/P ratio (ml/g.)
H01-P00-L13	1	1.3
H03-P00-L13	3	
H05-P00-L13	5	
H10-P00-L13	10	
H20-P00-L13	20	
H30-P00-L13	30	
H01-P00-L15	1	1.5
H03-P00-L15	3	
H05-P00-L15	5	
H10-P00-L15	10	
H20-P00-L15	20	
H30-P00-L15	30	

Note:

Hxx   *was referred to the sample produced with the H_2O_2 concentration of xx wt%*
Pyy   *was referred to the sample produced with the PMMA content of xx wt%*
Lzz   *was referred to the sample produced with the L/P ratio of 1.3 or 1.5 ml/g*

ศูนย์วิทยทรัพยากร
จุฬาลงกรณ์มหาวิทยาลัย

3.2.3 Combination Technique using PMMA and H$_2$O$_2$

The poly-methyl-methacrylate granules (PMMA) being commercial grade was applied as a pore former for sacrificial template technique, while hydrogen peroxide solution (H$_2$O$_2$) was used as a foaming agent for direct foaming technique.

Figure 3.5 displayed the flow chart of the preparation process of porous HA specimens via combination technique using PMMA granules and H$_2$O$_2$ solution. The fabrication started with preparing the homogeneous mixture of the HA powder, PMMA granules and H$_2$O$_2$ solution. After mixing, the paste was the paste was poured into the removable cylindrical molds with a diameter of 25 mm and the bar-shaped molds with dimensions of 10×40×20 mm (width×length×height) and then left in atmosphere for 15 minutes for expansion. In order to remove the remain H$_2$O$_2$, the foamed paste was kept at 60°C for 2 hours in a vacuum oven overnight. Afterwards, the green samples were demolded and heat-treated in a furnace.

Table 3.3 presented the experimental plan and sample names for the HA samples prepared via combination technique using PMMA granules and H$_2$O$_2$ solution. To investigate the effect of both PMMA content and H$_2$O$_2$ concentration, the mixture was prepared using PMMA granule at various contents (0, 5, 10, 20, 30, 40 and 50 wt%) and H$_2$O$_2$ solution at the different concentration (0, 5, 10, 20 and 30 wt%), with the L/P ratio of 1.3 ml./g.

Table 3.3   Experimental plan and sample names for the HA samples prepared via combination technique using PMMA granules and H$_2$O$_2$ solution

% PMMA Content (wt%)	% H$_2$O$_2$ Concentration (wt%)				L/P ratio (ml./g)
	5 wt%	10 wt%	20 wt%	30 wt%	
0	H05-P00-L13	H10-P00-L13	H20-P00-L13	H30-P00-L13	
5	H05-P05-L13	H10-P05-L13	H20-P05-L13	H30-P05-L13	
10	H05-P10-L13	H10-P10-L13	H20-P10-L13	H30-P10-L13	
20	H05-P20-L13	H10-P20-L13	H20-P20-L13	H30-P20-L13	1.3
30	H05-P30-L13	H10-P30-L13	H20-P30-L13	H30-P30-L13	
40	H05-P40-L13	H10-P40-L13	H20-P40-L13	H30-P40-L13	
50	H05-P50-L13	H10-P50-L13	H20-P50-L13	H30-P50-L13	

Note:
Hxx   was referred to the sample produced with the H$_2$O$_2$ concentration of xx wt%
Pyy   was referred to the sample produced with the PMMA content of xx wt%
Lzz   was referred to the sample produced with the L/P ratio of 1.3 or 1.5 ml/g
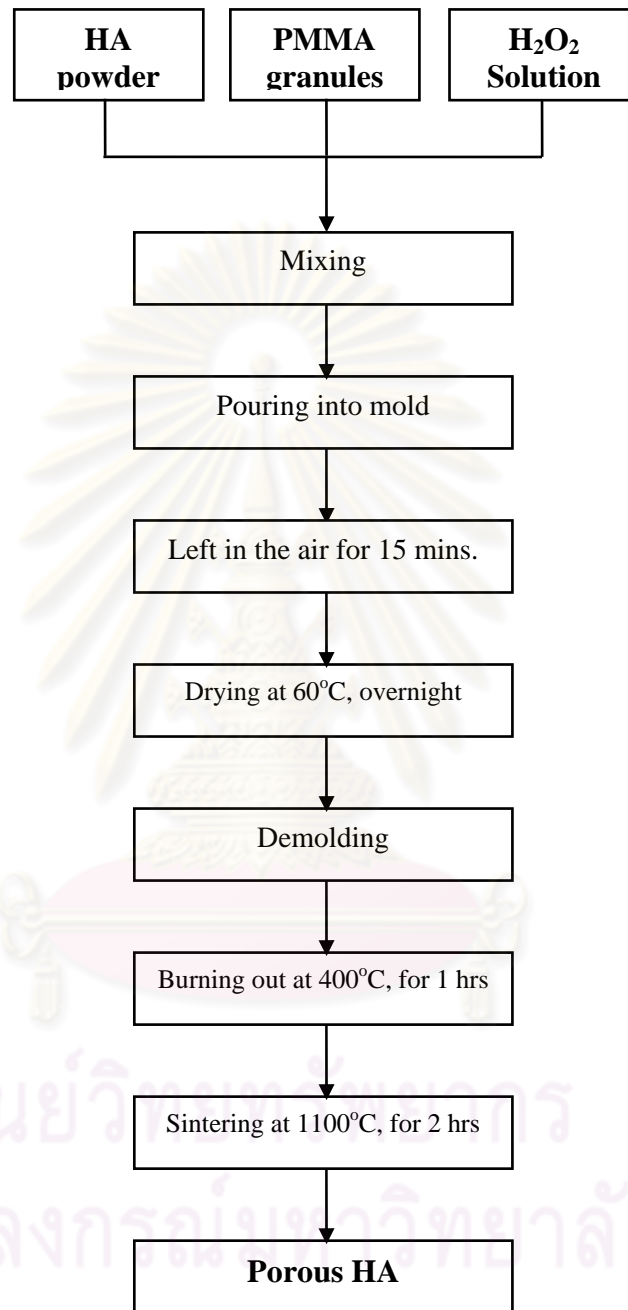
Figure 3.5   Flow chart of the preparation process of porous HA specimens via combination technique using PMMA granules and H_2O_2 solution

3.3 Fabrication of Porous Hydroxyapatite Samples with Surfactant

   To investigate the effect of addition of surfactant on the characteristics of porous HA, the food-grade agar powder (AGAR, Mermaid brand, Thailand) was selected as a surfactant. The fabrication procedures of the porous HA samples with surfactant via three pore forming techniques; including (1) sacrificial template using PMMA, (2) direct foaming using H_2O_2 and (3) combination technique using PMMA and H_2O_2 (combination between sacrificial template and direct foaming) were respectively explained.

3.3.1 Sacrificial Template Technique using PMMA

   Figure 3.6 presented the flow chart of the preparation process of porous HA via sacrificial template technique using PMMA granules with surfactant. To fabricate the porous samples through this technique, the HA powder was homogeneously mixed with PMMA granule and deionized water at the L/P ratio of 1.3 ml./g., as well as 1wt% agar powder. After mixing, the paste was placed into the removable cylindrical molds with a diameter of 25 mm and the bar-shaped molds with dimensions of 10×40×20 mm (width×length×height), and then kept at 60°C in a vacuum oven overnight. Afterwards, the green samples were removed from the mold and heat-treated in a furnace.

   Table 3.4 showed the experimental plan and sample names for the HA samples prepared via sacrificial template technique using PMMA granules with surfactant. To study the effect of PMMA content, the PMMA granule was varied with the content of 0, 5, 10, 20, 30, 40 and 50 wt%.
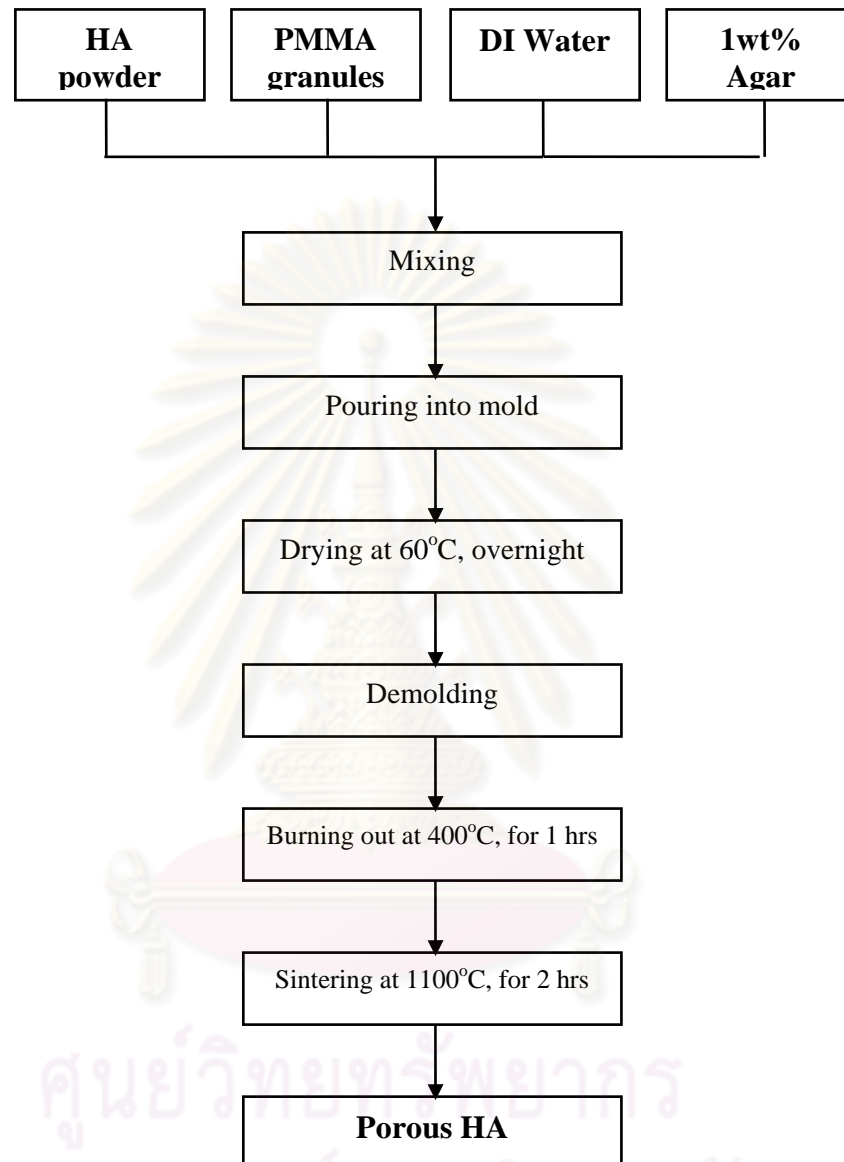
Figure 3.6   Flow chart of the preparation process of porous HA via sacrificial
             template technique using PMMA granules with surfactant

Table 3.4   Experimental plan and sample names for the HA samples prepared via
             sacrificial template technique using PMMA granules with surfactant

Sample Name	% PMMA content (wt%)	L/P ratio (ml/g.)	% Agar (wt%)
H00-P00-L13A	0		
H00-P05-L13A	5		
H00-P10-L13A	10		
H00-P20-L13A	20	1.3	1wt%
H00-P30-L13A	30		
H00-P40-L13A	40		
H00-P50-L13A	50		

Note:

Hxx   *was referred to the sample produced with the H_2O_2 concentration of xx wt%*
Pyy   *was referred to the sample produced with the PMMA content of xx wt%*
Lzz   *was referred to the sample produced with the L/P ratio of 1.3 or 1.5 ml/g*
A   *was referred to the sample produced with the addition of 1wt% agar*

3.3.2 Direct Foaming Technique using H_2O_2

Figure 3.7 illustrated the flow chart of the preparation process of porous HA via direct foaming technique using H_2O_2 solution with surfactant. The procedure began with the mixture of the HA powder and H_2O_2 solution at the L/P ratio of 1.3 ml./g., and then added 1wt% agar powder, followed by homogeneous stirring. After mixing, the paste was poured into the removable cylindrical molds and the bar-shaped molds and then left in atmosphere for 15 minutes for expansion. To dry the sample and remove the remaining H_2O_2, the foamed paste was kept at 60^oC in a vacuum oven overnight. Afterwards, the green samples were removed from the mold and heat-treated in a furnace.

Table 3.5 exhibited the experimental plan and sample names for the HA samples prepared via direct foaming technique using H_2O_2 solution with surfactant. To examine the effect of concentration of H_2O_2, the concentration was varied using 0, 1, 3, 5, 10, 20 and 30 wt% at the L/P ratio of 1.3 ml./g.

3.3.3 Combination Technique using PMMA and H_2O_2

Figure 3.8 displayed the flow chart of the preparation process of porous HA specimens via combination technique using PMMA granules and H_2O_2 solution with surfactant. The fabrication started with preparing the homogeneous mixture of the HA powder, PMMA granules, H_2O_2 solution and 1 wt% agar powder at the L/P ratio of 1.3 ml/g. After mixing, the paste was the paste was poured into the removable cylindrical molds and the bar-shaped molds and then left in atmosphere for 15 minutes for expansion. In order to remove the remain H_2O_2, the foamed paste was kept at 60^oC for 2 hours in a vacuum oven overnight. Afterwards, the green samples were demolded and heat-treated in a furnace.

Table 3.6 presented the experimental plan and sample names for the HA samples prepared via combination technique using PMMA granules and H_2O_2 solution with surfactant. To investigate the effect of both PMMA content and H_2O_2 concentration, the mixture was prepared using PMMA granule at various contents (0, 5, 10, 20, 30, 40 and 50 wt%) and H_2O_2 solution at the different concentration (0, 5, 10, 20 and 30 wt%), with the L/P ratio of 1.3 ml/g.

```
┌──────────┐  ┌──────────┐  ┌──────────┐
│   HA     │  │  H₂O₂    │  │  1wt%    │
│  powder  │  │ Solution │  │  Agar    │
└──────────┘  └──────────┘  └──────────┘
```

$$\text{HA powder} \qquad \text{H}_2\text{O}_2 \text{ Solution} \qquad \text{1wt\% Agar}$$

Mixing

Pouring into mold

Left in the air for 15 mins.

Drying at 60°C, overnight

Demolding

Sintering at 1100°C, for 2 hrs
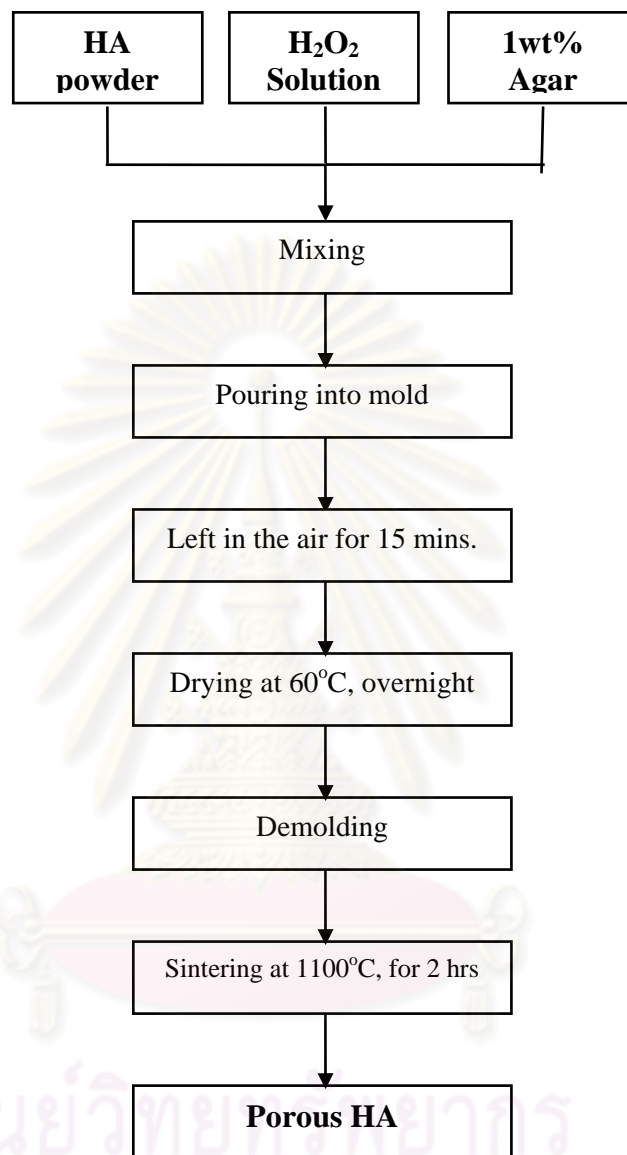
Porous HA

Figure 3.7   Flow chart of the preparation process of porous HA via direct

foaming technique using H_2O_2 solution with surfactant
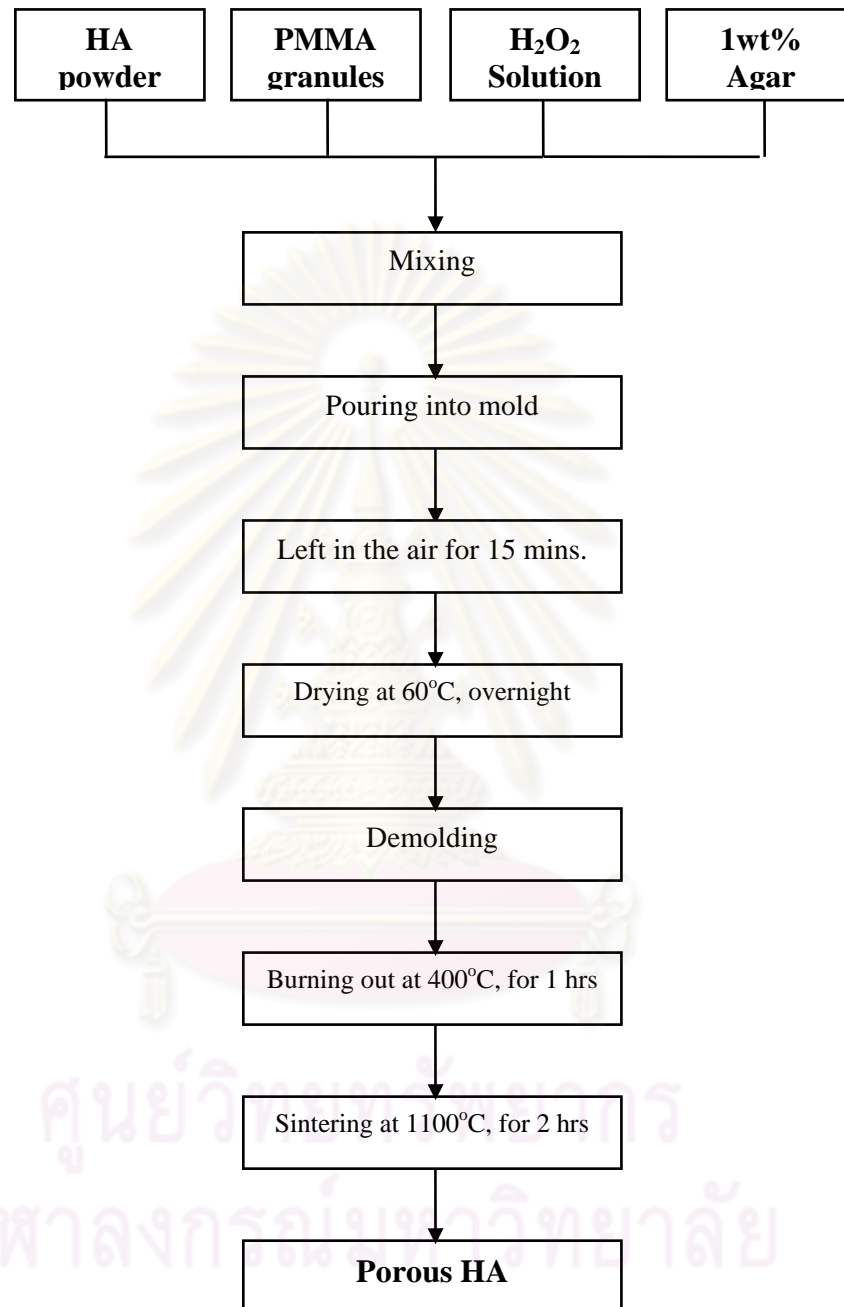
Figure 3.8   Flow chart of the preparation process of porous HA specimens via combination technique using PMMA granules and H_2O_2 solution with surfactant

Table 3.5   Experimental plan and sample names for the HA samples prepared via
direct foaming technique using H_2O_2 solution with surfactant.

Sample Name	% H_2O_2 concentration (wt%)	L/P ratio (ml/g.)	% Agar (wt%)
H01-P00-L13A	1		
H03-P00-L13A	3		
H05-P00-L13A	5		
H10-P00-L13A	10	1.3	1wt%
H20-P00-L13A	20		
H30-P00-L13A	30		

Note:

Hxx   *was referred to the sample produced with the H_2O_2 concentration of xx wt%*
Pyy   *was referred to the sample produced with the PMMA content of xx wt%*
Lzz   *was referred to the sample produced with the L/P ratio of 1.3 or 1.5 ml/g*
A   *was referred to the sample produced with the addition of 1wt% agar*

Table 3.6   Experimental plan and sample names for the HA samples prepared via
combination technique using PMMA granules and H_2O_2 solution with
surfactant

% PMMA Content (wt%)	% H_2O_2 Concentration (wt%)				L/P ratio (ml/g)	% Agar (wt%)
	5 wt%	10 wt%	20 wt%	30 wt%		
0	H05-P00-L13A	H10-P00-L13A	H20-P00-L13A	H30-P00-L13A		
5	H05-P05-L13A	H10-P05-L13A	H20-P05-L13A	H30-P05-L13A		
10	H05-P10-L13A	H10-P10-L13A	H20-P10-L13A	H30-P10-L13A		
20	H05-P20-L13A	H10-P20-L13A	H20-P20-L13A	H30-P20-L13A	1.3	1 wt%
30	H05-P30-L13A	H10-P30-L13A	H20-P30-L13A	H30-P30-L13A		
40	H05-P40-L13A	H10-P40-L13A	H20-P40-L13A	H30-P40-L13A		
50	H05-P50-L13A	H10-P50-L13A	H20-P50-L13A	H30-P50-L13A		

Note:

Hxx   *was referred to the sample produced with the H_2O_2 concentration of xx wt%*
Pyy   *was referred to the sample produced with the PMMA content of xx wt%*
Lzz   *was referred to the sample produced with the L/P ratio of 1.3 or 1.5 ml/g*
A   *was referred to the sample produced with the addition of 1wt% agar*

3.4 Heat Treatment

To find the suitable sintering temperature, the samples H10-P00-L13A, H10-P05-L13A, H10-P10-L13A and H10-P20-L13A were selected to be sintered at the various temperatures (at 1000^oC, 1050^oC and 1100^oC). Moreover, the effect of sintering temperature on porosity and mechanical properties of these samples was also investigated.

Figure 3.9 illustrated the heat treatment plan for the porous HA samples. After drying process, the dried samples were placed in the furnace and then heated at 400^oC for 1 hour with the slowly ramp rate of $1^oC/min$ to burn out the remaining PMMA granules and to avoid the cracking. Afterwards, the samples were sintered at 1100^oC for 2 hours with the ramp rate of $5^oC/min$ and then furnace cooled. The sintering temperature of 1100^oC, which was suitable for these porous HA samples, was obtained from the above experiment.
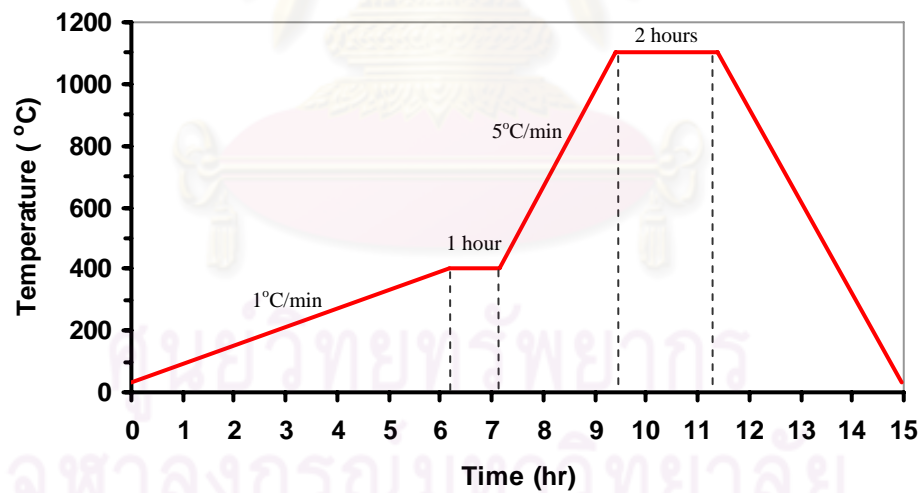
Figure 3.9   Heat treatment plan for the porous HA samples

3.5. Physical Characterization

3.5.1 Phase Purity Checking

To determine the phase purity of the synthesized HA, the sample powders were characterized on X-ray diffractometer (XRD), Fourier transform infrared spectrometer (FT-IR) and energy-dispersive X-ray analyzer (EDX).

(A) X-ray Diffraction (XRD)

The phase analysis of the synthesized HA powder sintered at $1100^{o}C$ for 2 hours was performed on X-ray diffractometer (XRD), using CuK_{α} radiation at a voltage of 40KV and a current of 40mA. The characterization procedures were based on ASTM F2024 (standard practice for X-ray diffraction determination of phase content of plasma-sprayed hydroxyapatite coating). To confirm the purity of the sample powder, the spectra of 3 samples were compared with the ICDD standard peak, according to ASTM F1185-03 (standard specification for composition of hydroxyapatite for surgical implants).

(B) Fourier transform infrared (FTIR)

To confirm the group of chemical component, the infrared spectrum of the sample powder was analyzed using Fourier transform infrared (FTIR) spectrometer. To prepare the specimen for FTIR analysis, a small amount of the sample powder was mixed with potassium bromide (KBr), which is transparent to infrared light, and then pressed into a thin coin which can be analyzed. The scanning was operated from 4000 to 400 cm^{-1}.

(C) Energy-dispersive X-ray (EDX)

The quantitative chemical composition of the sample powder was examined using energy dispersive X-ray (EDX) analyzer. This technique was used in a conjunction with scanning electron microscope (SEM). This analysis provides the composition of all elements detected in the sample. The composition of Ca and P elements measured from this analysis can be utilized for calculating the Ca/P molar ratio of the as-received HA powder.

3.5.2 Particle Size Analysis

The median particle size and particle size distribution of the sample powders, i.e. HA powders and PMMA granules, were assessed on laser particle size distribution analyzer using Malvern mastersizer S. Also, the Mastersizer software provided a series of particle sizes in diameter at the percentile of 0.1, 0.5 and 0.9. To confirm an accuracy of the measurement, the sample powders were characterized for 3 replications.

3.5.3 Thermogravimetric Analysis

To determine the decomposition temperature of the as-received PMMA granules, thermogravimetric analysis (TGA) was performed on simultaneous thermal analyzer (STA) with the heating rate of $10^{o}C/min$.

3.5.4 Microstructural Study

Scanning electron microscope (SEM) was employed to investigate the morphology of the powders and the microstructure of the porous samples. To perform the SEM analysis, the samples were prepared by coating with gold and then attached on a brass strut using a carbon adhesive tape. To avoid the discharge of electron on the surface of sample, the sample must be cleaned and dried before coating process and then kept in a closed container after coating process.

3.5.5 Bulk Density and Porosity

To calculate volume of the specimen, the dimensional measurements of the sintered HA specimens were performed by digital vernier caliper having an accuracy of 0.01 mm. Mass of the specimen was measured using digital weighing apparatus with an accuracy of 0.001 g. The volume and mass of the specimen were then used to calculate bulk density following in Equation 3.1. Additionally, porosity of the porous HA sample was determined using the bulk density of the sample and the theoretical density of hydroxyapatite (3.156 g/cm^3) as shown in Equation 3.2. (Hing *et al.*, 1999)

$$BD = \frac{M}{V} \tag{3.1}$$

$$P = \left(1 - \frac{BD}{D_{HA}}\right) \times 100\% \tag{3.2}$$

Where

BD	=	Bulk density (g/cm^3),
P	=	Porosity (%),
M	=	Mass (g),
V	=	Volume (cm^3), and
D_{HA}	=	Theoretical density of hydroxyapatite (3.156 g/cm^3).

3.6 Mechanical Characterization

To determine mechanical properties of the porous HA specimens, compressive and three point flexural tests were performed on multipurpose testing machine, SHIMADZU SERVOPULSER SFL 50kN. Compressive strength, flexural strength and stiffness were obtained from these following experiments.

3.6.1 Compressive Strength

Figure 3.10 exhibited the graphical schema of compressive test for the porous HA samples. In this study, the compressive test procedure was conducted according to ASTM C773-88 standard test method for compressive strength of ceramics. To prepare the test specimen, the sintered samples were machined to right cylinder and then cleaned by immersion in an ultrasonic bath filled with hot water and follow by drying at 90°C for 2 hours. The test started with placing the specimen carefully on the center between pressing and bearing plates, and then loading the specimen continuously until ultimate failure without impact shock, with the cross head speed of 2.5 mm/minute. The compressive strength of each specimen can be calculated as follows:

$$CS = \frac{P}{A} \times 10^6 \tag{3.3}$$

Where

CS =   Compressive strength of the specimen (Pa)

P =   Load on the specimen at failure (N)

A =   Cross sectional area of the bearing surface of the specimen (mm^2)
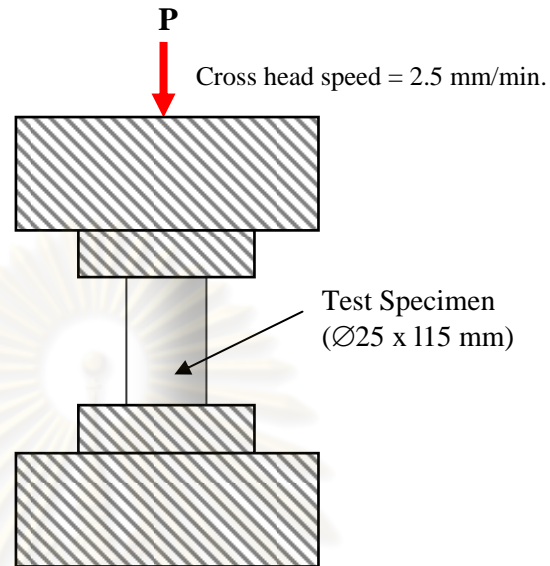
Figure 3.10   Graphical schema of compressive test for the porous HA samples
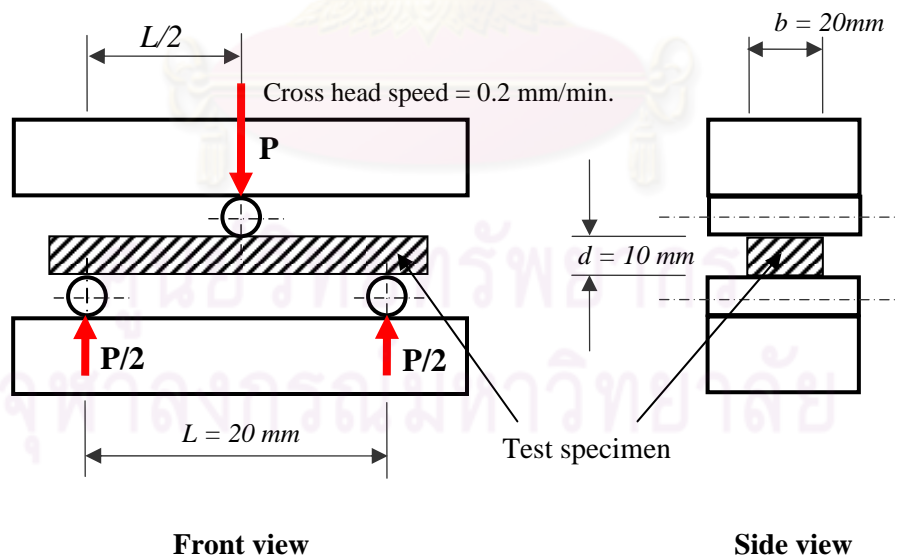
Figure 3.11   Graphical schema of three-point flexural test for the porous HA
                samples

3.6.2 Flexural Strength

Figure 3.11 illustrated graphical schema of three-point flexural test for the porous HA samples. In this work, three-point flexural test was carried out, following the standard test method of ASTM C1161-02c for ceramics at ambient temperature. The specimen was prepared into right dimension bar and then cleaned by immersion in an ultrasonic bath filled with hot water and follow by drying at 90°C for 2 hours. The test began with placing the specimen carefully on the center of the support span to preclude the possible damage and to ensure alignment of the specimen, and then slowly applying the load to the fixture until failure, with the cross head speed rate of 0.2 mm/minute. The flexural strength of the sample bar is as follows;

$$FS = \frac{3PL}{2bd^2} \times 10^6 \qquad\qquad (3.4)$$

Where

FS	=	Three-point flexural strength (Pa)
P	=	Load on the specimen at failure (N)
L	=	Long support span (mm)
b	=	Specimen width (mm)
d	=	Specimen thickness (mm)

3.6.3 Stiffness

Stiffness is a measure of the resistance of the materials offered by an elastic body to deformation. From the compressive and flexural tests, both compressive stiffness (E_C) and flexural stiffness (E_F) were obtained. The calculation formula for compressive stiffness is defined as;

$$E_C = \frac{P}{A.\varepsilon} \times 10^6 \qquad (3.4)$$

Where

E_C	=	Compressive Stiffness (N/m^2)
P	=	Load on the specimen at failure (N)
A	=	Cross sectional area of the specimen (mm^2)
ε	=	Compressive strain (mm/mm) = $\Delta l / l$
Δl	=	Displacement produced by the load (mm)
l	=	Height of the spherical specimen (mm)

And the calculation formula for flexural stiffness is as follows;

$$E_F = \frac{P}{y}\left(\frac{L^3}{4bd^3}\right) \times 10^6 \qquad (3.5)$$

Where

E_F	=	Flexural Stiffness (N/m^2)
P	=	Load on the specimen at failure (N)
y	=	Deflection due to the load P (mm)
L	=	Long support span (mm)
b	=	Specimen width (mm)
d	=	Specimen thickness (mm)

3.7 Statistical Analysis

3.7.1 Analysis of Variance

Analysis of variance (ANOVA) was performed to confirm the effect of fabrication factors on the responses of the porous HA samples prepared through (1) sacrificial template using PMMA, (2) direct foaming using H_2O_2 and (3) combination technique using PMMA and H_2O_2.

Table 3.7 listed the factors and responses of ANOVA test for porous HA samples prepared through various methods. Significant level (α) was set to be 0.05 due to a small sample size following upon previous research. Most importantly, the test was significant unless the P-value was over the significant level.

Table 3.7   Factors and responses of ANOVA test for porous HA samples prepared
            through various methods.

Factors	Responses

(1) Sacrificial template using PMMA
    1. PMMA content (C_P)
    2. L/P ratio (LP)
    3. Addition of agar
	1. Bulk density (BD)

(2) Direct foaming using H_2O_2
    1. H_2O_2 concentration (C_H)
    2. L/P ratio (LP)
    3. Addition of agar
	2. Porosity (P)
	
	3. Compressive strength (CS)
	
	4. Flexural strength (FS)

(3) Combination technique using PMMA and H_2O_2
    1. PMMA content (C_P)
    2. H_2O_2 concentration (C_H)
    3. Addition of agar
	5. Compressive stiffness (E_C)
	
	6. Flexural stiffness (E_F)

(4) Sintering temperature	

3.7.2 Regression Analysis

The experimental results were used to generate regression model to predict the responses, including porosity and mechanical strength. Moreover, analysis of variance (ANOVA) was carried out to investigate the significance of the model and R-square value of regression was also indicated by using significant level (α) of 0.05.

CHAPTER IV

EXPERIMENTAL RESULTS

This chapter described the experimental results of produced powder and porous hydroxyapatite ceramics, such as phase purity, particle size distribution, thermogravimetric analysis, microstructure, bulk density, porosity, and mechanical properties. The phase purity of HA powder analyzed using XRD, FTIR and EDX were reported. Particle size distributions and mean particle sizes of the HA powder and PMMA granules were explained. The TGA curve of PMMA granules was demonstrated. The SEM micrographs of HA particle, PMMA granules and some porous HA samples were investigated. Additionally, bulk density and porosity of the porous HA samples were summarized. Finally, compressive strength, flexural strength and its stiffness of the porous HA samples were represented.

4.1 Characteristics of the PMMA Granule

4.1.1 Particle Size Distribution

Figure 4.1 exhibited particle size distribution of the commercial PMMA granules. The distribution of the PMMA granules was a unimodal distribution with a peak of around 150 μm in particle size.

Table 4.1 summarized average and standard deviation of mean particle size of the PMMA granules. The average and standard deviation of median particle sizes (at d(0.5)) of the PMMA granules were 150.75±0.15 μm.

4.1.2 Thermogravimetric Curve

Figure 4.2 illustrated the TGA curve of the commercial PMMA granules. The weight of PMMA reduced gradually until the temperature of around $250^{o}C$ and then dropped rapidly. The PMMA granules have been completely decomposed at about $400^{o}C$, at which a stable weight was attained.
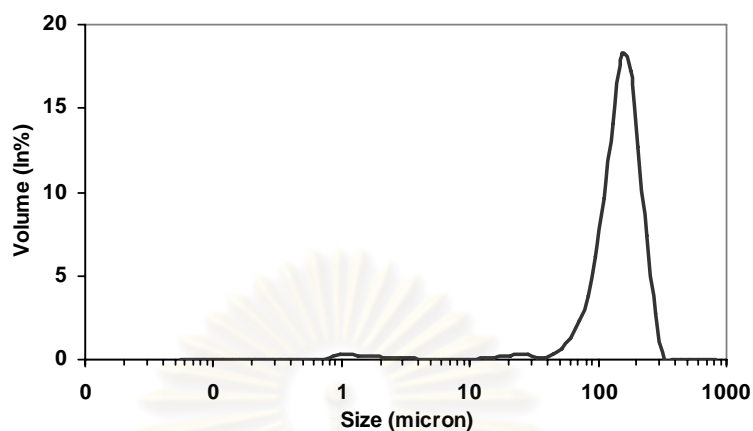
Figure 4.1   Particle size distribution of the commercial PMMA granules

Table 4.1   Average and standard deviation of particle sizes of the PMMA granules

Sample	Particle size (μm)		
	(d0.1)	(d0.5)	(d0.9)
PMMA granule			
Sample 1	82.96	150.92	222.83
Sample 2	82.42	150.65	223.49
Sample 3	82.69	150.69	222.53
Average ± SD	82.69 ± 0.27	150.75 ± 0.15	222.95 ± 0.49

Note: d0.1 was referred to the measured particle size of diameter at 10vol% of the particles
d0.5 was referred to the measured particle size of diameter at 50vol% of the particles
d0.9 was referred to the measured particle size of diameter at 90vol% of the particles
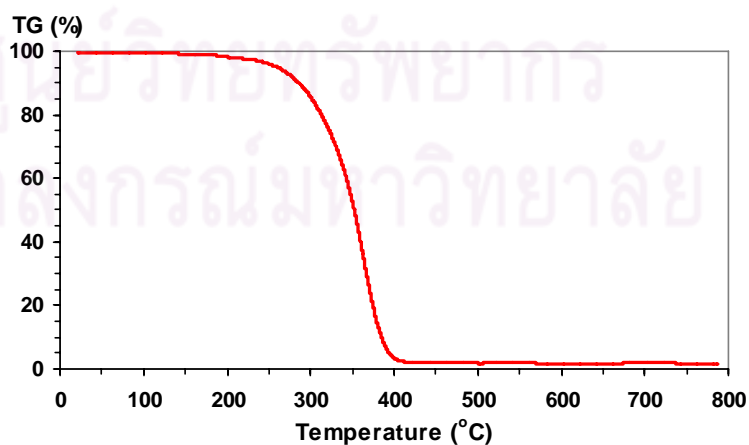
Figure 4.2   TGA curve of the commercial PMMA granules

4.1.3 Microstructure and Morphology

Figure 4.3 exhibited the SEM micrographs of the commercial PMMA granules at the magnification of (a) 100X, (b) 500X and (c) 800X. In Figure 4.9 (a), the particle of the PMMA granules had a spherical shape with various particle sizes. In Figure 4.9 (b), the large particle size was about 150 μm in diameter. In Figure 4.9 (c), the small particle size was approximately less than 50 μm in diameter. Moreover, surface of the PMMA granule was nearly smooth.
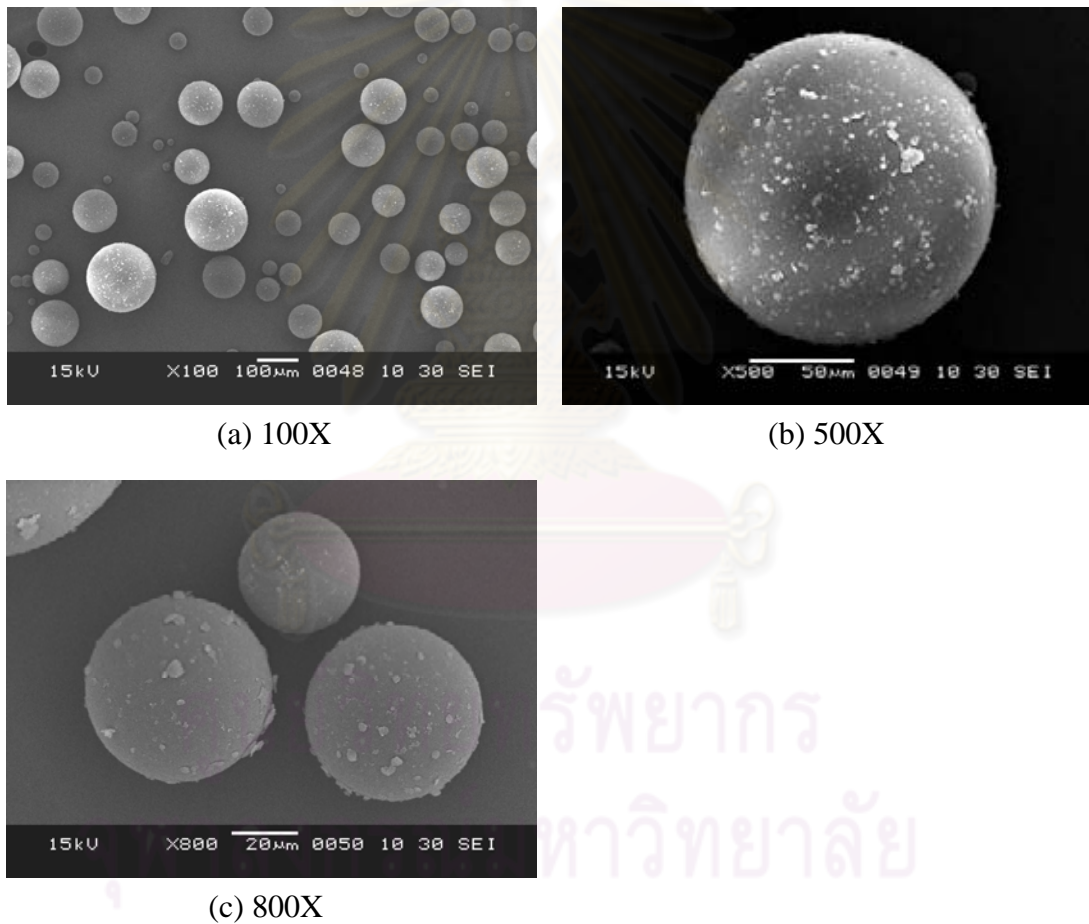
(a) 100X

(b) 500X

(c) 800X

Figure 4.3   SEM micrographs of the commercial PMMA granules at the
magnification of (a) 100X, (b) 500X and (c) 800X

4.2 Characteristics of the HA Powder

4.2.1 Phase Purity

(A) X-ray Diffraction (XRD)

Figure 4.4 displayed the XRD spectrum of the synthesized HA powder sintered at 1100^oC for 2 hours. The spectrum consisted of series of sharp and narrow diffraction peaks. According to ASTM F1185-03, the spectrum showed a single phase of HA, matching with ICDD standard peak of stoichiometric hydroxyapatite (standard No.09-0432).

(B) Fourier Transform Infrared (FTIR)

Figure 4.5 showed the FTIR spectrum of the synthesized HA powder. The spectrum was composed of water groups (H_2O), phosphate groups (PO_4^{3-}) and hydroxyl group (OH^-). The PO_4^{3-} groups was found at 564, 603 and 1034 cm^{-1}. While the OH^- groups was at 3570 and 630 cm^{-1}. Additionally, the H_2O groups were detected at 3420 and near 1640 cm^{-1}.

(C) Energy Dispersive X-ray (EDX)

Figure 4.6 illustrated the EDX spectrum of the synthesized HA powder sintered at 1100^oC for 2 hours. The spectrum was comprised of the desirable elements of Ca, P and O and other elements of C and Au. However, hydrogen (H) element can not be detected.

Table 4.2 listed the elemental compositions of the synthesized HA powder sintered at 1100^oC for 2 hours in term of weight and atomic percentage. The weight percentage of the O, P and Ca elements were 50.84%, 15.64% and 33.52%, respectively. While the atomic percentage of the O, P and Ca elements were 70.32%, 11.18% and 18.50%, respectively. Consequently, Ca/P atomic ratio of the HA powder was approximately 1.66 (= 18.50/11.18).
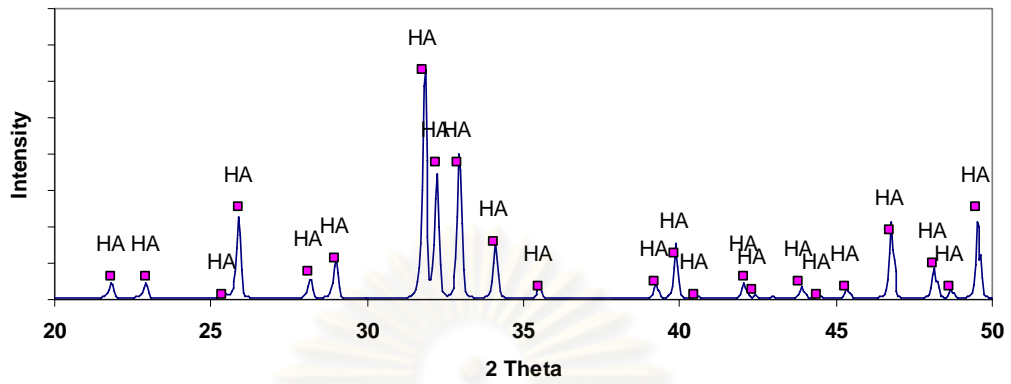
Figure 4.4   XRD spectrum of the synthesized HA powder sintered at 1100°C for
2 hours
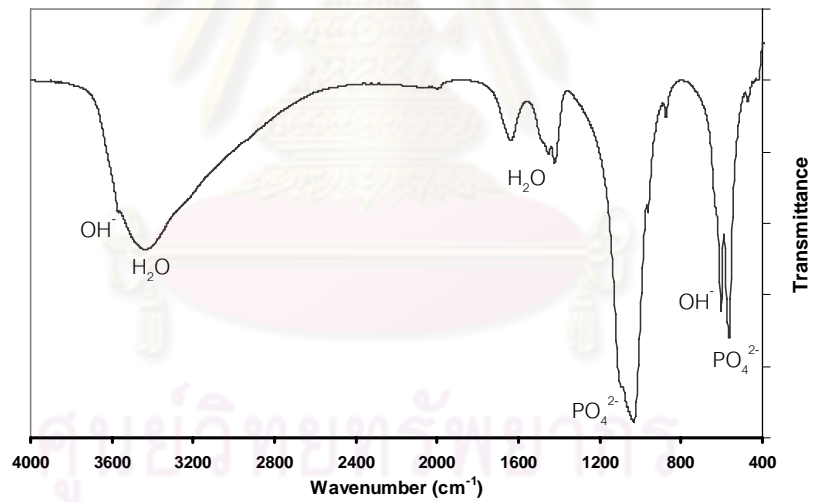
Figure 4.5   FTIR spectrum of the synthesized HA powder
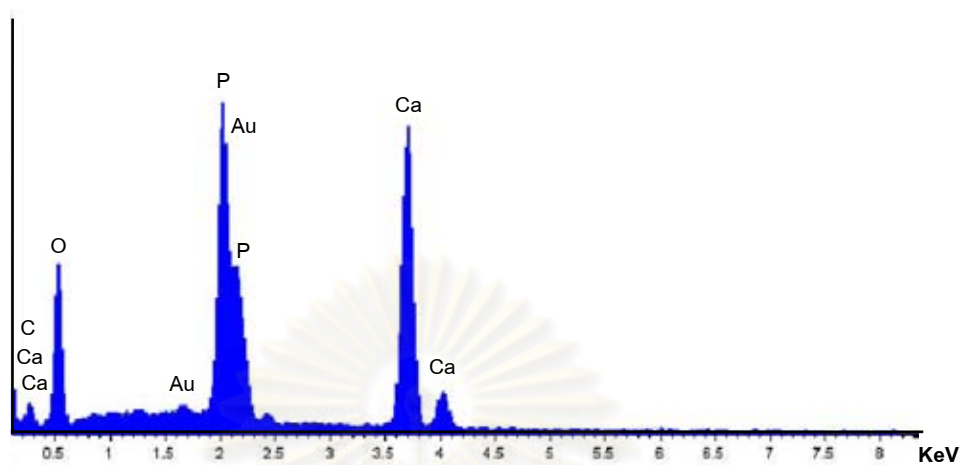
Figure 4.6   EDX spectrum of the synthesized HA powder sintered at 1100°C for 2 hours

Table 4.2   Elemental compositions of the synthesized HA powder

Element	Weight %	Atomic %
O	50.84	70.32
P	15.64	11.18
Ca	33.52	18.50
Total	100.00	100.00

4.2.2 Particle Size Distribution

        Figure 4.7 showed the particle size distribution of the synthesized HA powder. The distribution of the HA powder was a bimodal distribution with the peaks of approximately 4 μm and 20 μm in particle size.

        Table 4.3 summarized the average and standard deviation of mean particle sizes of the HA powders. The average and standard deviation of median particle size (at d(0.5)) of the HA powders was 4.97±0.03 μm.
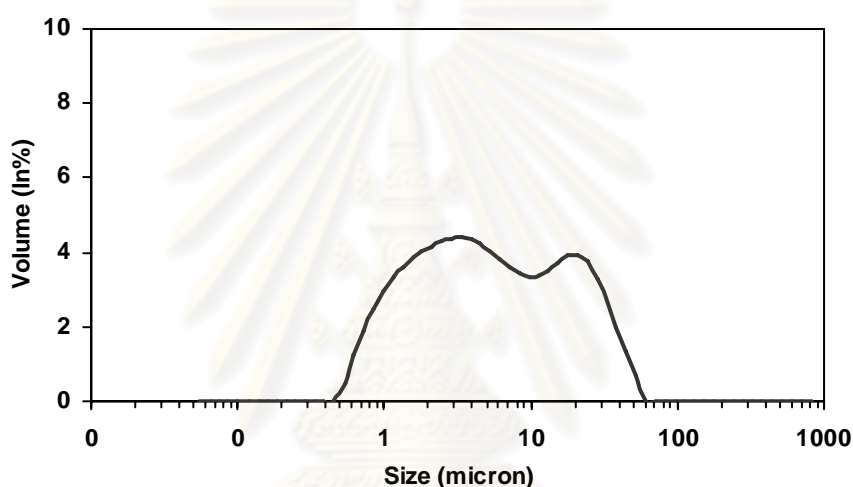
Figure 4.7   Particle size distribution of the synthesized HA powder

Table 4.3   Average and standard deviation of particle sizes of the HA powders

Sample	Particle size (μm)		
	(d0.1)	(d0.5)	(d0.9)
HA powder			
Sample 1	1.11	4.95	26.16
Sample 2	1.12	4.96	26.25
Sample 3	1.12	5.01	26.53
Average ± SD	1.12 ± 0.01	4.97 ± 0.03	26.31 ± 0.19

Note: d0.1 was referred to the measured particle size of diameter at 10vol% of the particles
*   d0.5 was referred to the measured particle size of diameter at 50vol% of the particles*
*   d0.9 was referred to the measured particle size of diameter at 90vol% of the particles*

4.2.3 Microstructure and Morphology

Figure 4.8 presented SEM micrographs of the synthesized HA powder before sintering at the magnifications of (a) 500X, (b) 2,500X and (c) 10,000X. In Figure 4.7 (a), the non-sintered HA powder had various particle sizes. In Figure 4.7 (b), the particle had an angular shape. In Figure 4.7 (c), the particle had a rough surface with some small particles attached.
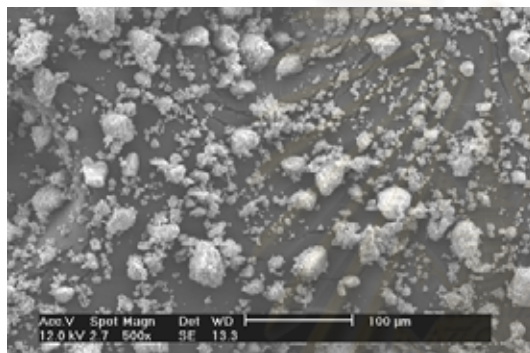
(a) 500X
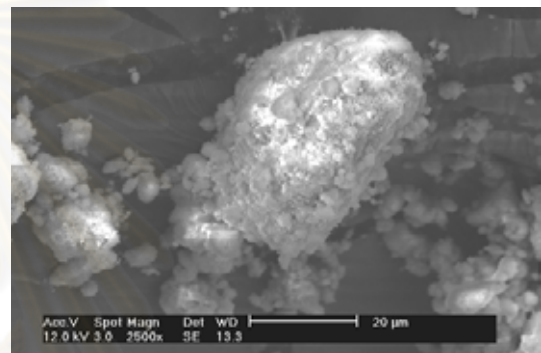
(b) 2,500X

(c) 10,000X

Figure 4.8   SEM micrographs of the synthesized HA powder before sintering at
                the magnifications of (a) 500X, (b) 2,500X and (c) 10,000X

Figure 4.9 illustrated SEM micrographs of the synthesized HA powder after sintering at 1100°C for 2 hr at the magnifications of (a) 500X, (b) 2,000X and (c) 10,000 X. In Figure 4.8 (a), the sintered HA powder had a wide range of particle size. In Figure 4.8 (b), shape of the sintered HA particle was also angular. In Figure 4.8 (c), the surface of the sintered HA particle was coarser than that of the non-sintered particle. Additionally, a large amount of smaller particles attached on the surface.

(a) 500X
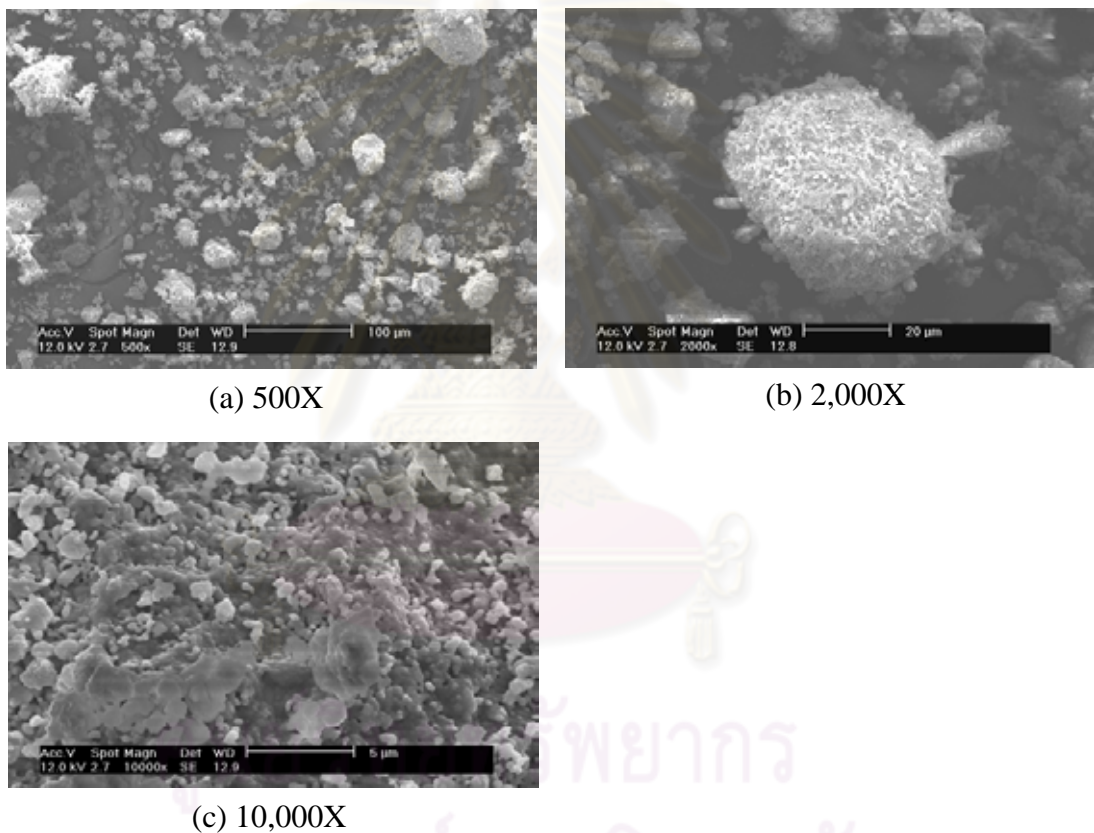
(b) 2,000X

(c) 10,000X

Figure 4.9   SEM micrographs of the synthesized HA powder after sintering at 1100°C for 2 hours at the magnifications of (a) 500X, (b) 2,000X and (c) 10,000 X

4.3 Selected Sintering Temperature

4.3.1 Bulk Density and Porosity

Table 4.4 summarized bulk density and porosity of the HA samples sintered at various temperatures. These porous HA samples were prepared through combination technique using PMMA and H_2O_2. At 1000°C, these porous samples showed the density ranging from 0.27 to 0.46 g/cm^3 and porosity ranging from 85.58% to 91.36%. At 1050°C, these samples had the density ranging between 0.29 and 0.62 g/cm^3 and porosity ranging between 80.47% and 90.74%. At 1100°C, all samples showed the density ranging from 0.42 to 0.59 g/cm^3 and porosity ranging from 81.35% to 86.55%.

Figure 4.10 illustrated the relationship between bulk density (BD) and PMMA content at L/P ratio of 1.3 ml/g with various sintering temperature of the porous HA samples from Table 4.9. At 1000°C, bulk density of these samples reduced with an increasing content of PMMA. At 1050°C, bulk density dropped until the PMMA content attained 10wt% and then unchanged. At 1100°C, bulk density was decreased slightly when PMMA content increased. The trend line of the sample sintering at 1100°C was over those sintering at 1050°C and 1000°C, respectively.

Figure 4.11 presented the relationship between porosity and PMMA content at L/P ratio of 1.3 ml/g with various sintering temperature of the porous HA samples from Table 4.9. At 1000°C, porosity of these samples raised from approximately 85% to 90% until the PMMA content was 10wt% and then increased slightly. At 1050°C, porosity also rose from ~82% to ~90% until the PMMA content was 10wt% and then was stable. At 1100°C, porosity was increased from about 82% to 85% and then increased slightly when the PMMA content was over 5wt%.

Table 4.4   Bulk density and porosity of the HA samples sintered at various
            temperatures

Sample	Bulk Density				Porosity			
	#	(g/cm³)	Average	SD	#	(%)	Average	SD
1000ºC								
H10-P00-L13A	1	0.46	**0.45**	0.01	1	85.58	**85.81**	0.33
	2	0.44			2	86.04		
H10-P05-L13A	1	0.40	**0.41**	0.02	1	87.48	**87.10**	0.54
	2	0.42			2	86.72		
H10-P10-L13A	1	0.33	**0.31**	0.03	1	89.43	**90.12**	0.98
	2	0.29			2	90.82		
H10-P20-L13A	1	0.27	**0.27**	0.00	1	91.36	**91.37**	0.01
	2	0.27			2	91.38		
1050ºC								
H10-P00-L13A	1	0.62	**0.58**	0.06	1	80.47	**81.78**	1.86
	2	0.53			2	83.09		
H10-P05-L13A	1	0.45	**0.46**	0.01	1	85.71	**85.54**	0.25
	2	0.46			2	85.36		
H10-P10-L13A	1	0.29	**0.33**	0.05	1	90.76	**89.56**	1.70
	2	0.37			2	88.36		
H10-P20-L13A	1	0.33	**0.33**	0.00	1	89.54	**89.44**	0.14
	2	0.34			2	89.34		
1100ºC								
H10-P00-L13A	1	0.57	**0.58**	0.01	1	81.94	**81.64**	0.42
	2	0.59			2	81.35		
H10-P05-L13A	1	0.50	**0.48**	0.03	1	84.23	**84.84**	0.87
	2	0.46			2	85.45		
H10-P10-L13A	1	0.46	**0.45**	0.01	1	85.54	**85.78**	0.33
	2	0.44			2	86.01		
H10-P20-L13A	1	0.44	**0.43**	0.01	1	86.12	**86.34**	0.30
	2	0.42			2	86.55		

Figure 4.10   Relationship between bulk density (BD) and PMMA content at L/P
                ratio of 1.3 ml/g with various sintering temperature of the porous HA
                samples H10-Pyy-L13A
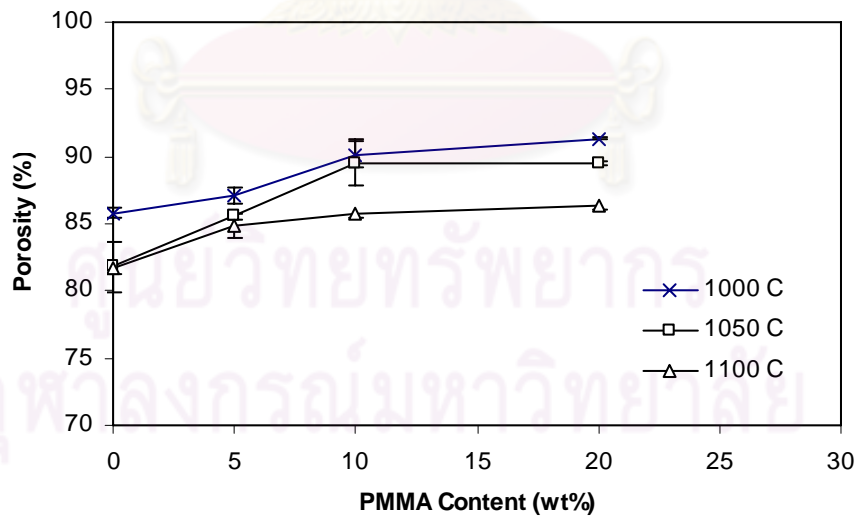
Figure 4.11   Relationship between porosity and PMMA content at L/P ratio of 1.3
                ml/g with various sintering temperature of the porous HA samples
                H10-Pyy-L13A

4.3.2 Mechanical Properties

Table 4.5 summarized the compressive strength and flexural strength of the HA samples sintered at various temperatures (i.e. 1,000^{o}C, 1,050^{o}C and 1,100^{o}C). At the sintering temperature of 1,000^{o}C, the highest compressive and flexural strengths were 0.13 MPa and 0.46 MPa, respectively, while the lowest strengths were 0.02 MPa and 0.10 MPa, respectively. At the temperature of 1,050^{o}C, the highest compressive strength increased to be 0.25 MPa and the highest flexural strength rose to be 0.56 MPa, whereas the lowest compressive and flexural strengths were slightly improved to be 0.03 MPa and 0.15 MPa, respectively. At the temperature of 1,100^{o}C, the highest compressive and flexural strengths were developed to be 0.50 MPa and 0.70 MPa, respectively, whilst the lowest compressive and flexural strengths were 0.06 MPa and 0.21 MPa, respectively.

Figure 4.12 displayed the relationship between compressive strength (CS) and PMMA content at L/P ratio of 1.3 ml/g with various sintering temperature of the porous HA samples H10-Pyy-L13A from Table 4.22. Obviously, an increase in sintering temperature improved the compressive strength of the samples. The samples sintering at 1100°C showed a distinct compressive strength over the other samples. Moreover, the compressive strength also showed a decrease as the PMMA content increased at all sintering temperatures.

Figure 4.13 depicted the relationship between flexural strength (FS) and PMMA content at L/P ratio of 1.3 ml/g with various sintering temperature of the porous HA samples H10-Pyy-L13A from Table 4.22. Seemingly, the flexural strength was increased when the sintering temperature rose. Furthermore, the flexural strength also decreased with an increasing content of PMMA at every sintering temperature.

Table 4.5   Compressive strength and flexural strength of the HA samples sintered at various temperatures

Sample	Compressive strength				Flexural strength			
	#	(MPa)	Average	SD	#	(MPa)	Average	SD
1000°C								
H10-P00-L13A	1	0.13	**0.12**	0.01	1	0.40	**0.43**	0.04
	2	0.11			2	0.46		
H10-P05-L13A	1	0.07	**0.07**	0.01	1	0.28	**0.28**	0.01
	2	0.08			2	0.29		
H10-P10-L13A	1	0.06	**0.05**	0.01	1	0.23	**0.24**	0.01
	2	0.05			2	0.24		
H10-P20-L13A	1	0.03	**0.02**	0.01	1	0.15	**0.13**	0.04
	2	0.02			2	0.10		
1050°C								
H10-P00-L13A	1	0.25	**0.20**	0.08	1	0.56	**0.52**	0.06
	2	0.14			2	0.48		
H10-P05-L13A	1	0.12	**0.13**	0.01	1	0.42	**0.41**	0.01
	2	0.14			2	0.40		
H10-P10-L13A	1	0.05	**0.06**	0.03	1	0.28	**0.31**	0.05
	2	0.08			2	0.35		
H10-P20-L13A	1	0.03	**0.03**	0.01	1	0.15	**0.17**	0.02
	2	0.04			2	0.18		
1100°C								
H10-P00-L13A	1	0.46	**0.48**	0.03	1	0.70	**0.67**	0.04
	2	0.50			2	0.64		
H10-P05-L13A	1	0.37	**0.35**	0.04	1	0.51	**0.49**	0.03
	2	0.32			2	0.47		
H10-P10-L13A	1	0.25	**0.22**	0.05	1	0.31	**0.34**	0.05
	2	0.19			2	0.38		
H10-P20-L13A	1	0.06	**0.06**	0.00	1	0.21	**0.24**	0.04
	2	0.06			2	0.26		

Figure 4.12   Relationship between compressive strength (CS) and PMMA content
at L/P ratio of 1.3 ml/g with various sintering temperature of the
porous HA samples H10-Pyy-L13A
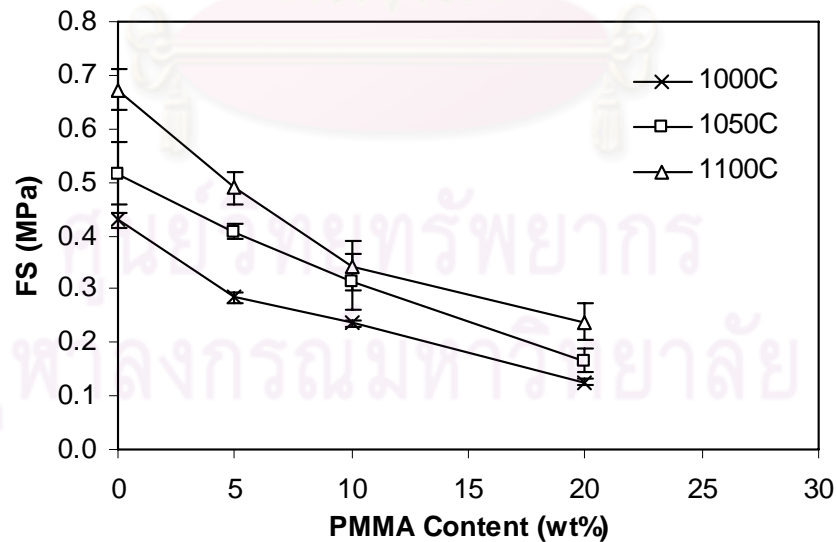
Figure 4.13   Relationship between flexural strength (FS) and PMMA content at
L/P ratio of 1.3 ml/g with various sintering temperature of the porous
HA samples H10-Pyy-L13A

Table 4.6 presented the compressive stiffness and flexural stiffness of the HA samples sintered at various temperatures (i.e. 1,000^{o}C, 1,050^{o}C and 1,100^{o}C). At the temperature of 1,000^{o}C, the compressive stiffness ranged from 21.33 to 81.60 kN/m^2, while the flexural stiffness ranged from 0.02 to 4.62 MN/m^2. At 1,050^{o}C, the compressive stiffness ranged between 34.08 and 122.05 kN/m^2, whilst the flexural stiffness ranged between 0.27 and 16.13 MN/m^2. At 1,100^{o}C, the compressive stiffness ranged from 54.01 to 464.94 kN/m^2, whereas the flexural stiffness ranged from 0.50 to 27.06 MN/m^2.

Figure 4.14 illustrated the relationship between compressive stiffness (E$_C$) and PMMA content at L/P ratio of 1.3 ml/g with various sintering temperature of the porous HA samples H10-Pyy-L13A from Table 4.23. Apparently, an increasing sintering temperature produced an increase in compressive stiffness. However, the compressive stiffness reduced with an increase of the PMMA content at all sintering temperatures.

Figure 4.15 showed the relationship between flexural stiffness (E$_F$) and PMMA content at L/P ratio of 1.3 ml/g with various sintering temperature of the porous HA samples H10-Pyy-L13A from Table 4.23. Supposedly, flexural stiffness showed an increase as the sintering temperature elevated. Moreover, the flexural stiffness reduced with an increasing content of PMMA at every sintering temperature.

Table 4.6　　Compressive stiffness and flexural stiffness of the HA samples sintered at various temperatures

Sample	Compressive stiffness				Flexural stiffness			
	#	(kN/m^2)	Average	SD	#	(MN/m^2)	Average	SD
1000°C								
H10-P00-L13A	1	83.32	**81.60**	2.44	1	4.56	**4.62**	0.08
	2	79.87			2	4.68		
H10-P05-L13A	1	50.68	**53.63**	4.17	1	0.17	**0.21**	0.06
	2	56.59			2	0.25		
H10-P10-L13A	1	49.65	**45.53**	5.83	1	0.19	**0.12**	0.10
	2	41.41			2	0.06		
H10-P20-L13A	1	26.85	**21.33**	7.80	1	0.03	**0.02**	0.00
	2	15.81			2	0.02		
1050°C								
H10-P00-L13A	1	185.33	**122.05**	89.50	1	19.56	**16.13**	4.85
	2	58.76			2	12.70		
H10-P05-L13A	1	70.16	**82.58**	17.55	1	4.18	**4.17**	0.02
	2	94.99			2	4.16		
H10-P10-L13A	1	47.39	**66.34**	26.80	1	0.39	**0.38**	0.01
	2	85.29			2	0.37		
H10-P20-L13A	1	21.72	**34.08**	17.49	1	0.36	**0.27**	0.13
	2	46.45			2	0.18		
1100°C								
H10-P00-L13A	1	383.10	**464.94**	115.73	1	34.96	**27.06**	11.18
	2	546.77			2	19.15		
H10-P05-L13A	1	195.55	**183.42**	17.15	1	8.86	**7.69**	1.65
	2	171.29			2	6.53		
H10-P10-L13A	1	138.20	**130.35**	11.10	1	2.34	**2.46**	0.17
	2	122.51			2	2.58		
H10-P20-L13A	1	72.11	**54.01**	25.59	1	0.56	**0.50**	0.08
	2	35.91			2	0.44		

Figure 4.14   Relationship between compressive stiffness (E_C) and PMMA content
               at L/P ratio of 1.3 ml/g with various sintering temperature of the
               porous HA samples H10-Pyy-L13A
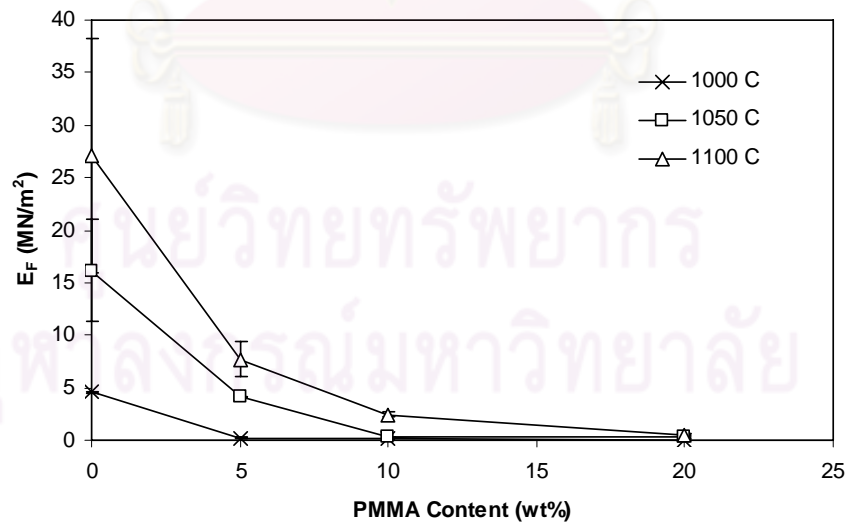
Figure 4.15   Relationship between flexural stiffness (E_F) and PMMA content at
               L/P ratio of 1.3 ml/g with various sintering temperature of the porous
               HA samples H10-Pyy-L13A

4.4 Characteristics of the Porous HA Samples

4.4.1 Microstructure

In this section, microstructure of the HA samples without surfactant, prepared by H_2O based technique, sacrificial template using PMMA, direct foaming using H_2O_2 and combination technique using PMMA and H_2O_2, were thoroughly explained.

(A) H_2O based Technique

Figure 4.16 showed the SEM micrographs of the HA sample H00-P00-L13 at the magnification of (a) 100X, (b) 500X, (c) 2,500X and (d) 5,000X. The HA sample H00-P00-L13 was prepared using 0wt% H_2O_2 and 0wt% PMMA at the L/P ratio of 1.3 ml/g. In Figure 4.16 (a) and (b), a small amount of pores with an average pore size of less than 50 μm were found. In Figure 4.16 (c), the pore had an irregular shape. In Figure 4.16 (d), the surface was densely smooth without any pores.

Figure 4.17 illustrated the SEM micrographs of the HA sample H00-P00-L15 at the magnification of (a) 100X, (b) 500X, (c) 2,500X and (d) 5,000X. The HA sample H00-P00-L15 was prepared using 0wt% H_2O_2 and 0wt% PMMA at the L/P ratio of 1.5 ml/g. In Figure 4.17 (a) and (b), a large number of small pores were investigated. The pore size was approximately less than 50 μm. In Figure 4.17 (c), the pore shape was also irregular. In Figure 4.17 (d), the sample had rough surface and a lot of tiny pores, less than 5 μm.

(a) 100X

(b) 500X
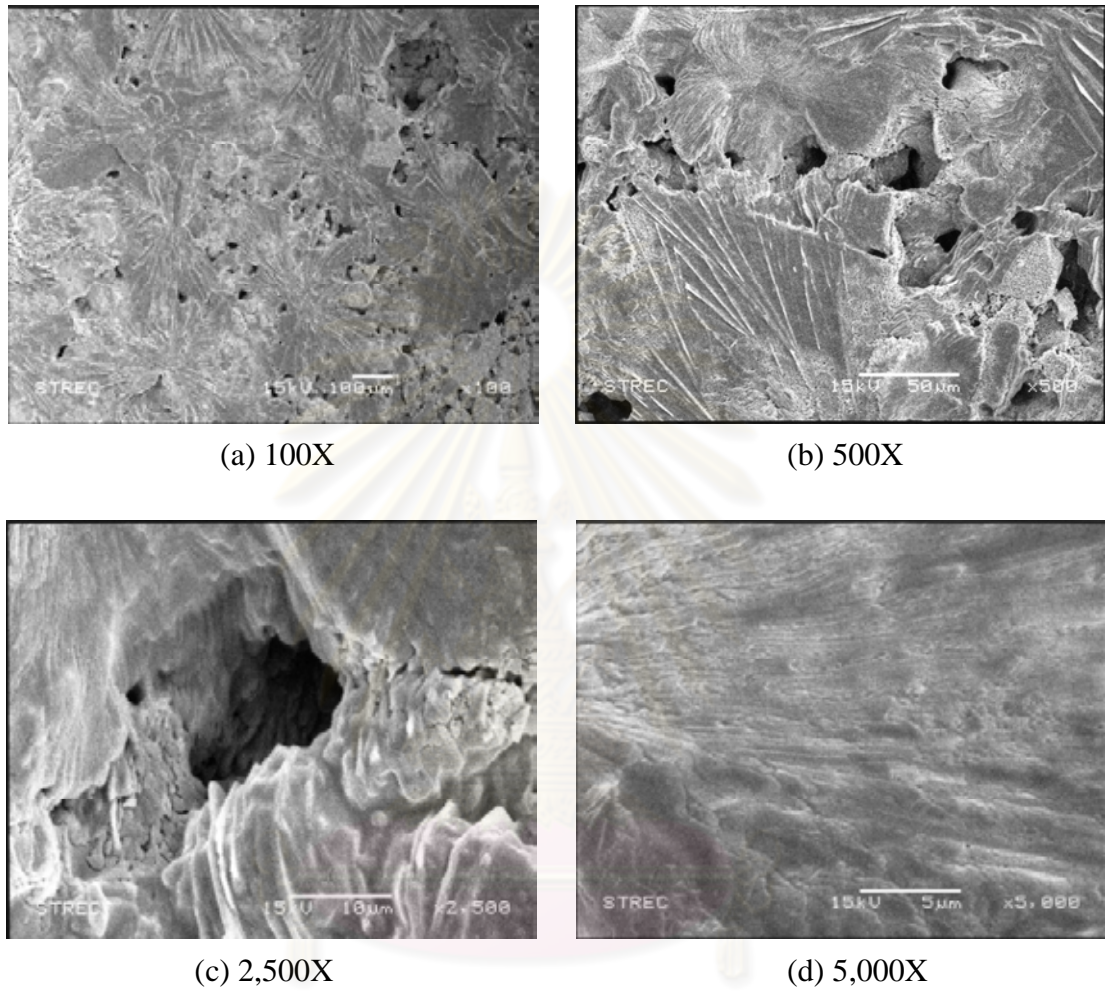
(c) 2,500X

(d) 5,000X

Figure 4.16   SEM micrographs of the HA sample H00-P00-L13 at the
                magnification of (a) 100X, (b) 500X, (c) 2,500X and (d) 5,000X

(a) 100X

(b) 500X
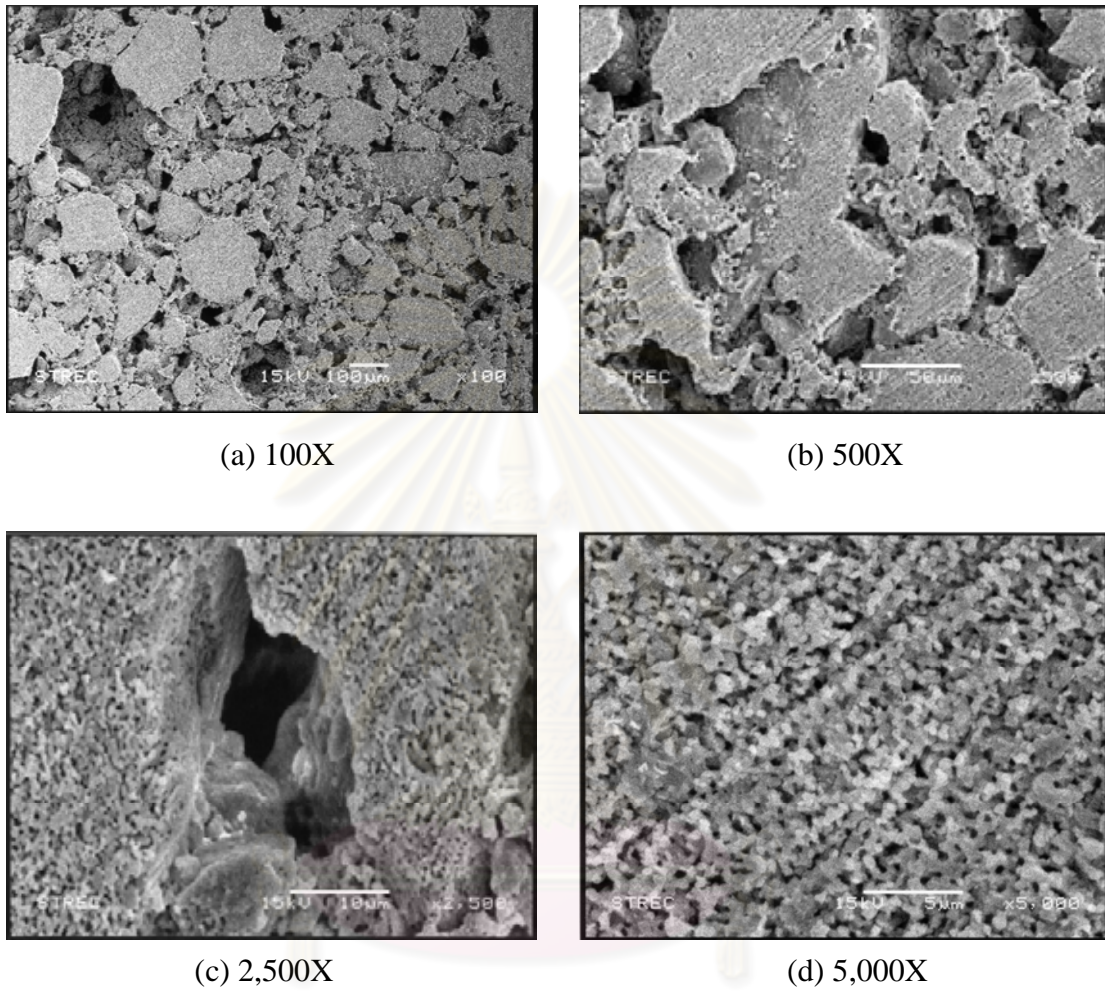
(c) 2,500X

(d) 5,000X

Figure 4.17   SEM micrographs of the HA sample H00-P00-L15 at the
magnification of (a) 100X, (b) 500X, (c) 2,500X and (d) 5,000X

(B) Sacrificial Template Technique using PMMA

Figure 4.18 demonstrated the SEM micrographs of the HA sample H00-P10-L13 at the magnification of (a) 100X, (b) 500X, (c) 1,000X and (d) 5,000X. The sample H00-P10-L13 was prepared by adding 10 wt% PMMA and 0 wt% H_2O_2 at L/P ratio of 1.3 ml/g. In Figure 4.18 (a) and (b), the sample contained two groups of pore size range. The former was the large pores with the size range of 100-200 μm. The latter was the small pores with the size of less than 50 μm. In Figure 4.18 (c), the pore with the diameter of approximately 30 μm had an irregular shape. In Figure 4.18 (d), the surface of this sample was composed of a number of very small pores less than 5 μm.

Figure 4.19 exhibited the SEM micrographs of the HA sample H00-P30-L13 at the magnification of (a) 100X, (b) 500X, (c) 2,500X and (d) 5,000X. . The sample H00-P30-L13 was made from 30 wt% PMMA and 0 wt% H_2O_2 with the L/P ratio of 1.3 ml/g. In Figure 4.19 (a) and (b), the sample also had two groups of pore size range. The large pores had pore size ranging from 100 to 300 μm, while the small pores had pore size less than 50 μm. Moreover, the large pore had a spherical shape. In Figure 4.19 (c), the small pore had an irregular shape. In Figure 4.19 (d), a few of very small pores less than 5 μm was observed.

(a) 100X

(b) 500X
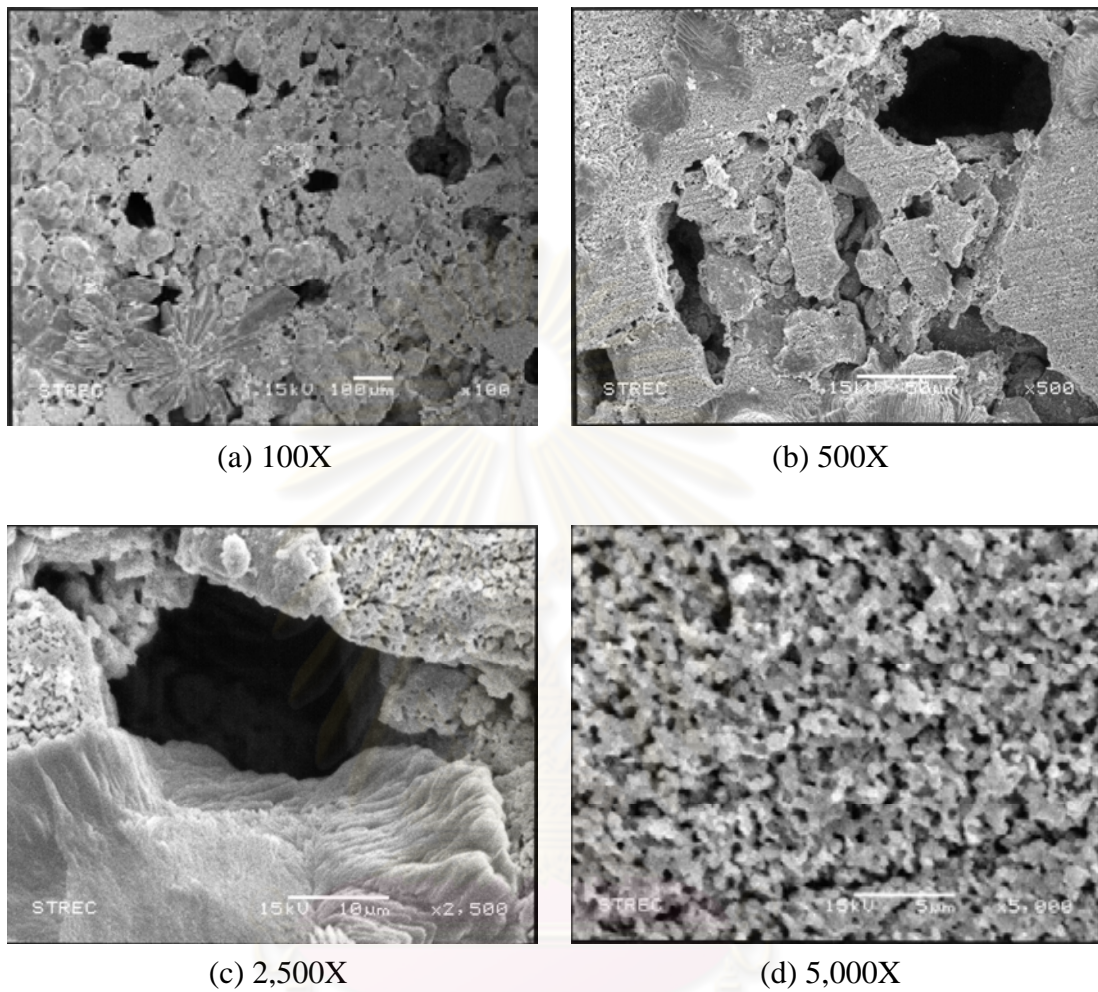
(c) 2,500X

(d) 5,000X

Figure 4.18   SEM micrographs of the HA sample H00-P10-L13 at the
magnification of (a) 100X, (b) 500X, (c) 2,500X and (d) 5,000X

(a) 100X

(b) 500X
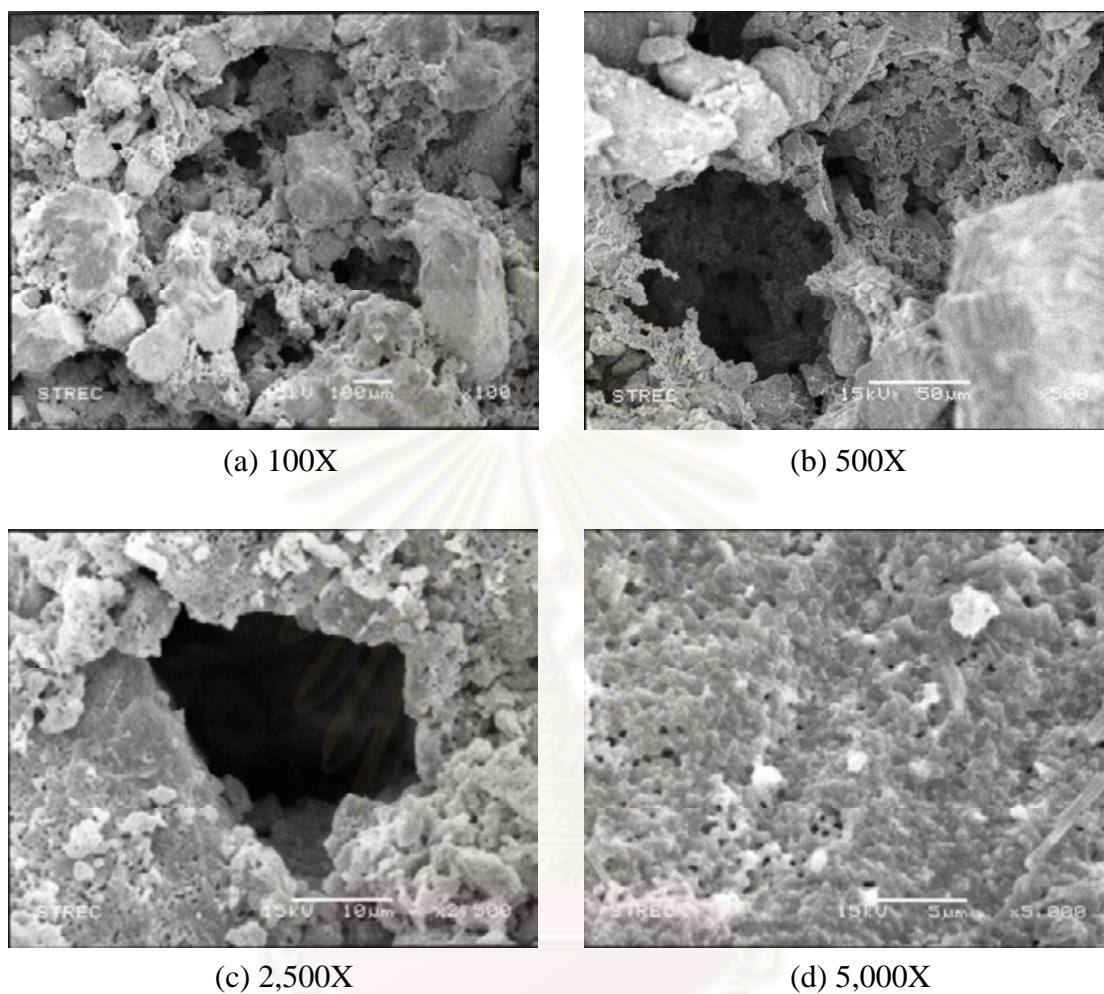
(c) 2,500X

(d) 5,000X

Figure 4.19   SEM micrographs of the HA sample H00-P30-L13 at the
magnification of (a) 100X, (b) 500X, (c) 2,500X and (d) 5,000X

(C) Direct Foaming Technique using H_2O_2

Figure 4.20 displayed the SEM micrographs of the HA sample H10-P00-L13 at the magnification of (a) 100X, (b) 500X, (c) 1,000X, (d) 5,000X and (e) 10,000X. The sample H10-P00-L13 was prepared from 10wt% H_2O_2 and 0wt% PMMA at the L/P ratio of 1.3 ml/g. In Figure 4.20 (a), the samples had a number of pores with the diameter of larger than 100 μm. In Figure 4.20 (b) and (c), some pores with the size of less than 100 μm were observed. In Figure 4.20 (d) and (e), surface of the sample consisted of a lot of tiny pores with the size of less than μm.

Figure 4.21 presented the SEM micrographs of the HA sample H10-P00-L15 at the magnification of (a) 100X, (b) 500X, (c) 1,000X, (d) 5,000X and (e) 10,000X. The sample H10-P00-L15 was made from 10wt% H_2O_2 and 0wt% PMMA at the L/P ratio of 1.5 ml/g. In Figure 4.21 (a), a very large pore with the size of over 500 μm was found. In Figure 4.21 (b) and (c), the sample still had some pores with the size of less than 100 μm. In Figure 4.21 (d) and (e), surface of the sample was composed of a great number of pores with the diameter of less than μm.

(D) Combination Techniques using PMMA and H_2O_2

Figure 4.22 presented SEM micrographs of the sample H10-P10-L13 at the magnification of (a) 50X, (b) 100X, (c) 500X, (d) 2,500X (e) 5,000X and (f) 10,000X. The HA sample H10-P10-L13 was prepared using 10wt% PMMA and 10wt% H_2O_2 with the L/P ratio of 1.3 ml/g. In Figure 4.22 (a) and (b), large pores over 500 μm in size and interconnected pores were observed. In Figure 4.22 (c), spherical and irregular shape pores were found. In Figure 4.22 (d), the irregular pore size was approximately 30 μm in diameter. In Figure 4.22 (e) and (f), surface of the sample consisted of a number of pores less than 1 μm in size and a bunch of agglomerated particles.

(a) 100X

(b) 500X

(c) 1,000X
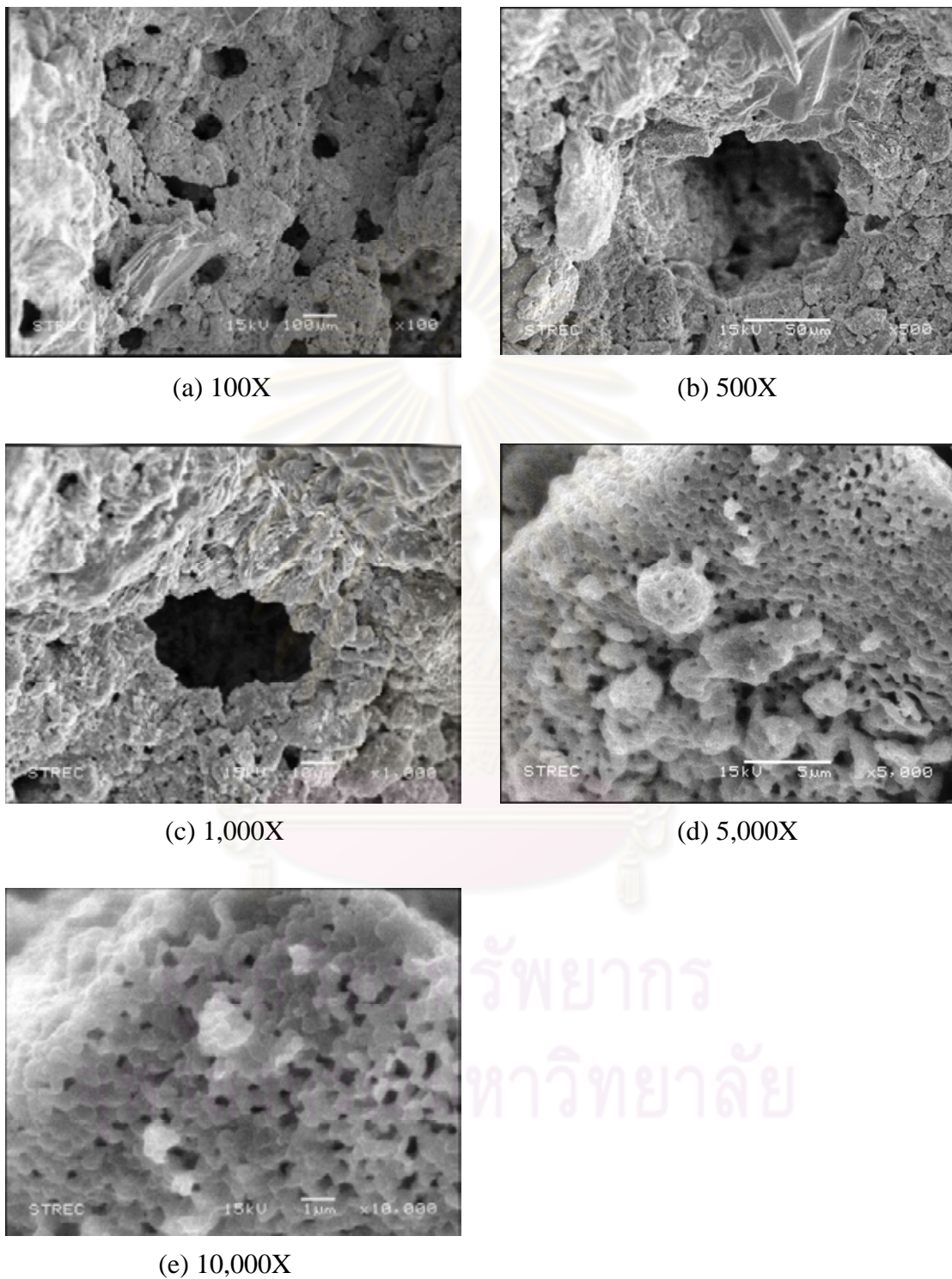
(d) 5,000X

(e) 10,000X

Figure 4.20   SEM micrographs of the HA sample H10-P00-L13 at the
magnification of (a) 100X, (b) 500X, (c) 1,000X, (d) 5,000X and (e)
10,000X

(a) 100X

(b) 500X

(c) 1,000X
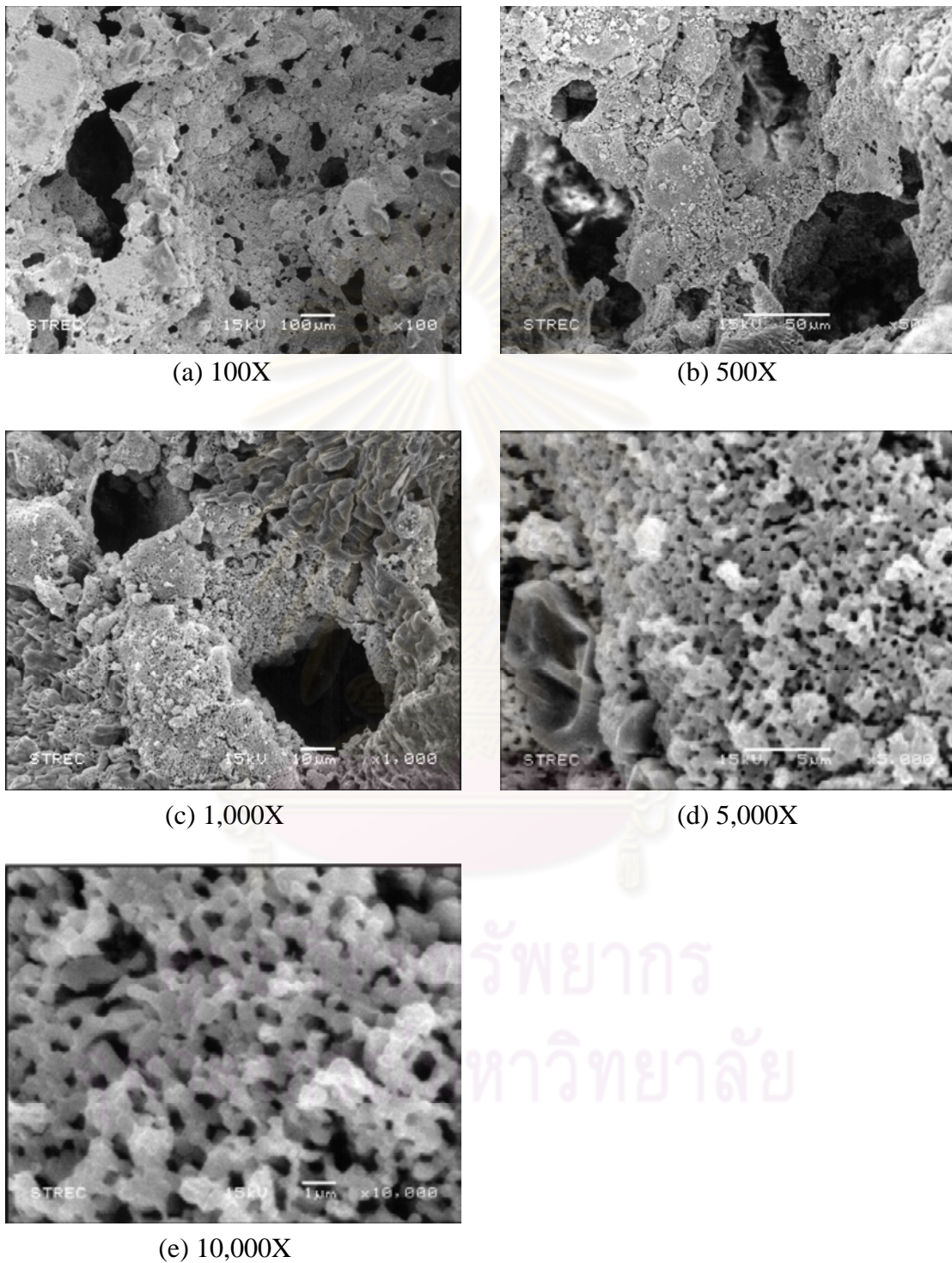
(d) 5,000X

(e) 10,000X

Figure 4.21   SEM micrographs of the sample H10-P00-L15 at the magnification of
(a) 100X, (b) 500X, (c) 1,000X, (d) 5,000X and (e) 10,000X

(a) 50X

(b) 100X

(c) 500X

(d) 2,500X
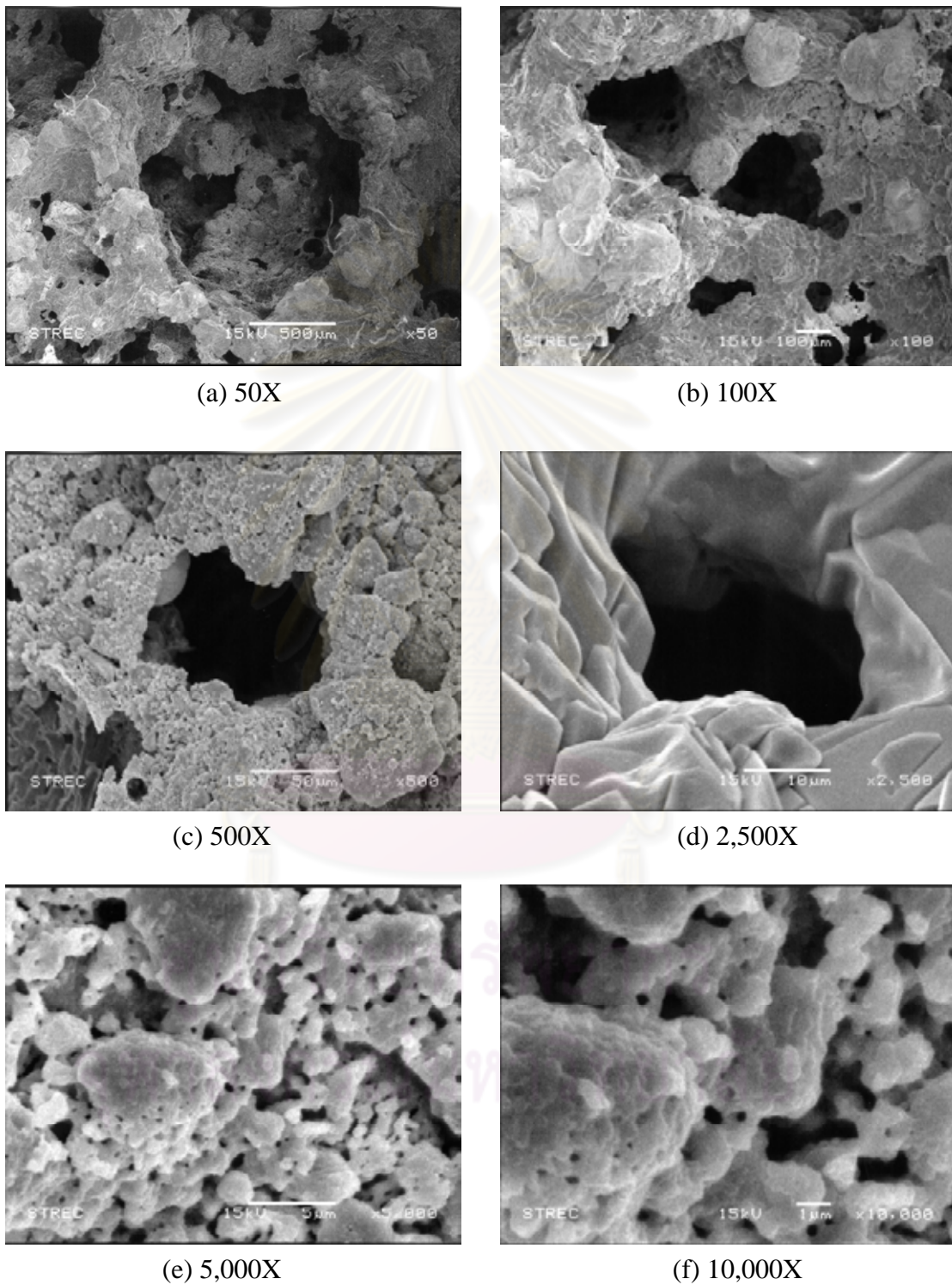
(e) 5,000X

(f) 10,000X

Figure 4.22   SEM micrographs of the sample H10-P10-L13 at the magnification of
(a) 50X, (b) 100X, (c) 500X, (d) 2,500X (e) 5,000X and (f) 10,000X

4.4.2 Bulk Density and Porosity

In this section, bulk density and porosity of the porous HA samples without surfactant, fabricated via sacrificial template using PMMA, direct foaming using H_2O_2 and combination technique using PMMA and H_2O_2, were described.

(A) Sacrificial Template Technique using PMMA

Table 4.7 summarized the bulk density and porosity of the HA samples, prepared via sacrificial template technique using PMMA granules. The samples using PMMA granules over 40 wt% were handless in every condition. The sample having the maximum bulk density of 1.51 g/cm^3 was H00-P00-L13, while the sample having the minimum bulk density of 0.84 g/cm^3 was H00-P00-L15. Moreover, the maximum porosity attained through this method was 73.59%, which was the sample H00-P40-L15. The minimum porosity was 52.04%, which was the sample H00-P00-L13.

Figure 4.23 illustrated the relationship between bulk density (BD) and PMMA content of the samples from Table 4.3. Average bulk density of all samples was decreased when the content of PMMA increased. Bulk density of the samples prepared at the L/P ratio of 1.5 ml/g was lower than those of the samples prepared at the L/P ratio of 1.3 ml/g.

Figure 4.24 presented the relationship between porosity and PMMA content of the samples from Table 4.3. Average porosity of all samples was increased when the content of PMMA increased. Porosity of the samples fabricated with the L/P ratio of 1.5 ml/g was higher than those of the samples prepared at the L/P ratio of 1.3 ml/g.

Table 4.7   Bulk density and porosity of the HA samples, prepared via sacrificial
             template technique using PMMA granules

Sample	#	(g/cm³)	Average	SD	#	(%)	Average	SD
		Bulk Density				**Porosity**		
H00-P00-L13	1	1.51	**1.51**	0.01	1	52.04	**52.17**	0.18
	2	1.51			2	52.30		
H00-P05-L13	1	1.49	**1.49**	0.00	1	52.65	**52.72**	0.11
	2	1.49			2	52.80		
H00-P10-L13	1	1.45	**1.46**	0.00	1	53.91	**53.81**	0.15
	2	1.46			2	53.70		
H00-P20-L13	1	1.28	**1.29**	0.01	1	59.51	**59.24**	0.38
	2	1.29			2	58.98		
H00-P30-L13	1	1.11	**1.10**	0.01	1	64.92	**65.19**	0.39
	2	1.09			2	65.47		
H00-P40-L13	1	0.88	**0.88**	0.00	1	71.96	**72.02**	0.08
	2	0.88			2	72.07		
H00-P50-L13	1	-	**-**	-	1	-	**-**	-
	2	-			2	-		
H00-P00-L15	1	1.49	**1.42**	0.10	1	52.72	**54.92**	3.11
	2	1.35			2	57.12		
H00-P05-L15	1	1.41	**1.40**	0.01	1	55.37	**55.62**	0.35
	2	1.39			2	55.87		
H00-P10-L15	1	1.38	**1.37**	0.02	1	56.14	**56.51**	0.52
	2	1.36			2	56.87		
H00-P20-L15	1	1.19	**1.20**	0.01	1	62.32	**62.11**	0.30
	2	1.20			2	61.90		
H00-P30-L15	1	1.02	**1.03**	0.02	1	67.78	**67.42**	0.51
	2	1.04			2	67.05		
H00-P40-L15	1	0.83	**0.84**	0.00	1	73.59	**73.52**	0.10
	2	0.84			2	73.45		
H00-P50-L15	1	-	**-**	-	1	-	**-**	-
	2	-			2	-		
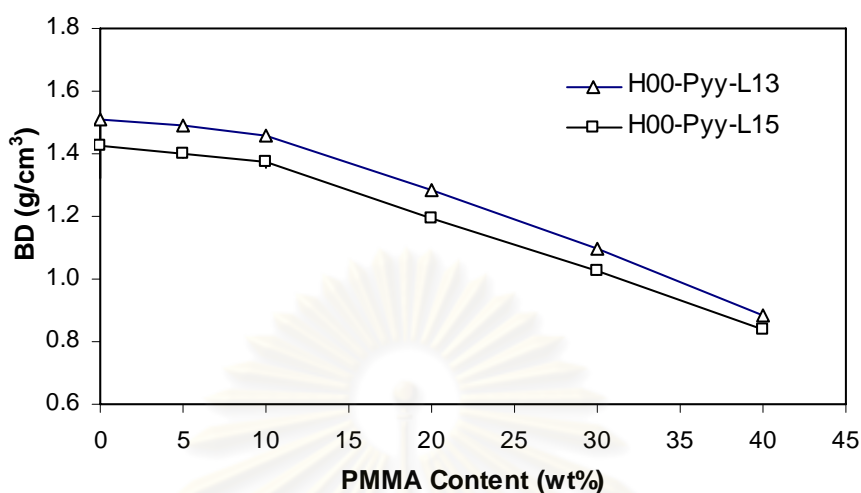
Figure 4.23   Relationship between bulk density (BD) and PMMA content of the
               HA samples, prepared via sacrificial template technique using PMMA
               granules with L/P ratio of 1.3 and 1.5 ml/g, respectively.
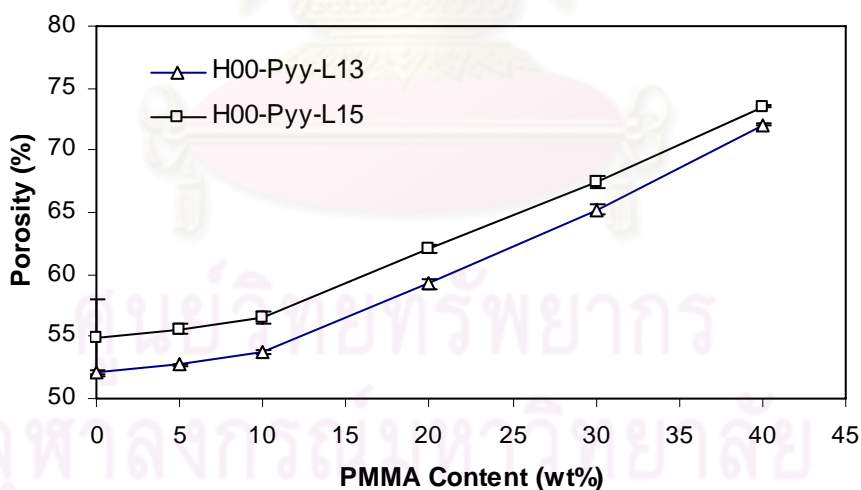
Figure 4.24   Relationship between porosity and PMMA content of the HA samples
               without surfactant, prepared via sacrificial template technique using
               PMMA granules with L/P ratio of 1.3 and 1.5 ml/g, respectively.

(B) Direct Foaming Technique using H_2O_2

Table 4.8 summarized the bulk density and porosity of the HA samples prepared via direct foaming using H_2O_2 solution. At the L/P ratio of 1.5 ml/g (H30-P00-L15), the samples fabricated through this method using over 20wt% H_2O_2 were handless. The minimum bulk density was 0.41 g/cm^3, whereas the maximum porosity attained was 86.99%, which was the sample H20-P00-L15. The minimum porosity was 52.04%, which was the sample H00-P00-L13.

Figure 4.25 exhibited the relationship between bulk density (BD) and H_2O_2 concentration of the samples from Table 4.4. Bulk density decreased slightly even with higher concentration of H_2O_2. The Bulk density of the sample with the L/P ratio of 1.5 ml/g. (Hxx-P00-L15) was lower than that of the sample with L/P ratio of 1.5 ml/g (Hxx-P00-L13).

Figure 4.26 displayed the relationship between porosity and H_2O_2 concentration of the samples from Table 4.4. Porosity increased slightly even with higher concentration of H_2O_2. The porosity of the sample with the L/P ratio of 1.5 ml/g. (Hxx-P00-L15) was higher than that of the sample with L/P ratio of 1.5 ml/g (Hxx-P00-L13).

Table 4.8   Bulk density and porosity of the HA samples prepared via direct foaming
using H_2O_2 solution

Sample	Bulk Density				Porosity			
	#	(g/cm^3)	Average	SD	#	(%)	Average	SD
H01-P00-L13	1	0.60	**0.61**	0.02	1	80.99	**80.64**	0.49
	2	0.62			2	80.30		
H03-P00-L13	1	0.59	**0.59**	0.00	1	81.39	**81.44**	0.08
	2	0.58			2	81.50		
H05-P00-L13	1	0.56	**0.56**	0.00	1	82.14	**82.24**	0.14
	2	0.56			2	82.34		
H10-P00-L13	1	0.55	**0.55**	0.00	1	82.62	**82.56**	0.09
	2	0.55			2	82.49		
H20-P00-L13	1	0.53	**0.53**	0.01	1	83.11	**83.30**	0.28
	2	0.52			2	83.50		
H30-P00-L13	1	0.44	**0.47**	0.03	1	85.99	**85.21**	1.11
	2	0.49			2	84.43		
H01-P00-L15	1	0.59	**0.60**	0.01	1	81.31	**81.10**	0.30
	2	0.60			2	80.89		
H03-P00-L15	1	0.49	**0.49**	0.00	1	84.48	**84.53**	0.08
	2	0.49			2	84.59		
H05-P00-L15	1	0.49	**0.48**	0.01	1	84.59	**84.86**	0.38
	2	0.47			2	85.13		
H10-P00-L15	1	0.47	**0.47**	0.00	1	85.23	**85.12**	0.15
	2	0.47			2	85.02		
H20-P00-L15	1	0.41	**0.43**	0.02	1	86.99	**86.50**	0.69
	2	0.44			2	86.02		
H30-P00-L15	1	-	**-**	-	1	-	**-**	-
	2	-			2	-		
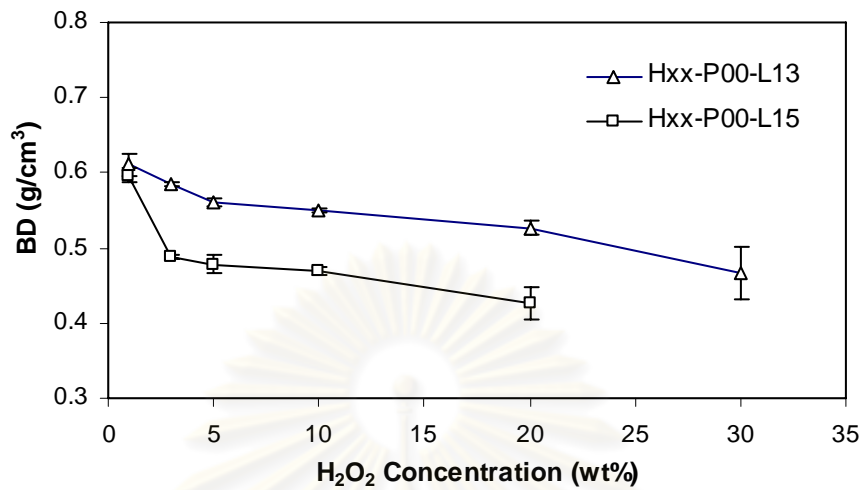
Figure 4.25   Relationship between bulk density (BD) and H_2O_2 concentration of
the HA samples prepared via direct foaming using H_2O_2 solution with
L/P ratio of 1.3 and 1.5 ml/g, respectively.

Figure 4.26   Relationship between porosity and H_2O_2 concentration of the HA
samples prepared via direct foaming using H_2O_2 solution with L/P
ratio of 1.3 and 1.5 ml/g, respectively.

(C) Combination Technique using PMMA and H_2O_2

Table 4.9 summarized the bulk density and porosity of the HA samples, prepared via combination technique using PMMA granule and H_2O_2 solution.

At 5wt% H_2O_2, the samples prepared through this method adding PMMA granules over 30 wt% were handless. Bulk density of the samples prepared at 5wt% H_2O_2 ranged between 0.36 and 0.56 g/cm^3, whilst porosity ranged from 82.14% to 88.66%.

At 10wt% H_2O_2, the samples prepared using PMMA over 20 wt% were handless. Bulk density of the samples prepared at 10wt% H_2O_2 ranged between 0.32 and 0.55 g/cm^3, while porosity ranged from 82.49% to 89.84%.

At 20wt% H_2O_2, the samples prepared using PMMA over 10 wt% were handless. Bulk density of the samples prepared at 5wt% H_2O_2 ranged between 0.36 and 0.53 g/cm^3, whilst porosity ranged from 83.11% to 88.59%.

At 30wt% H_2O_2, the samples prepared using PMMA over 10 wt% were handless. Bulk density of the samples prepared at 5wt% H_2O_2 ranged between 0.38 and 0.49 g/cm^3, whilst porosity ranged from 84.43% to 88.09%.

Figure 4.27 exhibited the effect of PMMA content and H_2O_2 concentration on bulk density (BD) of the HA samples from Table 4.5. Bulk density decreased with the increases of the PMMA content and the H_2O_2 concentration.

Figure 4.28 illustrated the effect of PMMA content and H_2O_2 concentration on porosity of the HA samples from Table 4.5. Porosity increased with the increases of the PMMA content and the H_2O_2 concentration.

Table 4.9   Bulk density and porosity of the HA samples, prepared via combination technique using PMMA granule and H_2O_2 solution.

Sample	Bulk Density				Porosity			
	#	(g/cm³)	Average	SD	#	(%)	Average	SD
H05-P00-L13	1	0.56	**0.56**	0.00	1	82.14	**82.24**	0.14
	2	0.56			2	82.34		
H05-P05-L13	1	0.52	**0.50**	0.03	1	83.48	**84.15**	0.94
	2	0.48			2	84.81		
H05-P10-L13	1	0.45	**0.46**	0.02	1	85.78	**85.40**	0.53
	2	0.47			2	85.02		
H05-P20-L13	1	0.40	**0.38**	0.02	1	87.37	**87.86**	0.69
	2	0.37			2	88.35		
H05-P30-L13	1	0.36	**0.36**	0.00	1	88.45	**88.56**	0.15
	2	0.36			2	88.66		
H05-P40-L13	1	-	**-**	-	1	-	**-**	-
	2	-			2	-		
H05-P50-L13	1	-	**-**	-	1	-	**-**	-
	2	-			2	-		
H10-P00-L13	1	0.55	**0.55**	0.00	1	82.62	**82.56**	0.09
	2	0.55			2	82.49		
H10-P05-L13	1	0.47	**0.44**	0.04	1	85.13	**85.93**	1.13
	2	0.42			2	86.73		
H10-P10-L13	1	0.37	**0.39**	0.02	1	88.27	**87.72**	0.78
	2	0.40			2	87.17		
H10-P20-L13	1	0.35	**0.33**	0.02	1	88.95	**89.40**	0.63
	2	0.32			2	89.84		
H10-P30-L13	1	-	**-**	-	1	-	**-**	-
	2	-			2	-		
H10-P40-L13	1	-	**-**	-	1	-	**-**	-
	2	-			2	-		
H10-P50-L13	1	-	**-**	-	1	-	**-**	-
	2	-			2	-		
H20-P00-L13	1	0.53	**0.53**	0.01	1	83.11	**83.30**	0.28
	2	0.52			2	83.50		
H20-P05-L13	1	0.39	**0.42**	0.04	1	87.61	**86.64**	1.37
	2	0.45			2	85.67		
H20-P10-L13	1	0.36	**0.39**	0.04	1	88.59	**87.59**	1.41
	2	0.42			2	86.59		
H20-P20-L13	1	-	**-**	-	1	-	**-**	-
	2	-			2	-		
H20-P30-L13	1	-	**-**	-	1	-	**-**	-
	2	-			2	-		
H20-P40-L13	1	-	**-**	-	1	-	**-**	-
	2	-			2	-		
H20-P50-L13	1	-	**-**	-	1	-	**-**	-
	2	-			2	-		

Table 4.9   Bulk density and porosity of the HA samples, prepared via combination technique using PMMA granule and H_2O_2 solution. (Continued)

Sample	Bulk Density				Porosity			
	#	(g/cm^3)	Average	SD	#	(%)	Average	SD
H30-P00-L13	1	0.44	**0.47**	0.03	1	85.99	**85.21**	1.11
	2	0.49			2	84.43		
H30-P05-L13	1	0.41	**0.41**	0.01	1	87.16	**86.95**	0.30
	2	0.42			2	86.74		
H30-P10-L13	1	0.39	**0.38**	0.01	1	87.73	**87.91**	0.25
	2	0.38			2	88.09		
H30-P20-L13	1	-	**-**	-	1	-	**-**	-
	2	-			2	-		
H30-P30-L13	1	-	**-**	-	1	-	**-**	-
	2	-			2	-		
H30-P40-L13	1	-	**-**	-	1	-	**-**	-
	2	-			2	-		
H30-P50-L13	1	-	**-**	-	1	-	**-**	-
	2	-			2	-		

123

Figure 4.27   Effect of PMMA content and H_2O_2 concentration on bulk density
                (BD) of the HA samples, prepared via combination technique using
                PMMA granules and H_2O_2 solution with L/P ratio of 1.3 ml/g
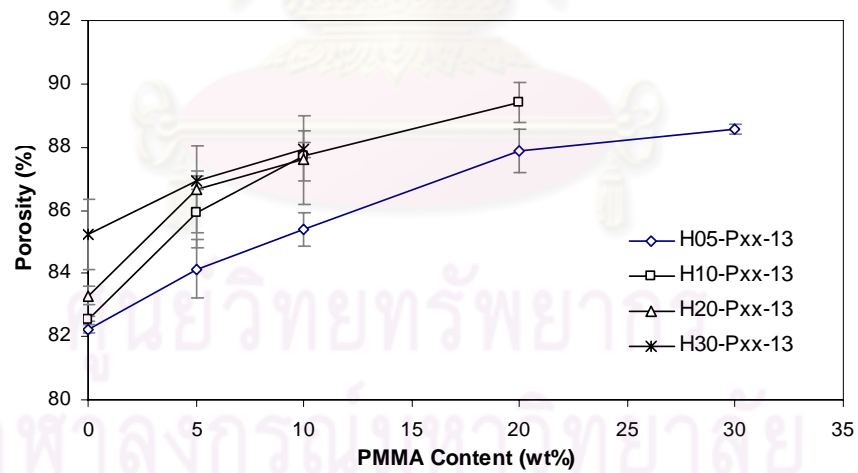
Figure 4.28   Effect of PMMA content and H_2O_2 concentration on porosity of the
                HA samples, prepared via combination technique using PMMA
                granules and H_2O_2 solution with L/P ratio of 1.3 ml/g

4.4.3 Mechanical Properties

(A) Sacrificial Template Technique using PMMA

Table 4.10 summarized the compressive strength and flexural strength of the HA samples prepared via sacrificial template technique using PMMA granules. Fabrication of HA specimen using PMMA over 40wt% was handleless. The average compressive strength of the samples prepared via this method at the L/P ratio of 1.3 ml/g and 1.5 ml/g ranged from 0.65 MPa to 34.45 MPa and ranged from 0.54 MPa to 31.04 MPa, respectively. The average flexural strength of the samples prepared at the L/P ratio of 1.3 ml/g and 1.5 ml/g ranged from 0.7 MPa to 5.98 MPa and ranged from 0.59 MPa to 5.06 MPa, respectively.

Figure 4.29 displayed the relationship between compressive strength (CS) and PMMA content of the HA samples from Table 4.10. Compressive strength of these samples decreased with an increase of PMMA content added. The samples with lower L/P ratio had a higher level of compressive strength than the other with the higher L/P ratio.

Figure 4.30 illustrated the relationship between flexural strength (FS) and PMMA content of the HA samples from Table 4.10. Flexural strength of all sample showed a decrease when PMMA content increased. The samples with the L/P ratio of 1.5 ml/g had the lowest strength in flexural.

Table 4.10 Compressive strength and flexural strength of the HA, prepared via sacrificial template technique using PMMA granules

Sample	Compressive strength				Flexural strength			
	#	(MPa)	Average	SD	#	(MPa)	Average	SD
H00-P00-L13	1	33.11	**34.45**	1.90	1	6.53	**5.98**	0.79
	2	35.80			2	5.42		
H00-P05-L13	1	27.11	**25.78**	1.88	1	4.93	**5.46**	0.75
	2	24.45			2	6.00		
H00-P10-L13	1	17.53	**17.16**	0.51	1	3.52	**3.31**	0.31
	2	16.80			2	3.09		
H00-P20-L13	1	7.25	**6.58**	0.95	1	1.72	**1.84**	0.16
	2	5.91			2	1.95		
H00-P30-L13	1	2.50	**2.51**	0.02	1	0.72	**1.44**	1.01
	2	2.53			2	2.15		
H00-P40-L13	1	0.68	**0.65**	0.05	1	0.58	**0.70**	0.17
	2	0.61			2	0.82		
H00-P50-L13	1	-	**-**	-	1	-	**-**	-
	2	-			2	-		
H00-P00-L15	1	33.46	**31.04**	3.42	1	5.23	**5.06**	0.23
	2	28.62			2	4.90		
H00-P05-L15	1	23.94	**22.95**	1.40	1	3.89	**3.85**	0.07
	2	21.97			2	3.80		
H00-P10-L15	1	14.65	**13.93**	1.02	1	3.25	**3.14**	0.16
	2	13.21			2	3.03		
H00-P20-L15	1	4.02	**4.22**	0.28	1	1.65	**1.77**	0.16
	2	4.41			2	1.88		
H00-P30-L15	1	2.00	**2.09**	0.13	1	0.69	**1.29**	0.85
	2	2.19			2	1.89		
H00-P40-L15	1	0.57	**0.54**	0.03	1	0.54	**0.59**	0.07
	2	0.52			2	0.64		
H00-P50-L15	1	-	**-**	-	1	-	**-**	-
	2	-			2	-		
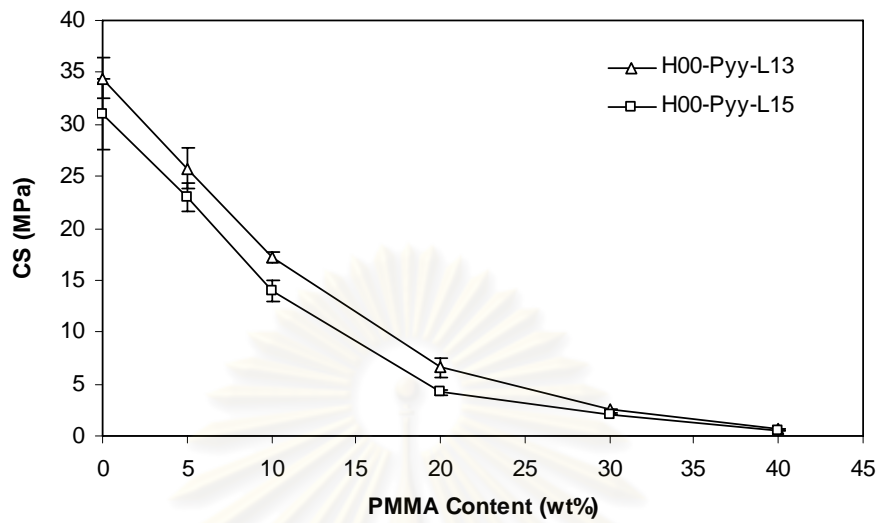
Figure 4.29   Relationship between compressive strength (CS) and PMMA content
                of the HA samples, prepared via sacrificial template technique using
                PMMA granules with L/P ratio of 1.3 and 1.5 ml/g, respectively.
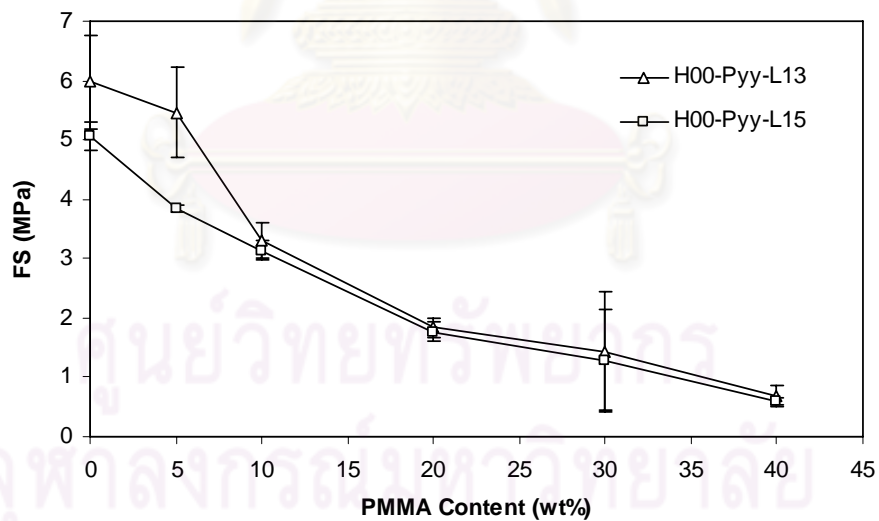
Figure 4.30   Relationship between flexural strength (FS) and PMMA content of
                the HA samples, prepared via sacrificial template technique using
                PMMA granules with L/P ratio of 1.3 and 1.5 ml/g, respectively.

Table 4.11 summed up the compressive stiffness and flexural stiffness of the HA samples, prepared via sacrificial template technique using PMMA granules. The samples using PMMA over 40wt% were handleless. The average compressive stiffness of the samples prepared through this method at the L/P ratio of 1.3 ml/g and 1.5 ml/g ranged from 401.15 to 5,150.50 kN/m^2 and ranged from 33.80 to 4,900.13 kN/m^2, respectively. The average flexural stiffness of the samples prepared at the L/P ratio of 1.3 ml/g and 1.5 ml/g ranged from 10.91 to 649.90 MN/m^2 and ranged from 8.45 to 362.31 MN/m^2, respectively.

Figure 4.31 presented the relationship between compressive stiffness (E_C) and PMMA content of the HA samples from Table 4.11. Compressive stiffness of these samples was reduced when the content of PMMA rose. The sample prepared at the L/P ratio of 1.3 ml/g (H00-Pyy-L13) had the higher compress stiffness than the sample prepared at the L/P ratio of 1.5 ml/g (H00-Pyy-L15).

Figure 4.32 showed the relationship between flexural stiffness (E_F) and PMMA content of the HA samples from Table 4.11. Flexural stiffness of the samples dropped until the PMMA content of 10wt% was attained and then decrease slowly until the PMMA content reached 40wt%. The sample prepared at the L/P ratio of 1.3 ml/g (H00-Pyy-L13) had the higher flexural stiffness than the sample prepared at the L/P ratio of 1.5 ml/g (H00-Pyy-L15).

Table 4.11   Compressive stiffness and flexural stiffness of the HA samples, prepared
via sacrificial template technique using PMMA granules

Sample		Compressive stiffness				Flexural stiffness		
	#	(kN/m^2)	Average	SD	#	(MN/m^2)	Average	SD
H00-P00-L13	1	4,881.59	**5,150.50**	380.30	1	729.17	**649.90**	112.11
	2	5,419.41			2	570.62		
H00-P05-L13	1	5,528.05	**4,821.28**	999.53	1	272.10	**328.04**	79.11
	2	4,114.51			2	383.98		
H00-P10-L13	1	3,384.33	**3,162.30**	313.99	1	212.23	**206.18**	8.56
	2	2,940.27			2	200.13		
H00-P20-L13	1	2,503.32	**2,268.81**	331.65	1	139.48	**172.55**	46.77
	2	2,034.29			2	205.62		
H00-P30-L13	1	1,926.54	**1,969.63**	60.93	1	67.58	**92.20**	34.81
	2	2,012.71			2	116.81		
H00-P40-L13	1	416.54	**401.15**	21.76	1	8.98	**10.91**	2.74
	2	385.76			2	12.85		
H00-P50-L13	1	-	**-**	-	1	-	**-**	-
	2	-			2	-		
H00-P00-L15	1	5,494.64	**4,900.13**	840.77	1	368.50	**362.31**	8.74
	2	4,305.61			2	356.13		
H00-P05-L15	1	4,892.23	**4,379.65**	724.91	1	252.71	**246.95**	8.15
	2	3,867.06			2	241.18		
H00-P10-L15	1	2,677.30	**2,531.17**	206.66	1	212.41	**200.02**	17.53
	2	2,385.04			2	187.63		
H00-P20-L15	1	1,375.37	**1,421.47**	65.20	1	120.48	**148.07**	39.01
	2	1,467.58			2	175.66		
H00-P30-L15	1	640.16	**706.03**	93.16	1	67.05	**79.75**	17.96
	2	771.91			2	92.44		
H00-P40-L15	1	32.99	**33.80**	1.15	1	7.75	**8.45**	0.99
	2	34.62			2	9.15		
H00-P50-L15	1	-	**-**	-	1	-	**-**	-
	2	-			2	-		
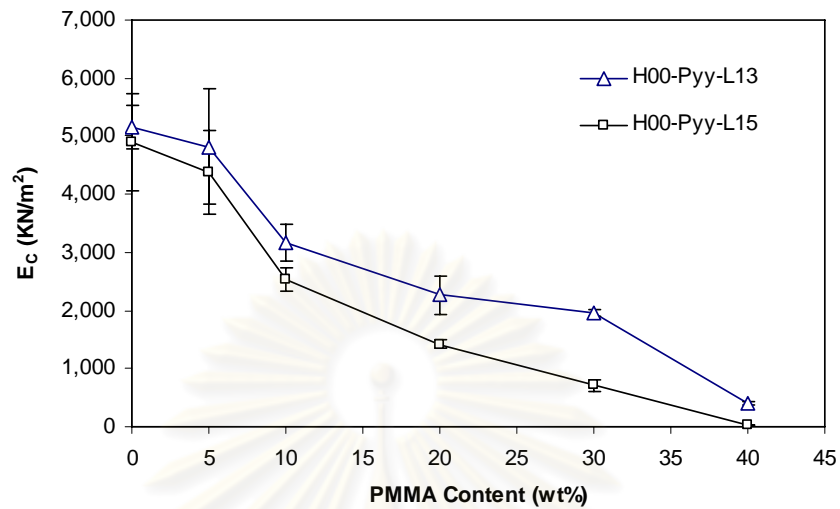
Figure 4.31   Relationship between compressive stiffness (E_C) and PMMA content of the HA samples, prepared via sacrificial template technique using PMMA granules with L/P ratio of 1.3 and 1.5 ml/g, respectively.
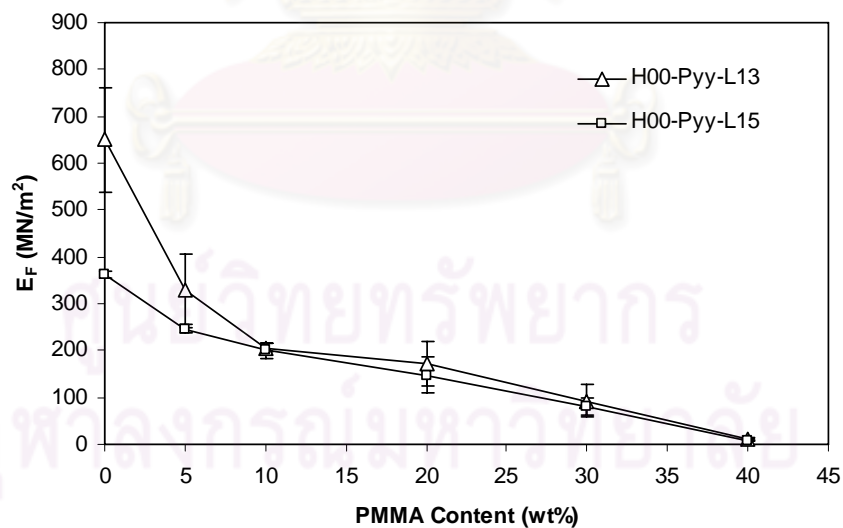
Figure 4.32   Relationship between flexural stiffness (E_F) and PMMA content of the HA samples, prepared via sacrificial template technique using PMMA granules with L/P ratio of 1.3 and 1.5 ml/g, respectively.

(B) Direct Foaming Technique using H_2O_2

Table 4.12 reported the compressive strength and flexural strength of the HA samples, prepared via direct foaming technique using H_2O_2 solution. At the L/P ratio of 1.5 ml/g, the samples using H_2O_2 over 20wt% were handleless. The average compressive strength of the samples prepared at the L/P ratio of 1.3 ml/g. and 1.5 ml/g. ranged from 0.15 to 0.40 MPa and ranged from 0.08 to 0.20 MPa, respectively. The average flexural strength of the samples prepared at the L/P ratio of 1.3 ml/g. and 1.5 ml/g. ranged from 0.22 to 0.81 MPa and ranged from 0.12 to 0.59 MPa, respectively.

Figure 4.33 exhibited the relationship between compressive strength (CS) and H_2O_2 concentration of the HA samples from Table 4.12. The compressive strength of these samples reduced with an increasing concentration of H_2O_2 solution. The compressive strength of the samples prepared at the L/P ratio of 1.3 ml/g. (Hxx-P00-L13) was higher than that of the samples prepared at the L/P ratio of 1.5 ml/g. (Hxx-P00-L15).

Figure 4.34 depicted the relationship between flexural strength (FS) and H_2O_2 concentration of the HA samples from Table 4.12. The flexural strength of these samples had non-linear trend line. The strength dropped rapidly until the concentration of H_2O_2 increased to 5wt%, then the strength decreased slowly after the concentration surpass 5wt%. The flexural strength of the samples prepared at the L/P ratio of 1.3 ml/g. (Hxx-P00-L13) was higher than that of the samples prepared at the L/P ratio of 1.5 ml/g. (Hxx-P00-L15).

Table 4.12 Compressive strength and flexural strength of the HA samples, prepared via direct foaming technique using H_2O_2 solution

Sample	Compressive strength				Flexural strength			
	#	(MPa)	Average	SD	#	(MPa)	Average	SD
H01-P00-L13	1	0.40	**0.40**	0.00	1	0.84	**0.81**	0.04
	2	0.40			2	0.78		
H03-P00-L13	1	0.38	**0.38**	0.00	1	0.69	**0.68**	0.03
	2	0.38			2	0.66		
H05-P00-L13	1	0.34	**0.33**	0.02	1	0.46	**0.51**	0.07
	2	0.32			2	0.56		
H10-P00-L13	1	0.28	**0.30**	0.02	1	0.41	**0.45**	0.06
	2	0.31			2	0.49		
H20-P00-L13	1	0.20	**0.19**	0.01	1	0.29	**0.30**	0.01
	2	0.19			2	0.31		
H30-P00-L13	1	0.12	**0.15**	0.03	1	0.22	**0.22**	0.01
	2	0.17			2	0.22		
H01-P00-L15	1	0.19	**0.20**	0.01	1	0.59	**0.59**	0.00
	2	0.21			2	0.59		
H03-P00-L15	1	0.17	**0.16**	0.00	1	0.44	**0.41**	0.04
	2	0.16			2	0.39		
H05-P00-L15	1	0.13	**0.15**	0.03	1	0.34	**0.34**	0.00
	2	0.17			2	0.34		
H10-P00-L15	1	0.15	**0.14**	0.00	1	0.24	**0.27**	0.04
	2	0.14			2	0.30		
H20-P00-L15	1	0.07	**0.08**	0.02	1	0.10	**0.12**	0.03
	2	0.09			2	0.14		
H30-P00-L15	1	-	**-**	-	1	-	**-**	-
	2	-			2	-		

ศูนย์วิทยทรัพยากร
จุฬาลงกรณ์มหาวิทยาลัย
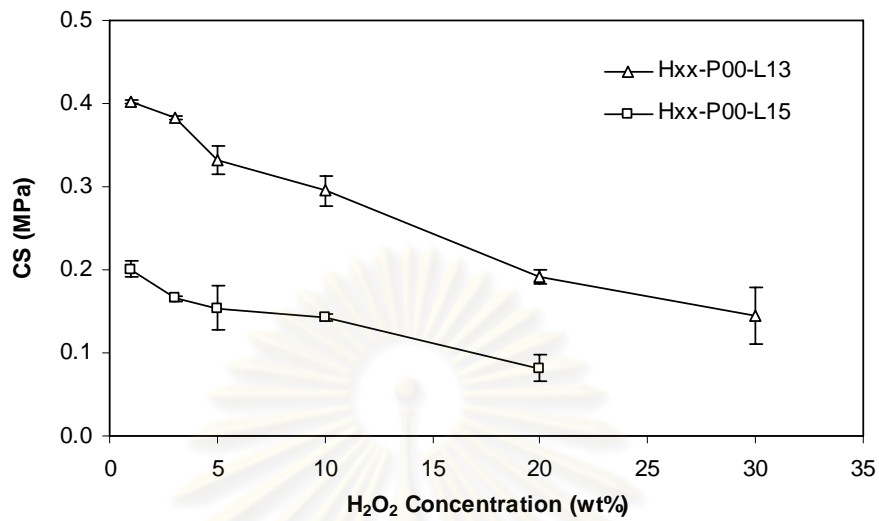
Figure 4.33   Relationship between compressive strength (CS) and H_2O_2
concentration of the HA samples, prepared via direct foaming
technique using H_2O_2 solution with L/P ratio of 1.3 and 1.5 ml/g,
respectively.
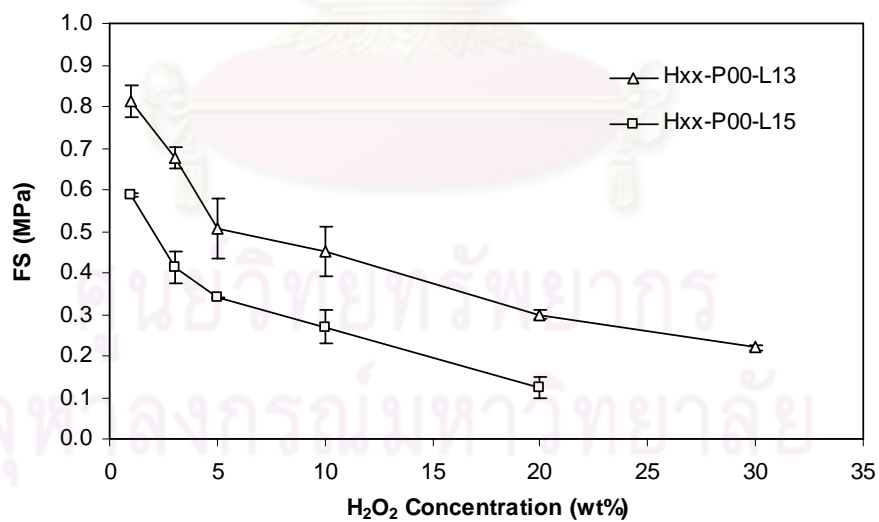
Figure 4.34   Relationship between flexural strength (FS) and H_2O_2 concentration
of the HA samples, prepared via direct foaming technique using H_2O_2
solution with L/P ratio of 1.3 and 1.5 ml/g, respectively.

Table 4.13 presented the compressive stiffness and flexural stiffness of the HA samples, prepared via direct foaming using H_2O_2 solution. At the L/P ratio of 1.5 ml/g, the samples using H_2O_2 over 20wt% were handleless. The average compressive stiffness of the samples prepared at the L/P ratio of 1.3 ml/g. and 1.5 ml/g. ranged from 79.48 to 398.13 kN/m^2 and ranged from 59.45 to 168.11 kN/m^2, respectively. The average flexural stiffness of the samples prepared at the L/P ratio of 1.3 ml/g. and 1.5 ml/g. ranged from 2.05 to 12.79 MN/m^2 and ranged from 1.64 to 10.52 MN/m^2, respectively.

Figure 4.35 illustrated the relationship between compressive stiffness (E_C) and H_2O_2 concentration of the HA samples from Table 4.13. The compressive stiffness increased with an increase of H_2O_2 concentration until the concentration of 5wt%. Then, the stiffness decreased with an increasing concentration of H_2O_2. The compressive stiffness of the porous HA samples prepared at the L/P ratio of 1.3 ml/g. (Hxx-P00-L13) was higher than that of the samples prepared at the L/P ratio of 1.5 ml/g. (Hxx-P00-L15).

Figure 4.36 displayed the relationship between flexural stiffness (E_F) and H_2O_2 concentration of the HA samples from Table 4.13. The flexural stiffness of these samples dropped dramatically until the H_2O_2 concentration was at 5wt% and then reduced gradually. However, the flexural stiffness of the samples prepared at the L/P ratio of 1.3 ml/g. (Hxx-P00-L13) was higher than that of the samples prepared at the L/P ratio of 1.5 ml/g. (Hxx-P00-L15).

Table 4.13   Compressive stiffness and flexural stiffness of the HA samples, prepared
via direct foaming technique using H_2O_2 solution

Sample		Compressive stiffness				Flexural stiffness		
	#	(kN/m^2)	Average	SD	#	(MN/m^2)	Average	SD
H01-P00-L13	1	346.08	**341.28**	6.79	1	13.41	**12.79**	0.87
	2	336.48			2	12.18		
H03-P00-L13	1	358.00	**341.26**	23.66	1	4.83	**5.89**	1.51
	2	324.53			2	6.96		
H05-P00-L13	1	419.54	**398.13**	30.27	1	3.34	**3.60**	0.37
	2	376.72			2	3.87		
H10-P00-L13	1	231.26	**210.22**	29.76	1	2.44	**2.66**	0.32
	2	189.18			2	2.89		
H20-P00-L13	1	116.29	**112.03**	6.02	1	2.15	**2.26**	0.15
	2	107.78			2	2.36		
H30-P00-L13	1	68.33	**79.48**	15.77	1	2.04	**2.05**	0.01
	2	90.62			2	2.06		
H01-P00-L15	1	60.67	**59.45**	1.72	1	10.83	**10.52**	0.44
	2	58.24			2	10.21		
H03-P00-L15	1	141.17	**151.17**	14.14	1	4.32	**4.23**	0.12
	2	161.17			2	4.15		
H05-P00-L15	1	180.12	**168.11**	16.99	1	2.87	**3.01**	0.20
	2	156.10			2	3.15		
H10-P00-L15	1	101.05	**108.39**	10.38	1	2.10	**2.43**	0.47
	2	115.74			2	2.77		
H20-P00-L15	1	68.53	**77.15**	12.19	1	1.48	**1.64**	0.23
	2	85.77			2	1.81		
H30-P00-L15	1	-	**-**	-	1	-	**-**	-
	2	-			2	-		

ศูนย์วิทยทรัพยากร
จุฬาลงกรณ์มหาวิทยาลัย
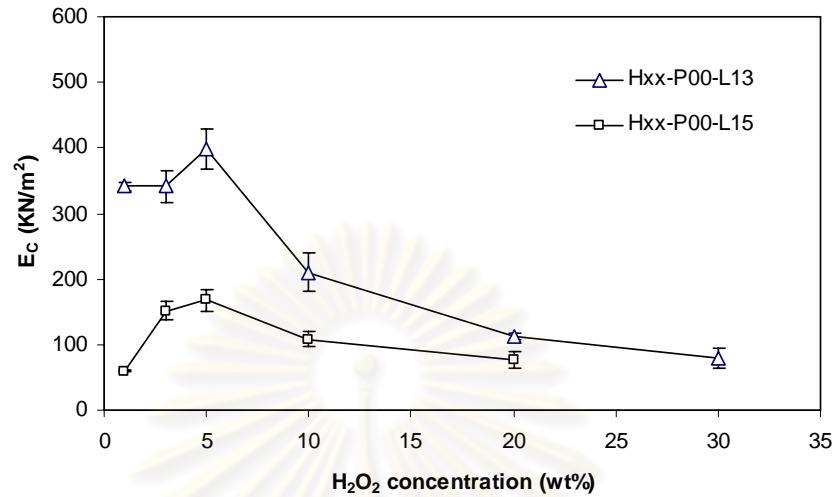
Figure 4.35   Relationship between compressive stiffness (E_C) and H_2O_2
               concentration of the HA samples, prepared via direct foaming
               technique using H_2O_2 solution with L/P ratio of 1.3 and 1.5 ml/g,
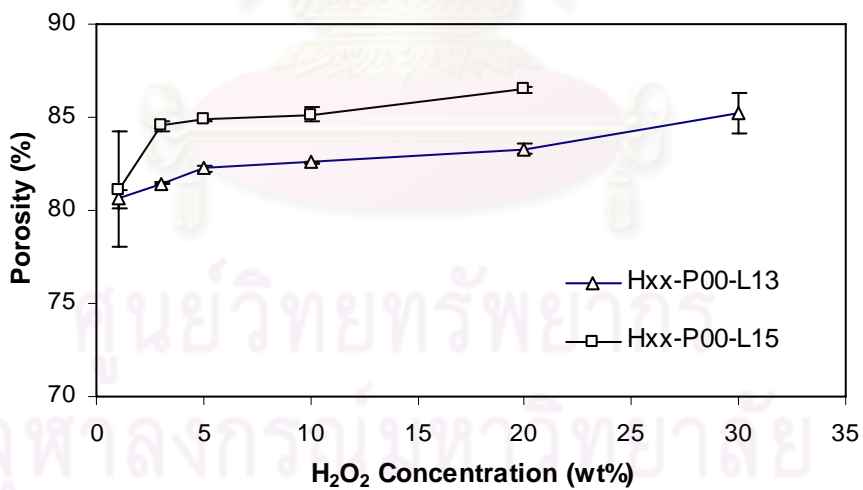   respectively.
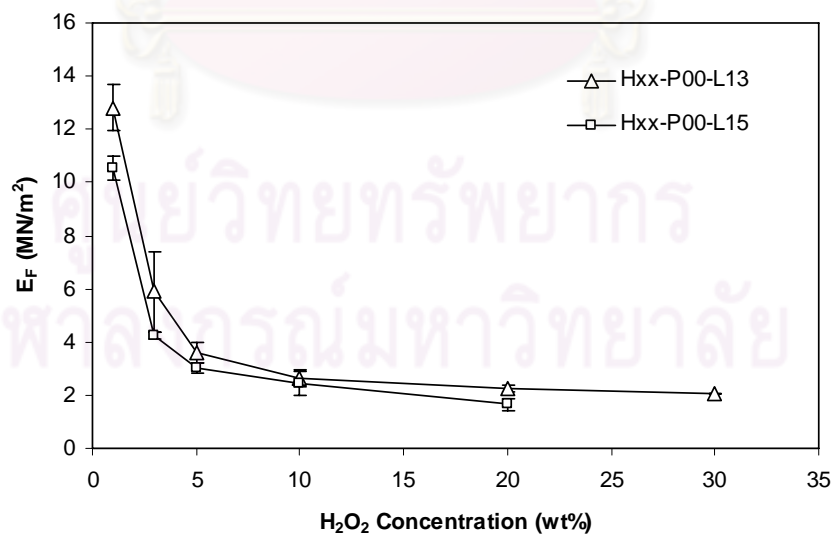
Figure 4.36   Relationship between flexural stiffness (E_F) and H_2O_2 concentration
               of the HA samples, prepared via direct foaming technique using H_2O_2
               solution with L/P ratio of 1.3 and 1.5 ml/g, respectively.

(C) Combination Technique using PMMA and H_2O_2

Table 4.14 summarized the compressive strength and flexural strength of the HA samples, prepared via combination technique using PMMA granules and H_2O_2 solution.

At 5wt% H_2O_2, the samples prepared through this method adding PMMA granules over 30 wt% were handless. The average compressive strength of the samples prepared at 5wt% H_2O_2 ranged between 0.04 and 0.33 MPa, whilst the average flexural strength ranged from 0.17 to 0.51 MPa.

At 10wt% H_2O_2, the samples prepared using PMMA over 20 wt% were handless. The average compressive strength of the samples prepared at 10 wt% H_2O_2 ranged between 0.03 and 0.30 MPa, while the average flexural strength ranged from 0.15 to 0.45 MPa.

At 20wt% H_2O_2, the samples prepared using PMMA over 10 wt% were handless. The average compressive strength of the samples prepared at 20wt% H_2O_2 ranged between 0.10 and 0.15 MPa, whereas the average flexural strength ranged from 0.18 to 0.30 MPa.

At 30wt% H_2O_2, the samples prepared using PMMA over 10 wt% were handless. The average compressive strength of the samples prepared at 30wt% H_2O_2 ranged between 0.03 and 0.15 MPa, whilst the average flexural strength ranged from 0.15 to 0.22 MPa.

Figure 4.37 showed the relationship between compressive strength (CS) and PMMA content of the HA samples from Table 4.14. The compressive strength decreased with the increases of both PMMA content and H_2O_2 concentration.

Figure 4.38 presented the relationship between flexural strength (FS) and PMMA content of the HA samples from Table 4.14. The flexural strength decreased with the increases of both PMMA content and H_2O_2 concentration. However, the variance of flexural strength showed a wider range than that of compressive strength.

Table 4.14   Compressive strength and flexural strength of the HA samples without surfactant, prepared via combination technique using PMMA granules and H_2O_2 solution.

Sample	Compressive strength				flexural strength			
	#	(MPa)	Average	SD	#	(MPa)	Average	SD
H05-P00-L13	1	0.34	**0.33**	0.02	1	0.46	**0.51**	0.07
	2	0.32			2	0.56		
H05-P05-L13	1	0.20	**0.19**	0.02	1	0.42	**0.43**	0.02
	2	0.17			2	0.45		
H05-P10-L13	1	0.12	**0.13**	0.01	1	0.41	**0.39**	0.04
	2	0.14			2	0.36		
H05-P20-L13	1	0.06	**0.05**	0.01	1	0.38	**0.32**	0.08
	2	0.04			2	0.27		
H05-P30-L13	1	0.04	**0.04**	0.00	1	0.17	**0.17**	0.01
	2	0.04			2	0.16		
H05-P40-L13	1	-	**-**	-	1	-	**-**	-
	2	-			2	-		
H05-P50-L13	1	-	**-**	-	1	-	**-**	-
	2	-			2	-		
H10-P00-L13	1	0.28	**0.30**	0.02	1	0.41	**0.45**	0.06
	2	0.31			2	0.49		
H10-P05-L13	1	0.17	**0.16**	0.01	1	0.37	**0.40**	0.05
	2	0.15			2	0.43		
H10-P10-L13	1	0.10	**0.11**	0.01	1	0.28	**0.31**	0.04
	2	0.12			2	0.33		
H10-P20-L13	1	0.03	**0.03**	0.00	1	0.16	**0.15**	0.02
	2	0.03			2	0.13		
H10-P30-L13	1	-	**-**	-	1	-	**-**	-
	2	-			2	-		
H10-P40-L13	1	-	**-**	-	1	-	**-**	-
	2	-			2	-		
H10-P50-L13	1	-	**-**	-	1	-	**-**	-
	2	-			2	-		
H20-P00-L13	1	0.20	**0.19**	0.01	1	0.29	**0.30**	0.01
	2	0.19			2	0.31		
H20-P05-L13	1	0.12	**0.13**	0.02	1	0.23	**0.24**	0.01
	2	0.14			2	0.25		
H20-P10-L13	1	0.11	**0.10**	0.01	1	0.23	**0.18**	0.08
	2	0.09			2	0.12		
H20-P20-L13	1	-	**-**	-	1	-	**-**	-
	2	-			2	-		
H20-P30-L13	1	-	**-**	-	1	-	**-**	-
	2	-			2	-		
H20-P40-L13	1	-	**-**	-	1	-	**-**	-
	2	-			2	-		
H20-P50-L13	1	-	**-**	-	1	-	**-**	-
	2	-			2	-		

Table 4.14   Compressive strength and flexural strength of the HA samples without surfactant, prepared via combination technique using PMMA granules and H_2O_2 solution (Continued).

Sample	Compressive strength				flexural strength			
	#	(MPa)	Average	SD	#	(MPa)	Average	SD
H30-P00-L13	1	0.12	**0.15**	0.03	1	0.22	**0.22**	0.01
	2	0.17			2	0.22		
H30-P05-L13	1	0.11	**0.11**	0.01	1	0.14	**0.18**	0.06
	2	0.10			2	0.23		
H30-P10-L13	1	0.10	**0.09**	0.02	1	0.18	**0.15**	0.05
	2	0.08			2	0.11		
H30-P20-L13	1	-	**-**	-	1	-	**-**	-
	2	-			2	-		
H30-P30-L13	1	-	**-**	-	1	-	**-**	-
	2	-			2	-		
H30-P40-L13	1	-	**-**	-	1	-	**-**	-
	2	-			2	-		
H30-P50-L13	1	-	**-**	-	1	-	**-**	-
	2	-			2	-		

Figure 4.37   Relationship between compressive strength (CS) and PMMA content
with various H_2O_2 concentration of the HA samples, prepared via
combination technique using PMMA granules and H_2O_2 solution with
L/P ratio of 1.3 ml/g
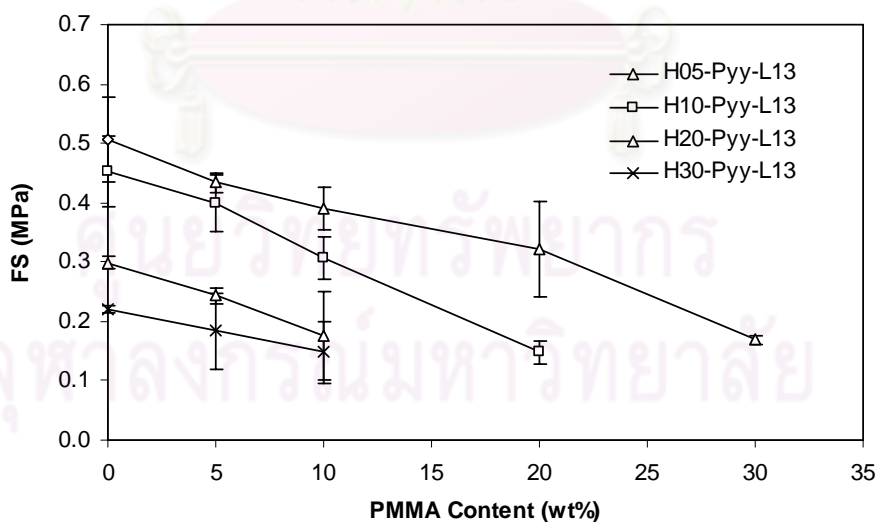
Figure 4.38   Relationship between flexural strength (FS) and PMMA content with
various H_2O_2 concentration of the HA samples, prepared via
combination technique using PMMA granules and H_2O_2 solution with
L/P ratio of 1.3 ml/g

Table 4.15 listed the compressive stiffness and flexural stiffness of the HA samples, prepared via combination technique using PMMA granules and H_2O_2 solution.

At 5wt% H_2O_2, the samples prepared through this method adding PMMA granules over 30 wt% were handless. The average compressive stiffness of the samples prepared at 5wt% H_2O_2 ranged between 41.58 and 434.03 kN/m^2, whilst the average flexural stiffness ranged from 0.42 to 3.60 MN/m^2.

At 10wt% H_2O_2, the samples prepared using PMMA over 20 wt% were handless. The average compressive stiffness of the samples prepared at 10wt% H_2O_2 ranged between 24.70 and 210.22 kN/m^2, whereas the average flexural stiffness ranged from 0.35 to 2.66 MN/m^2.

At 20wt% H_2O_2, the samples prepared using PMMA over 10 wt% were handless. The average compressive stiffness of the samples prepared at 20wt% H_2O_2 ranged between 91.68 and 121.81 kN/m^2, whilst the average flexural stiffness ranged from 0.93 to 2.26 MN/m^2.

At 30wt% H_2O_2, the samples prepared using PMMA over 10 wt% were handless. The average compressive stiffness of the samples prepared at 30wt% H_2O_2 ranged between 42.03 and 79.48 kN/m^2, while the average flexural stiffness ranged from 0.77 to 2.05 MN/m^2.

Figure 4.39 displayed the relationship between compressive stiffness (E_C) and PMMA content with various H_2O_2 concentration of the HA samples from Table 4.15. The compressive stiffness decreased with the increases of both PMMA content and H_2O_2 concentration.

Figure 4.40 illustrated the relationship between flexural stiffness (E_F) and PMMA content with various H_2O_2 concentration of the HA samples from Table 4.15. The flexural stiffness reduced with the increases of both PMMA content and H_2O_2 concentration.

Table 4.15 Compressive stiffness and flexural stiffness of the HA samples, prepared via combination technique using PMMA granules and H_2O_2 solution.

Sample	Compressive stiffness				Flexural stiffness			
	#	(kN/m²)	Average	SD	#	(kN/m²)	Average	SD
H05-P00-L13	1	431.98	**434.03**	2.91	1	3.34	**3.60**	0.37
	2	436.08			2	3.87		
H05-P05-L13	1	123.65	**99.77**	33.77	1	2.58	**2.89**	0.44
	2	75.89			2	3.20		
H05-P10-L13	1	76.06	**81.37**	7.50	1	2.35	**1.77**	0.82
	2	86.67			2	1.19		
H05-P20-L13	1	80.48	**62.37**	25.60	1	0.44	**0.55**	0.15
	2	44.27			2	0.66		
H05-P30-L13	1	31.73	**41.58**	13.93	1	0.34	**0.42**	0.11
	2	51.43			2	0.50		
H05-P40-L13	1	-	**-**	-	1	-	**-**	-
	2	-			2	-		
H05-P50-L13	1	-	**-**	-	1	-	**-**	-
	2	-			2	-		
H10-P00-L13	1	231.26	**210.22**	29.76	1	2.44	**2.66**	0.32
	2	189.18			2	2.89		
H10-P05-L13	1	122.27	**160.01**	53.38	1	1.69	**2.22**	0.75
	2	197.75			2	2.75		
H10-P10-L13	1	113.90	**112.96**	1.32	1	1.07	**1.12**	0.08
	2	112.03			2	1.18		
H10-P20-L13	1	12.73	**24.70**	16.92	1	0.36	**0.35**	0.02
	2	36.67			2	0.34		
H10-P30-L13	1	-	**-**	-	1	-	**-**	-
	2	-			2	-		
H10-P40-L13	1	-	**-**	-	1	-	**-**	-
	2	-			2	-		
H10-P50-L13	1	-	**-**	-	1	-	**-**	-
	2	-			2	-		
H20-P00-L13	1	116.29	**112.03**	6.02	1	2.15	**2.26**	0.15
	2	107.78			2	2.36		
H20-P05-L13	1	111.07	**121.81**	15.19	1	1.96	**1.89**	0.11
	2	132.55			2	1.81		
H20-P10-L13	1	117.13	**91.68**	35.99	1	0.98	**0.93**	0.07
	2	66.23			2	0.89		
H20-P20-L13	1	-	**-**	-	1	-	**-**	-
	2	-			2	-		
H20-P30-L13	1	-	**-**	-	1	-	**-**	-
	2	-			2	-		
H20-P40-L13	1	-	**-**	-	1	-	**-**	-
	2	-			2	-		
H20-P50-L13	1	-	**-**	-	1	-	**-**	-
	2	-			2	-		

Table 4.15 Compressive stiffness and flexural stiffness of the HA samples, prepared via combination technique using PMMA granules and H_2O_2 solution (Continued).

Sample	Compressive stiffness				Flexural stiffness			
	#	(kN/m^2)	Average	SD	#	(kN/m^2)	Average	SD
H30-P00-L13	1	68.33	**79.48**	15.77	1	2.04	**2.05**	0.01
	2	90.62			2	2.06		
H30-P05-L13	1	68.29	**57.69**	15.00	1	1.35	**1.77**	0.59
	2	47.08			2	2.18		
H30-P10-L13	1	45.74	**42.03**	5.24	1	0.98	**0.77**	0.30
	2	38.32			2	0.55		
H30-P20-L13	1	-	**-**	-	1	-	**-**	-
	2	-			2	-		
H30-P30-L13	1	-	**-**	-	1	-	**-**	-
	2	-			2	-		
H30-P40-L13	1	-	**-**	-	1	-	**-**	-
	2	-			2	-		
H30-P50-L13	1	-	**-**	-	1	-	**-**	-
	2	-			2	-		

Figure 4.39   Relationship between compressive stiffness (E_C) and PMMA content
with various H_2O_2 concentration of the HA samples, prepared via
combination technique using PMMA granules and H_2O_2 solution with
L/P ratio of 1.3 ml/g
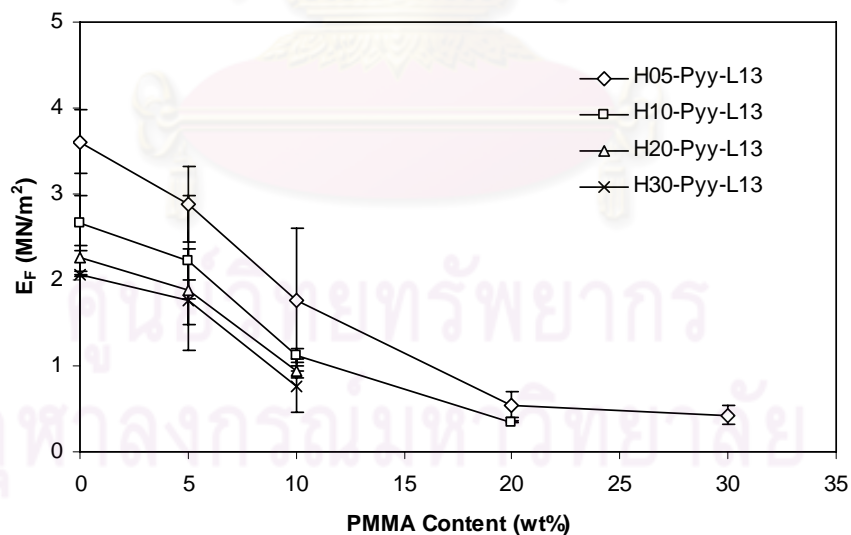
Figure 4.40   Relationship between flexural stiffness (E_F) and PMMA content with
various H_2O_2 concentration of the HA samples, prepared via
combination technique using PMMA granules and H_2O_2 solution with
L/P ratio of 1.3 ml/g

4.5 Characteristics of the Porous HA Samples with Surfactant

   To study the effect of addition of surfactant, a preliminary experiment on the porous HA samples with surfactant was conducted. The results found that the addition of 1wt% agar powder could affect on characteristics of the porous HA samples prepared through various methods. Therefore, the microstructure, bulk density, porosity and mechanical properties of the porous samples were investigated and reported as follows.

4.5.1 Microstructure

   In this section, microstructure of the HA samples with surfactant, prepared by H_2O based technique, direct foaming using H_2O_2 and combination technique using PMMA and H_2O_2, were explained.

   (A) H_2O based Technique

   Figure 4.41 presented SEM micrographs of the HA sample H00-P00-L13A at the magnification of (a) 100X, (b) 500X, (c) 1,000X and (d) 5,000X. The sample H00-P00-L13A was prepared using 0wt% H_2O_2, 0wt% PMMA and 1wt% agar at the L/P ratio of 1.3 ml/g. In Figure 4.41 (a) and (b), the sample was composed of large agglomerated particles, forming some pores. In Figure 4.41 (c), the pore had irregular and angular shape. In Figure 4.41 (d), the surface contained some clusters of pores with the size of less than 5 μm.

   (B) Direct Foaming Technique using H_2O_2

   Figure 4.42 showed SEM micrographs of the HA sample H10-P00-L13A at the magnification of (a) 100X, (b) 500X, (c) 1,000X, (d) 5,000X and (e) 10,000X. The HA sample H10-P00-L13A was prepared by adding 1wt% agar into the mixture of 10wt% H_2O_2 and 0wt% PMMA at the L/P ratio of 1.3 ml/g. In Figure 4.42 (a) and (b), a number of pores larger than 100 μm were found. In Figure 4.42 (c), pores with the size less than 50 μm was observed. In Figure 4.42 (d) and (e), surface of the sample was made from thousands of crystal bars.

Figure 4.43 illustrated SEM micrographs of the HA sample H20-P00-L13A at the magnification of (a) 50X, (b) 100X, (c) 500X, (d) 1,000X and (e) 5,000X. The HA sample H20-P00-L13A was prepared by adding 1wt% agar into the mixture of 20wt% H_2O_2 and 0wt% PMMA at the L/P ratio of 1.3 ml/g. In Figure 4.43 (a) and (b), the pores with the size of over 100 μm were noticed. In Figure 4.43 (c) and (d), the pore with the size of less than 50 μm remained in the sample. In Figure 4.43 (e), surface of this sample had some pore with the size of less than 1 μm.

(C) Combination Technique using PMMA and H_2O_2

Figure 4.44 showed SEM micrographs of the sample H10-P10-L13A at the magnification of (a) 50 X, (b) 100X, (c) 500X, (d) 1,000X and (e) 5,000X. The HA sample H10-P10-L13A was prepared using 10wt% PMMA, 10wt% H_2O_2 and 1 wt% agar with the L/P ratio of 1.3 ml/g. In Figure 4.44 (a) and (b), the pores with the size of over 500 μm and the interconnected pores were still noticed. In Figure 4.44 (c) and (d), pores with the size of around 50 μm were observed. In Figure 4.44 (e), the tiny pores (less than 1 μm) in surface on this sample were barely found. A few agglomerated particles remained on the surface.

(a) 100X

(b) 500X
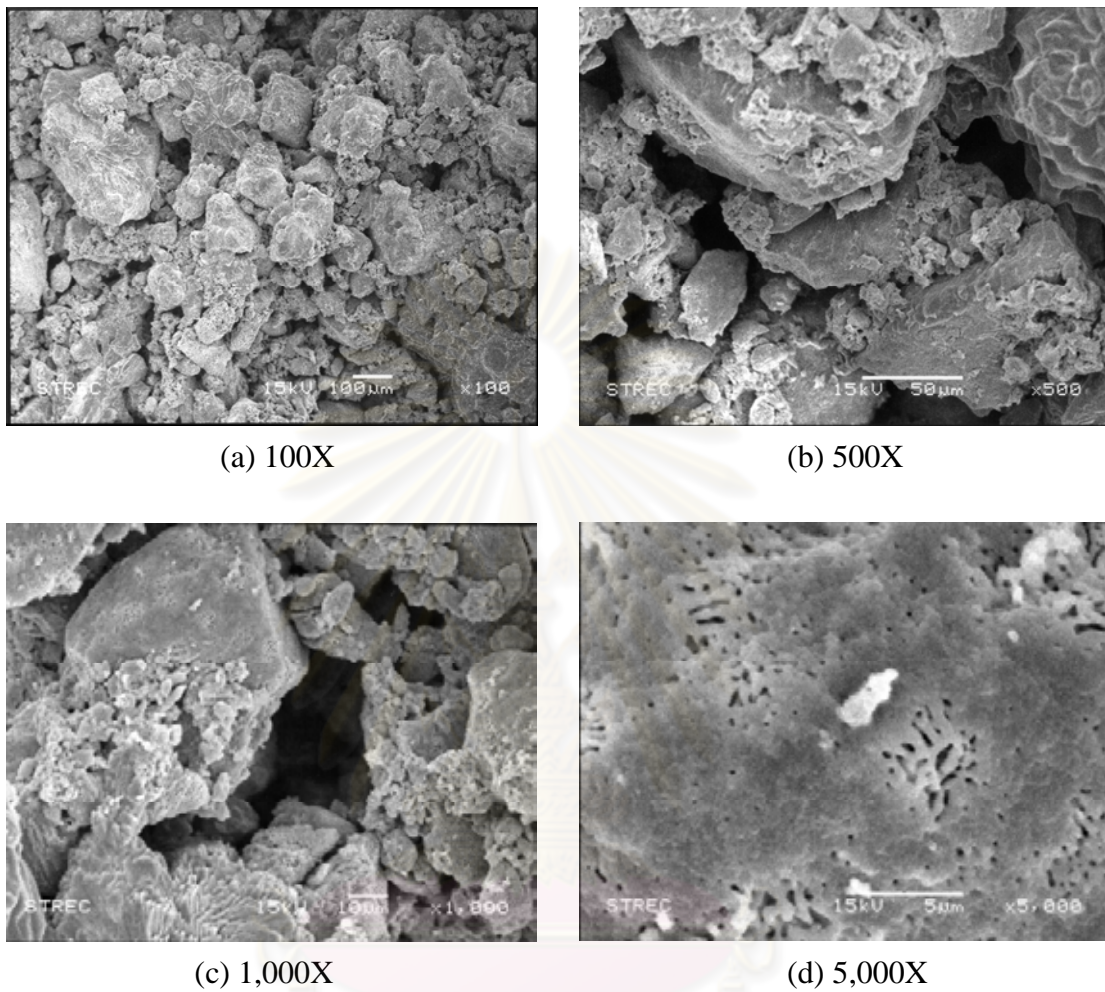
(c) 1,000X

(d) 5,000X

Figure 4.41   SEM micrographs of the HA sample with 1wt% agar of the sample
H00-P00-L13A at the magnification of (a) 100X, (b) 500X, (c)
1,000X and (d) 5,000X

(a) 100X

(b) 500X

(c) 1,000X
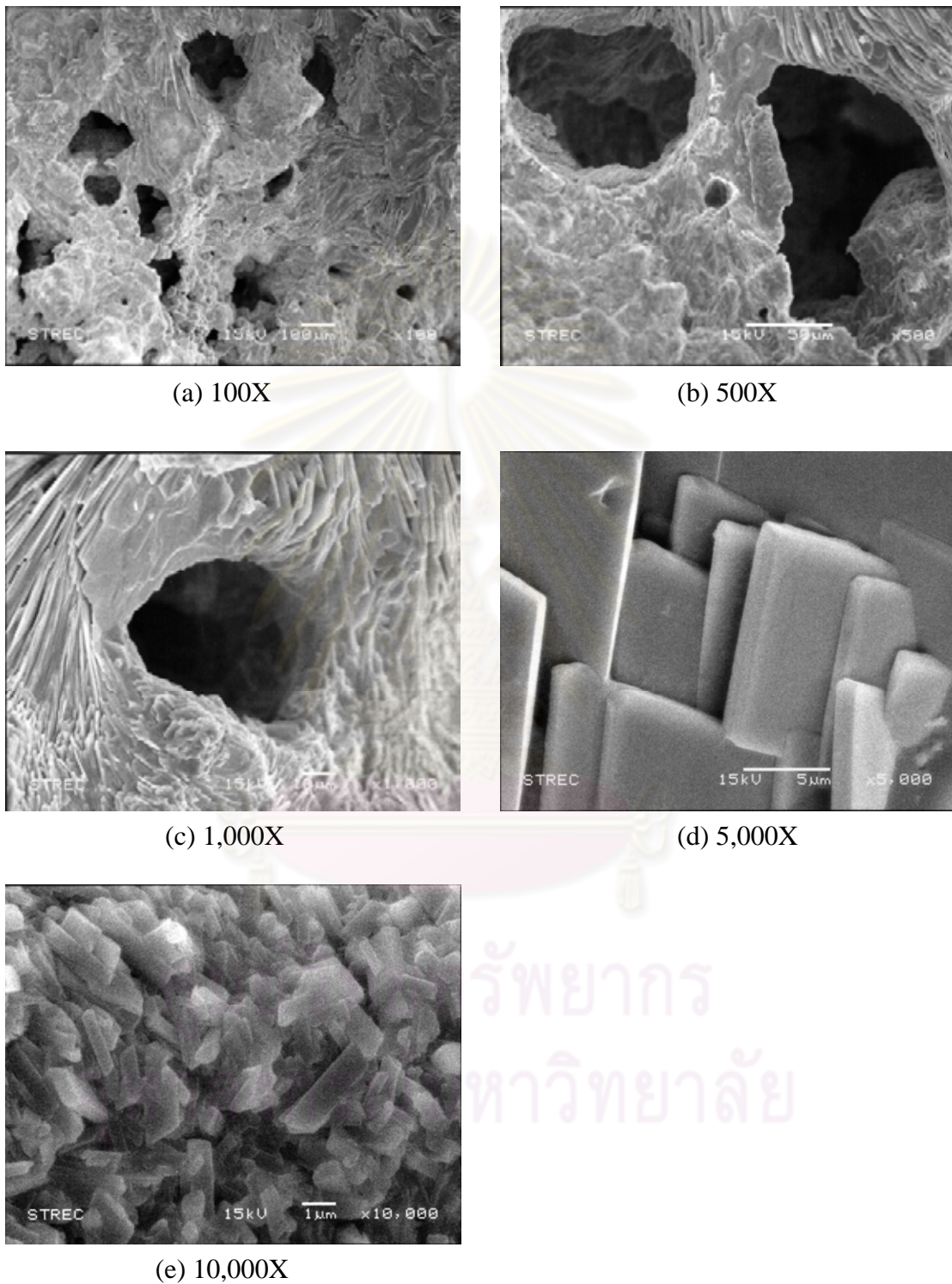
(d) 5,000X

(e) 10,000X

Figure 4.42   SEM micrographs of the HA sample with 1wt% agar of the sample
                H10-P00-L13A at the magnification of (a) 100X, (b) 500X, (c)
                1,000X, (d) 5,000X and (e) 10,000X

(a) 50X

(b) 100X

(c) 500X
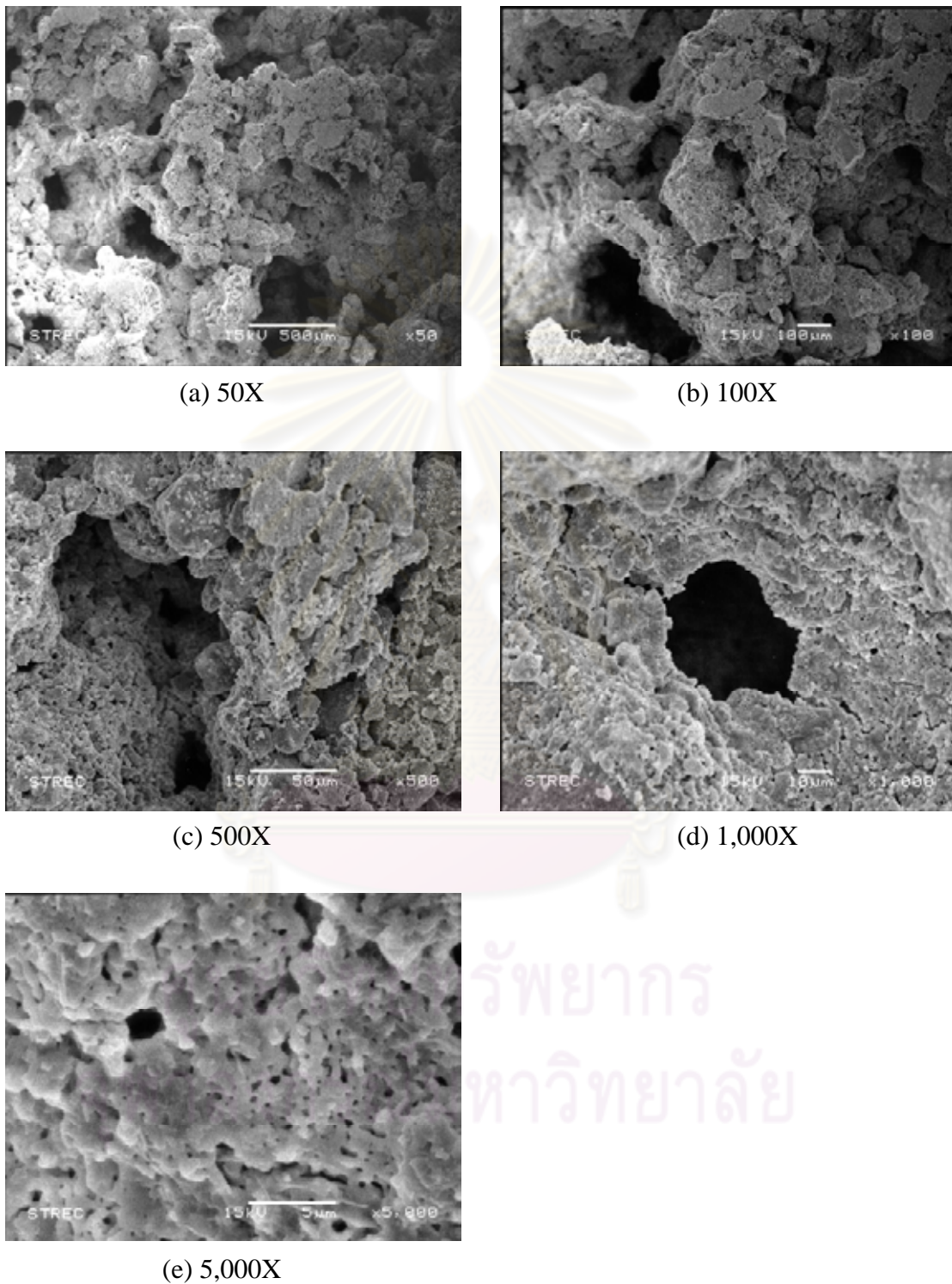
(d) 1,000X

(e) 5,000X

Figure 4.43   SEM micrographs of the HA sample with 1wt% agar of the sample
                H20-P00-L13A at the magnification of (a) 100X, (b) 500X, (c)
                1,000X, (d) 5,000X and (e) 10,000X

(a) 50X

(b) 100X

(c) 500X
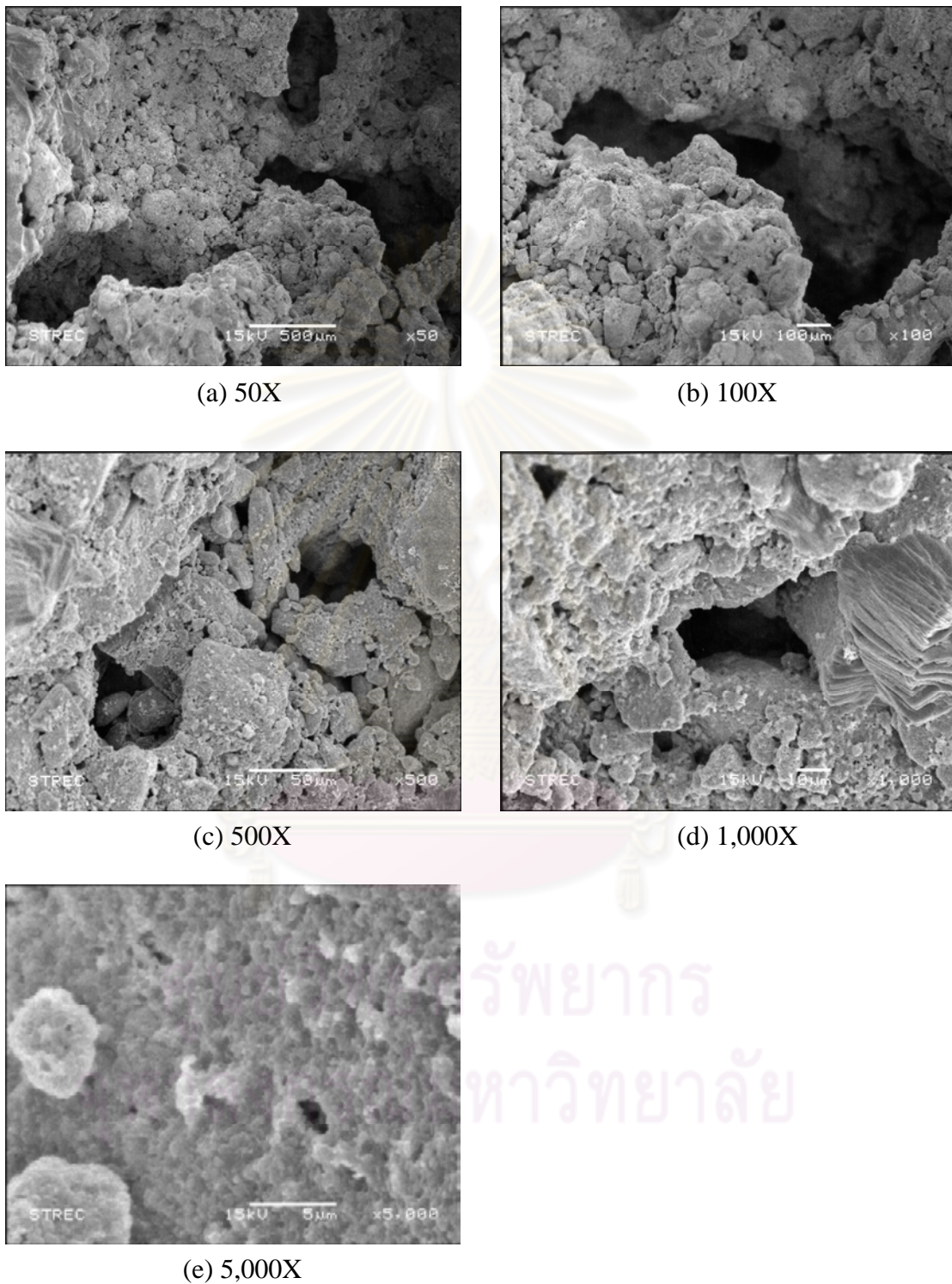
(d) 1,000X

(e) 5,000X

Figure 4.44   SEM micrographs of the HA sample with 1wt% agar of the sample
H10-P10-L13A at the magnification of (a) 50 X, (b) 100X, (c) 500X,
(d) 1,000X and (e) 5,000X

4.5.2 Bulk Density and Porosity

(A) Sacrificial Template Technique using PMMA

Table 4.16 summarized the bulk density and porosity of the HA samples with surfactant, prepared via sacrificial template technique using PMMA granules. The sample using PMMA over 40 wt% was handless. The average bulk density and porosity of these samples ranged from 0.91 to 1.46 g/cm^3 and ranged from 53.70% to 71.28%, respectively.

Figure 4.45 illustrated the effect of adding surfactant and PMMA content on bulk density (BD) of the HA samples prepared via sacrificial template technique using PMMA granules. The bulk density of both samples decreased with an increase of PMMA content. However, Addition of surfactant (agar) resulted in a decrease of bulk density of the samples prepared using PMMA between 0wt% and 30wt%. Over 30wt% PMMA, the samples adding agar showed better bulk density than the other without surfactant.

Figure 4.46 presented the effect of adding surfactant and PMMA content on porosity of the HA samples prepared via sacrificial template technique using PMMA granules. The porosity of both samples increased with an increase of PMMA content. Moreover, Addition of surfactant (agar) caused an increase of porosity of the HA samples prepared using PMMA between 0wt% and 30wt%. Over 30wt% PMMA, the porosity of the sample adding agar was lower than the other without surfactant.

Table 4.16   Bulk density and porosity of the HA samples with surfactant, prepared
via sacrificial template technique using PMMA granules.

Sample	Bulk Density				Porosity			
	#	(g/cm^3)	Average	SD	#	(%)	Average	SD
H00-P00-L13A	1	1.46	**1.46**	0.00	1	53.60	**53.70**	0.15
	2	1.46			2	53.81		
H00-P05-L13A	1	1.44	**1.43**	0.01	1	54.45	**54.64**	0.27
	2	1.43			2	54.82		
H00-P10-L13A	1	1.49	**1.42**	0.09	1	52.91	**54.90**	2.81
	2	1.36			2	56.88		
H00-P20-L13A	1	1.22	**1.23**	0.02	1	61.42	**61.06**	0.52
	2	1.24			2	60.69		
H00-P30-L13A	1	1.12	**1.10**	0.03	1	64.54	**65.10**	0.80
	2	1.08			2	65.66		
H00-P40-L13A	1	0.90	**0.91**	0.00	1	71.36	**71.28**	0.11
	2	0.91			2	71.20		
H00-P50-L13A	1	-	**-**	-	1	-	**-**	-
	2	-			2	-		

ศูนย์วิทยทรัพยากร
จุฬาลงกรณ์มหาวิทยาลัย

Figure 4.45   Effect of adding surfactant and PMMA content on bulk density (BD)
                of the HA samples prepared via sacrificial template technique using
                PMMA granules

Figure 4.46   Effect of adding surfactant and PMMA content on porosity of the HA
                samples prepared via sacrificial template technique using PMMA
                granules

(B) Direct Foaming Technique using H_2O_2

Table 4.17 summarized the bulk density and porosity of the HA samples with surfactant, prepared via direct foaming technique using H_2O_2 solution. The average bulk density and porosity of these samples ranged from 0.47 to 0.61 g/cm^3 and ranged from 80.62% to 85.14%, respectively.

Figure 4.47 exhibited the effect of adding surfactant and H_2O_2 concentration on bulk density (BD) of the HA samples prepared via direct foaming technique using H_2O_2 solution. The bulk density of both samples decreased with an increasing concentration of H_2O_2. Moreover, addition of surfactant (agar) resulted in an improvement of bulk density.

Figure 4.48 displayed the effect of adding surfactant and H_2O_2 concentration on porosity of the HA samples prepared via direct foaming technique using H_2O_2 solution. The porosity of both samples increased with an increasing concentration of H_2O_2. Furthermore, the porosity of the sample adding agar was lower than that of the sample without surfactant.

Table 4.17   Bulk density and porosity of the HA samples with surfactant, prepared via direct foaming technique using H_2O_2 solution.

Sample		Bulk Density				Porosity		
	#	(g/cm^3)	Average	SD	#	(%)	Average	SD
H01-P00-L13A	1	0.60	**0.61**	0.01	1	80.88	**80.62**	0.37
	2	0.62			2	80.36		
H03-P00-L13A	1	0.57	**0.60**	0.03	1	81.79	**81.10**	0.97
	2	0.62			2	80.41		
H05-P00-L13A	1	0.60	**0.60**	0.01	1	81.07	**80.88**	0.26
	2	0.61			2	80.70		
H10-P00-L13A	1	0.57	**0.58**	0.01	1	81.94	**81.64**	0.42
	2	0.59			2	81.35		
H20-P00-L13A	1	0.55	**0.56**	0.02	1	82.53	**82.13**	0.57
	2	0.58			2	81.72		
H30-P00-L13A	1	0.43	**0.47**	0.06	1	86.38	**85.14**	1.76
	2	0.51			2	83.90		
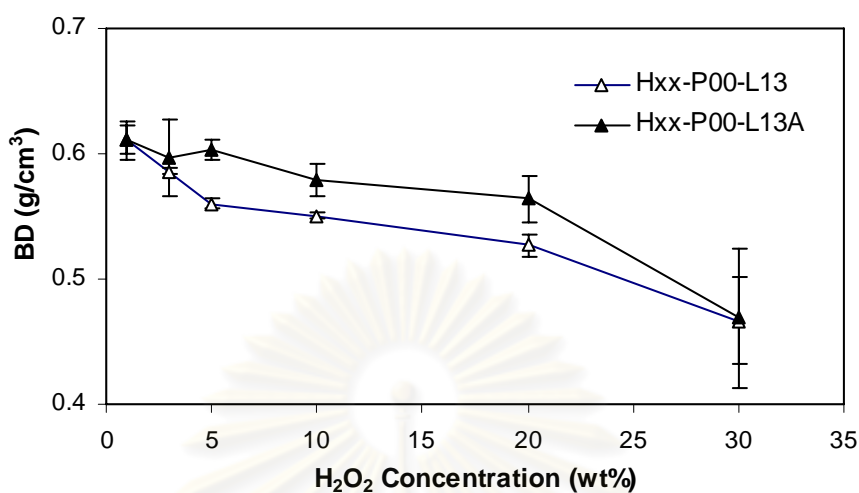
Figure 4.47   Effect of adding surfactant and H_2O_2 concentration on bulk density
              (BD) of the HA samples prepared via direct foaming technique using
              H_2O_2 solution
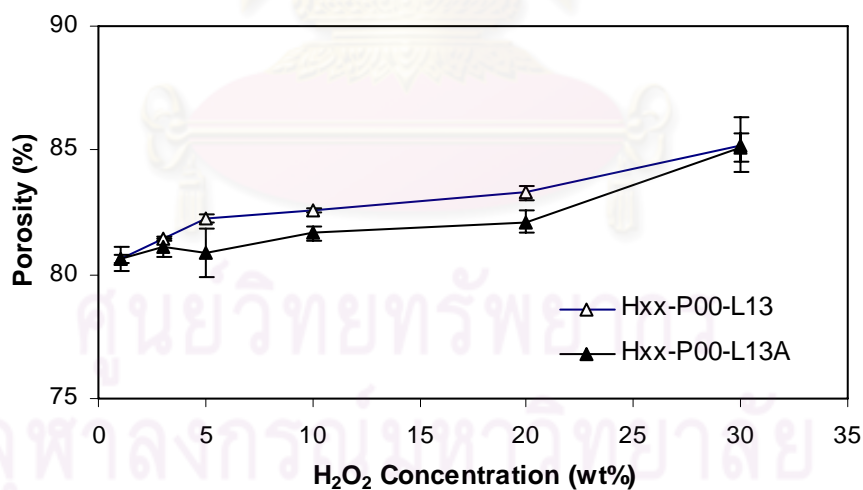
Figure 4.48   Effect of adding surfactant and H_2O_2 concentration on porosity of the
              HA samples prepared via direct foaming technique using H_2O_2
              solution

(C) Combination Technique using PMMA and H_2O_2

Table 4.18 summarized the bulk density and porosity of the HA samples with surfactant, prepared via combination technique using PMMA granule and H_2O_2 solution. The average bulk density of the samples adding surfactant ranged between 0.43 and 0.60 g/cm^3 at 5wt% H_2O_2; ranged between 0.43 and 0.58 g/cm^3 at 10wt% H_2O_2; ranged between 0.44 and 0.56 g/cm^3 at 20wt% H_2O_2; and ranged between 0.40 and 0.47 g/cm^3 at 30wt% H_2O_2. The average porosity of the samples adding agar ranged between 80.88% and 86.38% at 5wt% H_2O_2; ranged between 81.64% and 86.34% g/cm^3 at 10wt% H_2O_2; ranged between 82.13% and 86.19% at 20wt% H_2O_2; and ranged between 85.14% and 87.28% at 30wt% H_2O_2.

Figure 4.49 showed effect of PMMA content and H_2O_2 concentration on bulk density (BD) of the HA samples with surfactant, prepared via combination technique using PMMA granules and H_2O_2 solution with L/P ratio of 1.3 ml/g. The bulk density of the HA samples adding agar decreased with the increases of both PMMA content and H_2O_2 concentration.

Figure 4.50, Figure 4.51, Figure 4.52 and Figure 4.53 illustrated the effect of adding surfactant and PMMA content on bulk density (BD) of the HA samples prepared via combination technique using PMMA granules and H_2O_2 solution, at 5wt%, 10wt%, 20wt% and 30wt% H_2O_2, respectively. The bulk density of the sample adding agar was higher than that of the sample without surfactant. At 30wt% H_2O_2, the sample adding agar had a bit higher bulk density than the other without surfactant.

Table 4.18   Bulk density and porosity of the HA samples with surfactant, prepared
via combination technique using PMMA granule and H_2O_2 solution

Sample	Bulk Density				Porosity			
	#	(g/cm^3)	Average	SD	#	(%)	Average	SD
H05-P00-L13A	1	0.60	**0.60**	0.01	1	81.07	**80.88**	0.26
	2	0.61			2	80.70		
H05-P05-L13A	1	0.59	**0.57**	0.03	1	81.18	**81.82**	0.90
	2	0.55			2	82.46		
H05-P10-L13A	1	0.51	**0.52**	0.02	1	83.97	**83.48**	0.69
	2	0.54			2	82.99		
H05-P20-L13A	1	0.46	**0.45**	0.02	1	85.31	**85.83**	0.74
	2	0.43			2	86.36		
H05-P30-L13A	1	0.42	**0.43**	0.01	1	86.54	**86.38**	0.23
	2	0.43			2	86.22		
H05-P40-L13A	1	-	**-**	-	1	-	**-**	-
	2	-			2	-		
H05-P50-L13A	1	-	**-**	-	1	-	**-**	-
	2	-			2	-		
H10-P00-L13A	1	0.57	**0.58**	0.01	1	81.94	**81.64**	0.42
	2	0.59			2	81.35		
H10-P05-L13A	1	0.50	**0.48**	0.03	1	84.23	**84.84**	0.87
	2	0.46			2	85.45		
H10-P10-L13A	1	0.46	**0.45**	0.01	1	85.54	**85.78**	0.33
	2	0.44			2	86.01		
H10-P20-L13A	1	0.44	**0.43**	0.01	1	86.12	**86.34**	0.30
	2	0.42			2	86.55		
H10-P30-L13A	1	-	**-**	-	1	-	**-**	-
	2	-			2	-		
H10-P40-L13A	1	-	**-**	-	1	-	**-**	-
	2	-			2	-		
H10-P50-L13A	1	-	**-**	-	1	-	**-**	-
	2	-			2	-		
H20-P00-L13A	1	0.55	**0.56**	0.02	1	82.53	**82.13**	0.57
	2	0.58			2	81.72		
H20-P05-L13A	1	0.44	**0.46**	0.02	1	85.90	**85.41**	0.70
	2	0.48			2	84.91		
H20-P10-L13A	1	0.42	**0.44**	0.02	1	86.69	**86.19**	0.70
	2	0.45			2	85.70		
H20-P20-L13A	1	-	**-**	-	1	-	**-**	-
	2	-			2	-		
H20-P30-L13A	1	-	**-**	-	1	-	**-**	-
	2	-			2	-		
H20-P40-L13A	1	-	**-**	-	1	-	**-**	-
	2	-			2	-		
H20-P50-L13A	1	-	**-**	-	1	-	**-**	-
	2	-			2	-		

Table 4.18   Bulk density and porosity of the HA samples with surfactant, prepared
             via combination technique using PMMA granule and H_2O_2 solution
             (Continued)

Sample	Bulk Density				Porosity			
	#	(g/cm^3)	Average	SD	#	(%)	Average	SD
H30-P00-L13A	1	0.43	**0.47**	0.06	1	86.38	**85.14**	1.76
	2	0.51			2	83.90		
H30-P05-L13A	1	0.44	**0.44**	0.00	1	86.21	**86.19**	0.01
	2	0.44			2	86.18		
H30-P10-L13A	1	0.39	**0.40**	0.01	1	87.59	**87.28**	0.44
	2	0.41			2	86.97		
H30-P20-L13A	1	-	**-**	-	1	-	**-**	-
	2	-			2	-		
H30-P30-L13A	1	-	**-**	-	1	-	**-**	-
	2	-			2	-		
H30-P40-L13A	1	-	**-**	-	1	-	**-**	-
	2	-			2	-		
H30-P50-L13A	1	-	**-**	-	1	-	**-**	-
	2	-			2	-		

Figure 4.49   Effect of PMMA content and H_2O_2 concentration on bulk density
             (BD) of the HA samples with surfactant, prepared via combination
             technique using PMMA granules and H_2O_2 solution with L/P ratio of
             1.3 ml/g
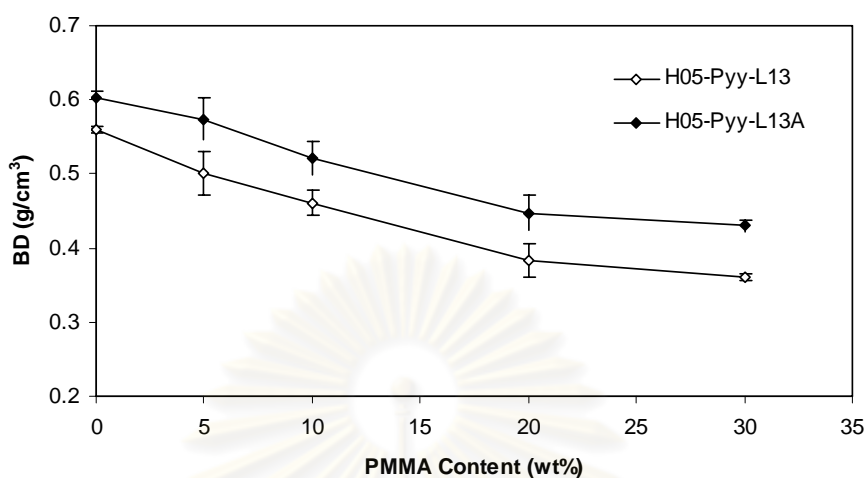
Figure 4.50   Effect of adding surfactant and PMMA content on bulk density (BD) of the HA samples prepared via combination technique using PMMA granules and H_2O_2 solution, at 5wt% H_2O_2 solution with L/P ratio of 1.3 ml/g
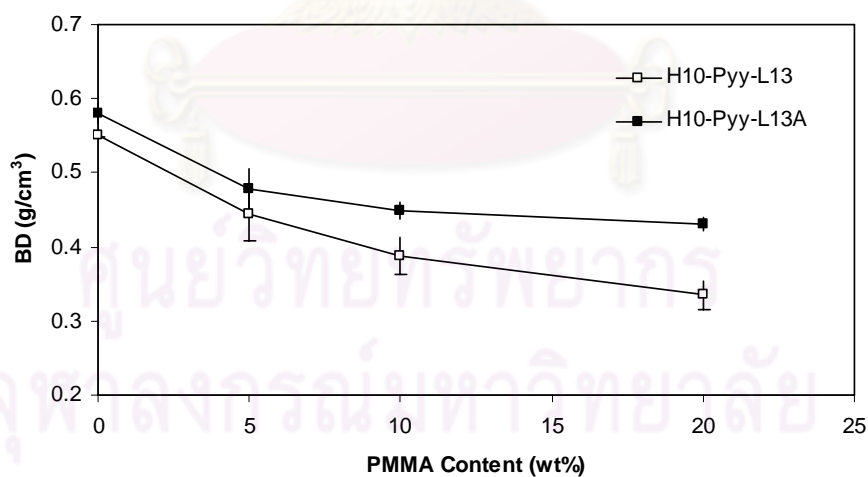
Figure 4.51   Effect of adding surfactant and PMMA content on bulk density (BD) of the HA samples prepared via combination technique using PMMA granules and H_2O_2 solution, at 10wt% H_2O_2 solution with L/P ratio of 1.3 ml/g
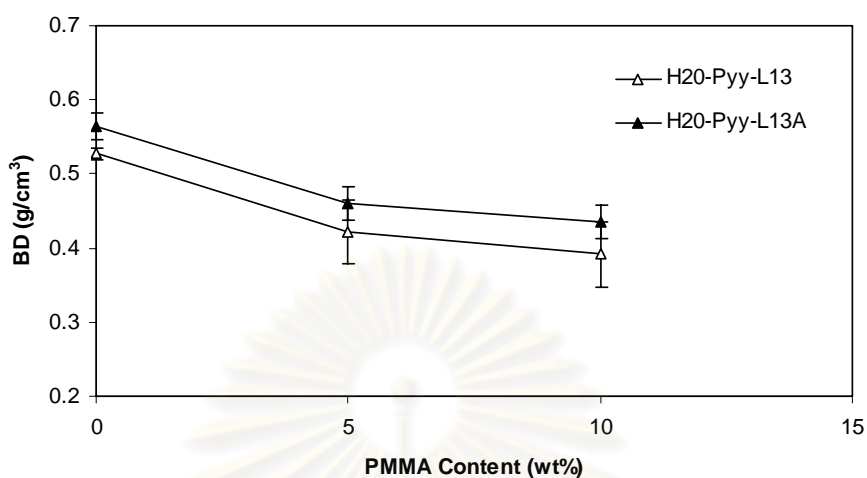
Figure 4.52   Effect of adding surfactant and PMMA content on bulk density (BD) of the HA samples prepared via combination technique using PMMA granules and H_2O_2 solution, at 20wt% H_2O_2 solution with L/P ratio of 1.3 ml/g
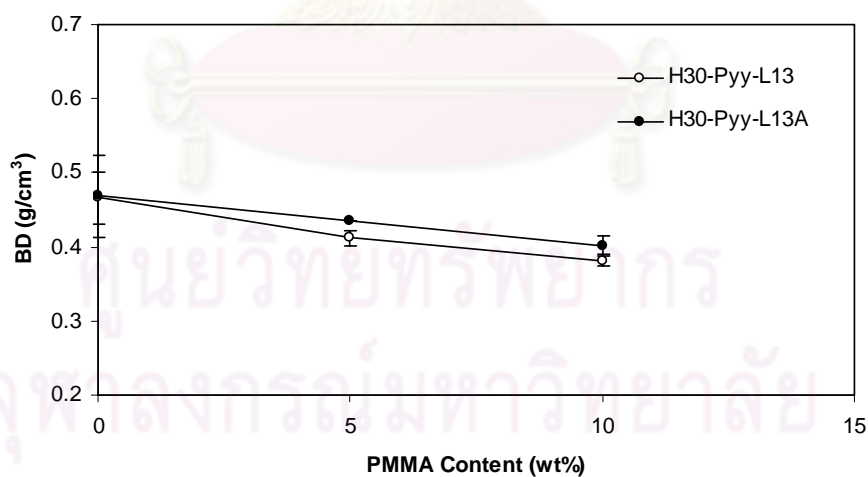
Figure 4.53   Effect of adding surfactant and PMMA content on bulk density (BD) of the HA samples prepared via combination technique using PMMA granules and H_2O_2 solution, at 30wt% H_2O_2 solution with L/P ratio of 1.3 ml/g

Figure 4.54 displayed the effect of PMMA content and H_2O_2 concentration on porosity of the HA samples with surfactant, prepared via combination technique using PMMA granules and H_2O_2 solution with L/P ratio of 1.3 ml/g. The porosity of the HA samples adding surfactant (agar) increased with the increases of both PMMA content and H_2O_2 concentration.

Figure 4.55, Figure 4.56, Figure 4.57 and Figure 4.58 presented the effect of adding surfactant and PMMA content on bulk density (BD) of the HA samples prepared via combination technique using PMMA granules and H_2O_2 solution with L/P ratio of 1.3 ml/g, at 5wt%, 10wt%, 20wt% and 30wt% H_2O_2, respectively. The porosity of the sample adding agar was lower than that of the sample without surfactant.
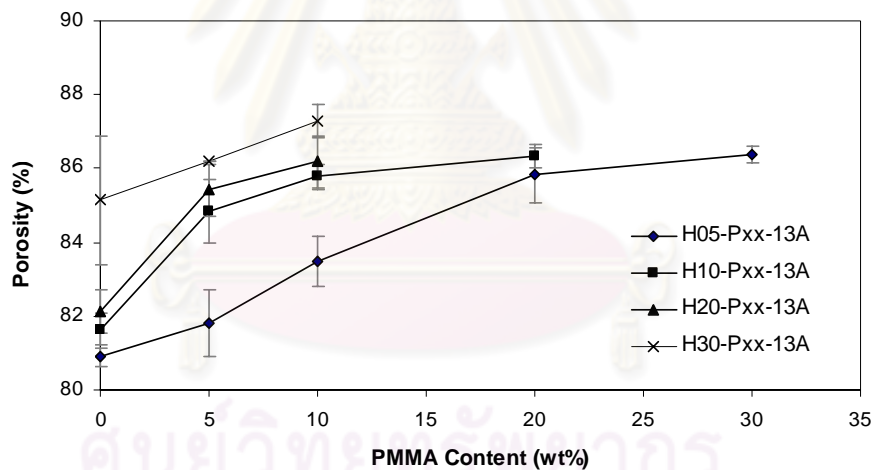
Figure 4.54   Effect of PMMA content and H_2O_2 concentration on porosity of the HA samples with surfactant, prepared via combination technique using PMMA granules and H_2O_2 solution with L/P ratio of 1.3 ml/g
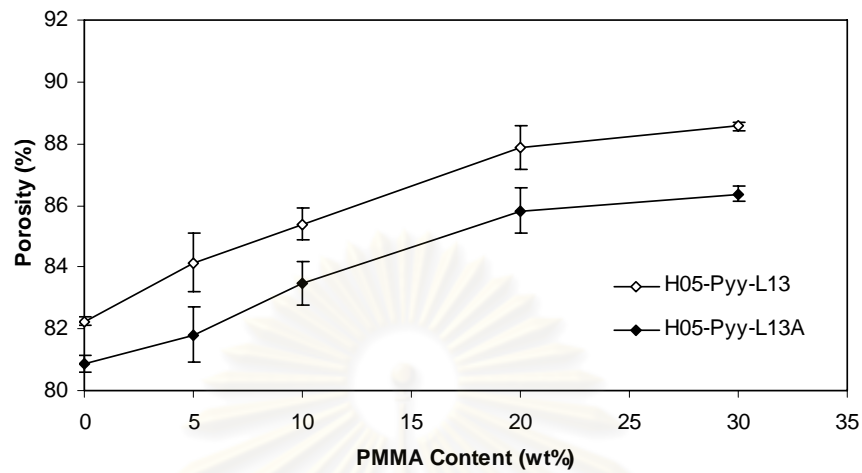
Figure 4.55   Effect of adding surfactant and PMMA content on porosity of the HA
samples prepared via combination technique using PMMA granules
and H_2O_2 solution, at 5wt% H_2O_2 solution with L/P ratio of 1.3 ml/g
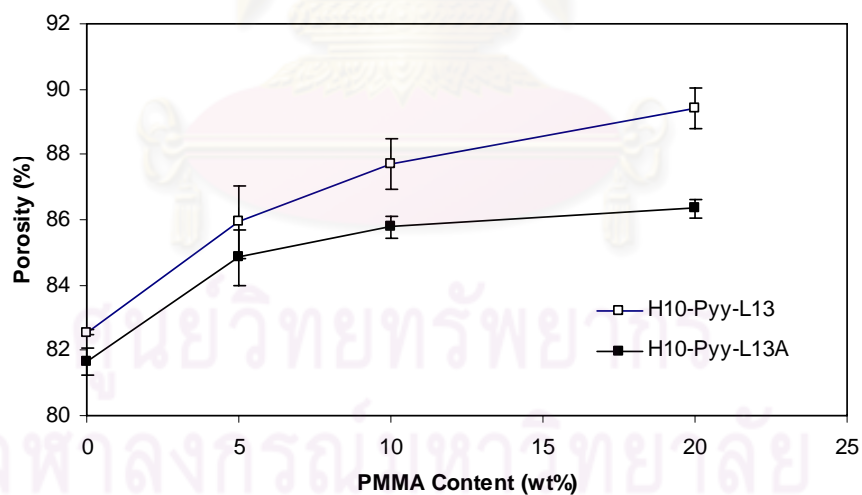
Figure 4.56   Effect of adding surfactant and PMMA content on porosity of the HA
samples prepared via combination technique using PMMA granules
and H_2O_2 solution, at 10wt% H_2O_2 solution with L/P ratio of 1.3 ml/g
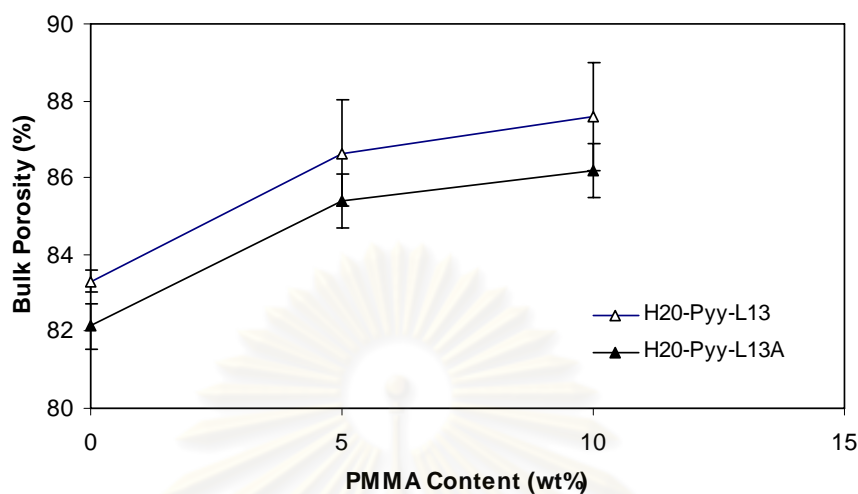
Figure 4.57   Effect of adding surfactant and PMMA content on porosity of the HA
samples prepared via combination technique using PMMA granules
and H_2O_2 solution, at 20wt% H_2O_2 solution with L/P ratio of 1.3 ml/g
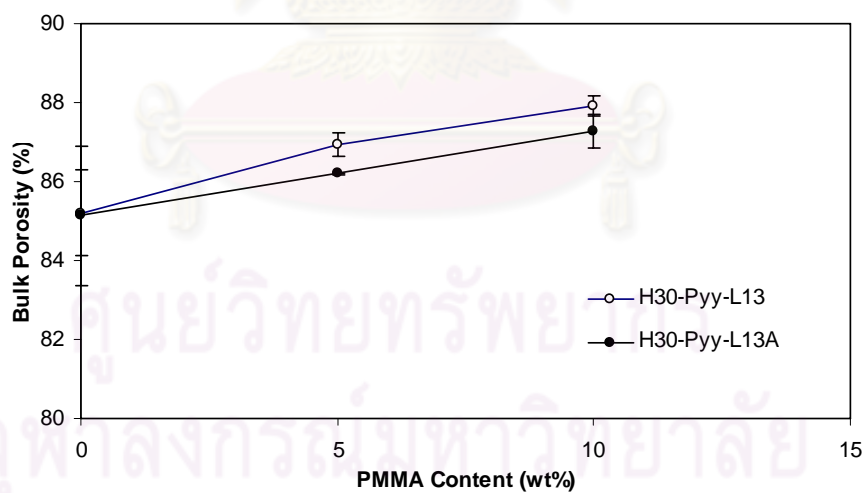
Figure 4.58   Effect of adding surfactant and PMMA content on porosity of the HA
samples prepared via combination technique using PMMA granules
and H_2O_2 solution, at 30wt% H_2O_2 solution with L/P ratio of 1.3 ml/g

4.5.3 Mechanical Properties

(A) Sacrificial Template Technique using PMMA

Table 4.19 summarized the HA samples with surfactant, prepared via sacrificial template technique using PMMA granules. Fabrication of HA specimen with surfactant using PMMA over 40wt% was handleless. The average compressive strength and flexural strength ranged from 0.75 to 34.17 MPa and ranged from 1.17 to 7.05 MPa, respectively.
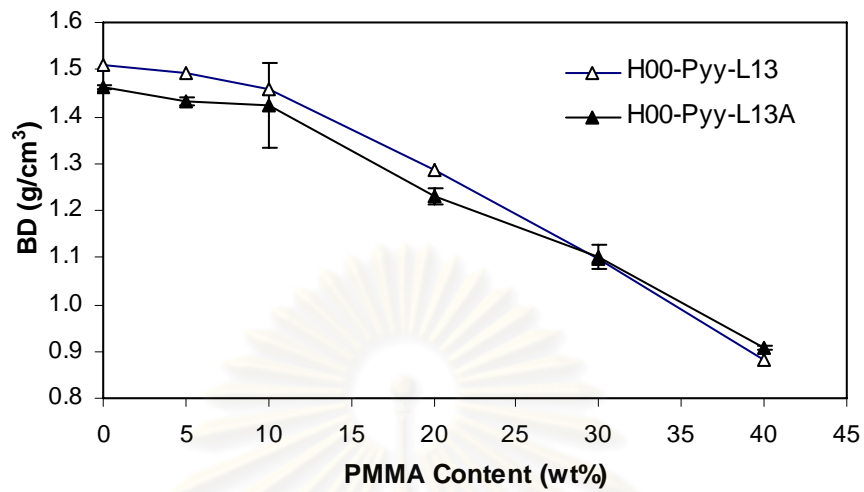
Figure 4.59 displayed the effect of adding surfactant and PMMA content on compressive strength (CS) of the HA samples prepared via sacrificial template technique using PMMA granules with L/P ratio of 1.3 ml/g. The compressive strength of both samples reduced with an increasing PMMA content. Moreover, addition of surfactant (agar) showed an unclear effect on compressive strength. At 5wt% and 10wt% PMMA, the compressive strength of the sample adding agar was slightly higher than that of the sample without surfactant.

Figure 4.60 illustrated the effect of adding surfactant and PMMA content on flexural strength (FS) of the HA samples prepared via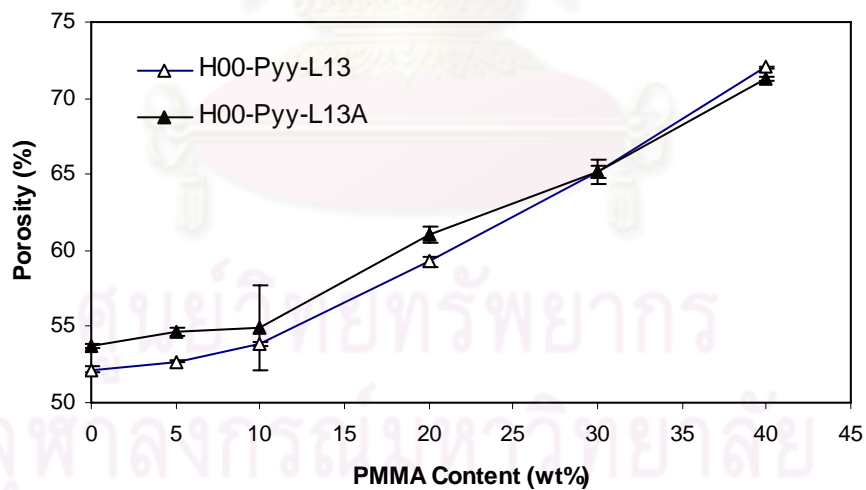 sacrificial template technique using PMMA granules with L/P ratio of 1.3 ml/g. The flexural strength of both samples decreased with an increase of PMMA content. Furthermore, addition of agar resulted in an improvement of the flexural strength, except at 5wt% PMMA.

Table 4.19   Compressive strength and flexural strength of the HA samples with surfactant, prepared via sacrificial template technique using PMMA granules.

Sample	Compressive strength				Flexural strength			
	#	(MPa)	Average	SD	#	(MPa)	Average	SD
H00-P00-L13A	1	36.04	**34.17**	2.65	1	7.26	**7.05**	0.30
	2	32.29			2	6.84		
H00-P05-L13A	1	24.72	**26.55**	2.58	1	4.86	**5.02**	0.23
	2	28.37			2	5.18		
H00-P10-L13A	1	17.52	**18.49**	1.36	1	3.61	**3.55**	0.08
	2	19.45			2	3.50		
H00-P20-L13A	1	6.19	**6.28**	0.12	1	2.58	**2.63**	0.07
	2	6.36			2	2.68		
H00-P30-L13A	1	2.70	**2.67**	0.04	1	1.89	**1.72**	0.25
	2	2.64			2	1.54		
H00-P40-L13A	1	0.74	**0.75**	0.01	1	1.33	**1.17**	0.22
	2	0.76			2	1.02		
H00-P50-L13A	1	-	**-**	-	1	-	**-**	-
	2	-			2	-		

Figure 4.59   Effect of adding surfactant and PMMA content on compressive
               strength (CS) of the HA samples prepared via sacrificial template
               technique using PMMA granules with L/P ratio of 1.3 ml/g
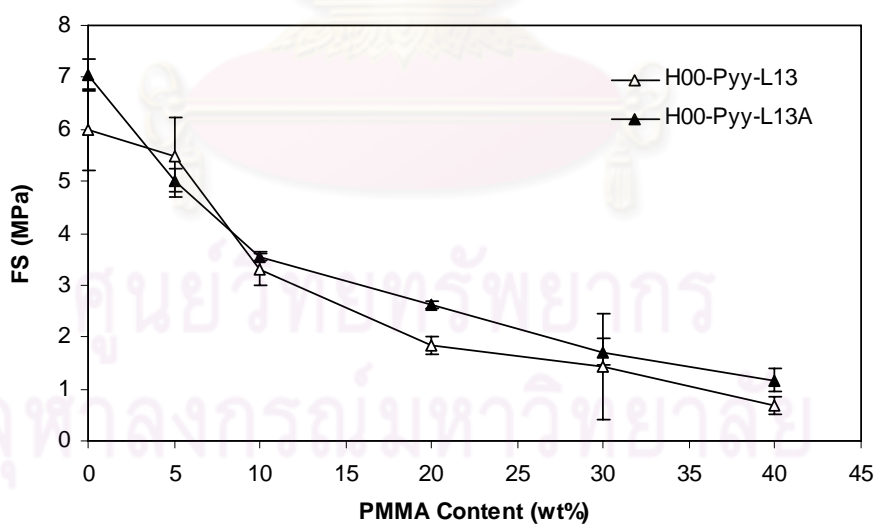
Figure 4.60   Effect of adding surfactant and PMMA content on flexural strength
               (FS) of the HA samples prepared via sacrificial template technique
               using PMMA granules with L/P ratio of 1.3 ml/g

Table 4.20 summed up the compressive stiffness and flexural stiffness of the HA samples with surfactant, prepared via sacrificial template technique using PMMA granules. The HA sample with surfactant using PMMA over 40wt% were handleless. The average compressive stiffness and flexural stiffness of the sample with surfactant ranged from 40.84 to 4,006.24 KN/m^2 and ranged from 9.86 to 526.32 MN/m^2, respectively.

Figure 4.61 presented the effect of adding surfactant and PMMA content on compressive stiffness (E_C) of the HA samples prepared via sacrificial template technique using PMMA granules. The compressive stiffness of both samples decreased with an increase of PMMA content. Moreover, the compressive stiffness of the sample adding agar was lower than that of the sample without surfactant.

Figure 4.62 showed the effect of adding surfactant and PMMA content on flexural stiffness (E_F) of the HA samples prepared via sacrificial template technique using PMMA granules. The flexural stiffness of both samples also reduced with an increasing PMMA content. Furthermore, addition of agar showed an unclear effect on the flexural stiffness. At less than 10wt% PMMA, the flexural stiffness was decreased when the PMMA granule was added.

Table 4.20   Compressive stiffness and flexural stiffness of the HA samples with surfactant, prepared via sacrificial template technique using PMMA granules

Sample	Compressive stiffness				Flexural stiffness			
	#	(kN/m^2)	Average	SD	#	(MN/m^2)	Average	SD
H00-P00-L13A	1	3,699.57	**4,006.24**	433.71	1	372.80	**526.32**	217.11
	2	4,312.92			2	679.84		
H00-P05-L13A	1	2,880.88	**2,658.22**	314.89	1	241.20	**278.02**	52.06
	2	2,435.56			2	314.83		
H00-P10-L13A	1	2,648.60	**2,436.35**	300.16	1	221.34	**211.54**	13.87
	2	2,224.10			2	201.73		
H00-P20-L13A	1	425.34	**439.61**	20.18	1	158.01	**165.27**	10.26
	2	453.87			2	172.52		
H00-P30-L13A	1	205.23	**195.25**	14.11	1	100.42	**98.14**	3.22
	2	185.27			2	95.86		
H00-P40-L13A	1	35.01	**40.84**	8.25	1	11.67	**9.86**	2.57
	2	46.68			2	8.04		
H00-P50-L13A	1	-	**-**	-	1	-	**-**	-
	2	-			2	-		

Figure 4.61   Effect of adding surfactant and PMMA content on compressive
              stiffness (E_C) of the HA samples prepared via sacrificial template
              technique using PMMA granules with L/P ratio of 1.3 ml/g
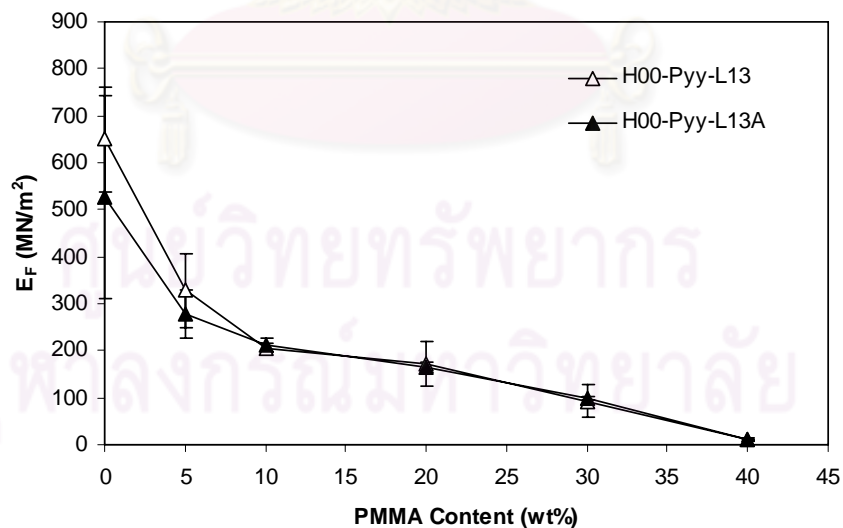
Figure 4.62   Effect of adding surfactant and PMMA content on flexural stiffness
              (E_F) of the HA samples prepared via sacrificial template technique
              using PMMA granules with L/P ratio of 1.3 ml/g

(B) Direct Foaming Technique using H_2O_2

Table 4.21 summarized the compressive strength and flexural strength of the HA samples with surfactant, prepared via direct foaming technique using H_2O_2 solution. The average compressive strength and flexural strength of these samples adding surfactant ranged from 0.18 to 0.67 MPa and ranged from 0.28 to 1.07 MPa, respectively.

Figure 4.63 showed the effect of adding surfactant and H_2O_2 concentration on compressive strength (CS) of the HA samples prepared via direct foaming technique using H_2O_2. The compressive strength of both samples decreased with an increase of H_2O_2 concentration. Moreover, addition of surfactant (agar) improved the compressive strength of the HA sample prepared through direct foaming technique.

Figure 4.64 illustrated the Effect of adding surfactant and H_2O_2 concentration on flexural strength (FS) of the HA samples prepared via direct foaming technique using H_2O_2. The flexural strength also reduced with an increasing H_2O_2 concentration. Furthermore, addition of agar caused an increase of compressive strength of the HA sample prepared by this technique.

Table 4.21   Compressive strength and flexural strength of the HA samples with surfactant, prepared via direct foaming technique using H_2O_2 solution.

Sample	Compressive strength				Flexural strength			
	#	(MPa)	Average	SD	#	(MPa)	Average	SD
H01-P00-L13A	1	0.66	**0.67**	0.02	1	1.05	**1.07**	0.03
	2	0.69			2	1.09		
H03-P00-L13A	1	0.57	**0.60**	0.04	1	0.79	**0.80**	0.01
	2	0.63			2	0.81		
H05-P00-L13A	1	0.50	**0.51**	0.02	1	0.80	**0.73**	0.11
	2	0.53			2	0.65		
H10-P00-L13A	1	0.46	**0.48**	0.03	1	0.70	**0.67**	0.04
	2	0.50			2	0.64		
H20-P00-L13A	1	0.38	**0.33**	0.06	1	0.43	**0.43**	0.00
	2	0.29			2	0.43		
H30-P00-L13A	1	0.20	**0.18**	0.02	1	0.25	**0.28**	0.04
	2	0.17			2	0.30		

Figure 4.63   Effect of adding surfactant and H_2O_2 concentration on compressive strength (CS) of the HA samples prepared via direct foaming technique using H_2O_2 solution with L/P ratio of 1.3 ml/g

Figure 4.64   Effect of adding surfactant and H_2O_2 concentration on flexural strength (FS) of the HA samples prepared via direct foaming technique using H_2O_2 solution with L/P ratio of 1.3 ml/g

Table 4.22 presented the compressive stiffness and flexural stiffness of the HA samples with surfactant, prepared via direct foaming technique using H_2O_2 solution. The average compressive stiffness and flexural stiffness of these samples adding surfactant ranged from 90.50 to 464.94 KN/m^2 and ranged from 2.31 to 6.98 MN/m^2, respectively.

Figure 4.65 illustrated the effect of adding surfactant and H_2O_2 concentration on compressive stiffness (E_C) of the HA samples prepared via direct foaming technique using H_2O_2 solution with L/P ratio of 1.3 ml/g. The compress stiffness of both samples decreased with an increasing H_2O_2 concentration. Moreover, addition of surfactant (agar) improved the compressive stiffness of the HA sample prepared via direct foaming technique.

Figure 4.66 displayed the effect of adding surfactant and H_2O_2 concentration on flexural stiffness (E_F) of the HA samples prepared via direct foaming technique using H_2O_2 solution with L/P ratio of 1.3 ml/g. The flexural stiffness of both samples was dropped when the H_2O_2 concentration was lower than 5wt% and then gradually decreased with an increasing H_2O_2 concentration. Furthermore, addition of agar resulted in an increase of flexural stiffness of the HA samples prepared through this technique.

Table 4.22 Compressive stiffness and flexural stiffness of the HA samples with surfactant, prepared via direct foaming technique using H_2O_2 solution.

Sample		Compressive stiffness				Flexural stiffness		
	#	(kN/m^2)	Average	SD	#	(MN/m^2)	Average	SD
H01-P00-L13A	1	380.48	**373.16**	10.34	1	65.22	**69.83**	6.52
	2	365.85			2	74.44		
H03-P00-L13A	1	281.35	**283.16**	2.56	1	40.55	**44.60**	5.72
	2	284.97			2	48.64		
H05-P00-L13A	1	353.01	**394.04**	58.02	1	45.01	**32.58**	17.59
	2	435.06			2	20.14		
H10-P00-L13A	1	383.10	**464.94**	115.73	1	34.96	**27.06**	11.18
	2	546.77			2	19.15		
H20-P00-L13A	1	179.27	**207.01**	39.23	1	14.34	**21.02**	9.45
	2	234.75			2	27.70		
H30-P00-L13A	1	97.88	**90.50**	10.44	1	2.36	**2.31**	0.08
	2	83.12			2	2.25		
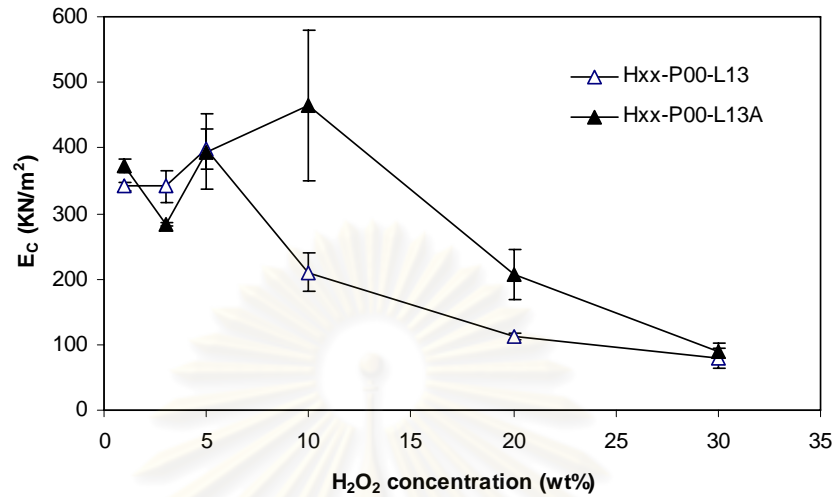
Figure 4.65   Effect of adding surfactant and H_2O_2 concentration on compressive
stiffness (E_C) of the HA samples prepared via direct foaming
technique using H_2O_2 solution with L/P ratio of 1.3 ml/g
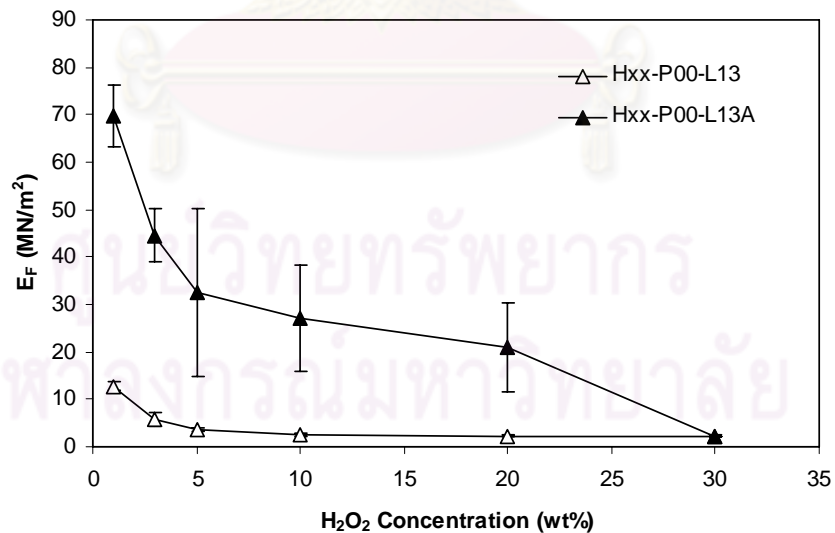
Figure 4.66   Effect of adding surfactant and H_2O_2 concentration on flexural
stiffness (E_F) of the HA samples prepared via direct foaming
technique using H_2O_2 solution with L/P ratio of 1.3 ml/g

(C) Combination Technique using PMMA and H_2O_2

Table 4.23 summarized the compressive strength and flexural strength of the HA sample with surfactant, prepared via combination technique using PMMA granules and H_2O_2 solution. The average compressive strength of the sample with surfactant ranged between 0.05 and 0.51 MPa at 5wt% H_2O_2; ranged between 0.06 and 0.48 MPa at 10wt% H_2O_2; ranged between 0.12 and 0.33 MPa at 20wt% H_2O_2; and ranged between 0.03 and 0.18 MPa at 30wt% H_2O_2. The average flexural strength of the sample with surfactant ranged between 0.29 and 0.67 MPa at 5wt% H_2O_2; ranged between 0.24 and 0.67 MPa at 10wt% H_2O_2; ranged between 0.22 and 0.47 MPa at 20wt% H_2O_2; and ranged between 0.20 and 0.31 MPa at 30wt% H_2O_2.

Figure 4.67 exhibited the effect of PMMA content and H_2O_2 concentration on compressive strength (CS) of the HA sample with surfactant, prepared via combination technique using PMMA granules and H_2O_2 solution with L/P ratio of 1.3 ml/g. The compressive strength of the sample adding surfactant (agar) decreased with the increases of both PMMA content and H_2O_2 concentration.

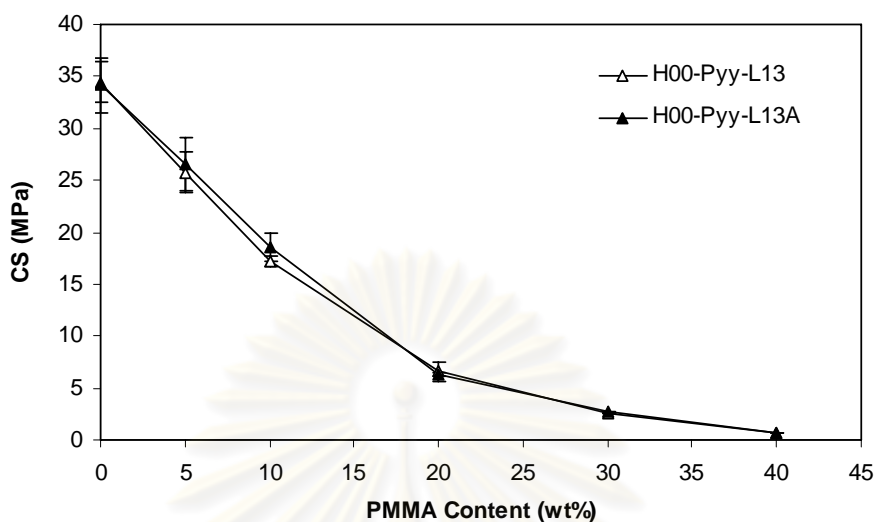Figure 4.68, Figure 4.69, Figure 4.70 and Figure 4.71 illustrated the effect of adding surfactant and PMMA content on compressive strength (CS) of the HA sample prepared via combination technique using PMMA granules and H_2O_2 solution with L/P ratio of 1.3 ml/g, at 5wt%, 10wt%, 20wt% and 30wt% H_2O_2, respectively. The compressive strength of the sample adding agar was higher than that of the sample without surfactant.

Table 4.23   Compressive strength and flexural strength of the HA sample with surfactant, prepared via combination technique using PMMA granules and H_2O_2 solution.

Sample	Compressive strength				Flexural strength			
	#	(MPa)	Average	SD	#	(MPa)	Average	SD
H05-P00-L13A	1	0.50	**0.51**	0.02	1	0.70	**0.67**	0.04
	2	0.53			2	0.64		
H05-P05-L13A	1	0.37	**0.36**	0.01	1	0.50	**0.51**	0.02
	2	0.36			2	0.52		
H05-P10-L13A	1	0.24	**0.25**	0.01	1	0.42	**0.43**	0.03
	2	0.25			2	0.45		
H05-P20-L13A	1	0.11	**0.10**	0.02	1	0.42	**0.41**	0.01
	2	0.08			2	0.40		
H05-P30-L13A	1	0.06	**0.05**	0.00	1	0.27	**0.29**	0.02
	2	0.05			2	0.30		
H05-P40-L13A	1	-	**-**	-	1	-	**-**	-
	2	-			2	-		
H05-P50-L13A	1	-	**-**	-	1	-	**-**	-
	2	-			2	-		
H10-P00-L13A	1	0.46	**0.48**	0.03	1	0.70	**0.67**	0.04
	2	0.50			2	0.64		
H10-P05-L13A	1	0.37	**0.35**	0.04	1	0.51	**0.49**	0.03
	2	0.32			2	0.47		
H10-P10-L13A	1	0.25	**0.22**	0.05	1	0.31	**0.34**	0.05
	2	0.19			2	0.38		
H10-P20-L13A	1	0.06	**0.06**	0.00	1	0.21	**0.24**	0.04
	2	0.06			2	0.26		
H10-P30-L13A	1	-	**-**	-	1	-	**-**	-
	2	-			2	-		
H10-P40-L13A	1	-	**-**	-	1	-	**-**	-
	2	-			2	-		
H10-P50-L13A	1	-	**-**	-	1	-	**-**	-
	2	-			2	-		
H20-P00-L13A	1	0.38	**0.33**	0.06	1	0.49	**0.47**	0.02
	2	0.29			2	0.45		
H20-P05-L13A	1	0.20	**0.17**	0.03	1	0.26	**0.30**	0.07
	2	0.15			2	0.35		
H20-P10-L13A	1	0.12	**0.12**	0.01	1	0.16	**0.22**	0.09
	2	0.11			2	0.28		
H20-P20-L13A	1	-	**-**	-	1	-	**-**	-
	2	-			2	-		
H20-P30-L13A	1	-	**-**	-	1	-	**-**	-
	2	-			2	-		
H20-P40-L13A	1	-	**-**	-	1	-	**-**	-
	2	-			2	-		
H20-P50-L13A	1	-	**-**	-	1	-	**-**	-
	2	-			2	-		

Table 4.23 Compressive strength and flexural strength of the HA sample with surfactant, prepared via combination technique using PMMA granules and H_2O_2 solution (Continued).

Sample	Compressive strength				flexural strength			
	#	(MPa)	Average	SD	#	(MPa)	Average	SD
H30-P00-L13A	1	0.20	**0.18**	0.02	1	0.28	**0.31**	0.04
	2	0.17			2	0.34		
H30-P05-L13A	1	0.14	**0.13**	0.01	1	0.25	**0.26**	0.02
	2	0.13			2	0.28		
H30-P10-L13A	1	0.09	**0.09**	0.00	1	0.22	**0.20**	0.03
	2	0.10			2	0.17		
H30-P20-L13A	1	-	**-**	-	1	-	**-**	-
	2	-			2	-		
H30-P30-L13A	1	-	**-**	-	1	-	**-**	-
	2	-			2	-		
H30-P40-L13A	1	-	**-**	-	1	-	**-**	-
	2	-			2	-		
H30-P50-L13A	1	-	**-**	-	1	-	**-**	-
	2	-			2	-		

Figure 4.67 Effect of PMMA content and H_2O_2 concentration on compressive strength (CS) of the HA sample with surfactant, prepared via combination technique using PMMA granules and H_2O_2 solution with L/P ratio of 1.3 ml/g
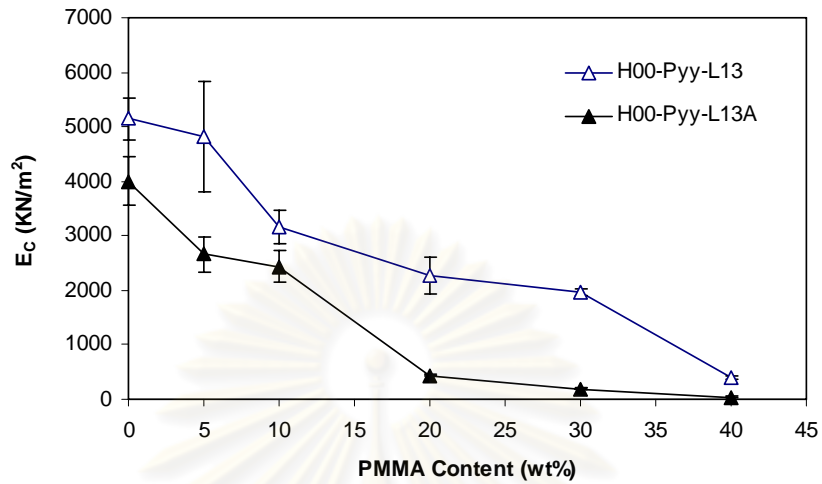
Figure 4.68 Effect of adding surfactant and PMMA content on compressive strength (CS) of the HA sample prepared via combination technique using PMMA granules and H_2O_2 solution, at 5wt% H_2O_2 solution with L/P ratio of 1.3 ml/g

Figure 4.69 Effect of adding surfactant and PMMA content on compressive strength (CS) of the HA sample prepared via combination technique using PMMA granules and H_2O_2 solution, at 10 wt% H_2O_2 solution with L/P ratio of 1.3 ml/g

Figure 4.70   Effect of adding surfactant and PMMA content on compressive
strength (CS) of the HA sample prepared via combination technique
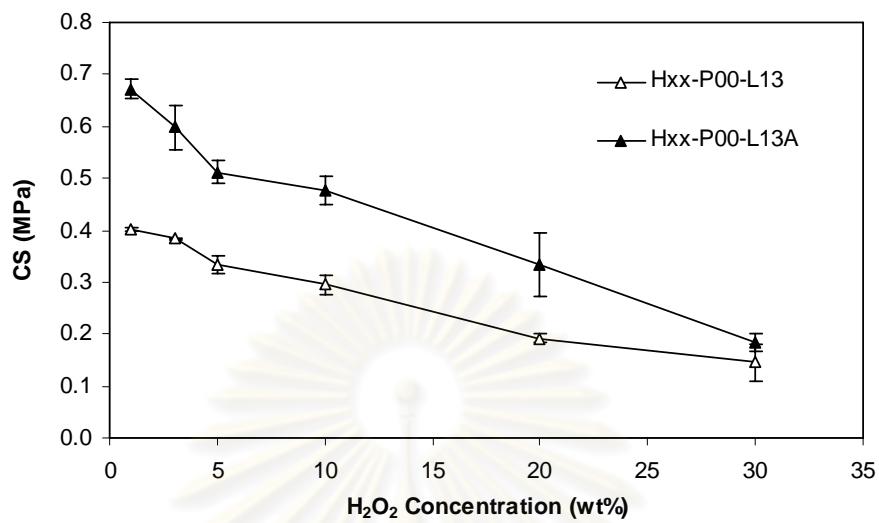using PMMA granules and H_2O_2 solution, at 20 wt% H_2O_2 solution
with L/P ratio of 1.3 ml/g

Figure 4.71   Effect of adding surfactant and PMMA content on compressive
strength (CS) of the HA sample prepared via combination technique
using PMMA granules and H_2O_2 solution, at 30 wt% H_2O_2 solution
with L/P ratio of 1.3 ml/g

Figure 4.72 showed the effect of PMMA content and H_2O_2 concentration on flexural strength (FS) of the HA sample with surfactant, prepared via combination technique using PMMA granules and H_2O_2 solution with L/P ratio of 1.3 ml/g. The flexural strength of the HA samples adding surfactant (agar) decreased with the increases of both PMMA content and H_2O_2 concentration.

Figure 4.73, Figure 4.74, Figure 4.75 and Figure 4.76 presented the effect of adding surfactant and PMMA content on flexural strength (FS) of the HA sample prepared via combination technique using PMMA granules and H_2O_2 solution with L/P ratio of 1.3 ml/g, at 5wt%, 10wt%, 20wt% and 30wt% H_2O_2, respectively. The HA sample adding agar had a better flexural strength than the sample without surfactant.
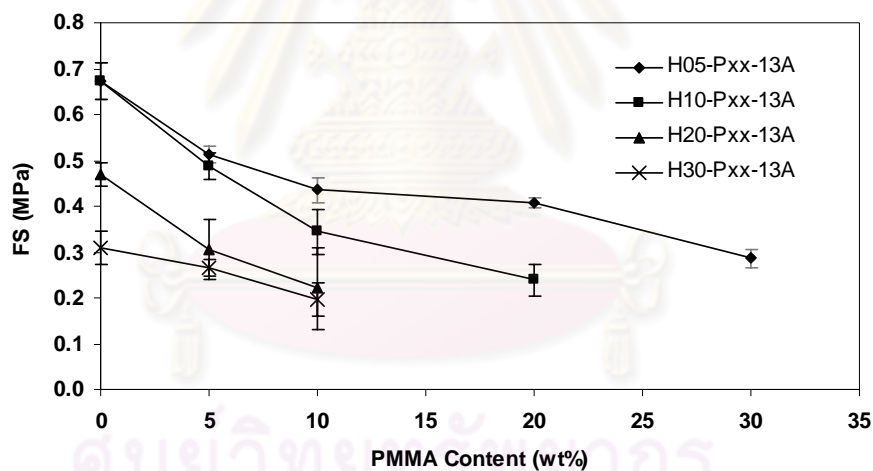
Figure 4.72   Effect of PMMA content and H_2O_2 concentration on flexural strength (FS) of the HA sample with surfactant, prepared via combination technique using PMMA granules and H_2O_2 solution with L/P ratio of 1.3 ml/g

Figure 4.73   Effect of adding surfactant and PMMA content on flexural strength
                (FS) of the HA sample prepared via combination technique using
                PMMA granules and H_2O_2 solution, at 5wt% H_2O_2 solution with L/P
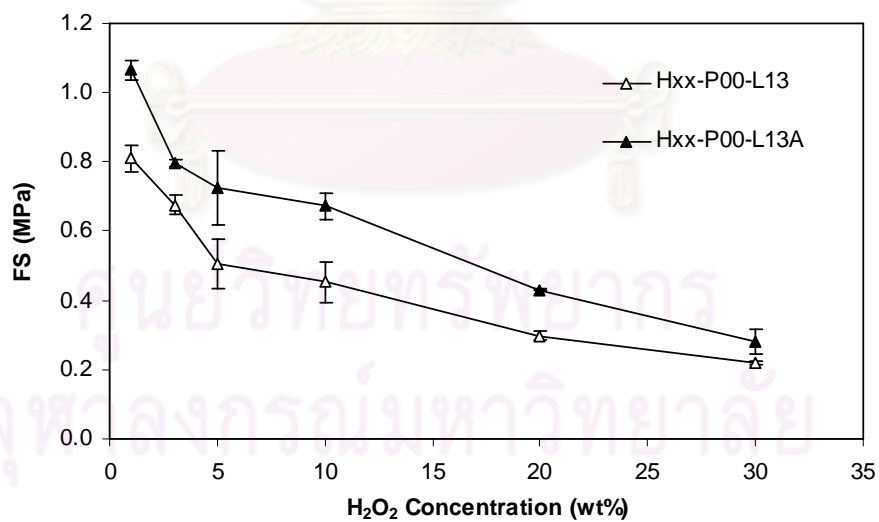   ratio of 1.3 ml/g

Figure 4.74   Effect of adding surfactant and PMMA content on flexural strength
                (FS) of the HA sample prepared via combination technique using
                PMMA granules and H_2O_2 solution, at 10wt% H_2O_2 solution with L/P
                ratio of 1.3 ml/g

Figure 4.75   Effect of adding surfactant and PMMA content on flexural strength
               (FS) of the HA sample prepared via combination technique using
               PMMA granules and H_2O_2 solution, at 20wt% H_2O_2 solution with L/P
               ratio of 1.3 ml/g

Figure 4.76   Effect of adding surfactant and PMMA content on flexural strength
               (FS) of the HA sample prepared via combination technique using
               PMMA granules and H_2O_2 solution, at 30wt% H_2O_2 solution with L/P
               ratio of 1.3 ml/g

Table 4.24 summarized the compressive stiffness and flexural stiffness of the HA sample with surfactant, prepared via combination technique using PMMA granules and H_2O_2 solution. The compressive stiffness of the HA sample adding surfactant (agar) ranged between 44.32 and 394.04 kN/m^2 at 5wt% H_2O_2; ranged between 54.01 and 464.94 kN/m^2 at 10wt% H_2O_2; ranged between 103.45 and 207.01 kN/m^2 at 20wt% H_2O_2; and ranged between 53.21 and 90.50 kN/m^2 at 30wt% H_2O_2. The flexural stiffness of the HA sample adding agar ranged between 0.58 and 32.58 kN/m^2 at 5wt% H_2O_2; ranged between 0.50 and 27.01 kN/m^2 at 10wt% H_2O_2; ranged between 1.25 and 21.02 kN/m^2 at 20wt% H_2O_2; and ranged between 1.10 and 2.31 kN/m^2 at 30wt% H_2O_2.

Figure 4.77 showed the effect of PMMA content and H_2O_2 concentration on compressive stiffness (E_C) of the HA sample with surfactant, prepared via combination technique using PMMA granules and H_2O_2 solution with L/P ratio of 1.3 ml/g. The compressive stiffness of the sample adding surfactant (agar) decreased with the increases of both PMMA content and H_2O_2 concentration.

Figure 4.78, Figure 4.79, Figure 4.80 and Figure 4.81 presented the effect of adding surfactant on compressive stiffness (E_C) of the HA sample prepared via combination technique using PMMA granules and H_2O_2 solution with L/P ratio of 1.3 ml/g, at 5wt%, 10wt%, 20wt% and 30wt% H_2O_2, respectively. Addition of agar resulted in an increase of the compressive stiffness of the sample prepared by combination technique.

Table 4.24 Compressive stiffness and flexural stiffness of the HA sample with surfactant, prepared via combination technique using PMMA granules and H_2O_2 solution.

Sample		Compressive stiffness				Flexural stiffness		
	#	(kN/m²)	Average	SD	#	(MN/m²)	Average	SD
H05-P00-L13A	1	353.01	**394.04**	58.02	1	45.01	**32.58**	17.59
	2	435.06			2	20.14		
H05-P05-L13A	1	132.90	**126.52**	9.02	1	4.42	**4.61**	0.27
	2	120.15			2	4.80		
H05-P10-L13A	1	83.82	**80.14**	5.21	1	2.78	**2.48**	0.42
	2	76.45			2	2.19		
H05-P20-L13A	1	65.40	**58.80**	9.33	1	0.69	**0.68**	0.01
	2	52.21			2	0.67		
H05-P30-L13A	1	39.25	**44.32**	7.18	1	0.53	**0.58**	0.07
	2	49.40			2	0.63		
H05-P40-L13A	1	-	**-**	-	1	-	**-**	-
	2	-			2	-		
H05-P50-L13A	1	-	**-**	-	1	-	**-**	-
	2	-			2	-		
H10-P00-L13A	1	383.10	**464.94**	115.73	1	34.96	**27.06**	11.18
	2	546.77			2	19.15		
H10-P05-L13A	1	195.55	**183.42**	17.15	1	8.86	**7.69**	1.65
	2	171.29			2	6.53		
H10-P10-L13A	1	138.20	**130.35**	11.10	1	2.34	**2.46**	0.17
	2	122.51			2	2.58		
H10-P20-L13A	1	72.11	**54.01**	25.59	1	0.56	**0.50**	0.08
	2	35.91			2	0.44		
H10-P30-L13A	1	-	**-**	-	1	-	**-**	-
	2	-			2	-		
H10-P40-L13A	1	-	**-**	-	1	-	**-**	-
	2	-			2	-		
H10-P50-L13A	1	-	**-**	-	1	-	**-**	-
	2	-			2	-		
H20-P00-L13A	1	179.27	**207.01**	39.23	1	14.34	**21.02**	9.45
	2	234.75			2	27.70		
H20-P05-L13A	1	117.28	**136.57**	27.28	1	2.31	**3.06**	1.06
	2	155.87			2	3.81		
H20-P10-L13A	1	112.06	**103.45**	12.19	1	1.16	**1.25**	0.13
	2	94.83			2	1.34		
H20-P20-L13A	1	-	**-**	-	1	-	**-**	-
	2	-			2	-		
H20-P30-L13A	1	-	**-**	-	1	-	**-**	-
	2	-			2	-		
H20-P40-L13A	1	-	**-**	-	1	-	**-**	-
	2	-			2	-		
H20-P50-L13A	1	-	**-**	-	1	-	**-**	-
	2	-			2	-		

Table 4.24　Compressive stiffness and flexural stiffness of the HA sample with
surfactant, prepared via combination technique using PMMA granules
and H_2O_2 solution (Continued).

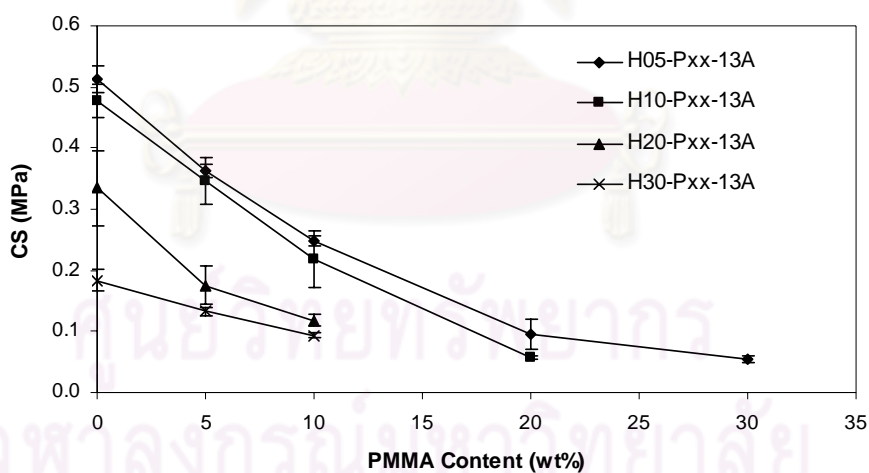| Sample	Compressive stiffness				Flexural stiffness			
	#	(kN/m²)	Average	SD	#	(MN/m²)	Average	SD
H30-P00-L13A	1	97.88	**90.50**	10.44	1	2.36	**2.31**	0.08
	2	83.12			2	2.25		
H30-P05-L13A	1	87.33	**82.84**	6.35	1	2.25	**1.90**	0.50
	2	78.35			2	1.55		
H30-P10-L13A	1	49.22	**53.21**	5.65	1	1.25	**1.10**	0.22
	2	57.21			2	0.94		
H30-P20-L13A	1	-	**-**	-	1	-	**-**	-
	2	-			2	-		
H30-P30-L13A	1	-	**-**	-	1	-	**-**	-
	2	-			2	-		
H30-P40-L13A	1	-	**-**	-	1	-	**-**	-
	2	-			2	-		
H30-P50-L13A	1	-	**-**	-	1	-	**-**	-
	2	-			2	-		

Figure 4.77　Effect of PMMA content and H_2O_2 concentration on compressive
stiffness (E_C) of the HA sample with surfactant, prepared via
combination technique using PMMA granules and H_2O_2 solution with
L/P ratio of 1.3 ml/g
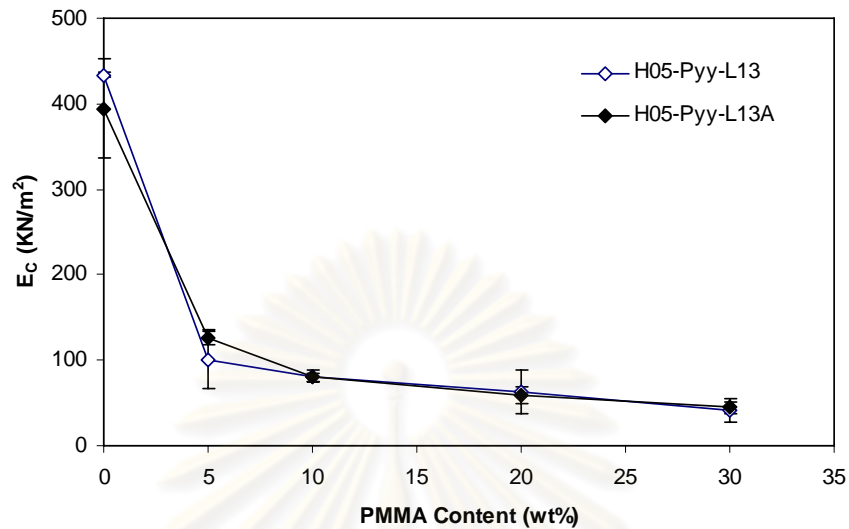
Figure 4.78   Effect of adding surfactant and PMMA content on compressive
stiffness (E_C) of the HA sample prepared via combination technique
using PMMA granules and H_2O_2 solution, at 5wt% H_2O_2 solution
with L/P ratio of 1.3 ml/g
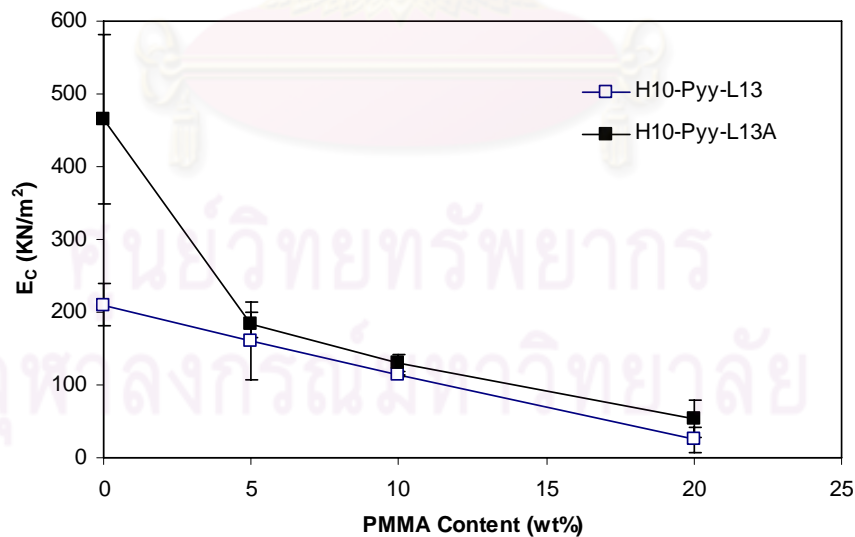
Figure 4.79   Effect of adding surfactant and PMMA content on compressive
stiffness (E_C) of the HA sample prepared via combination technique
using PMMA granules and H_2O_2 solution, at 10wt% H_2O_2 solution
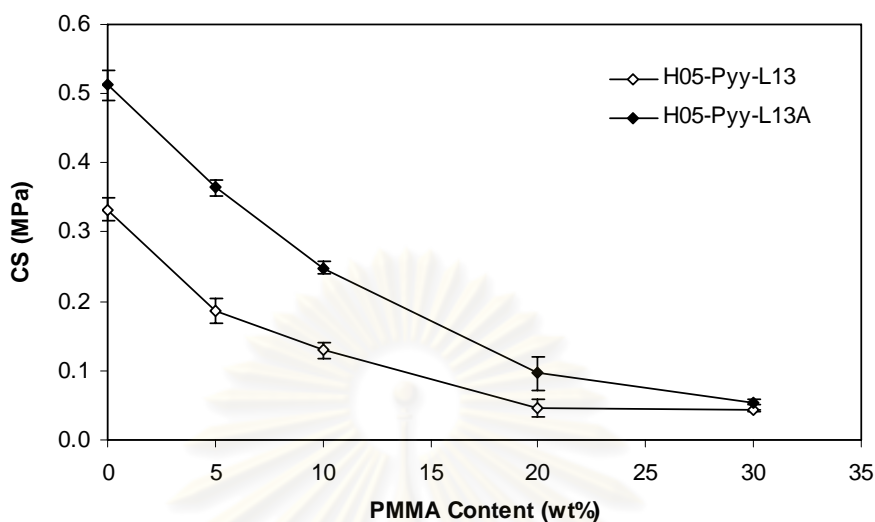with L/P ratio of 1.3 ml/g
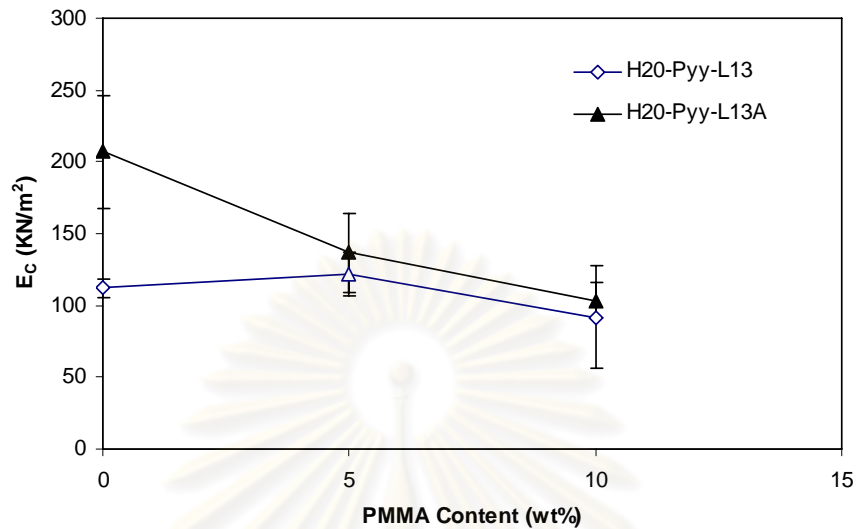
Figure 4.80   Effect of adding surfactant and PMMA content on compressive
               stiffness (E_C) of the HA sample prepared via combination technique
               using PMMA granules and H_2O_2 solution, at 20wt% H_2O_2 solution
               with L/P ratio of 1.3 ml/g
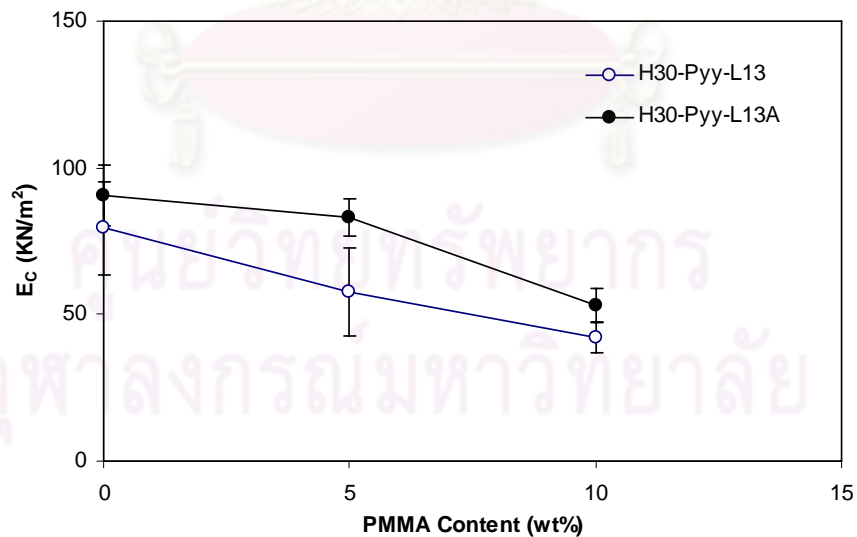
Figure 4.81   Effect of adding surfactant and PMMA content on compressive
               stiffness (E_C) of the HA sample prepared via combination technique
               using PMMA granules and H_2O_2 solution, at 30wt% H_2O_2 solution
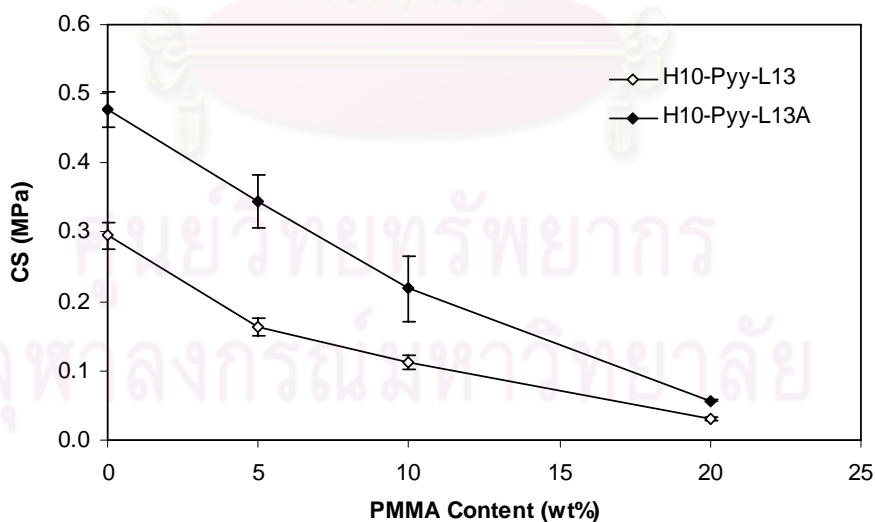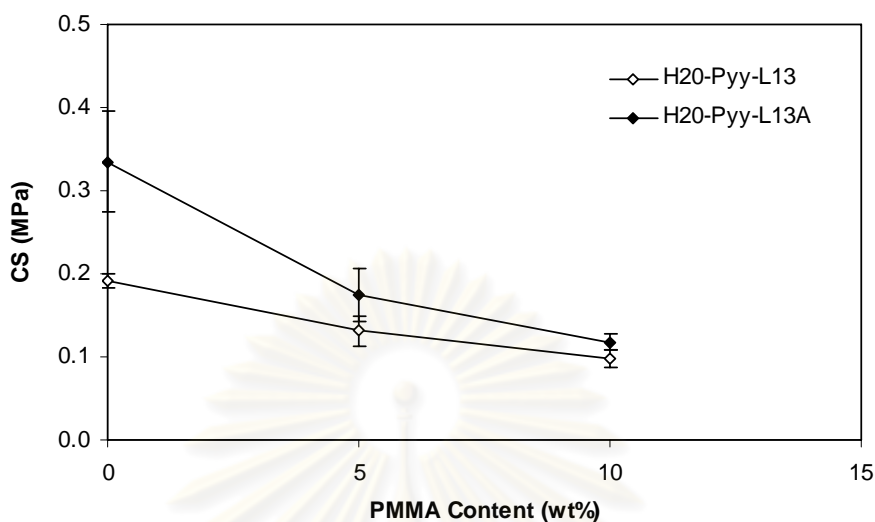   with L/P ratio of 1.3 ml/g

Figure 4.82 displayed the effect of PMMA content and H_2O_2 concentration on flexural stiffness (E_F) of the HA sample with surfactant, prepared via combination technique using PMMA granules and H_2O_2 solution with L/P ratio of 1.3 ml/g. The flexural stiffness of the HA samples adding agar also decreased with the increases of both PMMA content and H_2O_2 concentration.

Figure 4.83, Figure 4.84, Figure 4.85 and Figure 4.86 exhibited the effect of adding surfactant and PMMA content on flexural stiffness (E_F) of the HA sample prepared via combination technique using PMMA granules and H_2O_2 solution with L/P ratio of 1.3 ml/g, at 5wt%, 10wt%, 20wt% and 30wt% H_2O_2, respectively. Less than 10wt% PMMA, addition of agar improved obviously the flexural stiffness of the HA sample prepared by combination technique.
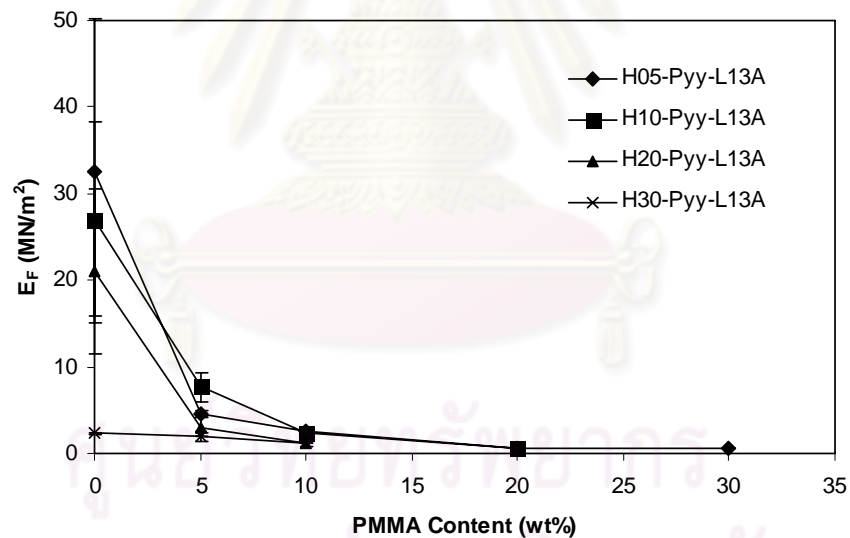
Figure 4.82   Effect of PMMA content and H_2O_2 concentration on flexural stiffness (E_F) of the HA sample with surfactant, prepared via combination technique using PMMA granules and H_2O_2 solution with L/P ratio of 1.3 ml/g
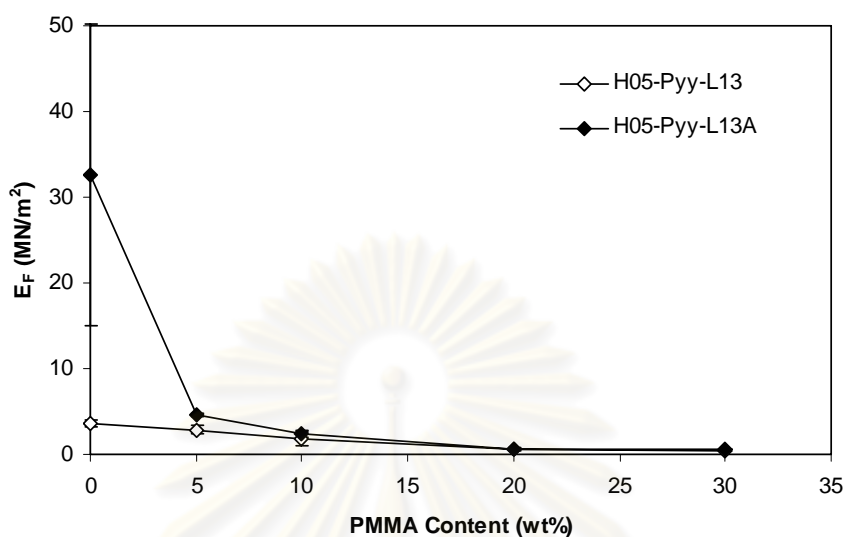
Figure 4.83   Effect of adding surfactant and PMMA content on flexural stiffness
(E_F) of the HA sample prepared via combination technique using
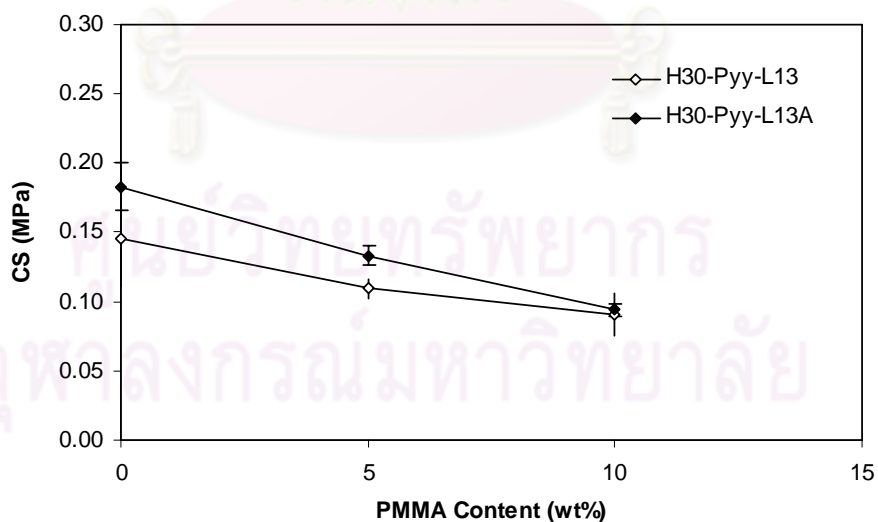PMMA granules and H_2O_2 solution, at 5wt% H_2O_2 solution with L/P
ratio of 1.3 ml/g
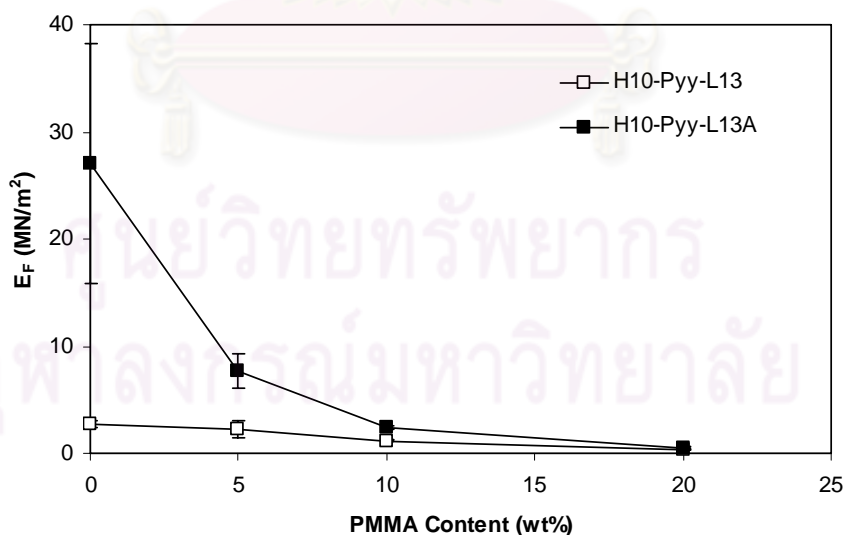
Figure 4.84   Effect of adding surfactant and PMMA content on flexural stiffness
(E_F) of the HA sample prepared via combination technique using
PMMA granules and H_2O_2 solution, at 10wt% H_2O_2 solution with L/P
ratio of 1.3 ml/g
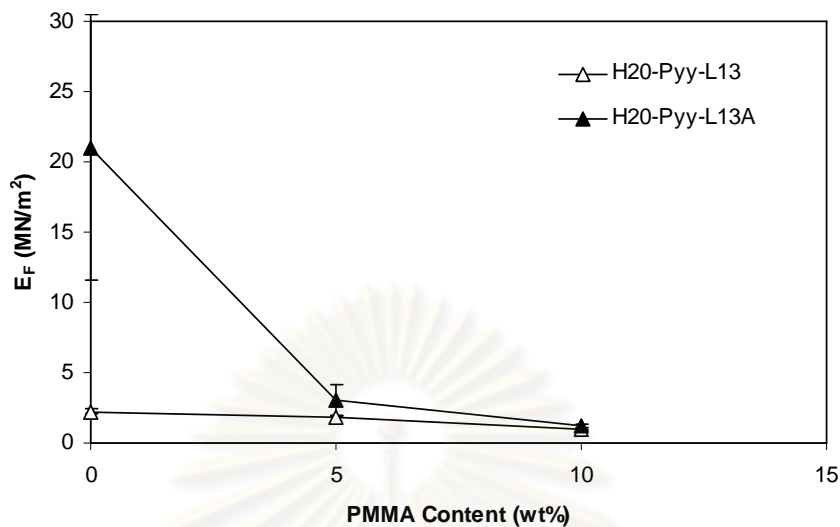
Figure 4.85   Effect of adding surfactant and PMMA content on flexural stiffness
              (E_F) of the HA sample prepared via combination technique using
              PMMA granules and H_2O_2 solution, at 20wt% H_2O_2 solution with L/P
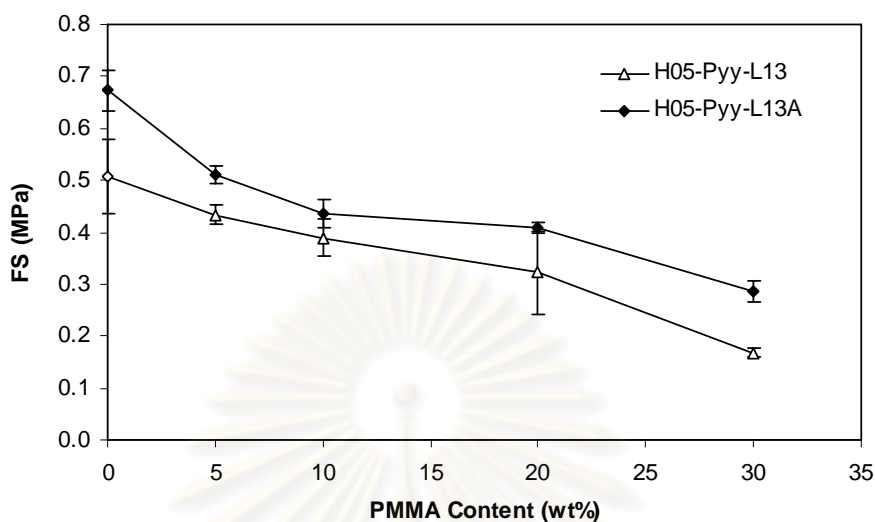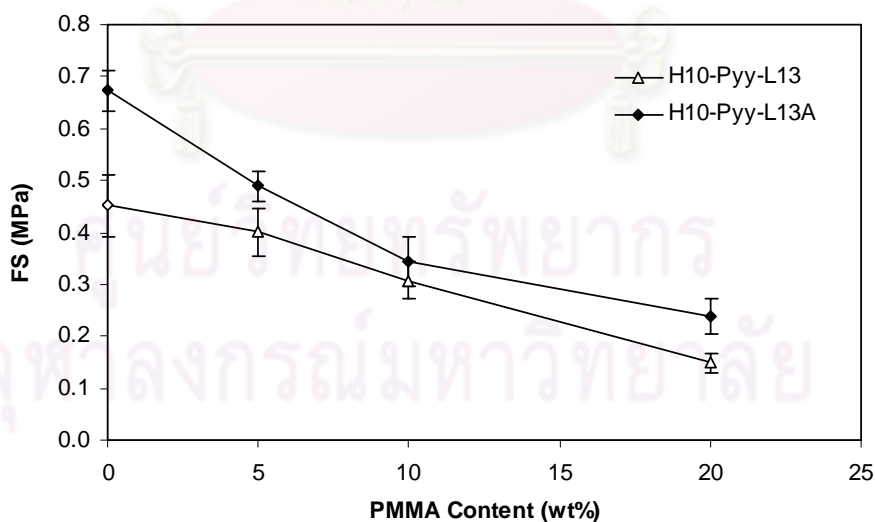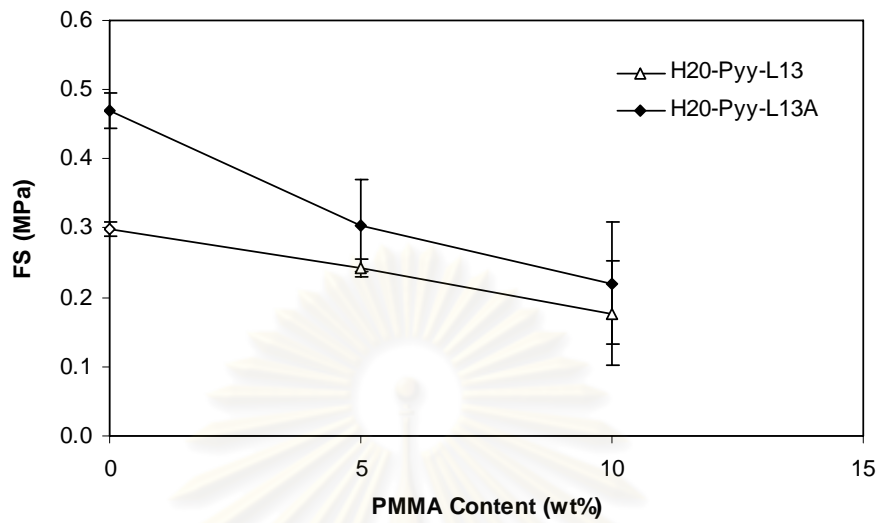   ratio of 1.3 ml/g
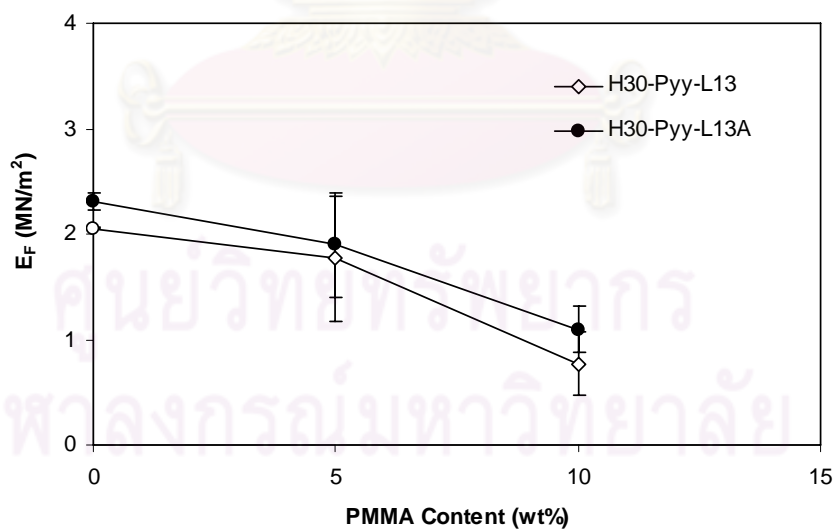
Figure 4.86   Effect of adding surfactant and PMMA content on flexural stiffness
              (E_F) of the HA sample prepared via combination technique using
              PMMA granules and H_2O_2 solution, at 30wt% H_2O_2 solution with L/P
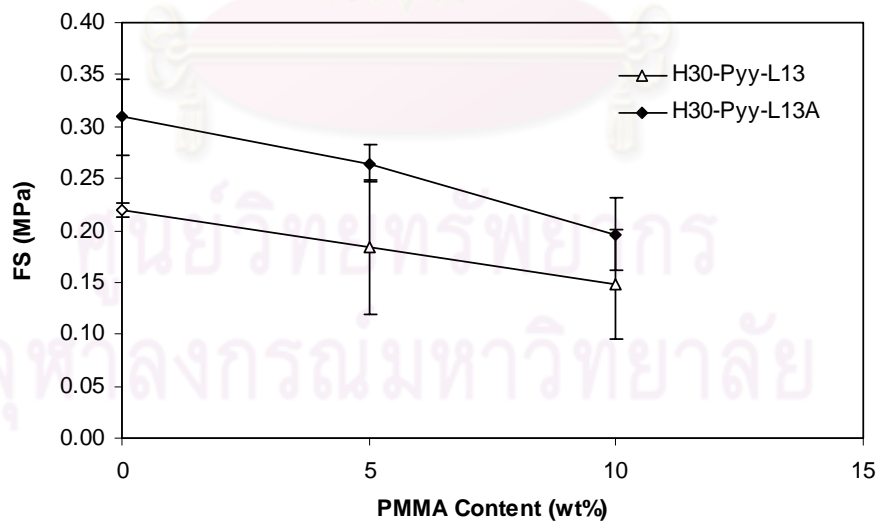   ratio of 1.3 ml/g

CHAPTER V

STATISTICAL ANALYSIS

5.1 Analysis of Variance

Experimental data in Chapter IV including bulk density, porosity, compressive strength, flexural strength, compressive stiffness and flexural stiffness from various fabrication conditions were analyzed by analysis of variance (ANOVA).

5.1.1 Effect of Forming Factors on Bulk Density

Table 5.1 summarized the analysis of variance (ANOVA) for bulk density of the porous HA samples prepared by various methods (at $\alpha = 0.05$). For sacrificial template technique, the significant factor was the content of PMMA granules. For direct foaming method, the significant factors were the concentration of H_2O_2 solution and the liquid to powder ratio (L/P ratio). For combination technique, the content of PMMA showed a significant effect on bulk density at the H_2O_2 concentration of 5wt% and 10wt%. Moreover, the sintering temperature also had a significant influence on bulk density for the porous HA samples prepared through combination technique at 10wt% H_2O_2.

5.1.2 Effect of Forming Factors on Porosity

Table 5.2 presented the analysis of variance (ANOVA) for porosity of the porous HA samples prepared by various methods (at $\alpha = 0.05$). For sacrificial template technique, the significant factor was the PMMA content. For direct foaming method the significant factors were the H_2O_2 concentration and the L/P ratio. For combination technique, the content of PMMA showed a significant effect on bulk density at the H_2O_2 concentration of 5wt% and 10wt%. Furthermore, the sintering temperature also showed an effect on bulk density for the sample H10-Pyy-L13A.

Table 5.1   Analysis of variance for bulk density of the porous HA samples prepared by various methods (at $\alpha = 0.05$)

Methods	Factors	P-value
1. Sacrificial template using PMMA	- Content of PMMA *	**< 0.001**
	- Liquid to powder ratio	0.422
	- Addition of agar	0.771
2. Direct foaming using H_2O_2	- Concentration of H_2O_2 *	**0.001**
	- Liquid to powder ratio *	**0.023**
	- Addition of agar	0.319
3. Combination technique using PMMA and H_2O_2		
3.1. at 5wt% H_2O_2	- Content of PMMA *	**< 0.001**
	- Addition of agar	0.092
3.2. at 10wt% H_2O_2	- Content of PMMA *	**0.003**
	- Addition of agar	0.162
3.3. at 20wt% H_2O_2	- Content of PMMA	0.060
	- Addition of agar	0.305
3.4. at 30wt% H_2O_2	- Content of PMMA	0.071
	- Addition of agar	0.533
	- Sintering Temperature *	**0.031**

Note: "" was referred to the significant factor.*

Table 5.2   Analysis of variance for porosity of the porous HA samples prepared by various methods (at $\alpha = 0.05$)

Methods	Factors	P-value
1. Sacrificial template using PMMA	- Content of PMMA *	**< 0.001**
	- Liquid to powder ratio	0.421
	- Addition of agar	0.758
2. Direct foaming using H_2O_2	- Concentration of H_2O_2 *	**0.001**
	- Liquid to powder ratio *	**0.021**
	- Addition of agar	0.319
3. Combination technique using PMMA and H_2O_2		
3.1. at 5wt% H_2O_2	- Content of PMMA *	**0.001**
	- Addition of agar	0.086
3.2. at 10wt% H_2O_2	- Content of PMMA *	**0.003**
	- Addition of agar	0.168
3.3. at 20wt% H_2O_2	- Content of PMMA	0.066
	- Addition of agar	0.320
3.4. at 30wt% H_2O_2	- Content of PMMA	0.061
	- Addition of agar	0.530
	- Sintering Temperature *	**0.030**

Note: "" was referred to the significant factor.*

5.1.3 Effect of Forming Factors on Compressive Strength

        Table 5.3 summarized the analysis of variance for compressive strength of the porous HA samples prepared by various methods (at $\alpha = 0.05$). The significant factors affecting on bulk density for sacrificial template technique was the PMMA content; for direct foaming method were the concentration of H_2O_2, the L/P ratio and the addition of 1wt% agar; as well as for combination technique were the PMMA content which was effective at the H_2O_2 concentration of 5wt%, 10wt% and 20wt%. Additionally, the sintering temperature was also the significant factor for compressive strength.

Table 5.3   Analysis of variance for compressive strength of the porous HA samples prepared by various methods (at $\alpha = 0.05$)

Methods	Factors	P-value
1. Sacrificial template using PMMA	- Content of PMMA *	**< 0.001**
	- Liquid to powder ratio	0.690
	- Addition of agar	0.957
2. Direct foaming using H_2O_2	- Concentration of H_2O_2 *	**< 0.001**
	- Liquid to powder ratio *	**< 0.001**
	- Addition of agar *	**0.006**
3. Combination technique using PMMA and H_2O_2		
3.1. at 5wt% H_2O_2	- Content of PMMA *	**< 0.001**
	- Addition of agar	0.125
3.2. at 10wt% H_2O_2	- Content of PMMA *	**< 0.001**
	- Addition of agar	0.088
3.3. at 20wt% H_2O_2	- Content of PMMA *	**0.010**
	- Addition of agar	0.189
3.4. at 30wt% H_2O_2	- Content of PMMA	0.178
	- Addition of agar	0.264
	- Sintering Temperature *	**0.002**

Note: "" was referred to the significant factor.*

5.1.4 Effect of Forming Factors on Flexural Strength

Table 5.4 reported the analysis of variance for flexural strength of the porous HA samples prepared by various methods (at $\alpha = 0.05$). The significant factors affecting on flexural strength for sacrificial template technique was the PMMA content; for direct foaming method was the H_2O_2 concentration; as well as for combination technique were the PMMA content which was effective at the H_2O_2 concentration of 5wt% and 10wt%, and the addition of agar which was effective at the H_2O_2 concentration of 30wt%.

Table 5.4   Analysis of variance for flexural strength of the porous HA samples prepared by various methods (at $\alpha = 0.05$)

Methods	Factors	P-value
1. Sacrificial template using PMMA	- Content of PMMA *	**< 0.001**
	- Liquid to powder ratio	0.525
	- Addition of agar	0.645
2. Direct foaming using H_2O_2	- Concentration of H_2O_2 *	**< 0.001**
	- Liquid to powder ratio	0.092
	- Addition of agar	0.106
3. Combination technique using PMMA and H_2O_2		
3.1. at 5wt% H_2O_2	- Content of PMMA *	**0.007**
	- Addition of agar	0.114
3.2. at 10wt% H_2O_2	- Content of PMMA *	**0.006**
	- Addition of agar	0.176
3.3. at 20wt% H_2O_2	- Content of PMMA	0.158
	- Addition of agar	0.135
3.4. at 30wt% H_2O_2	- Content of PMMA	0.392
	- Addition of agar *	**0.040**
	- Sintering Temperature	0.104

Note: "" was referred to the significant factor.*

5.1.5 Effect of Forming Factors on Compressive Stiffness

Table 5.5 summarized the analysis of variance for compressive stiffness of the porous HA samples prepared by various methods (at $\alpha = 0.05$). The factors having a significant effect on compressive stiffness for sacrificial template technique was the PMMA content; for direct foaming method was the H_2O_2 concentration; and for combination technique was the PMMA content which was effective at the H_2O_2 concentration of 5wt% and 10wt%.

Table 5.5   Analysis of variance for compressive stiffness of the porous HA samples prepared by various methods (at $\alpha = 0.05$)

Methods	Factors	P-value
1. Sacrificial template using PMMA	- Content of PMMA *	**< 0.001**
	- Liquid to powder ratio	0.528
	- Addition of agar	0.100
2. Direct foaming using H_2O_2	- Concentration of H_2O_2 *	**< 0.001**
	- Liquid to powder ratio *	**0.032**
	- Addition of agar	0.202
3. Combination technique using PMMA and H_2O_2		
3.1. at 5wt% H_2O_2	- Content of PMMA *	**< 0.001**
	- Addition of agar	0.810
3.2. at 10wt% H_2O_2	- Content of PMMA *	**0.001**
	- Addition of agar	0.473
3.3. at 20wt% H_2O_2	- Content of PMMA	0.057
	- Addition of agar	0.129
3.4. at 30wt% H_2O_2	- Content of PMMA	0.107
	- Addition of agar	0.121
	- Sintering Temperature	0.149

Note: "" was referred to the significant factor.*

5.1.6 Effect of Forming Factors on Flexural Stiffness

Table 5.6 presented the analysis of variance for flexural stiffness of the porous HA samples prepared by various methods (at $\alpha = 0.05$). The significant factors affecting on the flexural stiffness for sacrificial template technique was the PMMA content; for direct foaming method were the concentration of H_2O_2 and the addition of agar; as well as for combination technique was the content of PMMA which was effective at the H_2O_2 concentration between 5wt% and 20wt%.

Table 5.6   Analysis of variance for flexural stiffness of the porous HA samples prepared by various methods (at $\alpha = 0.05$)

Methods	Factors	P-value
1. Sacrificial template using PMMA	- Content of PMMA *	**< 0.001**
	- Liquid to powder ratio	0.351
	- Addition of agar	0.734
2. Direct foaming using H_2O_2	- Concentration of H_2O_2 *	**<0.001**
	- Liquid to powder ratio	0.753
	- Addition of agar *	**<0.001**
3. Combination technique using PMMA and H_2O_2		
3.1. at 5wt% H_2O_2	- Content of PMMA *	**0.003**
	- Addition of agar	0.177
3.2. at 10wt% H_2O_2	- Content of PMMA *	**0.015**
	- Addition of agar	0.087
3.3. at 20wt% H_2O_2	- Content of PMMA *	**0.003**
	- Addition of agar	0.153
3.4. at 30wt% H_2O_2	- Content of PMMA	0.085
	- Addition of agar	0.530
	- Sintering Temperature	0.159

Note: "" was referred to the significant factor.*

5.2 Regression Analysis

Experimental data were also used to construct regression equations for porosity (P), compressive strength (CS) and flexural strength (FS). The insignificant factors were eliminated to reduce the terms from the equations. Porosity was estimated in terms of the forming factors namely the content of PMMA (C_P), the concentration of H_2O_2 (C_H), and the liquid to powder ratio (LP). Moreover, compressive strength and flexural strength were also predicted in term of porosity to explain their mechanical behaviors.

5.2.1 Porosity (P)

Table 5.7 summarized the regression models of porosity (P) for the porous HA samples prepared by various methods, including (1) sacrificial template using PMMA, (2) direct foaming using H_2O_2, and (3) combination technique using PMMA and H_2O_2. The regression model of porosity for the porous sample prepared via sacrificial template using PMMA in Equation 5.1 was dependent on the PMMA content (C_P), having the R-square of 0.9960. The regression model of porosity for the sample prepared by direct foaming using H_2O_2 in Equation 5.2 was dependent on the H_2O_2 concentration (C_H) and the liquid to powder ratio (LP), having the R-square of 0.8855. Additionally, the regression model of porosity for the sample prepared via combination technique using PMMA and H_2O_2 in Equation 5.3 was dependent on the PMMA content (C_P) and the H_2O_2 concentration (C_H), having the R-square of 0.9350.

Table 5.7   Regression models of porosity (P) for the porous HA samples prepared by various methods (at $\alpha = 0.05$)

Methods		Regression Models		R-square
1. Sacrificial template using PMMA	(5.1)	$P = 0.008C_P^2 + 0.204C_P + 51.716$	; $0 \le C_P \le 40$	0.9960
2. Direct foaming using H_2O_2	(5.2)	$P = -0.015C_H^2 + 0.480C_H + 11.935LP + 64.342$	; $0 < C_H \le 30$; $1.3 \le LP \le 1.5$	0.8855
3. Combination technique using PMMA and H_2O_2	(5.3)	$P = -0.012C_P^2 + 0.538C_P + 0.298C_H + 80.2$	; $0 \le C_P \le 20$; $0 < C_H \le 10$	0.9350

5.2.2 Compressive Strength (CS)

Table 5.8 summarized the regression models of compressive strength (CS) for the porous HA samples prepared by various methods, including (1) sacrificial template using PMMA, (2) direct foaming using H_2O_2, and (3) combination technique using PMMA and H_2O_2. The regression models of compressive strength for all fabrication methods were expressed in term of exponential equation.

Figure 5.1 showed the relationship between compressive strength (CS) and porosity (P) of the porous HA sample prepared via sacrificial template technique using PMMA granule For sacrificial template technique, the regression model of compressive strength was demonstrated in Equation 5.4, having the R-square of 0.9684.

Figure 5.2 illustrated the relationship between compressive strength (CS) and porosity (P) of the porous HA sample prepared via direct foaming technique using H_2O_2 solution. For direct foaming technique, the regression model of compressive strength was shown in Equation 5.5, having the R-square of 0.7691.

Figure 5.3 presented the relationship between compressive strength (CS) and porosity (P) of the porous HA sample prepared via combination technique using PMMA granule and H_2O_2 solution. For combination technique using PMMA and H_2O_2, the regression model of compressive strength was stated in Equation 5.6, having the R-square of 0.7650.

Figure 5.4 displayed the relationship between compressive strength (CS) and porosity (P) of the porous HA sample prepared via various methods. The regression models of compressive strength for the porous samples prepared through these methods could be summarized in Equation 5.7, having the R-square of 0.9596.
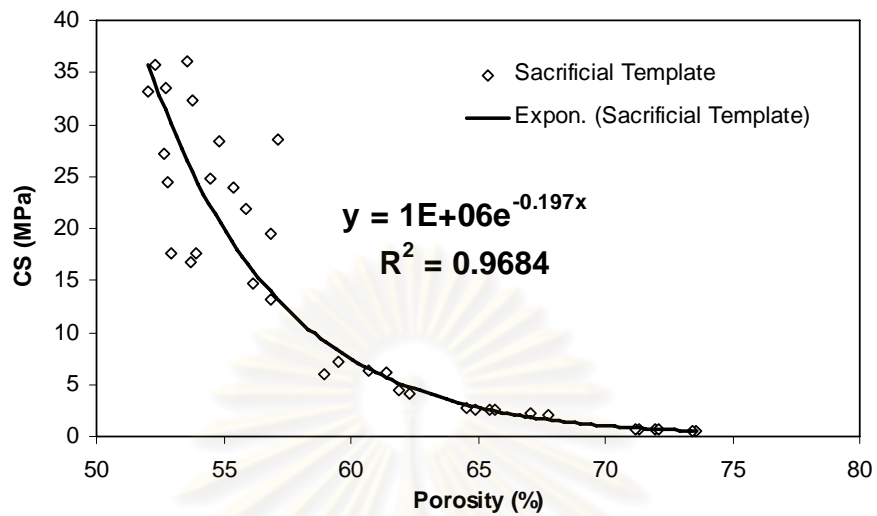
Figure 5.1   Relationship between compressive strength (CS) and porosity (P) of
              the porous HA sample prepared via sacrificial template technique
              using PMMA granule
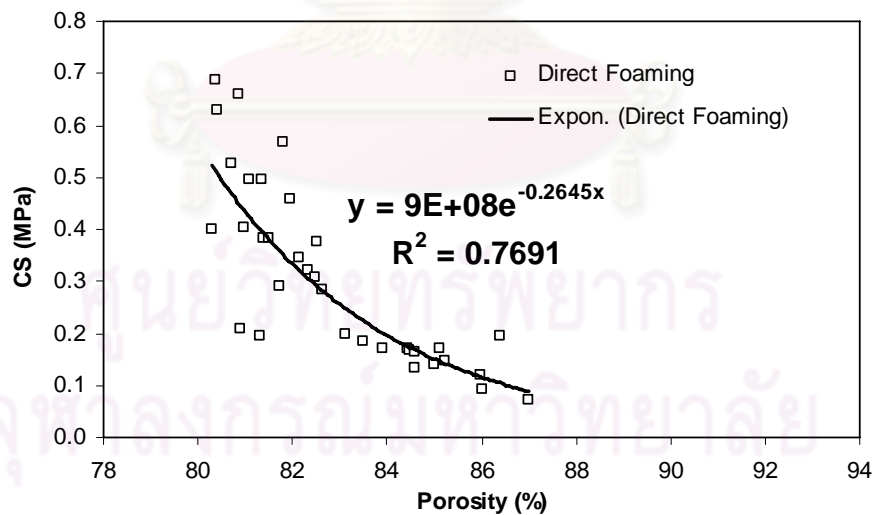
Figure 5.2   Relationship between compressive strength (CS) and porosity (P) of
              the porous HA sample prepared via direct foaming technique using
              H_2O_2 solution
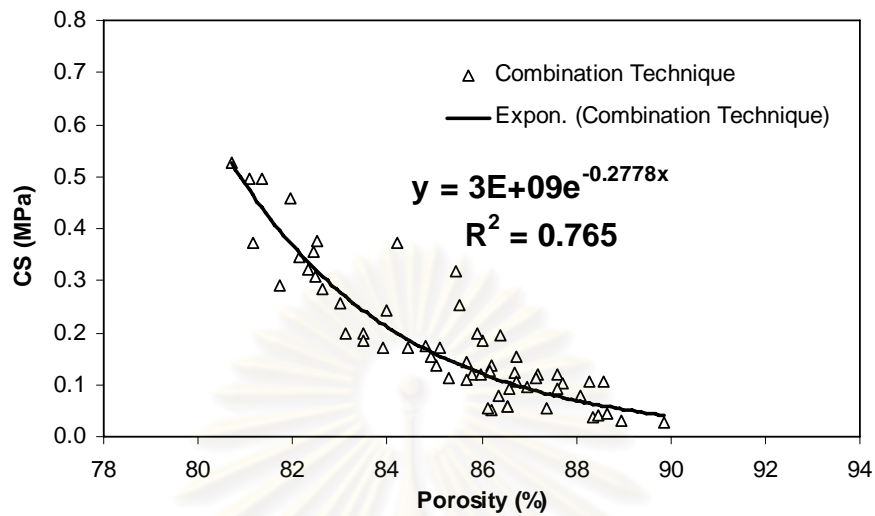
Figure 5.3   Relationship between compressive strength (CS) and porosity (P) of
the porous HA sample prepared via combination technique using
PMMA granule and H_2O_2 solution
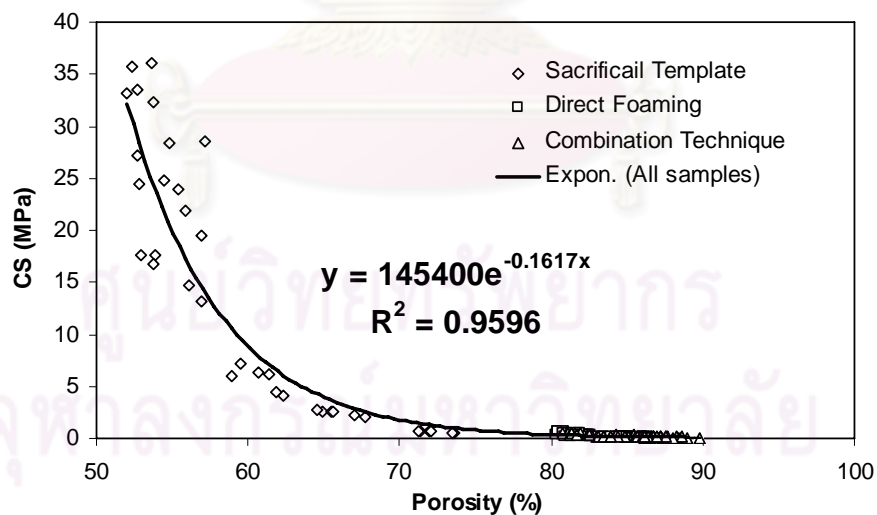
Figure 5.4   Relationship between compressive strength (CS) and porosity (P) of
the porous HA sample prepared via various methods

Table 5.8   Regression models of compressive strength (CS) for the porous HA samples prepared by various methods (at $\alpha = 0.05$)

Methods		Regression Models	R-square
1. Sacrificial template using PMMA	(5.4)	$CS = 1.015 \times 10^6 \, e^{-0.197 \, P}$	0.9684
2. Direct foaming using H_2O_2	(5.5)	$CS = 8.751 \times 10^8 \, e^{-0.265 \, P}$	0.7691
3. Combination technique using PMMA and H_2O_2	(5.6)	$CS = 2.883 \times 10^9 \, e^{-0.278 \, P}$	0.7650
All samples	(5.7)	$CS = 1.454 \times 10^5 \, e^{-0.162 \, P}$	0.9596

Table 5.9   Regression models of flexural strength (FS) for the porous HA samples prepared by various methods (at $\alpha = 0.05$)

Methods		Regression Models	R-square
1. Sacrificial template using PMMA	(5.8)	$FS = 372.877 \, e^{-0.081 \, P}$	0.7119
2. Direct foaming using H_2O_2	(5.9)	$FS = 6.008 \times 10^8 \, e^{-0.252 \, P}$	0.7909
3. Combination technique using PMMA and H_2O_2	(5.10)	$FS = 4.943 \times 10^4 \, e^{-0.140 \, P}$	0.3447
All samples	(5.11)	$FS = 537.275 \, e^{-0.086 \, P}$	0.8759

5.2.3 Flexural Strength (CS)

Table 5.9 summarized the regression models of flexural strength (FS) for the porous HA samples prepared by various methods, including (1) sacrificial template using PMMA, (2) direct foaming using H_2O_2, and (3) combination technique using PMMA and H_2O_2. The regression models of flexural strength for all pore forming methods were also expressed in term of exponential equation.

Figure 5.5 illustrated the relationship between flexural strength (FS) and porosity (P) of the porous HA sample prepared via sacrificial template technique using PMMA granule. For sacrificial template technique, the regression model of compressive strength was presented in Equation 5.8 and Figure 5.5, having the R-square of 0.7119.

Figure 5.6 showed the relationship between flexural strength (FS) and porosity (P) of the porous HA sample prepared via direct foaming technique using H_2O_2 solution. For direct foaming technique, the regression model of compressive strength was shown in Equation 5.9, having the R-square of 0.7909.

Figure 5.7 presented the relationship between flexural strength (FS) and porosity (P) of the porous HA sample prepared via combination technique using PMMA granule and H_2O_2 solution. For combination technique, the regression model of compressive strength was demonstrated in Equation 5.10, having the R-square of 0.3447.

Figure 5.8 exhibited the relationship between flexural strength (FS) and porosity (P) of the porous HA sample prepared via various methods. The regression models of compressive strength for all samples prepared through these methods were summarized in Equation 5.11, having the R-square of 0.9596.
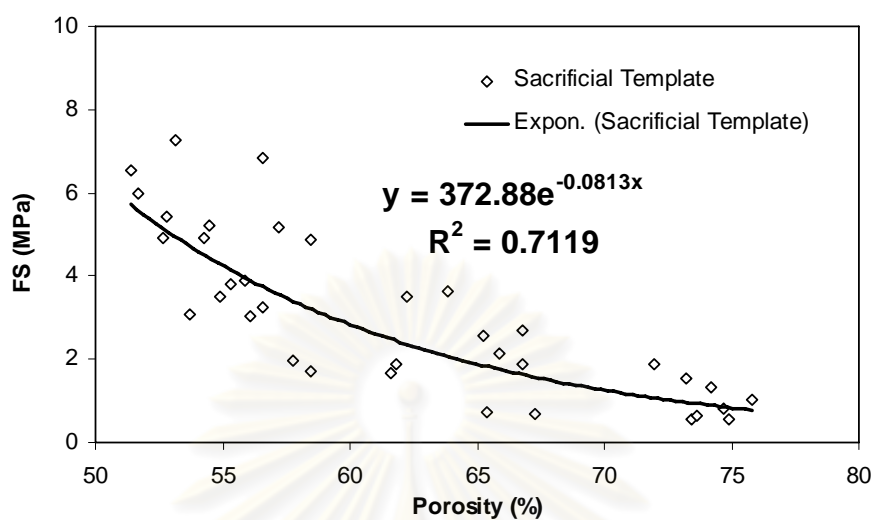
Figure 5.5   Relationship between flexural strength (FS) and porosity (P) of the
              porous HA sample prepared via sacrificial template technique using
              PMMA granule
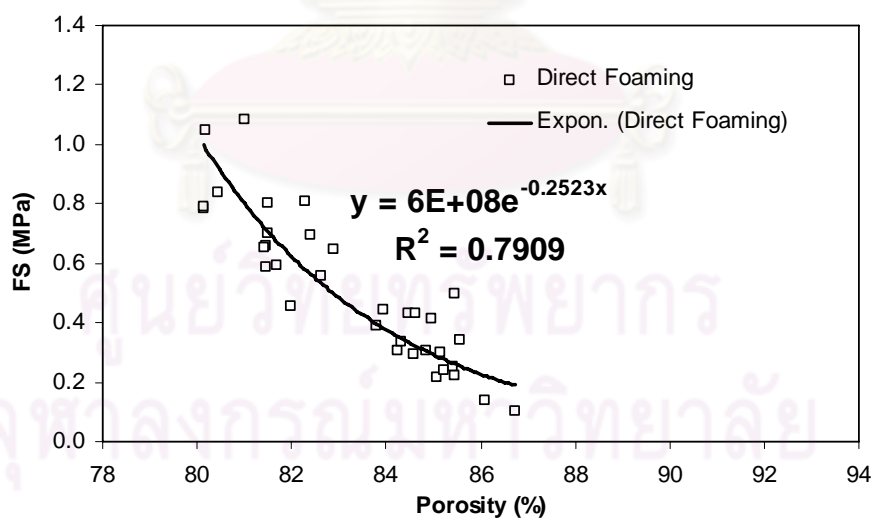
Figure 5.6   Relationship between flexural strength (FS) and porosity (P) of the
              porous HA sample prepared via direct foaming technique using H_2O_2
              solution
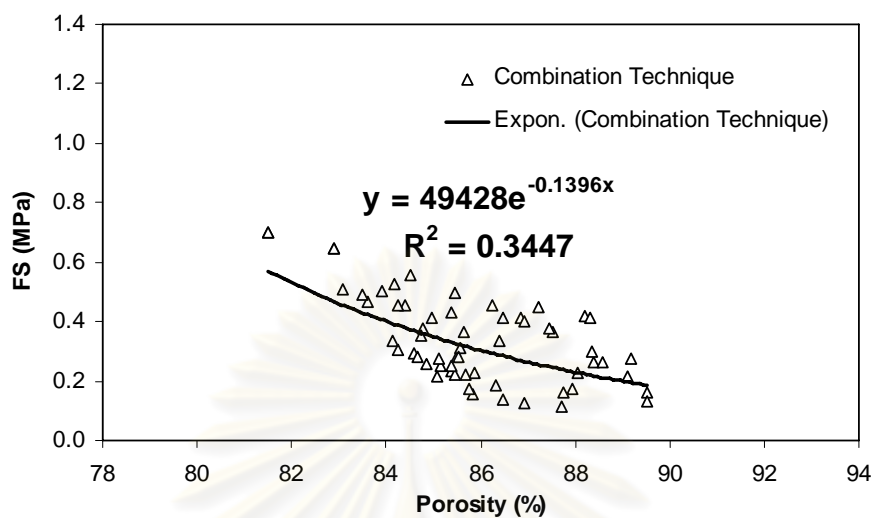
Figure 5.7   Relationship between flexural strength (FS) and porosity (P) of the
              porous HA sample prepared via combination technique using PMMA
              granule and H_2O_2 solution
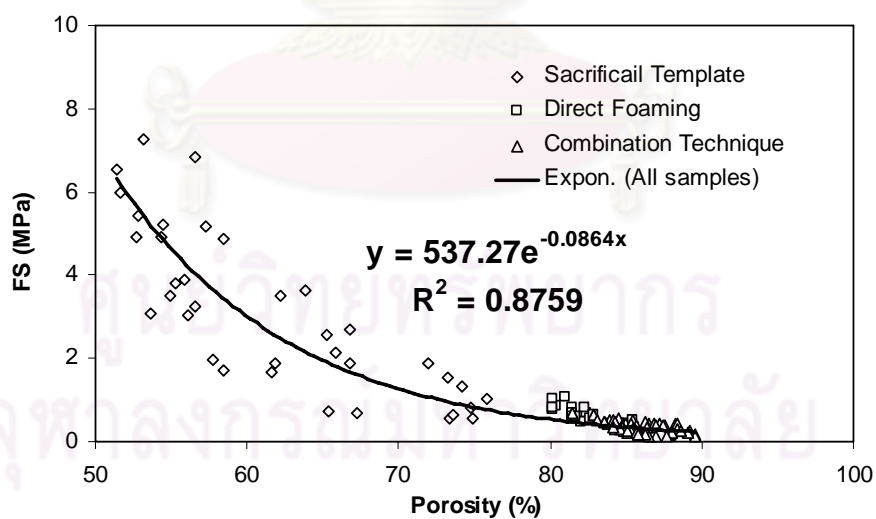
Figure 5.8   Relationship between flexural strength (FS) and porosity (P) of the
              porous HA sample prepared via various methods

CHAPTER VI

DISCUSSION

In this chapter, the results from characterizations of the synthesized HA powder and porous HA samples were discussed. Moreover, the effects of forming factors on porosity, compressive strength, flexural strength and stiffness were also mentioned.

6.1 The Synthesized HA Powder

In this research, the HA ceramic was synthesized through an aqueous precipitation method between calcium hydroxide and orthophosphoric acid. The synthesized HA powder was pulverized using pestle and mortar and then sieved.

6.1.1 Phase Purity

From the results of XRD analysis in the Chapter IV, the spectrum of the synthesized HA powder was consistent with the ICDD standard peak of stoichiometric Hydroxyapatite (No. 09-0432). Furthermore, the result of sintering the HA powder at $1100^{o}C$ for 2 hours agreed with a previous study of Patel and colleague (2001) in that sintering at high temperature resulted in the sharp and narrow diffraction peaks.

From FTIR analysis, the spectrum of the HA powder in Figure 4.2 showed the presence of PO_4^{3-} groups at 564, 603 and 1034 cm^{-1}. Absorption bands at 3570 cm^{-1} and near 630 cm^{-1} of hydroxyl group in HA ($Ca_{10}(PO_4)_6(OH)_2$) were barely detectable in the spectrum due to overlapping with the strong water band near 3420 cm^{-1}. Additionally, the strong absorption band near 1640 cm^{-1} can be attributed to the water absorbed.

From the EDX spectrum in Figure 4.3, the element of Ca, P and O, the component elements of HA, were detected excepting the element of H which hardly detected by this technique. Although the undesirable elements (C and Au) were also detected, they were obtained from the sample preparation step for SEM. The element

of carbon was from a carbon adhesive tape using to attach the sample to a strut. The element of gold was from the coating of the sample.

6.1.2 Particle Size and Morphology

From the characterization results of the HA powder in Chapter VI, the SEM micrographs indicated that the synthesized HA powder had an angular shape. Moreover, the particle size distribution of the powder showed a bimodal distribution with the peaks of ~4 μm and ~20 μm. These were because the HA powder used in this research was prepared by manual pestle and mortar grinding which hardly controlled the uniformity of power.

Figure 6.1 illustrated the SEM micrograph of (a) the HA powder produced by Direct Method (Patel *et al*., 2001) and (b) the HA powder prepared in this research. Interestingly, the morphology of the HA powder prepared in this research was similar to the HA powder produced by Direct Method from the previous study of Patel *et al.* (2001), which also had an angular shape as shown in Figure 6.1. The HA powder produced by the Direct Method was prepared by manual grinding and then ball milling. While the HA powder produced in this research was prepared by on manual grinding using pestle and mortar.

(a)   (b)
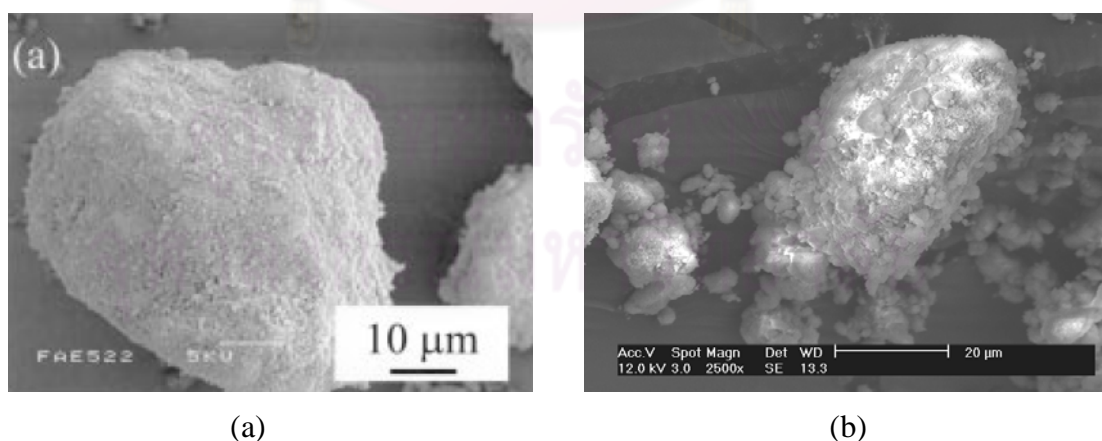
Figure 6.1   SEM micrographs of (a) the HA powder produced by Direct Method
(Patel *et al*., 2001) and (b) the HA powder prepared in this research.

6.2 Pore Morphology of Porous HA Samples

6.2.1 H_2O Based Technique

From Chapter IV, the sample prepared through H_2O based technique was named as the sample H00-P00, because the samples were prepared by casting without any pore former (i.e. PMMA and H_2O_2). In Figure 4.10, the sample H00-P00-L13, produced at the L/P ratio of 1.3 ml/g, showed a few small pores with the diameter of less than 50 μm. In Figure 4.11, the HA cement H00-P00-L15, prepared at the L/P ratio of 1.5 m;/g, also had the similar pores. Apparently, such pores were derived from driving out of water during drying process.

Figure 6.2 exhibited SEM micrographs at the magnification of 100X of the HA sample (a) H00-P00-L13 and (b) H00-P00-L15. By comparison between two samples, it seemed that the higher L/P ratio resulted in the higher number of pores derived from water, as shown in Figure 6.2. This idea was confirmed by the results of porosity in Table 4.3 that the porosity increased from 52.17% to 54.92% in average when the L/P ratio rose from 1.3 ml/g to 1.5 ml/g. Moreover, this result also agreed with a previous study of Almirall *el al.* (2004) in that the porosity of the sample increased with an increasing L/P ratio used.

(a) H00-P00-L13   (b) H00-P00-L15
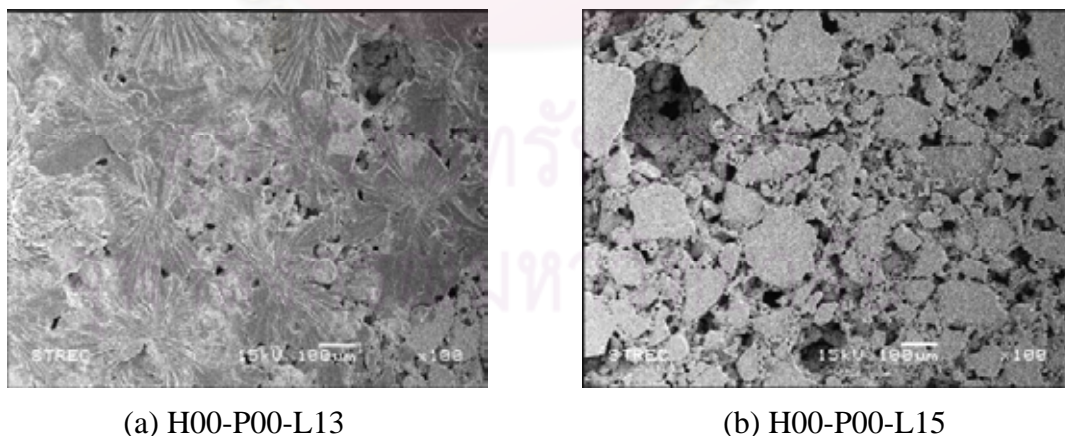
Figure 6.2   SEM micrographs at the magnification of 100X of the HA sample
(a) H00-P00-L13 and (b) H00-P00-L15

6.2.2 Sacrificial Template Technique using PMMA

From the experimental results in Chapter IV, the porous HA sample prepared through sacrificial template using PMMA granule were composed of two groups of pore size range. The former was small pores with the pore size of less than 50 μm. The latter was large pores having the diameter range of 100-300 μm. It seemed that the small pores were similar to the pore derived from water vaporization. While, the large pores were arisen from the disposal of PMMA granules as confirmed by SEM micrographs.

Figure 6.3 displayed SEM micrographs of (a) the porous HA sample H00-P30-L13 and (b) PMMA granule. In Figure 6.3, the large pores found in the sample H00-P30-L13 were rounded hole, which matched with the spherical shape of the PMMA granules. The pore size of the sample H00-P30-L13 was approximately 100 μm, which was smaller than the median particle size of the PMMA granule (approximately 150 μm). This was possible that sintering or heat treatment could result in the shrinkage of the ceramic sample and the pore, as reported by Yao *et al*. (2005).

(a)   (b)
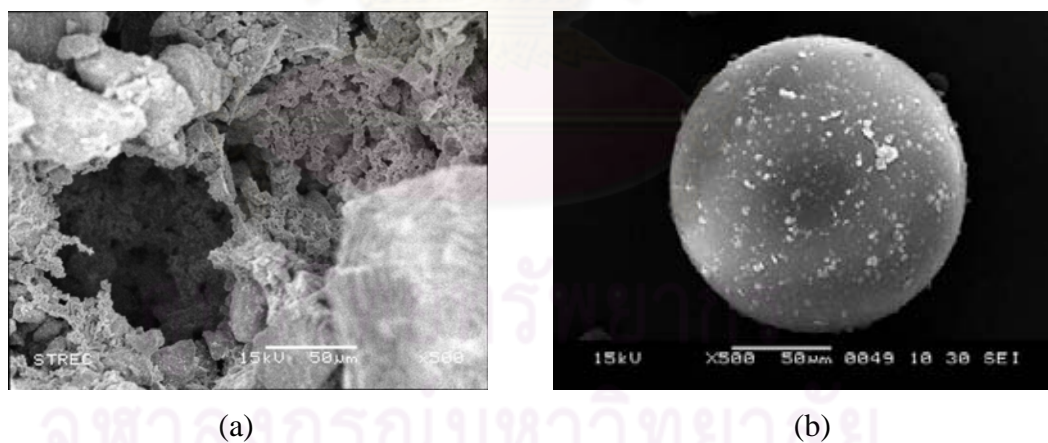
Figure 6.3   SEM micrographs of (a) the porous HA sample H00-P30-L13 and
(b) PMMA granule.

6.2.3 Direct Foaming Technique using H_2O_2

From the results in Chapter IV, the porous HA samples prepared by direct foaming method using H_2O_2 solution showed a number of pores with the size larger than 100 μm. In comparison between the sample H10-P00-L13A and H20-P00-L13A, the number and size of pores increased when the H_2O_2 concentration increased, as illustrated in Figure 4.17 and Figure 4.18. Moreover, it seemed that the L/P ratio also had an influence on the pore size as shown in Figure 4.15 and Figure 4.16. Furthermore, Almirall *et al.* (2004) confirmed the fact that both L/P ratio and H_2O_2 concentration resulted in the size of pores.

6.2.4 Combination Technique using PMMA and H_2O_2

From the experimental results, the porous HA sample prepared through combination technique using PMMA and H_2O_2 consisted of the large pores in the ceramic body and the small pores in the ceramic wall, as shown in Figure 4.19 and Figure 4.20. The size of the large pores was up to 1,000 μm in diameter, while the size of the small pores ranged between 100 and 300 μm in diameter. The large pores were possibly resulted from H_2O_2, while small pores might be from PMMA granules. In addition to the closed pores, the interconnected pores were also observed. Lu and colleague (1999) stated the definition of interconnected pores that was the pathways between pores conducting cells and vessels between pores and thus favor bone ingrowth inside ceramics.

Based on previous study of Karageorgiou and Kaplan (2005), the minimum requirement for pore size is considered to be around 100 μm due to cell size, migration requirements and transport. However, pore sizes over 300 μm was favorable to enhanced new bone formation and cell regeneration. Therefore, the sample prepared by combination technique using both PMMA and H_2O_2 can provide the pores attaining these requirements.

6.3 Effect of Forming Factors on Porosity

From the experimental results in Section 4.5, the porous HA samples prepared through sacrificial template technique using PMMA at the content of over 40wt% were handless, while the samples prepared through direct foaming technique using H_2O_2 solution at the concentration of over 20wt% were very brittle. To prepare the porous samples by combination technique using both PMMA and H_2O_2, a balance between the PMMA content and the H_2O_2 concentration must be considered.

Figure 6.4 illustrated graphical schemas of pore formation for the sample prepared via (a) sacrificial template using PMMA and (b) direct foaming using H_2O_2. For sacrificial template technique using PMMA, the content of PMMA were the only forming factor affecting significantly on porosity of the samples, as shown in Table 5.1. The relation between the porosity (P) and the content of PMMA (C_P) was explained by the regression model in Equation 5.1. Obviously, the porosity increased gradually, depending on the content of PMMA used. This mechanism was explained by the graphical illustration in Figure 6.4 (a). The PMMA granules remained until drying process. Then, the PMMA granule was removed by firing at the temperature of 400^oC, at which the PMMA was completely decomposed as shown in Figure 4.6. Afterwards, the former resident of PMMA granules became the pores. This result was agreed with Yao *et al*. (2005). At the L/P ratio of 1.3 ml/g, porosity of the samples reached approximately 72% at the PMMA content of 40wt%.

For direct foaming method using H_2O_2 solution, the significant factors having an influence on porosity were the concentration of H_2O_2 and the L/P ratio. The effect of the concentration of H_2O_2 (C_H) and the L/P ratio (LP) on porosity (P) was explained by the regression model in Equation 5.2. The porosity increased slightly with an increase of the H_2O_2 concentration and/or the L/P ratio. However, the porosity surged suddenly when the H_2O_2 solution was introduced. Even a small amount of H_2O_2, porosity could be enhanced up to 30%. The mechanism of pore formation was graphically illustrated in Figure 6.4 (b). At the liquid phase, the addition of H_2O_2 into ceramic slurry produced O_2 and H_2 gases, resulting in expansion of ceramic paste. At this state, the deformation of gas voids was possible. Then, the paste was stored at 60^oC to remove O_2 and H_2 gases. After drying process, the gas voids remaining in the

paste became the pores in porous dry bodies. Finally, the sintering process resulted in the shrinkage of pore size. This idea was confirmed by Almirall *et al.* (2004).

For combination technique using both PMMA and H_2O_2, Both of the PMMA content (C_P) and the H_2O_2 concentration (C_H) had a significant influence on porosity for the porous HA sample prepared through this technique. From Analysis of variance (ANOVA), the H_2O_2 concentration (C_H) was significant at lower than 10wt%, whereas the PMMA content was effective at lower than 20wt%. The porosity could be predicted by the regression model in Equation 5.3. Compared to the effect of H_2O_2, addition of PMMA was barely affected on porosity. It seemed that the porosity derived from PMMA granules was dominated by H_2O_2 solution. This was because PMMA granule formed pores by decomposition at above $400^{o}C$ in solid state while H_2O_2 produced pores by expansion of gas voids in liquid phase, which provide the higher porosity than PMMA.

Additionally, it seemed that the sintering temperature was also a significant factor affecting on porosity. From the experimental results in Chapter IV, the porosity reduced with an increase of sintering temperature. This result was consistent with the previous works of Mostasfa (2005) and He *et al.* (2008) in that the agglomeration of HA particle increased with an increasing temperature, resulting an increasing density and a decreasing porosity.
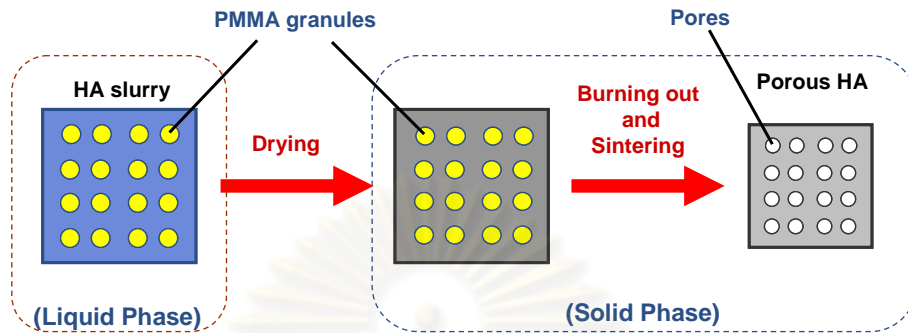
(a) Sacrificial template using PMMA
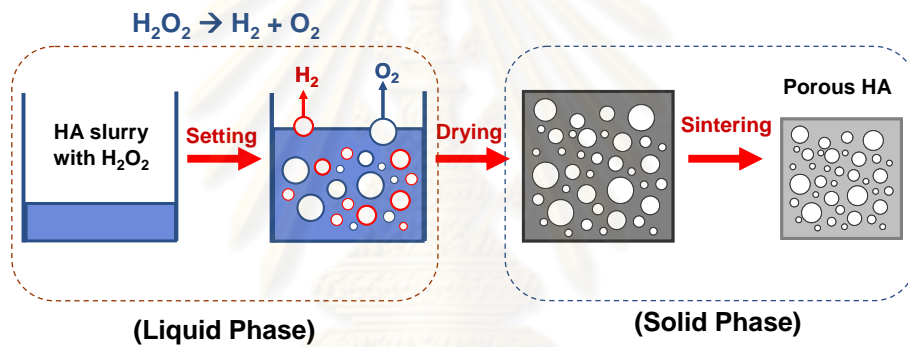
(b) Direct foaming using H_2O_2

Figure 6.4   Graphical schemas of pore formation for the sample prepared via

(a) sacrificial template using PMMA and (b) direct foaming using H_2O_2

6.4 Effect of Forming Factors on Compressive Strength

From the statistical analysis in Chapter V, many forming factors showed an influence on compressive strength of porous HA samples performed by sacrificial template technique using PMMA, direct foaming technique using H_2O_2 and combination technique using PMMA and H_2O_2. In this study, the compressive strength ranged between 0.03 MPa and 36 MPa with the porosity ranging between 52% and 90%.

Table 6.1 summarized compressive strength (CS) of porous HA ceramics from previous works. In comparison to the previous works, the average compressive strength obtained from this study was lower than those reported by Sepulveda *et al.* (2000); Deville *et al.* (2006); Lee *et al.* (2007); and Potoczek (2008). This was because of an addition of additives, enhanced the mechanical properties of porous sample. Besides, Zhang and Zhu (2006) improved the strength of the samples by uniaxially pressing at 50 MPa.

Table 6.1　Summary of compressive strength (CS) of porous HA ceramics from previous works.

Authors (year)	Methods	Additives	Porosity (%)	CS (MPa)
Sepulveda *et al* (2000)	Gelcasting (Direct foaming)	- Displex A40, polyacrylate derivatives (disperaant) - Acrylic monomers, ammonium persulfate, and N'-tetramethylethylen diamine (gelling agent) - Tergitol TMN10 (surfactant)	N/A	1.6- 5.8
Potoczek (2008)	Gelcasting (Direct foaming)	- Darvan 811, ammonium polymethacrylate (dispersant) - Agar (surfactant)	73-92 %	0.8-5.9
Deville *et al* (2006)	Water based freeze casting (Sacrificial template)	- Darvan 811 (dispersant) - PVA (binder)	40-65 %	65-145
Zhang and Zhu (2007)	Uniaxial press at 50 MPa and using rod-like urea particle (Sacrificial template)	- None	50-75 %	1.3-7.6
Lee *et al* (2007)	Camphene based freeze casting (Sacrificial template)	- oligomeric polyester (dispersant) - polystyrene (binder)	56-75 %	0.94-17

Statistically, the porosity seemed to have a significant effect on this strength, which could be described by the regression model in Equation 5.7. The compressive strength reduced exponentially with an increase of porosity, as reported by Kwon *et al.* (2002).

The significant factor affecting on compressive strength for the samples prepared by sacrificial template using PMMA was the content of PMMA (C_P) with the P-value of less than 0.001, as shown in Table 5.3. This finding was consistent with the results of porosity in that PMMA let to the pore formation resulting in mechanical strength of the specimen.

By direct foaming method using H_2O_2, compressive strength was significantly influenced by the concentration of H_2O_2 (C_H), the L/P ratio (LP) and addition of agar, which was supported by Almirall *et al.* (2004). Additionally, effect of adding agar was explained in the review of Studart *et al.* (2006) that direct foaming required a setting agent or surfactant to consolidate the foam microstructure before extensive coalescence and disproportionation take place.

By combination technique using PMMA and H_2O_2, the concentration of H_2O_2 (C_H) and the content of PMMA (C_P) resulted effectively in compressive strength at the H_2O_2 concentration of lower than 20wt%.

Moreover, sintering temperature also showed a significant influence on compressive strength. This result was supported by the previous study of White *et al.* (2007).

6.5 Effect of Forming Factors on Flexural Strength

From the statistical analysis in Chapter V, many forming factors showed an influence on flexural strength of porous HA samples performed by sacrificial template, direct foaming and combination between sacrificial template and direct foaming. In this study, the flexural strength ranged between 0.2 MPa and 7.5 MPa with the porosity ranging between 52% and 90%. However, these strengths seemed to be lower than those reported by Yao *et al.* (2005), ranging between 12 MPa and 27 MPa. Although Yao and colleagues prepared porous HA samples by sacrificial template technique using PMMA, they used the PMMA granule with lower particle size (around 50 μm) and also added polyvinyl alcohol (PVA) as a binder and polyacrylic acid (PAA) as a dispersant to improve the mechanical strength.

Statistically, the porosity seemed to have a significant effect on the flexural strength, which could be described by the regression model in Equation 5.11. As expected, the flexural strength also decreased exponentially with an increase of porosity. This result was supported by the previous study of Kwon *et al.* (2002).

The significant factor affecting on flexural strength for the samples prepared by sacrificial template technique using PMMA was the content of PMMA (C_P) with the P-value of less than 0.001, as shown in Table 5.3. This result agreed with the previous study of Yao *et al.* (2005).

By direct foaming technique using H_2O_2, flexural strength was significantly influenced by the concentration of H_2O_2 (C_H) with the P-value of less than 0.001.

By combination technique using PMMA and H_2O_2, the concentration of H_2O_2 (C_H) and the content of PMMA (C_P) were effective to flexural strength at the H_2O_2 concentration of lower than 10wt%.

However, the statistical result indicated that the sintering temperature had no significant influence on flexural strength. This result was also supported by White *et al.* (2007).

6.6 Effect of Forming Factors on Stiffness

From the experimental results in Chapter IV, many results showed the relation between stiffness and forming factors. In this dissertation, the compressive stiffness ranged approximately from 1 kN/m^2 to 250 kN/m^2, while the flexural stiffness ranged approximately between 10 kN/m^2 and 6,500 kN/m^2.

For sacrificial template using PMMA, the content of PMMA (C$_P$) showed a significant influence on both compressive stiffness and flexural stiffness with the P-value of less than 0.001.

For direct foaming using H$_2$O$_2$, the concentration of H$_2$O$_2$ (C$_H$) and the L/P ratio (LP) were the factors affecting significantly on compressive stiffness with the P-value of <0.001 and 0.032, respectively; while, the concentration of H$_2$O$_2$ (C$_H$) and addition of agar had a significant effect on flexural stiffness.

For combination technique using PMMA and H$_2$O$_2$, the content of PMMA (C$_P$) had a significant effect on compressive stiffness at the H$_2$O$_2$ concentration ranging between 5wt% and 10wt%, as well as the content of PMMA was also a significant factor flexural stiffness at the H$_2$O$_2$ concentration ranging between 5wt% and 20wt%.

However, sintering temperature showed an insignificant effect on stiffness, although it improved the stiffness of the porous samples slightly, as illustrated in Figure 4.61 and Figure 4.62.

Table 6.2 Comparison between the pore size, porosity, compressive strength (CS) and flexural strength (FS) of porous hydroxyapatite ceramics from previous works and this research.

Authors (year)	Methods	Pore Size (µm)	Porosity (%)	CS (MPa)	FS (MPa)
Rodriguez *et al* (1998)	ST (Starch consolidation)	80	45-69	n/a	2-14
Hing *et al* (1999)	RT (Hydrothermal treatment of cancellous bone)	500	n/a	1-11	n/a
Sepulveda *et al* (2000)	DT (Gelcasting)	17-122	n/a	1.6-5.8	n/a
Tempieri *et al* (2001)	RT (PU impregnation)	200-500	n/a	21-45	n/a
Tian and Tian (2001)	RT (PU impregnation)	150-400	58-80	2-15	n/a
Ramay and Zhang (2003)	RT (PU impregnation)	200-400	70-77	0.5-5	n/a
Kundu *et al* (2004)	ST (Cold isostatic pressing with Naphthalene)	100-250	75	9.7-10.3	n/a
Yao *et al* (2005)	ST (Casting with PMMA)	260-350	33.3-33.7	n/a	11.5-13.5
Deville *et al* (2006)	ST (H_2O based freeze casting)	>10	40-65	65-145	n/a
Zhang and Zhu (2007)	ST (Cold uniaxial pressing with urea)	120	50-75	1.3-7.6	n/a
Lee *et al* (2007)	ST (Camphene based freeze casting)	>10	56-75	0.9-17	n/a
Potoczek (2008)	DT (Gelcasting)	130-380	73-92	0.8-5.9	n/a
This research	ST (casting with PMMA)	100-300	52-74	0.5-36	0.6-7
	DT (casting with H_2O_2)	100-1000	80-85	0.07-0.7	0.1-1.1
	ST + DT (casting with PMMA and H_2O_2)	100-1000	82-90	0.03-0.5	0.1-0.7

Note: *'n/a' = No data available,*
'RT' =Replica technique,
'ST' = Sacrificial template technique, and
'DT' = Direct foaming technique

Table 6.2 compared the pore size, porosity, compressive strength and flexural strength of porous hydroxyapatite ceramics from previous works and this research. It seemed that both compressive strength and flexural strength decreased with an increasing porosity for all forming techniques. These results agreed with previous research by Yao *et al.* (2005) and Lee *et al.* (2007) that the mechanical strength of the sample was conversely relative to the amount of pore former used and final porosity. Furthermore, the samples with the porosity higher than 80% showed a fluctuation in strength, particularly flexural strength. On the other hand, the samples using H_2O_2 (i.e. direct foaming and combination technique) provided high variation in strength more than those using PMMA. This was because the porosity obtained from H_2O_2 could not be effectively controlled.

Nevertheless, the mechanical strengths of the samples in this research were lower than the minimum strength of cancellous bone. White *et al.* (2007) indicated that the minimum compressive strength and flexural strength of human cancellous bone were approximately 2 MPa and 10 MPa, respectively. Karageorgiou and Kaplan (2005) reported that the pore size favorable to bone formation and cell regeneration was over 300 μm. As well as Lu *et al.* (1999) stated that the interconnected pores favors to cell ingrowth inside the pore. However, there was no report on suitable porosity for these applications. As a result, such samples were not applicable for a scaffold in bone restoration due to the lack of strength. However, these materials could be applied for fabrication of an eye ball in orbital implant being porous bioceramics.

CHAPTER VII

CONCLUSION

In this chapter, the outcomes and limitations of this research for porous HA ceramic prepared through various methods were summarized. Additionally, the further research was also mentioned to improve the properties of porous HA ceramic.

7.1 Conclusions

From previous chapters, all results were summarized as follows:

(1) The porous HA ceramic produced by sacrificial template technique using PMMA granules had pore size ranging between 100 μm and 300 μm; porosity ranging between 52% and 74%; compressive strength ranging between 0.5 MPa and 36 MPa with compressive stiffness of 33 kN/m^2 and 5,530 kN/m^2; and flexural strength ranging between 0.6 MPa and 7 MPa with flexural stiffness of 8 MN/m^2 and 730 MN/m^2.

(2) The porous HA ceramic produced by direct foaming technique using H_2O_2 solution had pore size ranging between 100 μm and 1,000 μm; porosity ranging between 80% and 85%; compressive strength ranging between 0.07 MPa and 0.7 MPa with compressive stiffness of 60 kN/m^2 and 550 kN/m^2; and flexural strength ranging between 0.1 MPa and 1.1 MPa with flexural stiffness of 2 MN/m^2 and 75 kN/m^2.

(3) The porous HA ceramic produced by combination technique using PMMA granule and H_2O_2 solution had pore size ranging between 100 μm and 1,000 μm; porosity ranging between 82% and 90%; compressive strength ranging between 0.03 MPa and 0.5 MPa with compressive stiffness of 13 kN/m^2 and 440 kN/m^2; and flexural strength ranging between 0.1 MPa and 0.7 MPa with flexural stiffness of 0.5 MN/m^2 and 45 MN/m^2.

(4) The porous HA specimens were handleless when applied PMMA content was over 40wt% for sacrificial template technique and H_2O_2 concentration was over 20wt% for direct foaming technique, due to broken forming.

(5) Sacrificial template technique using PMMA was the best method to control the porosity of HA samples, due to the lowest variance of porosity.

(6) Combination technique using PMMA and H_2O_2 provided the interconnected pores, while sacrificial template technique using PMMA and direct foaming technique using H_2O_2 gave the closed pores.

(7) For sacrificial template technique, an increase of PMMA content affected an increase of porosity, while bulk density, compressive strength, flexural strength and stiffness were decreased.

(8) For direct foaming technique, an increase of H_2O_2 concentration and liquid to powder ratio resulted in an increasing pore size and porosity, whereas bulk density, compressive strength, flexural strength and stiffness were decreased.

(9) For combination between sacrificial template and direct foaming techniques, the increases of PMMA content and H_2O_2 concentration caused an increase of porosity; however, bulk density, compressive strength, flexural strength and stiffness were decreased.

(10) Addition of surfactant (i.e. agar) showed an effective improvement on compressive strength and flexural stiffness for only direct foaming method using H_2O_2 solution.

(11) An increase of sintering temperature resulted in a reduction of porosity, whereas bulk density, compressive strength, flexural strength and stiffness were increased.

(12) Compressive strength and flexural strength of the porous HA samples decreased exponentially as the porosity increased.

7.2 Research Limitations

The limitations of this research were summarized as follows:

(1) The precipitation reaction of the synthesized HA was the time-consuming process. To increase the production rate, the larger reactors were needed.

(2) The small particle size and uniform particle size distribution of the HA powder could improved the mechanical strength and reduced a deviation of the experimental results. To achieve these, ball milling and sieving machine were required.

(3) The mechanical strengths of the porous HA samples prepared via sacrificial template technique using PMMA granules were lower than those of previous studies. The addition of deflocculant could improve solid content of ceramic, resulting in an increase of mechanical strength.

(4) The pore size and shape of the porous HA sample prepared through direct foaming technique using H_2O_2 solution were hard to control due to uncontrollable air bubble in ceramic cake.

7.3 Further Researches

From this research work, there were some interesting aspects in the production of porous HA ceramic which could be further studied as follows,

(1) Mechanical strength of porous HA ceramic prepared by combination between sacrificial template and direct foaming techniques should be developed. Addition of some additive, such as binder, deflocculant or surfactant could improve the mechanical properties of porous ceramics.

(2) The porous ceramic prepared using hydrogen peroxide (H_2O_2) less than 5wt% concentration should be investigated, which was another way to improve the strength of the porous ceramics.

(3) Fabrication of porous ceramic using other sacrificial templates with various size ranges and different shapes should be studied, which could provide controllable pore size and result in different pore morphology.

REFERENCES

Aoki, H. 1994. Medical Applications of Hydroxyapatite Japan: Takayama Press.

Afshar, A., Ghorbam, M., Ehsanai, N., Saeri, M. R., and Sorrell, C. C. 2003. Some important factors in the wet precipitation process of hydroxyapatite, Materials and Design, 24: 197-202.

Almirall, A., et al. 2004. Fabrication of low temperature macroporous hydroxyapatite scaffolds by foaming and hydrolysis of an alpha-TCP paste. Biomaterials 25: 3671-3680.

Araki, K., and Halloran, J. W. 2005. Porous ceramic bodies with interconnected pore channels by a novel freeze casting technique. Journal of the American Ceramic Society 88(5): 1108-1114.

ASTM C773-88. 2006. Standard test method for compressive strength of fired whiteware materials, American Society for Testing and Materials, West Conshohocken, Pennsylvania, U.S.A.

ASTM C1161-02c. 2006. Standard test method for flexural strength of advanced ceramics at ambient temperature, American Society for Testing and Materials, West Conshohocken, Pennsylvania, U.S.A.

ASTM F1185-03. 2003. Standard specification for composition of hydroxylapatite for surgical implants, American Society for Testing and Materials, West Conshohocken, Pennsylvania, U.S.A.

ASTM F2024-00. 2000. Standard practice for X-ray diffraction derermination of phase content of plasma-sprayed hydroxyapatite coatings, American Society for Testing and Materials, West Conshohocken, Pennsylvania, U.S.A.

Bae, C. J., Kim, H. W., Koh, Y. H., and Kim, H. E. 2006. Hydroxyapatite bone scaffolds with controlled macrochannel pores. Journal of Materials Science: Materials in Medicine 17: 517-521.

Ban, S., and Hasegawa, J. 2002. Morphological regulation and crystal growth of hydrothermal-electrochemically deposited apatite. Biomaterials 23: 2965-2972.

Barbucci, R. 2002. Integrated Biomaterials Science New York, USA: Kluwer Academic Publishers.

Bartuli, C., et al. 2009. Mechanical properties of cellular ceramics obtained by gel casting: Characterization and modeling. Journal of the European Ceramic Society 29: 2979–2989.

Bezzi, G., et al. 2003. A novel sol-gel technique for hydroxyapatite preparation. Materials Chemistry adn Physics 78: 816-824.

Boanini, E., and Bigi, A. 2006. Biomimetic synthesis of carbonated hydroxyapatite thin films. Thin Solid Films 497: 53-57.

Bose, S., and Saha, S. K. 2003. Synthesis of hydroxyapatite nanopowders via sucrose-templated sol-gel method. Journal of the American Ceramic Society 86(6): 1055-1057.

Bouyer, E., Gitzhofer, F., and Boulos, M. I. 2000. Morphological study of hydroxyapatite nanocrystal suspension. Journal of Materials Science: Materials in Medicine 11: 523-531.

Brown, P. W., and Fulmer, M. 1991. Kinetics of Hydroxyapatite Formation at Low Temperature. Journal of the American Ceramic Society 74(5): 934-940.

Cao, L.Y., Zhang, C.B., and Huang, J.F. 2005. Influence of temperature, [Ca^{2+}], Ca/P ratio and ultrasonic power on the crystallinity and morphology of hydroxyapatite nanoparticles prepared with a novel ultrasonic precipitation method. Material Letters 59: 1902-1906.

Chu, T. M. G., Halloran, J. W., Hollister, S. J., and Feinberg, S. E. 2001. Hydroxyapatite implant with designed internal architecture. Journal of Materials Science: Materials in Medicine 12: 471-478.

DeOliveira, J. F., DeAguiar, P. F., Rossi, A. M., and Soares, G. A. 2003. Effect of process parameters on the characteristics of porous calcium phosphate ceramics for bone tissue scaffolds. International Society for Artificial Organs 27(5): 406-411.

Deville, S., Saiz, E., and Tomsia, A. P. 2006. Freeze casting of hydroxyapatite scaffolds for bone tissue engineering. Biomaterials 27: 5480-89.

Engin, O. N., and Tas, C. A. 2000. Preparation of porous HA and β-TCP bioceramics. Journal of the American Ceramic Society 83(7): 1581-1584.

Fanovich, M. A., and Porto Lopez, J. M. 1998. Influence of temperature and additives on the microstructure and sintering behaviour of hydroxyapatite with different Ca/P ratios. Journal of Materials Science: Materials in Medicine 9: 53-60.

Fidancevska, E., Ruseska, G., Bossert, J., Lin, Y. M., and Boccaccini, A. R. 2007. Fabrication and characterization of porous bioceramics composites based on hydroxyapatite and titania. Materials Chemistry and Physics 103: 95-100.

Flautre, B., Descamps, M., Delecourt, C., Blary, M. C., and Hardouin, P. 2001. Porous HA ceramic for bone replacement: Role of the pores and interconnections – experimental study in the rabbit. Journal of Materials Science: Materials in Medicine 12: 679-682.

Friefs, W., and Warner, J. 2002. Biomedical Applications. Handbook of Porous Solids, Volume 5 Viley-VCH: 2923-2970.

Fuji, M., Kato, T., Zhang, F.Z., and Takahashi, M. 2006. Effects of surfactants on the microstructure and some intrinsic properties of porous building ceramics fabricated by gelcasting. Ceramics International 32: 797-802.

Gibson, I. R., Ke, S., Best, S. M., and Bonfield, W. 2001. Effect of powder characteristics on the sinterability of hydroxyapatite powders. Journal of Materials Science: Material in Medicine 12: 163-171.

Graham, S., and Brown, P. W. 1996. Reactions of octacalcium phosphate to form hydroxyapatite. Journal of Crystal Growth 165: 106-115.

Gregorova, E., Zivcova, Z., and Pabst, W. 2006. Porosity and pore space characteristics of starch-processed porous ceramics. Journal of Materials Science 41: 6119-6122.

Guelcher, S. A., and Hollenger, J. O. 2006. An Introduction to Biomaterials USA: CRC Press.

Hamdi, M., and Ide-Ektessabi, A. 2007. Dissolution behavior of simultaneous vapor deposited calcium phosphate coatings in vitro. Materials Science and Engineering: C 27: 670-674.

He, L. H., Standard, O. C., Huang, T. T. Y., Latella, B. A., and Swain, M. V. 2008. Mechanical behaviour of porous hydroxyapatite. Acta Biomaterialia 4: 577-586.

Hench, L. L. 1998. Bioceramics. Journal of the American Ceramic Society 81, 7: 1705-1728.

Hing, K. A., Best, S. M., and Bonfield, W. 1999. Characterization of porous hydroxyapatite. Journal of Materials Science: Materials in Medicine 10: 135-145.

Hing, K. A. 2005. Bioceramic Bone Graft Substitutes: Influence of Porosity and Chemistry. Applied Ceramic Technology 2: 184-199.

Hsieh, M. F., Chin, T. S., Perng, L. H., and Perng, H. G. 2001. Gel-to-ceramic conversion during hydroxyapatite synthesis. Journal of the American Ceramic Society 84(9): 2123-2125.

Hsieh, M. F., Perng, L. H., and Chin, T. S. 2002. Formation mechanisms of sol-gel-derived hydroxyapatite using different thermal processing. Journal of Sol-Gel Science and Technology 23: 205-214.

Hsu, Y. H., Turner, I. G., and Miles, A. W. 2007. Fabrication of porous bioceramics with porosity gradients similar to the bimodal structure of cortical and cancellous bone. Journal of Materials Science: Materials in Medicine 18: 2251-56.

Hu, J., Russell, J. J., Ben-Nissan, B., and Vago, R. 2001. Production and analysis of hydroxyapatite from Australian corals via hydrothermal process. Journal of Materials Science Letter 20: 85-87.

Hutchens, S. A., Benson, R. S., Evans, B. R., O'Neill, H. M., and Rawn, C. J. 2006. Biomimetic synthesis of calcium-deficient hydroxyapatite in a natural hydrogel. Biomaterials 27: 4661-4670.

Jinawath, S., Pongkao, D., and Yoshimura, M. 2002. Hydrothermal synthesis of hydroxyapatite from natural source. Journal of Materials Science: Materials in Medicine 13: 494-494.

Juang, H. Y., and Hon, M. H. 1996. Effect of calcination on sintering of hydroxyapatite. Biomaterials 17: 2059-2064.

Karageorgiou, V., and Kaplan, D. 2005. Porosity of 3D biomaterial scaffolds and osteogenesis. Biomaterials 26: 5474-5491.

Kawata, M., et al. 2004. Development of porous ceramics with well-controlled porosities and pore sizes form apatite fibers and their evaluations. Journal of Materials Science: Materials in Medicine 15: 817-823.

Kim, W., and Saito, F. 2001. Sonochemical synthesis of hydroxyapatite from H_3PO_4 solution with $Ca(OH)_2$. Ultrasonics Sonochemistry 8: 85-88.

Kivrak, N., and Tas, C. A. 1998. Synthesis of Calcium Hydroxyapatite–Tricalcium Phosphate (HA–TCP) Composite Bioceramic Powders and Their Sintering Behavior, Journal of the American Ceramic Society 81 (9): 2245-2252.

Koh, Y. H., Son, J. H., Lee, E. J., and Kim, H. E. 2006. Freezing dilute ceramic/camphene slurry for ultra-high porosity ceramics with completely interconnected pore networks. Journal of the American Ceramics Society 89(10): 3089-93.

Komlev, V. S., and Barinov, S. M. 2002. Porous hydroxyapatite ceramics of bi-modal pore size distribution. Journal of Materials Science: Materials in Medicine 13: 295-299.

Kothapalli, C., Wei, M., Vasiliev, A., and Shaw, M. T. 2004. Influence of temperature and concentration on the sintering behavior and mechanical properties of hydroxyapatite. Acta materialia 52: 5655-5663.

Kundu, B., Sunha, M. K., Mitra, M. K., and Basu, D. 2004. Fabrication and characterization of porous hydroxyapatite ocular implant followed by and in vivo study in dogs. Bulletin of Materials Science 27(2): 133-140.

Kuo, M. C., and Yen, S. K. 2002. The process of electrochemical deposited hydroxyapatite coatings on biomedical titanium at room temperature. Materials Science and Engineering 20: 153-160.

Kwan, Y. B. P., and Alcock, J. R. 2002. The impact of water impregnation method on the accuracy of open porosity measurements. Journal of Materials Science 37: 2557-2561.

Kweh, S. W. K., Khor, K. A., and Cheang, P. 1999. The production and characterization of hydroxyapatite (HA) powders. Journal of Materials Processing Technology 80-90: 373-377.

Kwon, S. H., et al. 2002. Calcium phosphate bioceramics with various porosities and dissolution rates. Journal of the American Ceramic Society 85(12): 3129-3131.

Kwon, S. H., Jun, Y. K., Hong, S. H., and Kim, H. E. 2003. Synthesis and dissolution behavior of beta-TCP and HA/beta-TCP composite powders. Journal of the European Ceramic Society 23: 1039-1045.

Layrolle, P., Ito, A., and Tateishi, T. 1998. Sol-gel synthesis of amorphous calcium phosphate and sintering into microporous hydroxyapatite bioceramics. Journal of the American Ceramic Society 81(6): 1421-1428.

Lazic, S., Zec, S., Miljevic, N., and Milonjic, S. 2001. The effect of temperature on the properties of hydroxyapatite precipitated from calcium hydroxide and phosphoric acid. Thermochimica Acta 374: 13-22.

Lee, E. J., Koh, Y. H., Yoon, B. H., Kim, H. E., and Kim, H. W. 2007. Highly porous hydroxyapatite bioceramics with interconnected pore channels using camphene-based freeze casting. Materials Letters 61: 2270-73.

Lemos, A. F., and Ferreira, J. M. F. 2000. Porous bioactive calcium carbonate implants processed by starch consolidation. Materials Science and Engineering: C 11: 35-40.

Lewis A. J. 2000. Colloidal processing of ceramics. Journal of the American Ceramics Society 83(10): 2341-59

Li, S. H., de Wijn, J. R., Layrolle, P., and de Groot, K. 2003. Novel method to manufacture porous hydroxyapatite by dual-phase mixing. Journal of American Ceramics Society 86(1): 65-72.

Li, B., et al. 2009. Fabrication and cellular biocompatibility of porous carbonated biphasic calcium phosphate ceramics with a nanostructure. Acta Biomaterialia 5: 134-143.

Liu, D. M. 1997. Fabrication of hydroxyapatite ceramic with controlled porosity. Journal of Materials Science: Materials in Medicine 8: 227-232.

Lloyd, A. W., Garagher, R. G. A., and Denyer, S. P. 2001. Ocular biomaterials and implants. Biomaterials 22: 769-785.

Lu, J. X., et al. 1999. Role of interconnections in porous bioceramics on bone recolonization in vitro and in vivo. Journal of Materials Science: Materials in Medicine 10: 111-120.

Madhavi, S., Ferraris, C., and White, T. J. 2005. Synthesis and crystallization of macroporous hydroxyapatite. Journal of Solid State Chemistry 178: 2838-2845.

Mao, X. J., Wang, S. W., and Shimai, S. 2008. Porous ceramics with tri-modal pores prepared by foaming and starch consolidation. Ceramics International 34: 107-112.

Mastrogiacomo, M., et al. 2006. Role of scaffold internal structure on in vivo bone formation in macroporous calcium phosphate bioceramics. Biomaterials 27: 3230-3237.

Miao, X., Hu, Y., Liu, J., and Wong, A. P. 2004. Porous calcium phosphate ceramics prepared by coating polyurethane foams with calcium phosphate cements. Materials Letters 58: 397-402.

Miranda, P., Saiz, E., Gryn, K., and Tomsia, A. P. 2006. Sintering and robocasting of β-tricalcium phosphate scaffolds for orthopedic applications. Acta Biomaterialia 2: 457-466.

Mostafa, N. Y. 2005. Characterization, thermal stability and sintering of hydroxyapatite powders prepared by different routes, Materials Chemistry and Physics, 94: 333-341.

Murugan, R., and Ramakrishna, S. 2005. Development of nanocomposites for bone grafting: review. Composites Science and Technology 65: 2385-2406.

Nakahira, A., Murakami, T., Onoki, T., Hashida, T., and Hosoi, K. 2005. Fabrication of porous hydroxyapatite using hydrothermal hot pressing and post-sintering. Journal of the American Ceramic Society 88(5): 1334-1336.

Padilla, S., Roman, J., and Vallet-Regi, M. 2002. Synthesis of porous hydroxyapatite by combination of gelcasting and foams burn out methods. Journal of Materials Science: Materials in Medicine 13: 1193-1197.

Pang, Y. X., and Bao, X. 2003. Influence of temperature, ripening time and calcination on the morphology and crystallinity of hydroxyapatite nanoparticles. Journal of the European Ceramic Society 23: 1697-1704.

Park, J., and Lakes, R. S. 2007. Biomaterials: An Introduction, 3rd Edition New York: Springer.

Patel, N., Gibson, I. R., Ke, S., Best, S. M., and Bonfield, W. 2001. Calcining influence on the powder properties of hydroxyapatite. Journal of Material Science: Materials in Medicine 12: 181-188.

Paul, W., and Sharma, C. P. 1999. Development of porous spherical hydroxyapatite granules: application towards protein delivery. Journal of Materials Science: Materials in Medicine 10: 383-388.

Potoczek, M. 2008. Hydroxyapatite foams produced by gelcasting using Agarose. Material Letters 62: 1055-57.

Ramay, H. R., and Zhang, M. 2003. Preparation of porous hydroxyapatite scaffolds by combination of the gel-casting and polymer sponge methods. Biomaterials 24: 3293-3302.

Rice, R. W. 1998. Porosity of ceramic New York: Marcel Dekker.

Rivera-Munoz, E., Diaz, J. R., Rodriguez, J. R., Brostow, W., and Castano, V. M. 2001. Hydroxyapatite spheres with controlled porosity for eye ball prosthesis: processing and characterization. Journal of Materials Science: Materials in Medicine 12: 305-311.

Rocha, J. H. G., et al. 2005. Scaffolds for bone restoration from cuttlefish. Bone 37: 850-857.

Rodriguez-Lorenzo, L. M., Ferreira, J. M. F., and Vallet-Regi M. 1998. Processing of porous hydroxyapatite by starch consolidation. Bioceramics 11: 89-92.

Roy, D. M. 1975. Porous biomaterials and method of making same. US Patent US3929971.

Saeri, M. R., Afshar, A., Ghorbani, M., Ehsani, N., and Sorrell, C.C. 2003. The wet precipitation process of hydroxyapatite. Materials Letters 57: 4064-4069.

Saiz, E., et al. 2007. Preparation of porous hydroxyapatite scaffolds. Materials Science and Engineering C 27: 546-550.

Sepulveda, P., and Binner, J. G. P. 1999. Processing of Cellular Ceramics by Foaming and in situ Polymerisation of Organic Monomers. Journal of the European Ceramic Society 19: 2059-2066.

Sepulveda, P., Ortega, F. S., Innocentini, D. M., and Pandolfelli, V. C. 2000. Properties of highly porous hydroxyapatite obtained by the gel-casting of foams. Journal of the American Ceramic Society 82(12): 3021-3024.

Shih, W. J., Chen, Y. F., Wang, M. C., and Hon, M. H. 2004. Crystal growth and morphology of the nanosized hydroxyapatite powders synthesized from $CaHPO_4.2H_2O$ and $CaCO_3$ by hydrolysis method. Journal of Crystal Growth 270: 211-218.

Shih, W. J., Wang, J. W., Wang, M. C., and Hon, M. H. 2006. A study on the phase transformation of the nanosized hydroxyapatite synthesized by hydrolysis using in situ high temperature X-ray diffraction. Materials Science and Engineering 26: 1434-1438.

Siva-Kumar, M., Sampath-Kumar, T. S., Shantha, K. L., and Panduranga, R. K. 1996. Development of hydroxyapatite derived from Indian coral. Biomaterials 17: 1709-1714.

Studart, A. R., Gonzenbach, U. T., Tervoort, E., and Gauckler, L. J. 2006. Processing Routes to Macroporous Ceramic: A Review. Journal of the American Ceramics Society 89(6): 1771-1789.

Sun, R., Li, M., Lu, Y., and Li, S. 2006. Dissolution behavior of hollow hydroxyapatite microspheres immersed in deionized water. Materials Research Bulletin 41: 1138-1145.

Tadic, D., Beckmann, F., Schwarz, K., and Epple, M. 2004. A novel method to produce hydroxyapatite objects with interconnecting porosity that avoids sintering. Biomaterials 25: 3335-3340.

Tampieri, A., Celotti, G., Sprio, S., and Mingazzini, C. 2000. Characteristics of synthetic hydroxyapatite and attempts to improve their thermal stability. Materials Chemistry and Physics 64: 54-61.

Tampieri, A., Celotti, G., Sprio, S., Delcogliano, A., and Franzese, S. 2001. Porosity-graded hydroxyapatite ceramics to replace natural bone. Biomaterials 22: 1365-1370.

Tancred, D. C., McCormack, B. A. O., and Carr, A. J. 1998. A synthetic bone implant macroscopically identical to cancellous bone. Biomaterials 19: 2303-2311.

Tang, F. Q., Fudouzi, H., and Sakka Y. 2003. Fabrication of macroporous alumina with tailored porosity. Journal of the American Ceramics Society 86(12): 2050-2054.

Tang, F. Q., Fudouzi, H., Uchikoshi, T., and Sakka Y. 2004. Preparation of porous materials with controlled pore size and porosity. Journal of the European Ceramics Society 24: 341-344.

Tas, C.A. 2000. Synthesis of biomimetic Ca-hydroxyapatite powders at $37^{o}C$ in synthetic body fluids. Biomaterials 21: 1429-1438.

Tas, C. A., Korkusuz, F., Timucin, M., and Akkas, N. 1997. An investigation of the chemical synthesis and high-temperature sintering behavior of calcium hydroxyapatite (HA) and tricalcium phosphate (TCP) bioceramics. Journal of Materials Science: Materials in Medicine 8: 91-96.

Tian, J. T., and Tian, J. M. 2001. Preparation of porous hydroxyapatite, Journal of Materials Science 36: 3061-3066.

Tulliani, J. M., Bartuli, C., Bemporad, E., Naglieri, V., and Sebastiani, M. 2009. Preparation and mechanical characterization of dense and porous zirconia produced by gel casting with gelatin as a gelling agent. Ceramics International 35: 2481-2491.

Vargas, G., Lopez, J., Acevedo, J., Mendez, J., and Mendez, M. 1998. Effect of ultrasonic vibration on the particle size distribution of hydroxyapatite chemically precipitated from $Ca(OH)_2$ and H_3PO_4. Bioceramics Volume II: 711-714.

Vaz, L., Lopez, A. B., and Almeida, M. 1999. Porosity control of hydroxyapatite implants. Journal of Materials Science: Materials in Medicine 10: 239-242.

Wang, F., Li, M., Lu, Y., and Qi, Y. 2005. A simple sol-gel method for preparing hydroxyapatite nanopowders. Materials Letters 59: 916-919.

Woodard, J. R., et al. 2007. The mechanical properties and osteoconductivity of hydroxyapatite bone scaffolds with multi-scale porosity. Biomaterials 28: 45-54.

White, E. W., Weber, J. N., and White, R. A. 1975. Materials useful for prosthetic devices and the like. US Patent US3890107.

White, A. A., Best, S. M., and Kinloach, I. A. 2007. Hydroxyapatite-Carbon Nanotube Composites for biomedical application: A review. Applied Ceramic Technology 4: 1-13.

Xu, Y., Wang, D., Yang, L., and Tang, H. 2001. Hydrothermal conversion of coral into hydroxyapatite. Materials Characterization 47: 83-87.

Yang, H. Y., et al. 2008. Sintering behavior of calcium phosphate filaments for use as hard tissue scaffolds. Journal of the European Ceramic Society 28: 159-167.

Yao, X. M., Tan, S. H., and Jiang, D. L. 2005. Fabrication of hydroxyapatite ceramics with controlled pore characteristics by slip casting. Journal of Materials Science: Materials in Medicine 16: 161-165.

Yeong, K. C. B., Wang, J., and Ng, S. C. 1999. Fabricating densified hydroxyapatite ceramics from a precipitated precursor, Materials letters 38: 208-213.

Yeong, B., Junmin, X., and Wang, J. 2001. Mechanochemical Synthesis of Hydroxyapatite from Calcium Oxide and Brushite. Journal of the American Ceramic Society 84(2): 465-467.

Yoon, S. Y., Park, Y. M., Park, S. S., Stevens, R., and Park, H. C. 2005. Synthesis of hydroxyapatite whiskers by hydrolysis of α-tricalcium phosphate using microwave heating. Materials Chemistry and Physics 91: 48-53.

Zhang, H., Li, S., and Yan, Y. 2001. Dissolution behavior of hydroxyapatite powder in hydrothermal solution. Ceramics International 27: 451-454.

Zhang, F. Z., Kato, T., Fuji, M., and Takahashi, M. 2006. Gelcasting fabrication of porous ceramics using a continuous process. Journal of the European Ceramic Society 26: 667-671.

Zhang, X., and Vecchio, K. S. 2006. Creation of dense hydroxyapatite (synthetic bone) by hydrothermal conversion of seashells. Materials Science & Engineering 26: 1445-1450.

Zhang, H. G., and Zhu, Q. S. 2007. Preparation of porous hydroxyapatite with interconnected pore architecture. Journal of Materials Science: Materials in Medicine 18: 1825-1829.

APPENDIX

Table A-1   Dimensions and weights of the cylindrical specimens prepared via sacrificial template technique using PMMA granule

Sample Name	#	Diameter (mm.)				Height (mm.)				Weight (g.)
		1	2	3	Average	1	2	3	Average	
H00-P00-13	1	18.24	18.21	18.25	18.23	5.55	5.47	5.49	5.50	2.175
	2	18.41	18.53	18.57	18.50	5.49	5.53	5.47	5.50	2.225
H00-P05-13	1	17.63	17.58	17.59	17.60	6.31	6.49	6.41	6.40	2.328
	2	17.69	17.71	17.66	17.69	5.82	5.89	5.84	5.85	2.141
H00-P10-13	1	17.18	17.23	17.22	17.21	6.14	6.23	6.17	6.18	2.091
	2	17.15	17.21	17.18	17.18	5.93	5.89	5.85	5.89	1.995
H00-P20-13	1	17.95	17.98	17.97	17.97	7.21	7.22	7.48	7.30	2.366
	2	17.86	17.87	17.64	17.79	7.23	7.16	7.21	7.20	2.317
H00-P30-13	1	17.98	18.02	18.03	18.01	8.21	8.28	8.07	8.19	2.309
	2	18.06	18.14	18.11	18.10	8.02	8.04	8.10	8.05	2.259
H00-P40-13	1	18.46	18.39	18.31	18.39	8.30	8.26	8.35	8.30	1.951
	2	18.32	18.28	18.29	18.30	8.33	8.28	8.27	8.29	1.922
H00-P00-13A	1	17.61	17.57	17.59	17.59	4.89	4.90	4.92	4.90	1.745
	2	17.82	17.84	17.79	17.82	5.86	5.80	5.74	5.80	2.108
H00-P05-13A	1	17.44	17.42	17.43	17.43	5.87	5.82	5.81	5.83	2.001
	2	17.35	17.35	17.33	17.34	6.11	6.14	6.08	6.11	2.058
H00-P10-13A	1	17.54	17.40	17.44	17.46	7.12	7.14	7.14	7.13	2.538
	2	17.65	17.67	17.61	17.64	8.01	7.95	7.91	7.96	2.647
H00-P20-13A	1	17.84	17.92	17.91	17.89	7.95	7.96	7.92	7.94	2.431
	2	17.95	17.91	17.92	17.93	7.44	7.45	7.47	7.45	2.334
H00-P30-13A	1	18.11	18.10	18.15	18.12	8.07	8.10	8.07	8.08	2.332
	2	18.12	18.13	18.12	18.12	8.05	8.07	8.10	8.07	2.257
H00-P40-13A	1	18.45	18.47	18.48	18.47	8.15	8.17	8.14	8.15	1.974
	2	18.33	18.32	18.37	18.34	8.03	8.10	8.05	8.06	1.935
H00-P00-15	1	18.21	18.17	18.23	18.20	5.76	5.63	5.66	5.68	2.207
	2	18.33	18.35	18.28	18.32	5.78	5.82	5.85	5.82	2.075
H00-P05-15	1	17.93	17.88	17.91	17.91	6.12	6.19	6.14	6.15	2.182
	2	17.99	17.91	17.95	17.95	5.82	5.89	5.84	5.85	2.062
H00-P10-15	1	17.68	17.72	17.71	17.70	6.14	6.14	6.13	6.14	2.091
	2	17.75	17.71	17.78	17.75	6.15	6.19	6.15	6.16	2.075
H00-P20-15	1	17.81	17.84	17.85	17.83	7.31	7.32	7.34	7.32	2.175
	2	17.88	17.89	17.86	17.88	7.32	7.33	7.35	7.33	2.213
H00-P30-15	1	18.01	18.03	18.03	18.02	8.18	8.21	8.17	8.19	2.124
	2	18.05	18.04	18.01	18.03	8.12	8.09	8.10	8.10	2.152
H00-P40-15	1	18.46	18.39	18.31	18.39	8.50	8.46	8.55	8.50	1.882
	2	18.32	18.28	18.29	18.30	8.53	8.49	8.50	8.51	1.874

Table A-2   Dimensions and weights of the bar-shape specimens prepared via sacrificial template technique using PMMA granule

Sample Name	#	Length (mm.)	Width (mm.)	Thickness (mm.)	Weight (g.)
H00-P00-13	1	29.19	20.00	10.00	1.528
	2	28.01	20.00	10.00	1.569
H00-P05-13	1	27.87	20.00	10.00	1.504
	2	28.13	20.00	10.00	1.456
H00-P10-13	1	28.11	20.00	10.00	1.575
	2	27.73	20.00	10.00	1.581
H00-P20-13	1	27.94	20.00	10.00	1.495
	2	28.03	20.00	10.00	1.494
H00-P30-13	1	27.83	20.00	10.00	1.375
	2	28.16	20.00	10.00	1.271
H00-P40-13	1	28.27	20.00	10.00	0.926
	2	28.21	20.00	10.00	0.892
H00-P00-13A	1	27.46	20.00	10.00	1.591
	2	27.70	20.00	10.00	1.527
H00-P05-13A	1	27.87	20.00	10.00	1.552
	2	28.10	20.00	10.00	1.640
H00-P10-13A	1	28.85	20.00	10.00	1.636
	2	27.70	20.00	10.00	1.427
H00-P20-13A	1	27.20	20.00	10.00	1.575
	2	27.22	20.00	10.00	1.403
H00-P30-13A	1	28.05	20.00	10.00	1.239
	2	28.25	20.00	10.00	1.365
H00-P40-13A	1	27.65	20.00	10.00	1.070
	2	28.02	20.00	10.00	1.304
H00-P00-15	1	29.16	20.00	10.00	1.558
	2	28.05	20.00	10.00	1.565
H00-P05-15	1	28.06	20.00	10.00	1.512
	2	28.13	20.00	10.00	1.505
H00-P10-15	1	27.85	20.00	10.00	1.412
	2	27.73	20.00	10.00	1.408
H00-P20-15	1	28.12	20.00	10.00	1.422
	2	28.03	20.00	10.00	1.413
H00-P30-15	1	28.16	20.00	10.00	1.355
	2	28.23	20.00	10.00	1.337
H00-P40-15	1	28.24	20.00	10.00	1.023
	2	28.13	20.00	10.00	1.041

Table A-3   Dimensions and weights of the cylindrical specimens prepared via direct foaming technique using H_2O_2 solution

Sample Name	#	Diameter (mm.)				Height (mm.)				Weight (g.)
		1	2	3	Average	1	2	3	Average	
H01-P00-13	1	18.20	18.13	18.28	18.20	10.48	10.53	10.63	10.55	1.647
	2	17.98	18.04	18.01	18.01	10.52	10.56	10.59	10.56	1.672
H03-P00-13	1	17.53	17.57	17.45	17.52	11.34	11.36	11.31	11.34	1.605
	2	17.65	17.65	17.67	17.66	10.28	10.25	10.23	10.25	1.466
H05-P00-13	1	16.96	16.93	16.95	16.95	12.78	12.75	12.73	12.75	1.621
	2	16.99	16.96	16.98	16.98	13.29	13.28	13.34	13.30	1.678
H10-P00-13	1	17.88	17.93	17.85	17.89	12.35	12.38	12.44	12.39	1.708
	2	17.64	17.85	17.76	17.75	9.51	9.57	9.58	9.55	1.306
H20-P00-13	1	18.43	18.32	18.33	18.36	11.98	12.01	11.95	11.98	1.691
	2	18.31	18.25	18.20	18.25	11.90	11.87	11.93	11.90	1.622
H30-P00-13	1	18.01	18.04	18.10	18.05	13.53	13.59	13.54	13.55	1.533
	2	18.19	18.15	18.11	18.15	14.55	14.46	14.41	14.47	1.840
H01-P00-13A	1	18.28	18.33	18.31	18.31	10.77	10.84	10.80	10.8	1.716
	2	18.20	18.20	18.21	18.20	9.66	9.63	9.65	9.65	1.556
H03-P00-13A	1	18.18	18.18	18.20	18.19	9.06	9.04	9.07	9.06	1.352
	2	18.44	18.34	18.46	18.41	8.75	8.87	8.79	8.80	1.449
H05-P00-13A	1	17.59	17.55	17.62	17.59	11.40	11.41	11.40	11.40	1.655
	2	17.79	17.73	17.79	17.77	13.21	13.17	13.24	13.21	1.995
H10-P00-13A	1	17.55	17.52	17.44	17.50	14.41	14.42	14.38	14.40	1.975
	2	17.08	17.10	17.12	17.10	17.58	17.50	17.46	17.51	2.368
H20-P00-13A	1	17.92	17.86	17.92	17.90	10.63	10.66	10.63	10.64	1.476
	2	17.91	17.87	17.94	17.91	11.84	11.77	11.79	11.80	1.714
H30-P00-13A	1	17.20	17.23	17.20	17.21	7.60	7.54	7.63	7.59	0.759
	2	17.00	16.93	17.06	17.00	7.35	7.28	7.30	7.31	0.843
H01-P00-15	1	18.08	18.10	18.10	18.09	8.23	8.18	8.22	8.21	1.245
	2	18.10	18.12	18.08	18.10	8.10	8.09	8.11	8.10	1.257
H03-P00-15	1	17.87	17.83	17.83	17.84	9.57	9.57	9.56	9.567	1.172
	2	17.80	17.83	17.81	17.81	8.91	8.85	8.84	8.87	1.075
H05-P00-15	1	17.04	16.93	17.01	16.99	10.14	10.14	10.13	10.14	1.118
	2	16.80	16.89	16.82	16.84	14.04	14.01	13.99	14.01	1.464
H10-P00-15	1	16.44	16.58	16.54	16.52	12.96	13.37	12.12	12.82	1.281
	2	16.50	16.51	16.50	16.50	13.04	13.02	13.03	13.03	1.318
H20-P00-15	1	17.05	17.03	16.89	16.99	14.77	14.82	14.80	14.80	1.377
	2	16.65	16.29	16.85	16.60	14.71	14.60	14.52	14.61	1.395

Table A-4   Dimensions and weights of the bar-shape specimens prepared via direct
             foaming technique using H_2O_2 solution

Sample Name	#	Length (mm.)	Width (mm.)	Thickness (mm.)	Weight (g.)
H01-P00-13	1	25.95	20.00	10.00	1.418
	2	27.35	20.00	10.00	1.485
H03-P00-13	1	26.84	20.00	10.00	1.210
	2	21.60	20.00	10.00	1.112
H05-P00-13	1	25.94	20.00	10.00	1.428
	2	26.02	20.00	10.00	1.185
H10-P00-13	1	24.27	20.00	10.00	1.169
	2	24.88	20.00	10.00	1.106
H20-P00-13	1	24.54	20.00	10.00	1.021
	2	25.14	20.00	10.00	1.085
H30-P00-13	1	27.32	20.00	10.00	1.067
	2	27.22	20.00	10.00	1.209
H01-P00-13A	1	28.33	20.00	10.00	1.259
	2	28.12	20.00	10.00	1.117
H03-P00-13A	1	30.15	20.00	10.00	1.648
	2	28.42	20.00	10.00	1.331
H05-P00-13A	1	27.56	20.00	10.00	1.356
	2	27.06	20.00	10.00	1.482
H10-P00-13A	1	26.62	20.00	10.00	1.231
	2	26.80	20.00	10.00	1.252
H20-P00-13A	1	26.50	20.00	10.00	1.098
	2	26.51	20.00	10.00	1.075
H30-P00-13A	1	27.18	20.00	10.00	1.182
	2	27.33	20.00	10.00	1.172
H01-P00-15	1	23.12	20.00	10.00	0.941
	2	23.11	20.00	10.00	1.012
H03-P00-15	1	25.28	20.00	10.00	0.935
	2	25.17	20.00	10.00	0.945
H05-P00-15	1	23.06	20.00	10.00	0.773
	2	22.62	20.00	10.00	0.717
H10-P00-15	1	23.42	20.00	10.00	0.714
	2	23.23	20.00	10.00	0.708
H20-P00-15	1	23.45	20.00	10.00	0.705
	2	23.77	20.00	10.00	0.711

Table A-5   Dimensions and weights of the cylindrical specimens prepared via combination technique using PMMA granule and H_2O_2 solution

Sample Name	#	Diameter (mm.)				Height (mm.)				Weight (g.)
		1	2	3	Average	1	2	3	Average	
H05-P00-13	1	16.96	16.93	16.95	16.95	12.78	12.75	12.73	12.75	1.621
	2	16.99	16.96	16.98	16.98	13.29	13.28	13.34	13.30	1.678
H05-P05-13	1	17.10	17.11	17.12	17.11	10.74	10.84	10.78	10.81	1.296
	2	16.94	16.84	16.90	16.89	12.84	12.78	12.80	12.79	1.374
H05-P10-13	1	18.65	18.67	18.64	18.65	13.26	13.24	13.24	13.24	1.624
	2	18.72	18.69	18.73	18.71	12.87	12.88	12.89	12.89	1.675
H05-P20-13	1	17.03	17.05	17.01	17.03	18.89	19.11	19.08	19.10	1.734
	2	17.00	17.02	17.00	17.01	12.37	12.42	12.41	12.42	1.037
H05-P30-13	1	18.08	18.12	18.09	18.10	11.95	12.04	12.02	12.00	1.125
	2	18.04	18.01	17.95	18.00	15.40	15.38	15.41	15.40	1.402
H05-P00-13A	1	17.59	17.55	17.62	17.59	11.40	11.41	11.40	11.40	1.655
	2	17.79	17.73	17.79	17.77	13.21	13.17	13.24	13.21	1.995
H05-P05-13A	1	18.38	18.35	18.31	18.35	13.50	13.57	13.47	13.51	2.122
	2	18.28	18.29	18.32	18.30	12.68	12.71	12.67	12.69	1.847
H05-P10-13A	1	18.18	18.15	18.12	18.15	10.25	10.21	10.23	10.23	1.339
	2	18.31	18.28	18.26	18.28	11.35	11.32	11.35	11.34	1.598
H05-P20-13A	1	16.69	16.72	16.68	16.70	11.03	11.12	11.15	11.10	1.127
	2	16.80	16.78	16.87	16.82	11.69	11.80	11.65	11.71	1.120
H05-P30-13A	1	17.12	17.09	17.11	17.11	11.02	11.03	10.95	11.00	1.074
	2	18.07	17.98	18.02	18.02	13.89	14.08	14.04	14.00	1.554
H10-P00-13	1	17.88	17.93	17.85	17.89	12.35	12.38	12.44	12.39	1.708
	2	17.64	17.85	17.76	17.75	9.51	9.57	9.58	9.55	1.306
H10-P05-13	1	17.30	17.38	17.35	17.34	13.60	13.63	13.62	13.63	1.511
	2	17.92	18.08	17.72	17.91	16.59	16.89	16.76	16.83	1.775
H10-P10-13	1	17.81	17.78	17.80	17.80	18.93	19.04	18.99	19.02	1.751
	2	17.47	17.96	17.66	17.70	14.77	14.88	14.75	14.82	1.475
H10-P20-13	1	17.81	17.68	17.89	17.79	12.77	12.65	12.68	12.67	1.098
	2	17.88	17.78	17.76	17.81	16.92	16.88	16.94	16.91	1.350
H10-P00-13A	1	17.55	17.52	17.44	17.50	14.41	14.42	14.38	14.40	1.975
	2	17.08	17.10	17.12	17.10	17.58	17.50	17.46	17.51	2.368
H10-P05-13A	1	17.65	17.97	17.75	17.79	13.39	13.34	13.33	13.35	1.652
	2	17.76	17.62	18.07	17.82	17.76	17.67	17.73	17.72	2.028
H10-P10-13A	1	18.14	18.24	18.23	18.20	16.41	16.45	16.41	16.42	1.950
	2	18.02	17.95	18.14	18.04	17.21	17.20	17.19	17.20	1.940
H10-P20-13A	1	17.21	17.23	17.20	17.21	17.33	17.32	17.25	17.30	1.763
	2	17.09	17.10	17.12	17.10	17.16	17.24	17.17	17.19	1.676

Table A-5   Dimensions and weights of the cylindrical specimens prepared via combination technique using PMMA granule and H_2O_2 solution(Cont.)

Sample Name	#	Diameter (mm.)				Height (mm.)				Weight (g.)
		1	2	3	Average	1	2	3	Average	
H20-P00-13	1	18.43	18.32	18.33	18.36	11.98	12.01	11.95	11.98	1.691
	2	18.31	18.25	18.20	18.25	11.90	11.87	11.93	11.90	1.622
H20-P05-13	1	17.47	17.50	17.52	17.50	14.46	14.57	14.51	14.51	1.364
	2	17.80	17.75	17.81	17.79	16.50	16.74	16.66	16.63	1.869
H20-P10-13	1	17.16	17.21	17.23	17.20	16.27	16.30	16.32	16.30	1.364
	2	17.25	17.21	17.18	17.21	14.36	14.39	14.46	14.40	1.419
H20-P00-13A	1	17.92	17.86	17.92	17.90	10.63	10.66	10.63	10.64	1.476
	2	17.91	17.87	17.94	17.91	11.84	11.77	11.79	11.80	1.714
H20-P05-13A	1	17.70	17.75	17.64	17.70	13.57	13.56	13.50	13.54	1.482
	2	17.92	17.92	17.95	17.93	15.33	15.35	15.26	15.31	1.841
H20-P10-13A	1	17.85	17.92	17.90	17.89	15.22	15.23	15.23	15.23	1.608
	2	18.03	18.14	18.09	18.09	14.45	14.42	14.38	14.42	1.672
H30-P00-13	1	18.01	18.04	18.10	18.05	13.53	13.59	13.54	13.55	1.533
	2	18.19	18.15	18.11	18.15	14.55	14.46	14.41	14.47	1.840
H30-P05-13	1	18.04	18.01	17.96	18.00	12.52	12.44	12.56	12.51	1.290
	2	18.24	18.25	18.26	18.25	11.02	10.98	10.99	11.0	1.204
H30-P10-13	1	18.10	18.09	18.13	18.11	12.40	12.44	12.35	12.40	1.236
	2	18.31	18.31	18.29	18.30	13.44	13.43	13.46	13.44	1.330
H30-P00-13A	1	17.20	17.23	17.20	17.21	7.60	7.54	7.63	7.59	0.759
	2	17.00	16.93	17.06	17.00	7.35	7.28	7.30	7.31	0.843
H30-P05-13A	1	17.85	17.86	17.85	17.85	13.82	13.88	13.81	13.84	1.508
	2	17.86	17.85	17.83	17.85	13.74	13.66	13.72	13.71	1.495
H30-P10-13A	1	17.59	17.55	17.52	17.55	12.15	12.16	12.15	12.15	1.152
	2	18.12	18.15	18.07	18.11	12.59	12.63	12.58	12.6	1.335

Table A-6   Dimensions and weights of the bar-shape specimens prepared via combination technique using PMMA granule and H_2O_2 solution

Sample Name	#	Length (mm.)	Width (mm.)	Thickness (mm.)	Weight (g.)
H05-P00-13	1	25.94	20.00	10.00	1.428
	2	26.02	20.00	10.00	1.185
H05-P05-13	1	27.53	20.00	10.00	1.039
	2	22.07	20.00	10.00	0.850
H05-P10-13	1	28.56	20.00	10.00	0.773
	2	26.46	20.00	10.00	0.915
H05-P20-13	1	28.32	20.00	10.00	0.826
	2	25.98	20.00	10.00	0.788
H05-P30-13	1	29.42	20.00	10.00	1.089
	2	28.04	20.00	10.00	1.104
H05-P00-13A	1	26.62	20.00	10.00	1.231
	2	26.80	20.00	10.00	1.252
H05-P05-13A	1	28.34	20.00	10.00	1.146
	2	28.43	20.00	10.00	1.130
H05-P10-13A	1	28.94	20.00	10.00	1.021
	2	28.52	20.00	10.00	1.055
H05-P20-13A	1	28.70	20.00	10.00	0.935
	2	28.57	20.00	10.00	0.799
H05-P30-13A	1	28.70	20.00	10.00	0.746
	2	29.20	20.00	10.00	0.705
H10-P00-13	1	24.27	20.00	10.00	1.169
	2	24.88	20.00	10.00	1.106
H10-P05-13	1	25.66	20.00	10.00	0.977
	2	27.10	20.00	10.00	0.908
H10-P10-13	1	28.57	20.00	10.00	1.178
	2	27.89	20.00	10.00	1.005
H10-P20-13	1	27.50	20.00	10.00	0.754
	2	26.01	20.00	10.00	0.718
H10-P00-13A	1	26.62	20.00	10.00	1.231
	2	26.80	20.00	10.00	1.252
H10-P05-13A	1	27.69	20.00	10.00	1.126
	2	27.94	20.00	10.00	1.340
H10-P10-13A	1	28.30	20.00	10.00	1.145
	2	27.67	20.00	10.00	1.094
H10-P20-13A	1	26.29	20.00	10.00	0.887
	2	25.86	20.00	10.00	0.858

Table A-6   Dimensions and weights of the bar-shape specimens prepared via combination technique using PMMA granule and H_2O_2 solution (Cont.)

Sample Name	#	Length (mm.)	Width (mm.)	Thickness (mm.)	Weight (g.)
H20-P00-13	1	24.54	20.00	10.00	1.021
	2	25.14	20.00	10.00	1.085
H20-P05-13	1	27.31	20.00	10.00	1.435
	2	27.11	20.00	10.00	1.335
H20-P10-13	1	27.35	20.00	10.00	1.123
	2	27.03	20.00	10.00	1.220
H20-P00-13A	1	26.50	20.00	10.00	1.098
	2	26.51	20.00	10.00	1.075
H20-P05-13A	1	26.77	20.00	10.00	1.287
	2	26.90	20.00	10.00	1.256
H20-P10-13A	1	26.72	20.00	10.00	1.207
	2	26.75	20.00	10.00	1.160
H30-P00-13	1	27.32	20.00	10.00	1.067
	2	27.22	20.00	10.00	1.209
H30-P05-13	1	27.36	20.00	10.00	0.918
	2	28.21	20.00	10.00	0.762
H30-P10-13	1	27.79	20.00	10.00	0.772
	2	28.76	20.00	10.00	0.910
H30-P00-13A	1	27.25	20.00	10.00	1.182
	2	27.33	20.00	10.00	1.172
H30-P05-13A	1	26.42	20.00	10.00	0.769
	2	24.49	20.00	10.00	0.709
H30-P10-13A	1	27.64	20.00	10.00	0.801
	2	29.06	20.00	10.00	0.923

BIOGRAPHY

Mr. Sujin Woottichaiwat was born in Bangkok, Thailand, on December 16, 1977. He graduated with Bachelor's degree of Engineering in Industrial Engineering from Kasetsart University in 1999 and Master's degree of Engineering in Industrial Engineering from Chulalongkorn University in 2002. He had worked for three years before has been studied for a Doctoral degree of Engineering in Industrial Engineering, Chulalongkorn University in 2004.